

UNIVERSITY OF NAPLES FEDERICO II

Department of Structures for Engineering and Architecture

PH.D. PROGRAMME IN SEISMIC RISK

COORDINATOR PROF. ALDO ZOLLO

XXV CYCLE



FABIO PETRUZZELLI

PH.D. THESIS

**Scale-dependent procedures
for seismic risk assessment and management
of industrial building portfolios**

ADVISOR: PROF. IUNIO IERVOLINO

2013

To my father Donato and my mother Mariella

ABSTRACT

In the last years the assessment and management of seismic risk in the manufacturing industry has received a continuously growing interest, due to the significant consequences, both direct and indirect, that can be triggered by earthquakes (e.g. (Tohoku, 2011; Emilia, 2012)).

The present thesis is focused on the development and the application to real case-studies of different procedures for seismic risk assessment and management in the industrial and insurance fields. The research addresses to the problem at different scales: (i) a “large scale”, typically the one of interest of the insurer, at which the number of buildings to deal with is of hundreds or thousands; a “meso scale”, typically the one of large industrial groups, at which the number of building is of tens to hundreds; (iii) a “site-specific” scale, that is the one of interest for a single plant.

At each one of the previously listed scales, a different procedure has been proposed.

At the “large scale”, a detailed assessment of vulnerability is, in general, unfeasible. Therefore, a prioritization scheme has been developed with the purpose of analysing a portfolio of structures and ranking their seismic risk in a coherent manner, in order to define a priority scale for further, more detailed, investigations. This approach is based on the evaluation of a conventional (or “nominal”) seismic risk index, on the basis of extremely poor and easy to retrieve data, at least the year of construction and geographic location, for the production of which it is not required any visual inspection of the structures. This index is defined as the gap between the current seismic demand and the seismic capacity, the latter evaluated on the basis of seismic demand at the time of the design, assuming a perfect code compliance. In the case of structures not designed in a seismic zone, the horizontal capacity may be obtained from the design for other horizontal actions, such as that from wind. In order to implement the proposed prioritization scheme and compare it to other similar ones, available in literature, a tool named “*NODE – NOminalDEficit – v1.1. beta*” has been developed.

This tool enables to compute location-specific code-based horizontal performance demands, according to Italian code and seismic classification evolution since 1909. Moreover it contains the evolution of wind design and a map of soil categories according to current seismic regulations for the whole Italian territory.

Thanks to the collaboration with *AXA Matrix Risk Consultants*, this approach has been applied to a real case-study of 19 Italian industrial plants, visually surveyed by means of knowledge forms realized ad-hoc.

At the “meso scale”, the number of buildings to deal with is of hundreds or thousands. It is believed that at this scale it is possible, according to the resources of the stakeholder, to achieve a level of knowledge about the structures sufficient to allocate a fragility curve to each structure of the portfolio or to classes of structures individuated in the portfolio. The proposed approach, therefore, consists in the rapid computation of expected loss due to earthquakes by the integration of hazard, fragility and exposure. Although the use of fragility curves can be considered a well-established methodology for computing seismic risk, significant differences exist among fragility functions computed in different geographical contexts, reflecting the differences in structural typologies, construction practice and materials. Therefore their practical use requires instruments for their managing, conversion and use along with hazard and exposure. In order to overcome this shortcomings, the software suite named “*FRAME - Fragility-based rapid seismic Risk AssessMEnt - v.1.0 beta*” has been developed with the aim of providing for the management, the manipulation and the homogenization of an inventory of fragility curves. The inclusion in the software of seismic hazard at the global scale and the possibility of including exposure allow the computation of the expected losses worldwide.

At the “site-specific scale”, the analysis of the seismic performance of an existing steel building has been performed in order to provide for the lack in fragility curves available in literature for this specific structural typology and to compute failure probabilities. The latter represent the most rational basis for assessing loss estimates and computing insurance premiums. Such an approach to seismic risk assessment, extremely demanding in terms of time and computational burden, is proposed to be applied at the scale of the single building, of a plant or, of a limited number of plants. The analysed structure is the main workshop building of one of the most risk-prone plants of the case-study portfolio, as resulting from the prioritization analysis. The study of such a structure, designed according to obsolete structural codes about both the definition of the seismic design action and the design of steel structures, allows to enlighten and critically discuss some peculiar modelling aspects. Moreover, some findings deriving from non-linear response history analysis, related to the onset of different failure modes and the inclusion of residual drift in the assessment, have been discussed.

Although on principle independent each other, the three procedures outlined in the thesis can be structured in order to provide a unified framework for management and assessment of seismic risk of large dimensions structural portfolios.

KEYWORDS: *Industrial buildings • Portfolio • Risk Management • Steel Structures • Nominal Deficit • Seismic Risk • Hazard • Fragility • Loss.*

ACKNOWLEDGEMENTS

I would express my sincere gratitude to my advisor, Prof. Iunio Iervolino, for his unwavering guidance, his technical advice and for the opportunity to work in an outstanding academic department.

I would like to thank Prof. Gaetano Della Corte for his patience, the thoughtful support of my work, and for never cutting a meeting short.

Their competence and devotion to research have been, and will be in the future, an example for me.

A great acknowledgment is due to AXA Matrix Risk Consultants, in particular the head of Italian office, Marcello Forte, for the openness and suggestions provided and Davide Spanò, for the support and the continuous exchange of opinions in this years.

I wish to acknowledge also the AXA Corporate Solutions group, in particular Bernard Laporte and Gilbert Kervella, for the interest shown in the work made in this years.

I wish to acknowledge the contribution of the Italian Network of University Laboratories for Earthquake Engineering (ReLUIIS), which has partially supported this research in the framework of ReLUIIS-DPC 2010-2013 project, funded by the Italian Department of Civil Protection.

I would like to acknowledge and express my appreciation to Dr. Fatemeh Jalayer for having introduced me to the world of research and wisely guided me in the first part of my Ph.D. and Prof. Nicola Augenti and Dr. Gerardo M. Verderame for the discussions and the interest shown in my work in this years.

I would like to thank all the friends and colleagues at the University of Naples, for having shared their knowledge with me, and making me fell like at home: Ludovica Elefante, Flavia De Luca, Raffaele De Risi, Vittorio Capozzi, Paolo Ricci, Vincenzo Giamundo, Crescenzo Petrone and Marianna Ercolino, Raffaele Frascadore, Alberto Zinno, Claudio D'Ambra.

I particularly wish to thank my roommates: Fulvio Parisi, Simona Esposito, Barbara Polidoro, Eugenio Chioccarelli and Carmine Galasso. Your friendship is one of the major results of my Ph.D.

I am grateful to my friends Ferdinando, Francesco, Giovanni and Alessandra for having endured me during these years and for having been there in the worst times and to Ornella, Bruno and Giorgia for the support and the care shown in these months.

My PhD was like a run, during which several times I fell and I lost a lot of things of my personal life, but I also found new ones.

A great, warm and loving thank goes to Ilaria, for having been beside me throughout this months. Your joy, love and care have made this goal possible.

My deepest gratitude goes to my family, to which I dedicate all the efforts and difficulties, as well as the good times and the joy of these years. In particular I would like to thank my parents, Donato and Mariella Petruzzelli, for their unconditional love. I can hardly express in words how much I am grateful to them for the sacrifices and their every-day support throughout the years. I have never said you how much I love you and how important is your role model to me. I would like to thank my loving sisters Mariangela and Alessia for all the love and patience they give me and Alex and Paolo for having brought happiness to our family.

Finally, a message to the “little bean” that is going to arrive, we do not know yet your name but thinking of you in this moment gives me the strength to face new challenges.

TABLE OF CONTENTS

ABSTRACT	I
ACKNOWLEDGEMENTS	III
TABLE OF CONTENTS	V
LIST OF TABLES	IX
LIST OF FIGURES	X
LIST OF ABBREVIATIONS	XVII
CHAPTER 1 – BACKGROUND AND MOTIVATION	1
1.1. FRAMEWORK	1
1.2. OBJECTIVES OF THE STUDY	4
1.3. OUTLINE OF THE THESIS	7
CHAPTER 2 – BASICS OF SEISMIC RISK	8
2.1. DEFINITION	8
2.2. SEISMIC RISK ASSESSMENT	9
2.2.1. LOSS ESTIMATION	13
2.3. COMPUTING INDIVIDUAL RISK COMPONENTS	15
2.3.1. Seismic Hazard	15
2.3.2. Vulnerability	16
2.3.2.1. Empirical methods	17
2.3.2.2. Analytical methods	19
2.3.2.3. Code-based methods	21
2.3.2.4. Expert Judgment-based methods	21
2.3.2.5. Hybrid methods	22
2.3.3. Exposure	22
2.4. MANAGEMENT AND MITIGATION OF SEISMIC RISK	23
CHAPTER 3 THE CASE-STUDY BUILDING PORTFOLIO	26
3.1. DESCRIPTION OF THE CASE-STUDY	26
3.2. HAZARD FORM FOR INDUSTRIAL PLANTS	36
3.3. KNOWLEDGE FORMS FOR INDUSTRIAL MANUFACTURING PLANTS	42
3.3.1. PLANT LAYOUT KNOWLEDGE FORM	42
3.3.2. BUILDING-LIKE STRUCTURES KNOWLEDGE FORM	46
3.3.3. SILOS/TANKS KNOWLEDGE FORM	51

CHAPTER 4 – RISK PRIORITIZATION BASED ON NOMINAL DEFICIT ...	53
4.1. INTRODUCTION	53
4.2. REVIEW OF DECISION-MAKING FRAMEWORKS AND PRIORITIZATION APPROACHES	54
4.2.1. Screening procedures	55
4.2.2. The ATC 3-06 procedure	59
4.2.3. The NZSEE (2003) approach	61
4.2.4. The Grant <i>et al.</i> , (2007) approach	66
4.2.5. The Crowley <i>et al.</i> , (2008) approach.....	71
4.2.6. The Borzi <i>et al.</i> , (2011) approach.....	72
4.3. PROPOSED RISK MANAGEMENT PROCEDURE	75
4.3.1. Fundamental period and soil conditions.....	80
4.3.2. Building designed in non-seismic zones: wind design.....	81
4.3.3. Updating seismic capacity.....	82
4.3.3.1. <i>The C10- Comma 10 - v.1.0 software</i>	82
4.4. EVOLUTION OF ITALIAN SEISMIC STRUCTURAL REQUIREMENTS	85
4.4.1. Early history	85
4.4.2. Modern era	87
4.4.3. State-of-the-art and current codes	88
4.5. EVOLUTION OF SEISMIC CLASSIFICATION (DESIGN HAZARD) IN ITALY	90
4.6. THE NODE – <i>NOMINAL DEFICIT</i> - v.1.1 BETA SOFTWARE	97
4.7. APPLICATION OF THE PROPOSED RISK MANAGEMENT PROCEDURE TO THE CASE-STUDY PORTFOLIO	103
4.7.1. Step 1 –Ranking based on $NODE_{PGA}$ index.....	104
4.7.2. Knowledge phase	111
4.7.3. Step 2 –Ranking based on $NODE_{Sa(T),soil}$ index.....	111
4.7.3.1. <i>Seismic horizontal capacity from wind design</i>	114
4.7.3.2. <i>Updating seismic capacity due to earthquake occurrence</i>	118
4.7.4. Knowledge phase and Step 3 – Loss assessment	120
4.7.5. Comparison of NODE with other indices	120
4.8. CONCLUSIONS.....	124
CHAPTER 5 – FRAGILITY-BASED RAPID SEISMIC RISK ASSESSMENT	130
5.1. INTRODUCTION	130
5.2. REVIEW OF EXISTING FRAGILITY CURVES	132
5.2.1. Methodologies for computing fragility curves	132
5.2.2. Intensity Measure types.....	138
5.2.3. Limit states	141
5.3. THE “ <i>FRAME – FRAGILITY-BASED RAPID SEISMIC RISK ASSESSMENT - v.1.0 BETA</i> ” SOFTWARE SUITE	143

6.6.4.2. <i>Probability of local failure</i>	239
6.7. CONCLUSIONS.....	240
CHAPTER 7 – SUMMARY AND CONCLUSIONS	243
7.1. PRIORITIZATION ANALYSIS BASED ON NOMINAL DEFICIT	243
7.2. FRAGILITY-BASED RAPID SEISMIC RISK ASSESSMENT	245
7.3. SEISMIC RISK ASSESSMENT OF AN EXISTING INDUSTRIAL STEEL BUILDING	246
7.4. FINAL REMARKS	249
REFERENCES	251
APPENDIX A - EVOLUTION OF WIND DESIGN PRESCRIPTIONS IN ITALY	273
APPENDIX B - MAIN CHARACTERISTICS OF THE CASE-STUDY PORTFOLIO	275
APPENDIX C - MAIN CHARACTERISTICS OF RECORDS EMPLOYED IN NON- LINEAR TIME-HISTORY ANALYSES	278

LIST OF TABLES

Table 3.1 Case study plants.	27
Table 3.2 Soil category and structural composition of the case-study portfolio.	30
Table 3.3 Number of production structures of case-study plants, ELR and OLR (*computed considering the cumulative occupants of all the structures of the plant).	35
Table 3.4 Comparison of soil classification in modern seismic codes worldwide (Pitilakis <i>et al.</i> , 2004).	39
Table 4.1 Grading system adopted in NZSEE (2003).	65
Table 4.2 Summary of the most important changes in horizontal seismic actions and classification of Italian territory, as per regulatory codes. The number of municipalities which changed classification is expressed with respect to the previous code; partially adapted from Di Pasquale <i>et al.</i> , (1999a and 1999b).	96
Table 4.3 Statistics of linear regression of hazard curves for different structural periods, obtained from median INGV data, for exceedance return periods of 475, 1000 and 2500 years.	98
Table 4.4 Typical weights of structural materials and elements (CEN, 2004; PCI, 2010)	114
Table 5.1 Comparison of Macroseismic intensity scales (Musson <i>et al.</i> , 2010).	141
Table 5.2 Comparison of damage scales (Rossetto and Elnashai, 2003).	142
Table 6.1 Summary of structural characteristics of the examined models.	194
Table 6.2 Selection criteria for records consistent with disaggregation of seismic hazard at the facility site. Different sets of records were considered at four different levels in which intensity has been divided.	214
Table 6.3 Summary of the performed analysis for each structural model.	215
Table 6.4 Summary of local failures of roof members.	227
Table 6.5 Probabilities of failure based on the peak transient drift.	237
Table 6.6 Probabilities of failure based on the bivariate distribution of peak transient and residual drift. In parentheses the percentage variations with respect to the univariate distribution of peak transient drift reported in Table (6.5).	239
Table 6.7 Annual probabilities of exceeding global drift ratio limits, given that no global collapse occurs.	239
Table A.1. Summary of the codes for wind design in Italy considered in the “large-scale” prioritization approach and implemented in <i>NODE v.1.0 beta</i>	274
Table B.1. Main characteristics of case-study structures.	275
Table C.1. Basic record characteristics for $T_R=50$ years set	279
Table C.2. Basic record characteristics for $T_R=475$ years set	279
Table C.3. Basic record characteristics for $T_R=975$ years set	280
Table C.4. Basic record characteristics for $T_R=2475$ years set	281

LIST OF FIGURES

Figure 1.1 Worldwide socio economic trends to earthquakes (1900-2011). Cumulative deaths and economic losses related to global 2011dollar GDP and population (Daniell and Vervaeck, 2011)..... 1

Figure 1.2 Schematic representation of the different scales (in terms of number of buildings) of seismic risk assessment and management in industry..... 3

Figure 1.3 Scheme of the three scale-dependent procedures for seismic risk assessment and management dealt in the thesis. 5

Figure 1.4 Framework for seismic risk assessment and management of large industrial portfolios..... 6

Figure 2.1 Overview of PEER seismic loss assessment methodology (adapted from Krawinkler, 2005)..... 9

Figure 2.2 Vision 2000 recommended seismic performance objectives for buildings (Porter, 2003 after SEAOC, 1995);..... 12

Figure 2.3 Illustration of performance-based earthquake engineering (from Parisi, 2010 after Hamburger)..... 12

Figure 2.4 Risk management cycle..... 24

Figure 3.1 Case-study plants represented over the map of PGA with 475 years return period on rock (Stucchi *et al.*, 2011)..... 26

Figure 3.2 Percentages relative to the use of structures of the case-study portfolio. 30

Figure 3.3 Composition of the case study portfolio for what concerns construction material (left) and year of design (right)..... 31

Figure 3.4 Age of design of steel structures used for production 32

Figure 3.5 Typology of main (left) and secondary (right) beams of surveyed steel structures used for production 32

Figure 3.6 Typology of column of surveyed steel structures used for production. 32

Figure 3.7 Design year of PRC structures used for production. 33

Figure 3.8 Types of main beams and roofing elements of surveyed PRC structures. 33

Figure 3.9 Column cross section dimensions of surveyed PRC structures. 34

Figure 3.10 Case study plant ranked from left to right in order of decreasing OLR and respective values of ELR and of PGA with 475 year return period on rock. 35

Figure 3.11 Individual seismogenic sources according to DISS v.3.1.1 (Basili *et al.*, 2009), on Google earth view, 41°07'19.17''N 1°42'07.86'' lev.-149m alt 1819.47km, 02/26/2013..... 37

Figure 3.12 Macroseismic Intensity with 10% of probability of exceedance in 50 years employing a Gaussian GMPE (left) and a binomial GMPE (right) (Albarello *et al.*, 2007)..... 38

Figure 3.13 Hazard form (1/2) 40

Figure 3.14 Hazard form (2/2) 41

Figure 3.15 Example of identification of structural aggregates. The * in the left panel refers to a structure for loading/unloading finished products not belonging to those under investigation that is, therefore, neglected.	43
Figure 3.16 Plant layout form (1/2).	45
Figure 3.17 Plant layout forms (2/2).	46
Figure 3.18 Example of identification of individual structural units and relative age of design.	48
Figure 3.19 First level building-like structures knowledge form (1/2).	49
Figure 3.20 First level building-like structures knowledge form (2/2).	50
Figure 3.21 Silos/Tanks knowledge form.	52
Figure 4.1 ATC 3-06 approach for risk reduction (form Grant <i>et al.</i> , 2006 based on ATC, 1978).	60
Figure 4.2 NZSEE (2003) active risk reduction programme. TA stands for territorial authority; Anairp for “As Near As Is Reasonably Practicable”. Other acronyms are explained in the text. (NZSEE, 2003)	62
Figure 4.3 Initial Evaluation Procedure (IEP) of NZSEE approach (NZSEE, 2003).	63
Figure 4.4 Occupancy Classification for ordinary buildings according to NZSEE (2203).	66
Figure 4.5 Framework of Grant <i>et al.</i> (2007) procedure for risk mitigation in Italian school buildings (Grant <i>et al.</i> , 2007).	67
Figure 4.6 Definition of the “effective PGA” (PGA_C) according to Grant <i>et al.</i> (2007).	68
Figure 4.7 Linear log-log hazard curves with gradient $-k_2$ and $-k_1$ (Grant <i>et al.</i> , 2007).	70
Figure 4.8 Proposed approach for priority ranking in large-worldwide spread portfolios of structures.	76
Figure 4.9 Normalised number of occupants raised to α versus normalised number of occupants relationship.	79
Figure 4.10 C10 – comma 10 – v.1.1 beta graphical user interface.	84
Figure 4.11 Composition of Italian building stock in terms of year of construction, according to 2001 census data (ISTAT 2001)	85
Figure 4.12 Reference seismic demand evolution for L’Aquila site (Lat: 42.36, Lon: 13.41).	90
Figure 4.13 Italian seismicity map after year 1909 (left), 1915 (right).	91
Figure 4.14 Italian seismicity map after year 1927 (left), 1937 (right).	91
Figure 4.15 Italian seismicity map after year 1962 (left) 1980 (right).	92
Figure 4.16 Italian seismicity map after year 1981 (left) 1984 (right).	92
Figure 4.17 1996 SSN (left) and 1998 GNDT-SSN (right) proposals for Italian hazard map.	94
Figure 4.18 Italian seismicity map after year 2003(left) and 2008 (right).	95
Figure 4.19 Gradient of hazard curve for PGA, obtained from linear regression of logarithms of median INGV data, considering 100, 475, 1000 and 2500 year return periods.	98
Figure 4.20 Subsoil category according to EC8 and NIBC seismic codes (Santo <i>et al.</i> , 2013).	99
Figure 4.21 NODE – Nominal Deficit - v.1.1 beta graphical user interface.	103
Figure 4.22 Performed procedure for risk management of case-study building portfolio.	104
Figure 4.23 Ranking of case-study structures based on $NODE_{PGA,rock}$ (grey bars) and PGA with 475 years return period on rock (black dotted line).	106

Figure 4.24 Ranking of case-study structures based on normalised $SRI_{PGA,rock}$ (blue bars), normalised $NODE_{PGA,rock}$ (grey bars), and normalised PGA with 475 years return period on rock (black dotted line). Red dotted line refers to the SRI level used for the selection of the 5 less risk-prone plants 108

Figure 4.25 Ranking of case-study structures based on normalised $SRI_{PGA,soil}$ (green bars), normalised $NODE_{PGA,soil}$ (grey bars), and normalised PGA with 475 years return period on effective soil (black dotted line). Red dotted line refers to the SRI level used for the selection of the 5 less risk-prone plants..... 110

Figure 4.26 Ranking of case-study structures based on normalised $SRI_{Sa(T),soil}$ (red bars for the structures selected after Step 1; green bars for the structures excluded from Step1), normalised $NODE_{Sa(T),soil}$ (grey bars) and normalised spectral acceleration with 475 years return period on effective soil (black dotted line). Red dotted line refers to the SRI level used for the selection of the 5 most risk-prone plants. 113

Figure 4.27 $NODE_{Sa(T),soil}$ indices computed considering wind design (red bars) and neglecting it (grey bars) for the case-study structures. 116

Figure 4.28 Ranking of case-study structures based on normalised $SRI_{Sa(T),soil}$ (light-red bars) and normalised $NODE_{Sa(T),soil}$ (grey bars) accounting for wind design in the definition of the nominal capacity. Red dotted line refers to the SRI level used for the selection of the 5 most risk-prone plants. 117

Figure 4.29 Ranking of case-study structures based on normalised $NODE_{Sa(T),soil}$ index (grey bars) updated after Emilia 2012. The ranking obtained before the updating is reported in dashed lines..... 119

Figure 4.30 Ranking of case-study structures based on normalised $NODE_{PGA,soil}$ index (red bars); $PGA_{deficit}$ by Grant *et al.* (2007) (blue bars) and PGA_{ratio} by Crowley *et al.* (2008) (green bars). 122

Figure 4.31 Ranking of case-study structures based on normalised $NODE_{PGA,soil}$ index (red bars) and SA_{ratio} by Crowley *et al.* (2008) (blue bars)..... 123

Figure 5.1 Second level procedure for seismic risk assessment 131

Figure 5.2 examples of: (a) Vulnerability curve; (b) Fragility curve 132

Figure 5.3 (a) Singhal and Kiremidjian (1997) curves for low-rise RC moment resisting frames (points updated with observational data are shown as the larger symbols in the shaded area) using the Park and Ang damage index; Right panel: (b) Mosalam *et al.* (1997) curves for low-rise RC MRF using inter-storey drift values to define damage (adapted from Rossetto and Elnashai, 2003). 133

Figure 5.4 Empirical fragility curves or different IMs (Rossetto and Elnashai, 2003) 134

Figure 5.5 Flowchart describing the main steps for the determination of analytical vulnerability functions and DPMs (adapted from Dumova-Jovanoska (2004))..... 135

Figure 5.6 Fragility curves for Mid-Rise frames (Singhal and Kiremidjian, 1996)..... 137

Figure 5.7 Vulnerability classes according to EMS-98 scale (Grüntal *et al.*, 1998)..... 139

Figure 5.8 Definition of quantities according to EMS-98 scale (Grüntal *et al.*, 1998) 140

Figure 5.9 Damage grades for reinforced concrete buildings according to EMS-98 scale (Grüntal *et al.*, 1998) 140

Figure 5.10 Example of Limit States and Damage States. 142

Figure 5.11 The <i>FRAME - Fragility-based rapid seismic Risk AssessMEnt - v.1.0 beta</i> software suite.....	144
Figure 5.12 “Conditional P_f ” analysis and “Absolute P_f ” analysis performed in <i>FRAME v.1.0</i>	146
Figure 5.13 <i>FRAME – Fragility-based rapid seismic Risk AssessMEnt – v1.0 beta</i> main GUI.....	147
Figure 5.14 <i>FRAME v.1.0 beta</i> loss assessment module.....	150
Figure 5.15 INGV hazard curves and UHS computation in <i>FRAME v.1.0 beta</i>	151
Figure 5.16 Input of a user defined hazard curve in <i>FRAME v.1.0 beta</i>	152
Figure 5.17 Adopted Taxonomy.....	154
Figure 5.18 <i>FRAME Manager tool</i> GUI (top) and windows allowing the input of empirical fragility curves (bottom-left) and taxonomy (bottom-right).....	155
Figure 5.19 <i>FRAME Comparison&Conversion tool</i> GUI.....	156
Figure 5.20 <i>FRAME Comparison&Conversion tool</i> GUI showing the comparison of an ensemble of fragility curves selected from the inventory.....	157
Figure 5.21 <i>FRAME Comparison&Conversion tool</i> : different options for computing statistics.....	158
Figure 5.22 <i>FRAME Comparison&Conversion tool</i> GUI showing the manipulation/homogeneization of limit states.....	160
Figure 5.23 <i>FRAME fragility filter</i> tool.....	161
Figure 6.1 Aerial (left) and close-up (right) view of the whole facility.....	165
Figure 6.2 Schematic drawing illustrating different portions of the case-study building.....	166
Figure 6.3 Full structural cross section in the x-direction.....	166
Figure 6.4 Single-bay structural cross-sections of trusses in direction X.....	167
Figure 6.5 Single-bay structural cross-sections of main frame trusses in direction Y.....	167
Figure 6.6 Single-bay structural cross-sections of trusses of the perimeter frame in direction Y.....	168
Figure 6.7 Close-up view showing roof gusset plate connections.....	168
Figure 6.8 Columns and base connections: (a) type A column, (b) type B column.....	169
Figure 6.9 (a) details at the top of type B columns; (b) columns and base connections of type C columns.....	170
Figure 6.10 Cyclic (left) and in-cycle strength degradation (right) (ATC, 2005).....	174
Figure 6.11 Cyclic moment-rotation response of type B column base connection.....	175
Figure 6.12 Allowed (a and b) and not allowed (c) connection geometries for the application of T-stub model.....	176
Figure 6.13 Component method according to EC3 (CEN, 2005).....	177
Figure 6.14 Tensile and compressive strengths in <i>type B</i> column base connection: (a) bending about x-x axis; (b) bending about y-y axis.....	178
Figure 6.15 Limit equilibrium conditions: (a) “large” eccentricity and tension failure; (b) “large” eccentricity and compression failure; (c) “small” eccentricity and compression failure.....	179
Figure 6.16 Moment-rotation relationships for different values of eccentricity.....	180

Figure 6.17 Tangent stiffness computed at $M^* = N_{G,s} \cdot e^*$ 181

Figure 6.18 Moment-rotation relationships for type C base plate at increasing values of eccentricity, in the case of bending about the x - x axis. 181

Figure 6.19 Considered T-stub in tension..... 182

Figure 6.20 Moment-rotation relationships for type C base plate at increasing values of eccentricity, in the case of bending about the y - y axis. 183

Figure 6.21 (a) tensile and compressive strengths in *type B* column base connection; (b) T-stub in tension; (c) characterization of tensile strength of the base plate through FEM modelling of the base plate portion marked by dashed box in panel *b*..... 184

Figure 6.22 Moment-rotation relationships for type A base plate at increasing values of eccentricity, in the case of bending about the y - y axis. 184

Figure 6.23 Decomposition of connection response into separate contributions. 185

Figure 6.24 Individual contributions to connection response. 186

Figure 6.25 Determination of k_{Δ} according to panel *b* of Figure (6.24). 187

Figure 6.26 Moment-rotation relationships for *type B* base plate. 189

Figure 6.27 Structural models for 1991 and 1971/79 portions of the case study buildings. 191

Figure 6.28 Aerial views of a 3-dimensional finite element model (1991 portion). 192

Figure 6.29 Bi-dimensional model of one central frame extracted from the 1991 structure in Y - (a) and X -direction (b). 192

Figure 6.30 Three-dimensional structural model of the 1991 building portion (*a*) and deformed shape according to the first mode (*b*)..... 194

Figure 6.31 Ensemble of pushover curves accounting for different positions of the control node. 196

Figure 6.32 FEMA 440 (ATC,2005) procedure for equivalent linearization of pushover curve and simplified verification of sensitivity to dynamic instability due to strength degradation. . 196

Figure 6.33 Implemented procedure for equivalent linearization. 198

Figure 6.34 Normalised pushover curves for the considered structural models. 198

Figure 6.35 Typical output of non-linear dynamic analyses: (a)MSA analysis; (b) IDA analysis; (c) SSA analysis; (d) Cloud analysis. (Jalayer, 2003)..... 202

Figure 6.36 Result of MSA analysis and computation of $P[failure/x,NC]$ 205

Figure 6.37 Peak transient (δ_p) - residual drift (δ_r) values at $S_d(T_1)=0.2 g$ for the *fully restrained* 1991-3D- Y model. δ_G is the drift due to gravitational loads; δ_l is the drift corresponding to the yielding of the first plastic hinge of the model. 207

Figure 6.38 Peak transient-residual drifts at given IM levels for the *fully continuous* 1991-3D model, analysed in direction Y . Each point refers to the output of a RHA for which no dynamic instability occurs..... 208

Figure 6.39 Joint lognormal probability density function of the EDPs, given the IM level, for non-collapse cases. 210

Figure 6.40 Truncated joint lognormal probability density function of the EDPs, given the IM level, for non-collapse cases. 210

Figure 6.41 Seismic sources affecting the hazard at the site (courtesy of E. Chioccarelli). 213

Figure 6.42 Exceedance probabilities for soft soil in 1 year, for the spectral acceleration at 1 s and 1.6 s.....213

Figure 6.43 Seismic hazard deaggregation of Sa(T)=1.0 s (a) and 1.6 s (b) at the building site for 50 yrs return period.215

Figure 6.44 Seismic hazard deaggregation of Sa(T)=1.0 s (a) and 1.6 s (b) at the building site for 475 yrs return period.216

Figure 6.45 Seismic hazard deaggregation of Sa(T)=1.0 s (a) and 1.6 s (b) at the building site for 975 yrs return period.216

Figure 6.46 Seismic hazard deaggregation of Sa(T)=1.0 s (a) and 1.6 s (b) at the building site for 2475 yrs return period.216

Figure 6.47 5% damped pseudo-acceleration response spectra of selected accelerograms for TR=50 years.217

Figure 6.48 5% damped pseudo-acceleration response spectra of selected accelerograms for TR=475 years.217

Figure 6.49 5% damped pseudo-acceleration response spectra of selected accelerograms for TR=975 years.217

Figure 6.50 5% damped pseudo-acceleration response spectra of selected accelerograms for TR=2475 years.218

Figure 6.51 Peak transient and residual drift ratios for 1971/79-2D-X model.....219

Figure 6.52 Peak transient and residual drift ratios for 1971/79-2D-Y model.....219

Figure 6.53 Peak transient and residual drift ratios for the 1991-2D-X model.....220

Figure 6.54 Peak transient and residual drift ratios for the 1991-2D-Y model.....220

Figure 6.55 Peak transient and residual drift ratios for the *fully continuous* 1991-3D-Y model.221

Figure 6.56 Peak transient and residual drift ratios for the *partially continuous* 1991-3D-Y model.221

Figure 6.57 Peak transient and residual drifts ratio for the 1991-3D-Y models and the corresponding 1991-2D-Y frame.222

Figure 6.58 Collapse mechanisms: (a) 1991-2D-Y frame; (b) 1991-2D-X frame; (c) 1991-3D-Y model.223

Figure 6.59 Counted median comparison for the analysed structural models.224

Figure 6.60 Results of MSA for *fully continuous* 1991-3D-Y model.....224

Figure 6.61 Results of MSA for *partially continuous* 3D-1991-Y model.225

Figure 6.62 Results of MSA for 2D-1971/79-2D-X model.225

Figure 6.63 Results of MSA for 2D-1971/79-2D-Y model.225

Figure 6.64 Results of MSA for 2D-1991-2D-X model.226

Figure 6.65 Results of MSA for 2D-1991-2D-Y model.226

Figure 6.66 Results of MSA in terms of member axial force for two elements of the 1991-2D-Y model.227

Figure 6.67 Fragility curves for 3D models.....228

Figure 6.68 Fragility curves for 1971/79 2D-models in X and Y direction.....229

Figure 6.69 Fragility curves for 1991 2D-models in X and Y direction.....230

Figure 6.70 Comparison of fragility curves of *fully continuous* 1991-3D-Y model, obtained under different assumptions regarding the bivariate distribution of the demands.231

Figure 6.71 Comparison of fragility curves of *partially continuous* 1991-3D-Y model, obtained under different assumptions regarding the bivariate distribution of the demands.231

Figure 6.72 Comparison of fragility curves of 1971/79-2D-X model, obtained under different assumptions regarding the bivariate distribution of the demands.231

Figure 6.73 Comparison of fragility curves of 1971/79-2D-Y model, obtained under different assumptions regarding the bivariate distribution of the demands.232

Figure 6.74 Comparison of fragility curves of 1991-2D-X model, obtained under different assumptions regarding the bivariate distribution of the demands.232

Figure 6.75 Comparison of fragility curves of 1991-2D-Y model, obtained under different assumptions regarding the bivariate distribution of the demands.232

Figure 6.76 Comparison of fragility curves obtained from univariate and bivariate distribution of demands for the *fully continuous* 1991-3D-Y model.....233

Figure 6.77 Comparison of fragility curves obtained from univariate and bivariate distribution of demands for the *partially continuous* 1991-3D-Y model.233

Figure 6.78 Comparison of fragility curves obtained from univariate and bivariate distribution of demands for the 1971/79-2D-X model.234

Figure 6.79 Comparison of fragility curves obtained from univariate and bivariate distribution of demands for the 1971/79-2D-Y model.234

Figure 6.80 Comparison of fragility curves obtained from univariate and bivariate distribution of demands for the 1991-2D-X model.234

Figure 6.81 Comparison of fragility curves obtained from univariate and bivariate distribution of demands for the 1991-2D-Y model.235

Figure 6.82 Fragility curves for two members belonging to 1991-2D-Y (a) and 1991-2D-X (b) models.....236

Figure 7.1 Scheme of the three scale-dependent procedures dealt in the thesis considered in a unified approach to seismic risk assessment and management250

LIST OF ABBREVIATIONS

ATC	Applied Technology Council
BI	Business Interruption
CCDF	Complementary Cumulative Density Function
CDF	Cumulative Density Function
CNR	Consiglio Nazionale delle Ricerche
CP	Collapse Prevention
CR	Capacity Ratio
CSM	Capacity Spectrum Method
DAP	Detailed Assessment Procedure
DBELA	Displacement-Based Earthquake Loss Assessment
DISS	Database of Individual Seismogenic Sources
DM	Damage Measure
DPC	Dipartimento Protezione Civile
DSA	Double Stripe Analysis
DSHA	Deterministic Seismic Hazard Analysis
DV	Decision Variable
EC3	Euro Code 3
EC8	Euro Code 8
EDP	Engineering Demand Parameter
EI	Exposure Index
ELR	Economic Loss Ratio
EMS	European Macroseismic Scale
FaMIVE	Failure Mechanism Identification and Vulnerability Evaluation
FEMA	Federal Emergency Management Agency
FRAME	Fragility-based rapid seismic Risk AssessMEnt
gBI	Group Business Interruption
GDP	Gross Domestic Product
GIS	Geographical Information System
GM	Ground Motion
GMPE	Ground Motion Prediction Equation
GNDT	Gruppo Nazionale Difesa Terremoti
HAZUS	HAZard in United States
IBC	International Building Code
ICC	International Code Council
IDA	Incremental Dynamic Analysis

IEG	Independent Evaluation Group
IEP	Initial Evaluation Procedure
IM	Intensity Measure
ING	Istituto Nazionale di Geofisica
INGV	Istituto Nazionale di Geofisica e Vulcanologia
IO	Immediate Occupancy
ISTAT	Istituto Nazionale di Statistica
ITACA	Italian ACcelerometric Archive
LS	Life Safety
MAF	Mean Annual Frequency
MCS	Mercalli Cancani Sieberg
MDOF	Multi-Degree-Of-Freedom
MFL	Maximum Foreseeable Loss
MMI	Modified Mercalli Intensity
MRF	Moment Resisting Frame
MSA	Multi Stripe Analysis
MSK	Medvedev Sponheuer Karnik
NIBC	New Italian Building Code
NODE	Nominal Deficit
NPC	Non- structural Performance Categories
NZSEE	New Zealand Society for Earthquake Engineering
OLR	Occupancy Loss Ratio
OP	Occupancy Potential
PA	Pushover Analysis
PAR	Performance Achievement Ratio
PBA	Performance Based Assessment
PBEE	Performance Based Earthquake Engineering
pBI	Plant Business Interruption
PD	Property Damage
PDF	Probability Density Function
PEER	Pacific Earthquake Engineering Research
PFG	Progetto Finalizzato geodinamica
PGA	Peak Ground Acceleration
PGV	Peak Ground Velocity
PRC	Precast Reinforced Concrete
PSDA	Probabilistic Seismic Demand Analysis
PSHA	Probabilistic Seismic Hazard Analysis
RC	Reinforced Concrete
RC	Reinforced Concrete

RHA	Response History Analysis
SAG	Seismic Attributes Grades
SDOF	Single-Degree-Of-Freedom
SP-BELA	Simplified Pushover-Based Earthquake Loss Assessment
SPC	Structural Performance Categories
SPS	Structural Performance Score
SRI	Seismic Risk Index
SSA	Single Stripe Analysis
SSSM	Seismic Safety Screening Method
TA	Territorial Administration
UBI	Unit Business Interruption
URM	Un-Reinforced Masonry
USD	United State Dollars

Chapter 1 – BACKGROUND AND MOTIVATION

1.1. Framework

In recent years the number of disasters following natural events worldwide has been rapidly raising. The World Bank (IEG, 2007) has reported that, from 1975 to 2005, the amount of disasters has increased by about 400% and recent studies have observed a death toll of about 699,000 deaths since the beginning of the decade due to large earthquakes (Holtzer and Savage, 2013). Looking at the losses due to earthquakes in the last Century (Fig. 1.1), casualties, direct and indirect losses, show a continuously increasing trend. This is due to the urbanization, which tends to concentrate people and goods exposing them to natural hazards more than in the past. Moreover, in the 21st century, an increasing in the death toll due to large catastrophic seismic events (>100,000 deaths) is expected, that could be estimated in 2.57 ± 0.64 million (Holtzer and Savage, 2013)

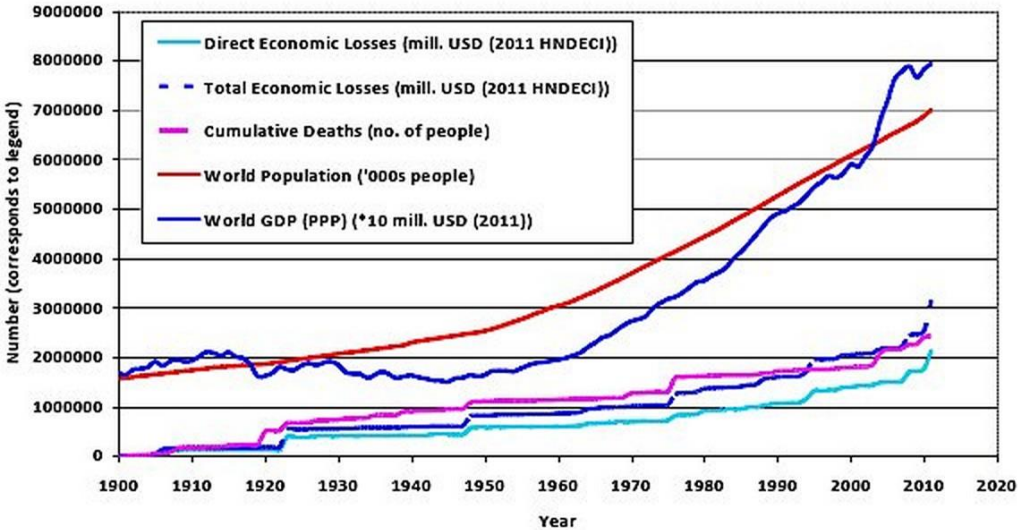


Figure 1.1 Worldwide socio economic trends to earthquakes (1900-2011). Cumulative deaths and economic losses related to global 2011 dollar GDP and population (Daniell and Vervaeck, 2011).

As regards specifically the industrial field, recent earthquakes in industrialized

countries (e.g., Tohoku, 2011, Emilia 2012) have shown the importance of performing seismic loss assessment in the manufacturing industry, because of the significant consequences caused by earthquakes in terms of property damage, business interruption and casualties. For example, The Great Tohoku Earthquake of 2011 and the subsequent tsunami caused approximately 19,295 deaths, a direct economic loss between 295 and 374 billion USD and an estimated total economic loss between 479 and 710 billion USD, corresponding to 10–15% of GDP (Daniell and Vervaeck, 2012). Moreover, serious losses were caused to the automotive and hi-tech worldwide industry, leading to production downtimes all over the World (MunichRe, 2012).

The previous issues have lead, in the last years, to a significant growing interest of the industry, insurance and research in the assessment of the seismic risk in the manufacturing industry. In fact, industry has a primary interest in efficient risk management procedures, insurance can use earthquake loss assessment to compute the premiums on rational basis, and research can provide the scientific instruments in order to quantify and manage/mitigate seismic risk.

In this context, the *AXA Matrix Risk Consultants* entered into a three-year agreement with the *Department of Structures for Engineering and Architecture of the University of Naples Federico II*, Italy, aimed at developing procedures for the seismic risk assessment and management of manufacturing industrial structural portfolios.

This implies addressing the problem of seismic risk assessment and management at different scales, which may vary from the one of a large size portfolio, composed of thousands of structures, to that of the single building.

As it can be observed in Figure (1.2), the first scale is typically the one at which the insurer operates, having to assess the seismic risk, in the most general case, for a portfolio of industrial groups. Each industrial group (e.g., a Corporate) can be structured, depending on its dimensions, in one or more plants (e.g., subsidiaries, local plants), worldwide spread and related each other by the supply chain. Each plant, in its turn, can be composed of a large variety and amount of structures, extremely different one another.

It is worth noting that in Figure (1.2), a schematic representation of the structure of large industrial groups is presented, with the aim of emphasizing the hierarchical organization and the differences in the scale of the object of the analysis in terms of number of structures to deal with (suppliers are, on purpose, neglected).

The above considerations suggest that a detailed assessment of seismic risk for each structure of the portfolio under investigation could not represent a suitable approach to seismic risk in the case of large industrial groups, insurance companies and risk consultants. In fact, such an approach would require an amount of resources, both financial and of time that is in general unavailable.

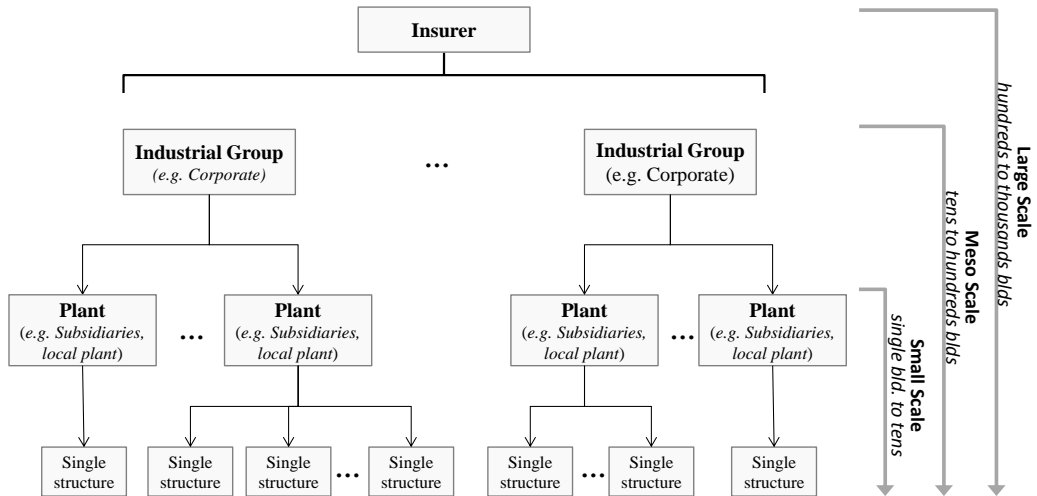


Figure 1.2 Schematic representation of the different scales (in terms of number of buildings) of seismic risk assessment and management in industry.

Therefore, it seems more suitable to approach the problem in a scale-dependent way, distinguishing: :

- a “*large scale*”: it is the scale of main interest for insurers, reinsurers and risk consultants, assessing the risk for a portfolio of industrial groups. The number of buildings expected at this scale is typically of hundreds to thousands. The knowledge about the structures composing the portfolio can be only limited and the interest of the stakeholder is primarily in the assessment and management of the risk from a “global” point of view, for example by ranking the risk across the whole structural portfolio.
- a “*meso scale*”: it is the scale of interest for large industrial groups, as well as for insurers. The number of buildings expected at this scale is of tens to hundreds, that is to say those composing a plant or a (limited) group of plants. A more detailed knowledge about the structures can be achieved, and this might allow a gross quantification of the losses from the plant in the case of an earthquake. In fact, it seems reasonable to assume that, at this scale, at least a visual survey of the structural portfolio could be feasible.
- a “*site-specific scale*”: it is the scale of primary interest for small industrial groups or single plants. The number of buildings expected at this scale ranges from the single building to tens. Primary interest is to quantify the expected loss due to earthquakes and eventually to reduce it by means of risk reduction strategies. In fact, at this scale, the knowledge about the structure could be sufficient to perform an analytical assessment of seismic risk.

Therefore, the need for different procedures that may operate at the different scales arises. Finally, it is worth to underline that the scales to which this study is referred to are expressed in terms of number of buildings to deal with; the problem of spatial distribution of plants or buildings is not addressed in this thesis.

1.2. Objectives of the study

The primary objective of this thesis is to face the problem of seismic risk assessment and management of industrial building portfolios at the different scales presented in the previous section, with reference to a real case-study portfolio of industrial buildings. The procedures that can be followed for risk assessment and management are strictly related to the number of buildings to deal with, that influences the input data that is possible to gather (i.e. the knowledge), the methodology that is possible to implement and the output (i.e. the objective) of the assessment.

As it can be observed in the Figure (1.3), at the three different scales of the problem the following procedures have been implemented in this thesis:

At “*large scale*”, a ***Risk management procedure based on Nominal deficit*** (also referred to as “***large scale procedure***” in the following) is proposed with the purpose of analysing a portfolio of structures and ranking their seismic risk in a coherent manner, in order to define a priority scale for further, more detailed investigations. This approach is based on the evaluation of a conventional (or “nominal”) seismic risk index, on the basis of data extremely poor and easy to retrieve, for the production of which it is not required any visual inspection of the structures (“desk study” or “off-line” assessment), or only a rapid visual screening. On the base of these assumptions, the output of such a procedure is a relative measure of the seismic risk.

In order to implement such a procedure for the Italian context, the *NODE – NOminal DEficit - v.1.1 beta software* was developed.

At the “*meso scale*”, a ***Fragility-based rapid seismic risk assessment procedure*** (also referred to as “***meso scale procedure***” in the following) is proposed. It consists in the explicit calculation of earthquake expected losses and it has been implemented worldwide by means of a software suite realized for the purpose (*FRAME – Fragility-based rapid seismic Risk AssessMENT, v.1.0 – beta*). This approach is thought to be applied at the scale of the single building, as well as to that of the single industrial plant or groups of industrial plants (tens or hundreds of buildings). In fact, at this scale, it is possible to achieve a level of knowledge of the building, such that a fragility function can be associated to the building, selecting it from those available in literature or computing it *ad-hoc*. This one can be used in conjunction with hazard and exposure to

assess the expected losses even if with significant approximation.

At the “*site-specific scale*”, the methodologies for computing losses due to earthquakes by means of mechanical modelling are rather well consolidated. Nevertheless a lack in fragility curves for specific industrial buildings is still present in literature; therefore, an ***analytical evaluation of the seismic risk*** (also referred to as “*site-specific scale procedure*” in the following), can be performed in order to develop fragility curves and to compute failure probabilities in a Performance Based Engineering (PBEE) approach. These can be employed for a rational evaluation of the losses due to earthquakes or insurance premiums.

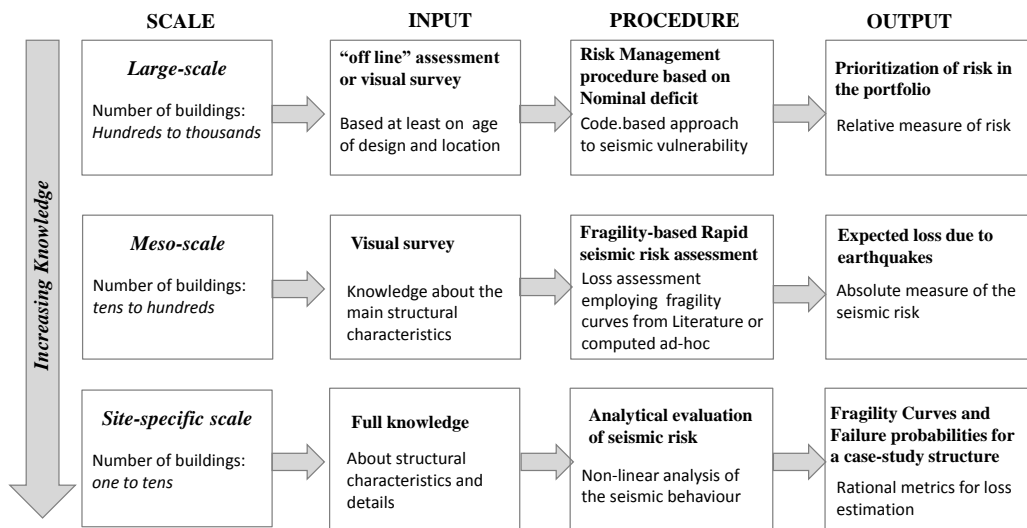


Figure 1.3 Scheme of the three scale-dependent procedures for seismic risk assessment and management dealt in the thesis.

The “*large-scale*” procedure for risk management has been applied to a real case study portfolio of Italian plants, belonging to one of the most important Corporate groups clients of *AXA Matrix*. The “*site-specific scale*” analytical evaluation of seismic risk has been applied to one industrial building belonging to the abovementioned case-study portfolio.

It should be noted that the three procedures outlined above are to be intended as alternative, i.e. the stakeholders can implement one of them according to the size of the portfolio under investigation.

Nevertheless, considering a large dimension structural portfolio, the three procedures could be linked together, as represented in Figure (1.4), in order to create a risk

management framework, operating as described hereinafter.

In a first step, on the basis of poor information, a large-scale procedure (i.e. a prioritization analysis of the portfolio) could be implemented, in order to select a number of buildings mostly exposed to risk. This portion of the portfolio, selected as a function of the available resources, could be inspected more in details and analysed by means of a second level procedure, given that a fragility curve is available for all the structures under investigations. Otherwise, an analytical evaluation of the fragility could be performed. In this way, the computed fragility curve could be added to the inventory of curves in the availability of the stakeholder.

Finally, it is worth to underline that, although it is known that a large part of losses in case of earthquakes are due to non-structural components and contents, in this thesis this issue is not directly addressed but only structural seismic risk is faced. In fact, the problem of the structural seismic risk assessment at different scales has been believed a priority.

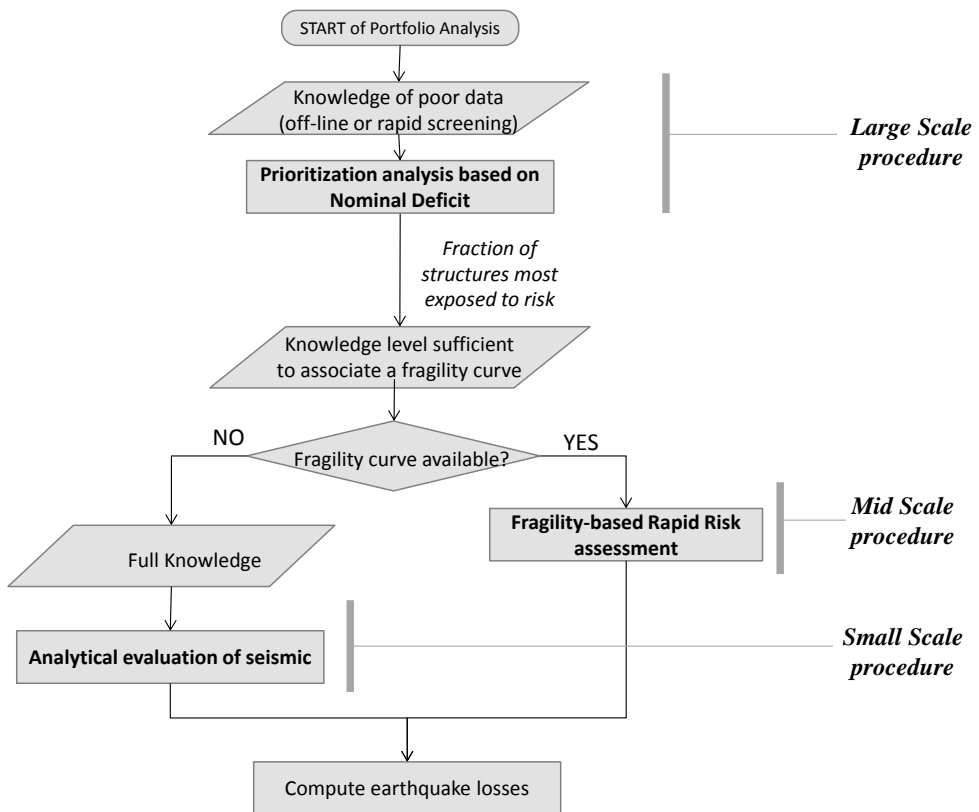


Figure 1.4 Framework for seismic risk assessment and management of large industrial portfolios.

1.3. Outline of the thesis

In **Chapter 2**, some general concepts regarding seismic risk assessment and its individual components are given first. In particular, available approaches to hazard, vulnerability, loss estimation, and risk mitigation strategies are briefly reviewed.

In **Chapter 3**, the case-study portfolio is presented. It consists of Italian plants, investigated by means of visual survey forms realized *ad-hoc*. Such forms provided the information necessary to apply the “large scale” prioritization analysis, specific object of **Chapter 4**. In this Chapter a review of risk management frameworks is performed first with particular emphasis on those ones employing “nominal deficit” for measuring risk. Subsequently, the proposed “large scale” procedure, based on “nominal” risk indices, is presented and compared with other similar approaches available in literature. The *NODE – NOminal DEficit - v.1.0 beta* software is then presented and employed for the analysis of the case study. The results of the comparison are critically discussed.

In **Chapter 5** the “mid-scale” procedure is discussed and, after a review of the fragility curves available in literature and a discussion about their main differences in terms of intensity measure and limit states, the *FRAME – Fragility-based rapid seismic Risk AssessMEnt – v1.0 beta* software suite is presented.

In **Chapter 6**, the analysis of the seismic performance of an existing steel structure, selected from the case-study portfolio, is performed. Some general modelling issues, that can characterize the seismic behaviour of existing steel structures, are highlighted and critically discussed. Fragility curves and failure probabilities are also computed.

In **Chapter 7**, the general outcomes deriving from the developing and the application of the proposed procedures are, finally, discussed.

Chapter 2 – BASICS OF SEISMIC RISK

2.1. Definition

Seismic risk can be defined as the probability that a pre-defined level of losses due to earthquakes is exceeded within a given reference period, in a specific territorial area of interest. By its definition, seismic risk is "cumulative" because it accounts for the overall losses, including fatalities, injuries and social-economic losses, generated by different earthquakes, evaluated in a given time period. Seismic risk is also "dynamic", since the variables which influence it continuously change over time, as well as in space. Seismic risk can be estimated at different territorial scales, from the global or regional one to that of a specific site, therefore the loss can be referred to an individual structure, to a business, to a community or to the entire infrastructure of a nation. It can also be expressed either in monetary terms (e.g. the repairing cost, loss of revenue, etc.), casualties (e.g. injuries and deaths) or loss of functionality (e.g. downtime) and its evaluation involves different scientific fields: seismology, geophysics, geology, geotechnical engineering, structural engineering, regional and urban planning, insurance engineering and estimio.

Seismic risk is a function of three main components: the seismic hazard; the seismic vulnerability and the exposure.

The *seismic hazard* represents any physical effect, both direct (such as the shaking of the ground) and induced (e.g. unstable slopes or the liquefaction of saturated loose soil) due to a seismic event, capable to cause adverse effects on human activities.

The *seismic vulnerability* is, on the contrary, the component of risk not attributable to the site but to the physical environment, both artificial and natural. In the simplest terms, it is the susceptibility of the physical environment to be damaged by seismic events with a given intensity.

The *exposure* term takes into account the location, consistency, quality and quantity of assets and activities that may be affected directly and indirectly by the seismicity of the site. Therefore, it represents an economic, in the broadest sense, quantification of the potential losses. Seismic hazard and vulnerability are linked together by a cause-effect relationship and their joint evaluation allows to obtain a probabilistic description of the damage due to seismic events (frequency of exceedance of a given damage level, in most cases). Exposure represents the translation of this probability into seismic risk (frequency of exceedance of loss). The ultimate goal of risk assessment is to provide elements for a rational decision-making and to implement risk management strategies.

2.2. Seismic Risk assessment

The Pacific Earthquake Engineering Research (PEER) framework (Cornell and Krawinkler, 2000; Krawinkler and Miranda, 2004; Moehle and Deierlein, 2004) represents the best current practice for seismic loss assessment of individual structures and a reference for modern large-scale loss assessment procedures.

It was developed with the primary objective to improve decision making procedures with regards to the seismic performance of facilities, therefore, it expresses the seismic risk as the exceeding rate of a Decision Variable (DV) that can represent a cost, the length of downtime, the number of casualties or any other variable useful to guide the stakeholder in the decision making. A key and preliminary issue in the seismic loss assessment process is, therefore, the identification and quantification of the decision variables of primary interest to the decision makers.

The PEER procedure is illustrated in Figure (2.1). It is composed of the following four stages: *hazard analysis*, consisting in the quantification of the frequency and intensity of earthquakes and of the ground motions that represent the effects of earthquakes at a particular site (see Section 2.3.1); *structural analysis*, aimed at the quantification of the structural response parameters; *damage analysis*, that is the quantification of damage states and their relation to response parameters (the last two are briefly dealt in Section 2.3.2), and *loss analysis*, involving evaluation of monetary loss, downtime and casualties, and their consequences for the owner and society (see Sect. 2.3.3) .

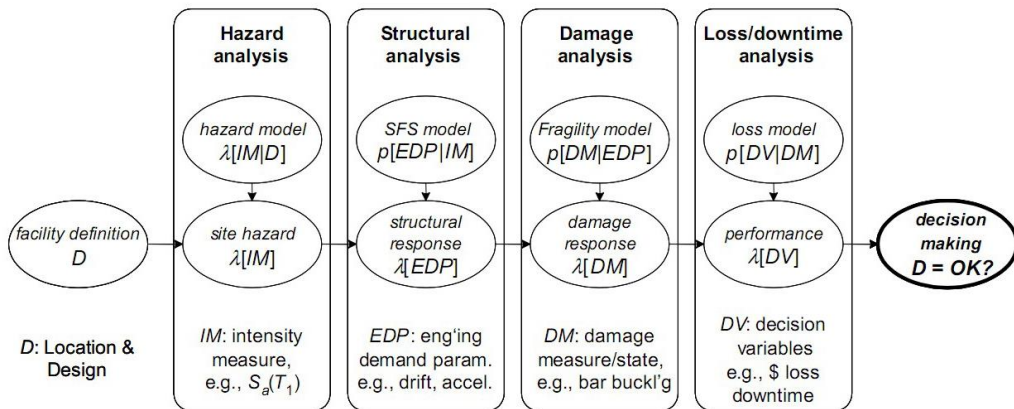


Figure 2.1 Overview of PEER seismic loss assessment methodology (adapted from Krawinkler, 2005)

In the *hazard analysis phase*, the frequency of exceedance of an Intensity Measure (IM) of the ground motion at the site is calculated. The IM is a parameter directly correlated to the ground shaking at the site of interest, that could be a scalar (e.g. the elastic spectral acceleration at the fundamental period of the structure, $S_a(T_1)$), as well

as a vector (e.g. a combination of the peak ground acceleration, PGA, and $S_a(T_I)$). The latter choices have shown some advantages in describing the ground motion (Baker and Cornell, 2005), especially in the case of near fault ground motions (Alavi and Krawinkler, 2004). As discussed in Section (2.3.1), the hazard analysis can be performed both deterministically and probabilistically. In the latter case, the output of the analysis is the mean annual frequency of exceedance of IM, namely $\lambda(IM)$, also known as *hazard curve*.

In the *structural analysis phase*, an analytical modelling of the building is performed to the aim of obtaining a vector of Engineering Demand Parameters (EDPs). An EDP is a structural response parameter that correlates well with damage in structural and non-structural components and contents of the structure. Examples of suitable EDPs are the interstorey drift or force demands to structural members, or any other structural parameter which allows controlling the evolutionary state of the structure up to collapse. Other examples are given in (Porter, 2002) or in ATC 58-2 document (ATC, 2004). The relationship between EDPs and IMs is typically obtained through inelastic dynamic analyses, but also other simplified methods among those presented in Section (2.3.2) can be employed. The output of this process, which is often referred to as Probabilistic Seismic Demand Analysis (PSDA), is $P[EDP \geq edp | IM = im]$, which is the conditional probability that the EDP exceeds a specified value edp , given that the IM is equal to a particular im . The integration of the previous probability over the hazard curve provides the mean annual frequency of exceedance of the EDP, $\lambda(EDP)$, reported in Figure (2.1). Details about PSDA are given in Chapter 6 or in (Jalayer, 2003).

In the *damage analysis phase*, the chosen EDPs are related to the damage measures in building components. These ones can be classified into structural components, non-structural components and contents. For each component of interest, a Damage Measure (DM) is defined, describing the level of damage experienced during an earthquake. The output of the damage analysis stage is a relationship between the EDPs and the DMs expressing the probability of being in a damage state dm , given that the EDP is equal to a given value edp , that is $P[DM = dm | EDP = edp]$. For example, referring to a building, the latter is the probability of observing various levels of damage to individual beams, columns, non-structural partitions, or building contents, as functions of various internal member forces, story drifts, etc. Such relationships, referred to as *fragility*, are computed, in general, by means of analytical modelling, laboratory test or field experience (Eberhard *et al.*, 2001).

In the last phase of the PEER procedure, that is *loss analysis*, the losses (i.e. DVs) due to the chosen DMs are evaluated. While DMs are defined at the component level, the DVs are defined at the system or building level. If the fragility functions for all

relevant damage states of all relevant components are known, the DVs of interest can be evaluated either directly or by means of cost functions that relate the damage states to repair/replacement costs (Aslani and Miranda, 2005; Mitrani-Reiser, 2007).

The steps previously described can be summarized in the following equation:

$$\lambda(dv) = \int \int \int G(dv | dm) |dG(dm | edp)| |dG(edp | im)| |d\lambda(im)| \quad (2.1)$$

expressing the mean annual frequency (MAF, λ) of exceeding of a DV. In Eq. (2.1), the function $G(x/y)=G(X \geq x/Y=y)$ is the complementary cumulative distribution function (CCDF) of X given Y ; $dG(x/y)$ and $d\lambda(z)$ are the differentials of $G(x/y)$ and $\lambda(z)$.

In Eq. (2.1), the damage measure is assumed to be a continuous random variable. However, it is common to deal with building or system components that are associated with discrete repair or replacement actions. Therefore, it was proposed (Miranda and Aslani, 2003; Krawinkler and Miranda, 2004) to compute earthquake losses considering discrete damage states triggering repairing or replacing actions for the components under consideration. In this case, the relationship between the EDP and DM is obtained, in practice, subtracting the probability of exceeding two subsequent damage states, given the value of EDP.

Such an approach presents the advantage of separating the computation of seismic risk into discipline-specific contribution (seismology, structural engineering, cost analysis, decision making). The key assumption is conditional independence of DV and DM from IM, of DV from EDP and IM. This implies that intermediate variables EDP and DM, used to relate IM to DV, are chosen so that the conditioning information is not “carried forward”. So, for example, the EDPs should be selected so that the DMs (and DVs) do not also vary with intensity, once the EDP is specified. Similarly, the intensity measures (IM) should be chosen so that, once it is given, the dynamic response (EDP) is not also further influenced by, say, magnitude or distance to the source. (Krawinkler, 2005)

The presented framework is coherent with Performance Based Earthquake Engineering (PBEE) approach (Cornell and Krawinkler, 2000). According to PBEE, the design of a new structure and the assessment of the seismic performance of an existing one have to comply a discrete number of “quantitative” requirements (structural or economic) corresponding to “qualitative” performance levels.

The definition of these performances were firstly addressed by SEAOC Vision 2000 (SEAOC, 1995) and subsequently in ATC-32 (1996a), ATC-40 (1996b), FEMA 356 (ASCE, 2000). The matrix in Figure (2.2) relates four earthquake performance levels with design earthquake levels expressed in terms of return period (see Sect 2.3.1). The

coupling of a specific seismic intensity level with a performance level of the structure is the *performance objective*. Different earthquake performance levels have been defined in literature, associated to different loss levels due to earthquake. Some of them are reported in Figure (2.3), overlapped to a typical base shear-top displacement evolutionary response of a structure (i.e. pushover curve).

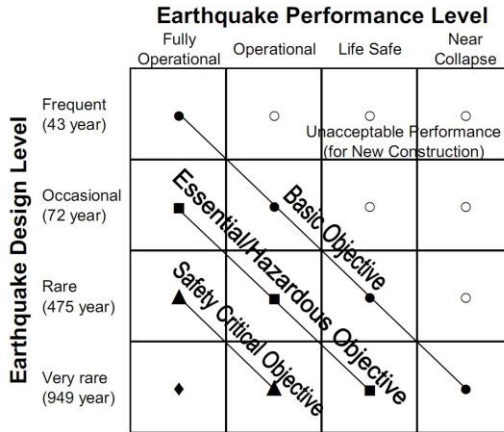


Figure 2.2 Vision 2000 recommended seismic performance objectives for buildings (Porter, 2003 after SEAOC, 1995);

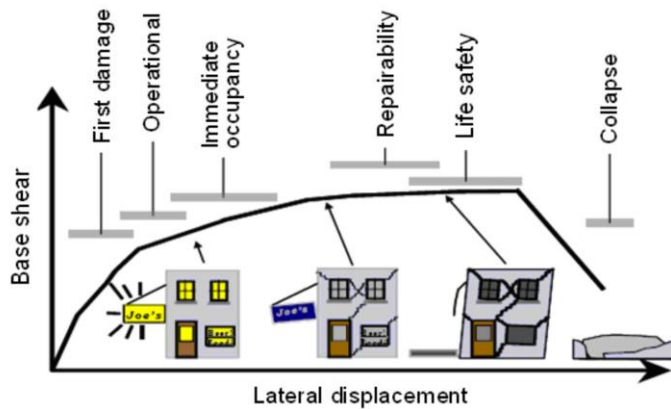


Figure 2.3 Illustration of performance-based earthquake engineering (from Parisi, 2010 after Hamburger)

If reference is made to these performance objectives, the PEER methodology allows to perform a Performance Based Assessment (PBA), and to estimate the frequency with which a particular performance metric will exceed various levels for a given design at a given location.

According to PBEE, the structural behaviour has to be checked with respect to given “limit states”, i.e. conditions after which the structure no longer meets the required performance levels, also referred to as “*failure*”. A structural limit state is usually defined by the structural behaviour at the onset of structural demand being equal to the capacity corresponding to that limit state.

More in detail, matching a performance level can be expressed by the values assumed by a so-called *limit state function*, generally defined so that, if non-positive, the *failure* condition is reached. Considering, as an example, a simple limit state function defined as the difference between the seismic demand, D , and the seismic capacity, C , the *failure rate* can be expressed as:

$$\lambda_f = \int_{im} P[D \geq C | im] \cdot |d\lambda(im)| \quad (2.2)$$

The term C in the previous equation, is the capacity for the specific limit state.

The failure probability can be expressed, assuming an homogeneous Poisson’s stochastic model, as:

$$P_f = 1 - e^{-\lambda_f T_L} \quad (2.3)$$

where T_L is the reference time period¹. If reference is made to the annual probability of exceedance of a given value of im , Eqs. (2.3) and (2.4) provides approximately the same result. The term $P[D \geq C/im]$ or, equivalently, $P[failure/im]$, is usually referred to as *fragility curve* or *fragility function*. It expresses the probability of exceeding a specific limit state (i.e. structural performance), given $IM=im$.

2.2.1. Loss estimation

There are many possible measure of economic loss that can be used to express the seismic performance (Miranda and Aslani, 2003; Aslani and Miranda, 2005; Zareian and Krawinkler, 2009). The ATC 58-1 project (ATC, 2003), aimed at the communication of seismic risk to stakeholders, concluded that while some stakeholders, in order to make decision, find more useful to work with simple measure of economic losses (such as the annual expected loss), others prefer more complex measures (such as the exceedance probability of a single earthquake loss in a given time period or the probable maximum loss associated with a major earthquake).

Some measures of the loss, ordered by increasing level of complexity are:

- **The expected loss for a given earthquake scenario.** This measure of the risk expresses the average loss in an earthquake scenario, defined by a given

¹ This period is the time interval in which earthquakes are observed. From a design standpoint, it is related to the nominal life of the construction, its expected occupancy level, and its importance for civil protection purposes.

ground motion intensity IM, with a given return period. It corresponds to the expected value of the total loss, conditioned to a given $IM=im$: $E[L|IM = im]$.

- **The expected loss for a set of earthquake scenarios.** This measure of the risk provides the average loss for a family of earthquake scenarios. It can be used to obtain the variation of the average losses at increasing IMs. .
- **The annual expected loss.** This measure provides the average loss produced in the building every year. Referring to a given structural performance (*failure*) and to the annual probability of failure, P_f , it is computed from the following equation:

$$E[L] = E[L|failure] \cdot P_f \quad (2.4)$$

The measures described above, do not express any information about the dispersion of the losses around average values, therefore, improved and more informative measures of the loss can be:

- **The probability of exceeding a specific loss in a given earthquake scenario.** This measure provides information about the possibility of facing an economic loss larger than a given amount, l , in an earthquake with an intensity im : $P[L>l|IM=im]$.
- **The probability of exceeding a specific loss for a set earthquake scenario.** It is the previous measure, repeated for different earthquake scenarios with increasing IM.
- **The probability of having a loss equal to or larger than a given amount.** This measure combines the probability of exceeding a given loss in a scenario earthquake, characterized by a specific im , with the annual probability of exceeding a ground motion intensity equal to or larger than im . It can provide the loss amount associated with a particular probability of being exceeded (e.g. the total loss that has the 2% of probability of being exceeded in 50 years).

The assessment of losses is not a specific purpose of this thesis, nevertheless, some measures of loss are considered, reflecting the approaches proposed at different scales. In risk prioritization analysis (Chapter 4) a relative index accounting for potential losses (in terms of monetary losses, business interruption and life losses) is considered, therefore no explicit computation of earthquake losses is given. In the procedures outlined in Chapters 5 and 6, two possible metrics of losses are considered: the expected loss given an earthquake scenario and the annual expected loss. These metrics were adopted, although synthetic, because they are believed to be useful to owners, insurers or other stakeholders to quantitatively compare, for example, expected annual losses and annual revenues.

2.3. Computing individual Risk components

2.3.1. Seismic Hazard

Seismic hazard is the totality of physical effects, both direct and indirect, induced by the earthquake and able to produce harmful consequences.

The intensity of the seismic ground motion (GM) in a specific site depends mainly on the following parameters: the input energy released by the seismic source (which is a function of the source dimensions and fracture mechanism); the seismic waves path (which prevalently depends on the source-site distance); and the local geotechnical conditions (local seismic response of soil deposits at the site). The first two factors affect the characteristics of seismic motion at the bedrock, namely the so-called *shakeability*, which is evaluated in ideal conditions of horizontal topographic surface and free field. The third accounts for the modification of the seismic signal from the bedrock to the surface due to the dynamic response and topography of soil deposits (Lanzo and Silvestri, 1999; Vinale, 2008). In fact, site conditions can influence the amplitude, frequency content, and duration of seismic ground motion.

Regarding the definition of seismic hazard for seismic risk analysis purposes, it can be defined through a probabilistic seismic hazard analysis (PSHA) or a deterministic seismic hazard analysis (DSHA).

The PSHA, originally proposed in the landmark paper by Cornell (1968), takes into consideration possible earthquakes that could affect a site and its output is the mean annual frequency of exceeding a ground motion intensity measure threshold, im :

$$\lambda(im) = \sum_{i=1}^n \nu_i \cdot \int \int G_{IM|M,R}(im|m,r) \cdot f_M(m) \cdot f_R(r) \cdot dm \cdot dr \quad (2.5)$$

In the previous equation, $f_M(m)$ and $f_R(m)$ are, respectively, the probability density functions (PDFs) of magnitude, M , and distance, R , (assuming that M and R are independent); $G_{IM|M,R}$ is the conditional probability that, for given M and R , a specific value of im is exceeded at the site. This probability is generally computed by means of a Ground Motion Prediction Equation (GMPE). Finally, ν_i is the rate of a threshold magnitude exceedance of the i -th source affecting the site.

The probability of exceedance of IM can be obtained, in most of the practical applications, assuming that the occurrence of seismic events follows an homogeneous Poisson's stochastic model:

$$P[IM > im] = 1 - e^{-T_L/T_R} = 1 - e^{-\lambda(im)T_L} \quad (2.6)$$

where T_R is the return period, that is the reciprocal of the annual rate of exceedance of the IM and T_L is the considered time period. From the previous formulation the expression of the return period derives:

$$T_R = \frac{1}{\lambda(im)} = -\frac{T_L}{\ln(1 - P[IM > im])} \quad (2.7)$$

It has to be noticed that Eq. (2.8) represents the complementary cumulative distribution (CCDF) of the intensity measure, therefore the probability distribution (PDF) of the intensity measure can be obtained from Eq.(2.7) by simply differentiation.

Regarding deterministic seismic hazard analysis (DSHA), it is based on the development of earthquake scenarios, defined by location and magnitude, which could affect the site under consideration.

Deterministic approaches are not dealt in this thesis; for details the reader should refer to Reiter (1990) and Kramer (1996). It seems worthwhile to enlighten that, besides their differences, DSHA and PSHA can be considered complementary analysis, chosen as a function of available data and objectives of the seismic risk assessment (McGuire, 2001). Probabilistic methods can be viewed as inclusive of all deterministic events with a finite probability of occurrence. This points out the complementary nature of deterministic and probabilistic analyses: deterministic events can be checked with a probabilistic analysis to ensure that the event is realistic (and that it has a finite probability of occurrence) and probabilistic analyses can be checked with deterministic events to see that rational, realistic hypotheses of concern have been included in the analyses. Typical example of this complementarity is, in fact, the possibility of selecting scenario earthquakes from deaggregation analysis (Bazzurro and Cornell, 1999) of the seismic hazard computed by a PSHA. A more comprehensive discussion about differences and similarities of the two methods is contained in Bommer (2002).

2.3.2. Vulnerability

Seismic vulnerability represents the proneness of physical environment to suffer damage under earthquakes. It can be evaluated according to different methodologies, mainly dependent on the scale of the problem, ranging from the one of the single structure to the regional or national scale. The object of the analysis, in fact, determines the quantity and quality of input data that can be gathered and the methods of analysis that can be pursued. According to the classification proposed by Dolce *et al.*, (1994), vulnerability assessment methods can be classified on the basis of the three quantities: input, method and output.

Regarding *input* data required for the analysis, they are strongly dependent on the size of the object of the analysis and on the chosen methodology. As a matter of fact, vulnerability assessment for a single structure requires an amount of information and a

level of detailing in modelling that are unfeasible at larger scales. Input data required for a vulnerability analysis can vary from the damage observed in past earthquakes to qualitative or quantitative characteristics about the structure, hazard studies for the specific site and geological and geotechnical information.

The *output* of vulnerability assessment can be expressed in terms of: (i) absolute vulnerability; (ii) relative vulnerability. *Absolute* vulnerability represents an actual measure of the damage suffered by structures during earthquakes while *relative* vulnerability is represented by indicators for which no direct correlation to the actual damage is available. Therefore, the latter is suitable for vulnerability ranking and prioritization analyses, rather than the assessment of the actual structural vulnerability.

Regarding possible *methods* for computing vulnerability, they can be classified into:

- empirical methods;
- analytical methods;
- expert judgment-based methods;
- hybrid methods;
- code-based methods.

The use of one of the above is strictly related to the methodology employed for computing hazard. In the following, a brief review of main vulnerability approaches available in literature, subdivided according to the employed methodology, is presented. Much more comprehensive reviews can be found in (Polesse,2002; Calvi *et al.*, 2006; Ricci, 2010).

2.3.2.1. Empirical methods

Empirical methods represent the first approaches pursued for seismic vulnerability assessment, dated the early 1970s, based on the observation of the damage suffered in past earthquakes. The observed damage is measured by means of Macroseismic intensity scales.

These approaches present the advantage of giving a realistic representation of the damage (they represent the real effect of earthquakes on physical environment), provided they are applied to a building stock with the same characteristics as the one damaged in past earthquakes. Notwithstanding, they present the following shortcomings: they account for vulnerability and hazard in a non-independent way and are calibrated on a particular territorial area, therefore they are not, in principle, exportable to other territories because of differences in seismological context, structural typologies, building practice and damage distributions.

Moreover they do not allow to model any mitigation strategy which employs the reduction of seismic vulnerability (e.g. a retrofit of a building) and they can be affected

by shortcomings related to availability of data or errors in filling post-earthquake assessment forms (Colombi *et al.*, 2008).

Different empirical methods are:

- damage probability matrices (DPMs);
- empirical damage functions;
- vulnerability Index method;
- screening methods.

A *Damage Probability Matrix* (DPM) represents, in discrete form, the conditional probability $P[D/I,T]$ of reaching a damage level D , given a ground motion intensity I expressed by a macroseismic scale, for a given structural typology T . Its use was firstly proposed by Witman *et al.* (1973), after the San Fernando earthquake of 1971. Other examples of DPMs are those proposed by Braga *et al.* (1982); Di Pasquale *et al.* (2005); Dolce *et al.* (2003); Giovinazzi and Lagomarsino (2004). Relationships between seismic intensity and expected damage based on empirical data can also be derived in a continuous form. In fact, empirical damage function (or curves) can be defined as the continuous form a DPM (e.g. Spence *et al.*, 1991; Orsini, 1999, Shinghal and Kiremidjian, 1997; Sabetta *et al.*, 1998; Rossetto and Elnashai, 2003)

The *Vulnerability Index Method* was proposed by Benedetti and Petrini (1984) and subsequently employed in (GNDT, 1993). It consists in an “indirect” measure of vulnerability because a relationship between the seismic action and the response is established through a vulnerability index, defined on the basis of the scores assigned, after a field survey, to eleven parameters believed to be correlated to the actual vulnerability of the building. This methodology, largely adopted both for national and international research projects (e.g. in the “Progetto Catania”, Faccioli *et al.*, 1999; Faccioli and Pessina, 2000 and “RISK-UE”, Mouroux and Le Brun, 2006), presents the advantage of allowing the vulnerability characteristics of the building stock under consideration to be determined; notwithstanding, it requires expert judgement to be applied in assessing the buildings, and in defining coefficients and weights (Calvi *et al.*, 2006).

Finally, *Screening methods* are aimed at providing an approximate evaluation of vulnerability employing visual surveys (Culver *et al.*, 1975; JBDPA, 1990). Their output is, in most cases, an “indirect” measure of the vulnerability, represented by descriptive ratings or vulnerability indices.

The forms employed in these methods for the visual survey are, in general, quite similar to “post-earthquake” survey forms employed for assessing the damage following an earthquake in order to guide decision on continued occupancy (e.g. Anagnostopoulos *et al.*, 1989; Baggio *et al.*, 2000). These methods, are in general aimed at the definition of a relative measure of the vulnerability of structures in large

portfolios and they are usually employed for prioritization analyses. For this reason, they will be dealt more in detail in Chapter 4.

2.3.2.2. Analytical methods

In analytical methods, the relationship between seismic intensity and expected damage is provided by a structural model with direct physical meaning. The analytical approach to vulnerability, allows to separate structural analysis from site hazard modelling. Furthermore, it allows to deal with structures characterised by different construction practices and to consider the effect of vulnerability mitigation strategies (Ricci, 2010). However, analytical approaches require, in general, an high level of knowledge about structural characteristics and detailing, as well as high computational burden. Moreover, some critical issues related to their use suggesting that the results provided by this kind of approaches should be, somehow, checked with real damage, exist. Examples are: the reliability of numerical modelling, the correlation of the chosen demand parameters with the actual structural performance and the influence of constructive errors and deficiencies, that usually are not considered in the analytical model (Verderame *et al.*, 2011) or investigated with a sufficient degree of accuracy (Petruzzelli *et al.*, 2010).

Several analytical methods for vulnerability assessment have been developed in literature. It is important to underline that the procedure for evaluation of the seismic vulnerability is closely dependent on the scale of the problem, since the size of the sample to be analysed actually determines the quality and quantity of data that can be retrieved (level of knowledge that is possible to achieve) and, therefore, the mechanical modelling. As a matter of fact, the more the sample size grows, the more it is necessary to renounce to a certain degree of accuracy and detail in mechanical modelling and to adopt approximated methods, which require a lower amount of input data.

For this reason, hereinafter, both methods that are suitable to the scale of the single building (for example, the analytical evaluation of fragility curves) and methods that have been conceived and developed to be applied to large samples will be briefly discussed. Depending on the mechanical model employed and on the structural analysis performed, they can be classified as follows:

- analytical fragility curves (or DPMs);
- collapse mechanism-based methods;
- capacity spectrum-based methods;
- displacement-based methods.

Analytical fragility curves and analytical DPMs express, respectively in continuous or discrete form, the probability of observing a given level of damage, conditioned to a value of IM. Several methodologies can be pursued for their computation both based

on static and dynamic analyses and reflecting uncertainties in the seismic demand (record to record variability) and in the capacity (e.g. Singhal and Kiremidjian, 1996; Dumova-Jovanoska 2004; Rossetto and Elnashai 2005). These methods will be dealt in presented more in detail in Chapter 5 and the analytical evaluation of fragility curves for existing steel structures is the specific object of Chapter 6.

Collapse mechanism-based procedures employ collapse multipliers and mechanical concepts to ascertain whether a mechanism will form and thus damage will occur.

Among these procedures, originally developed for masonry buildings, it is to recall the VULNUS method (Bernardini *et al.*, 1990), the Failure Mechanism Identification and Vulnerability Evaluation (FaMIVE) method (D'Ayala and Speranza, 2002) and the procedure proposed by Cosenza *et al.* (2005), for the evaluation of the seismic capacity of reinforced concrete (RC) building classes.

Capacity spectrum-based methods employ non-linear static procedures (NSPs) and Capacity Spectrum Method (CSM) by Freeman *et al.* (1975) for rapid assessment of the seismic risk of building classes. According to it, the seismic capacity obtained from a NSP can be compared to the demand in a plane having the spectral displacement on the abscisse axis and the spectral acceleration on the ordinates axis. The main scope is to assess seismic demand through a spectral representation of non-linear response, which is made possible by: (i) the idealisation of the actual multi-degree-of-freedom (MDOF) structure as an equivalent elasto-plastic single-degree-of-freedom (SDOF) system; and (ii) the transformation of the elastic demand in the inelastic demand by increasing structural damping or, alternatively, defining a global displacement ductility.

Among capacity spectrum-based methodologies for the analytical evaluation of vulnerability it is possible to count the HAZUS (HAZard in United States) method (FEMA, 2001; Kircher *et al.*, 1997a, Kircher *et al.*, 1997b; Whitman *et al.*, 1997). This is an earthquake loss estimation methodology including many components, among which a building fragility module based on capacity spectrum method.

Giovinazzi (2005) defined a methodology for the vulnerability assessment of RC and un-reinforced masonry (URM) building classes employing a CSM-based approach, in which the capacity curve was defined on the basis of code prescriptions enforced at the time of design.

Finally, the method by Iervolino *et al.* (2007), representing a complete seismic risk assessment framework for RC building classes and the one by Ricci (2010), for the seismic vulnerability assessment of existing bare, partially infilled and infilled RC buildings, has to be mentioned too.

Calvi (1999) first proposed an approach for the evaluation of the vulnerability of building classes based on the Displacement-Based method (Priestley, 1997). According

to this method, seismic demands are computed by means of displacement spectrum and displacements are employed as damage indicators. The methodology was subsequently developed (Pinho *et al.*, 2002; Glaister and Pinho, 2003; Crowley *et al.*, 2004; Crowley *et al.*, 2006) leading to the Displacement-Based Earthquake Loss Assessment (DBELA) procedure. The extension of the approach to masonry buildings was performed by Restrepo-Vélez and Magenes (2004), Restrepo-Vélez (2005), Modena *et al.* (2005) leading to the MeBaSe (Mechanical Based Procedure for the Seismic Risk Estimation of Unreinforced Masonry Buildings) Procedure.

The Simplified Pushover-Based Earthquake Loss Assessment (SP-BELA) by Borzi *et al.* (2008a) combines the class approach of DBELA with the definition of simplified static pushover curves in a way similar to Cosenza *et al.* (2005) and Iervolino *et al.* (2007).

2.3.2.3. Code-based methods

In Code-based methods the seismic capacity is derived from the seismic code prescriptions enforced at the time of design. The latter can be used either to define a simplified capacity curve, as in method by Giovinazzi (2005) previously discussed, either to define a so-called “nominal” capacity to be compared to the current seismic demand, as in the New Zealand Society for Earthquake Engineering guidelines (NZSEE, 2003) and Grant *et al.* (2007).

Such methods are based on the strong assumption that the design was performed in full compliance with the code and that, therefore, the demand to capacity ratio was, at the time of design, equal to one. For this reason, these methods are usually employed only for prioritization analysis of large building portfolios. This family of methods will be dealt in Chapter 4.

2.3.2.4. Expert Judgment-based methods

According to these methods an expert (or an expert panel) expresses, on the basis of his engineering judgement and experience, a qualitative judgment on the vulnerability of a structure or a class of structures. In general, they require ad-hoc damage functions in order to translate vulnerability indicators into damage and, subsequently, into economic losses.

An example of Damage Probability Matrices, derived from the expert judgement of more than 50 senior earthquake engineering experts, can be found in ATC-13 (ATC, 1985). Examples of the use of DPMs based on the ATC-13 approach for the assessment of risk and loss include the city of Basel (Fah *et al.*, 2001), Bogotá (Cardona and Yamin, 1997) and New Madrid (Veneziano *et al.*, 2002).

2.3.2.5. *Hybrid methods*

Hybrid methods consider empirical and analytical approaches as complementary, rather than mutually exclusive options for the vulnerability assessment.

They allow to produce fragility curves and damage probability matrices combining analytical modelling and observations of damage of past earthquakes. In fact, mechanical modelling can be used in order to provide for the lack in damage data at a given intensity level or, on the contrary, damage can be used in order to calibrate mechanical models. Examples are given in Kappos *et al.* (1995, 1998) and Barbat *et al.* (1996).

2.3.3. *Exposure*

Exposure can be defined as the economic losses due to seismic events and their associated probabilities. Therefore, it represents the term allowing to translate hazard and vulnerability concepts into risk. Its definition depends on the object of the risk assessment and it may include a single structure with its occupants, a portfolio of buildings, a urbanised area or a whole region. Generally speaking, losses can be classified as:

- direct losses;
- indirect losses.

Direct losses are those observed for a specific site as a direct result of the physical damage. They are expressed, in general, as the cost of repair or replacement, that is to say they represent the losses caused by an earthquake arising from the repair effort needed to return a damaged building to its undamaged state. In industrial and insurance field they are referred to as "Property damage".

Indirect losses, on the contrary, are those resulting from the temporary loss of function of the facility, or downtime. The downtime can be defined as the period of time between the occurrence of a seismic event and the completion of the building repair effort and the restoring of the full functionality (Comerio, 2006).

In Industry these losses are referred to as "Business Interruption" (BI), addressing all the possible consequences of a given downtime. For a single industrial facility these consequences can be: loss of production, loss of profit and of market shares, costs for the restart of the production activities, damage to image, etc. When dealing with portfolios of industrial structures or plants, besides the above mentioned damages, observed for one specific structure of the portfolio, also losses related to the disruption of the supply chain must be taken into account. These indirect consequences can represent the large part of the losses due to seismic events in Industry and can propagate themselves both upstream and downstream.

Strictly speaking, human casualties represent a direct loss, generally related to the collapse of the structure. Nevertheless they are in general considered separately from economic impacts, since equating or converting human lives to a monetary amount is considered problematic or involving social equality issues².

This suggests another possible classification of losses due to seismic events into:

- dollars,
- downtime,
- deaths;

that is the so-called “3D” approach, generally adopted in PEER approach.

2.4. Management and mitigation of seismic risk

“Risk assessment is all about risk management. The only reason you do an assessment is because somebody has to make a risk-management decision” (Smith, 2005). This sentence well summarizes the main function of the seismic risk assessment, which is to provide rational estimates to guide the decision making process and the implementation of mitigation strategies. The risk management cycle is represented in Figure (2.4). Once the analysis of seismic risk has provided the probability of exceeding a given loss in a reference period, or any other useful metric to express the loss (see Section 2.2.1), according to the risk management framework illustrated in Figure (2.4) the stakeholder has elements to judge if the risk level is acceptable or not. If acceptable, monitoring risks and identifying any new potential risk are the activities the decision maker should continue to pursue. If the risk level is deemed unacceptable, risk mitigation strategies have to be implemented.

In the obvious inability to reduce the hazard component of the seismic risk³, possible strategies for risk mitigation can be aimed at the reduction of seismic vulnerability, exposure or economic consequences.

Vulnerability reduction strategies could be:

- the retrofitting of existing structures;
- the development and continuous updating of seismic codes according to research advances.

² In order to overcome these problems, measures of the loss related to casualties alternate to the assessment of human life were proposed in Literature, (e.g. the disability adjusted life years, World Bank, 1993; or Economic Adjusted Life years, Scawthorn, 2011).

³ For completeness, it is to mention the possibility of relocating the building. Strictly speaking, this solution, feasible only in the design of a new structure, by changing the building location, actually changes the hazard.

Implementing vulnerability reduction strategies for existing buildings is a rather complex issue, especially for large portfolios of structure or for civil protection purposes. Two different approaches to seismic rehabilitation of existing buildings are possible: a “passive” one and an “active” one. According to the former, assessment and rehabilitation are required only in case the building owner applies for an alteration or change in use. Active programmes are, on the contrary, those that require owners to rehabilitate their buildings to a specific rehabilitation objective in a certain timeframe or, in the case of government or other owners of large inventories, to self-impose objectives and deadlines.

Issues regarding passive seismic risk reduction were addressed by Hoover (1992) and an example of active seismic risk reduction programme is contained in (NZSEE, 2003). Passive programmes reduce risk more slowly than active programmes but, on the other hand, they generally require much less efforts to be implemented. In both cases they are more rapid than modifications of seismic codes that, applying only to new constructions, produce a reduction of vulnerability delayed in time.

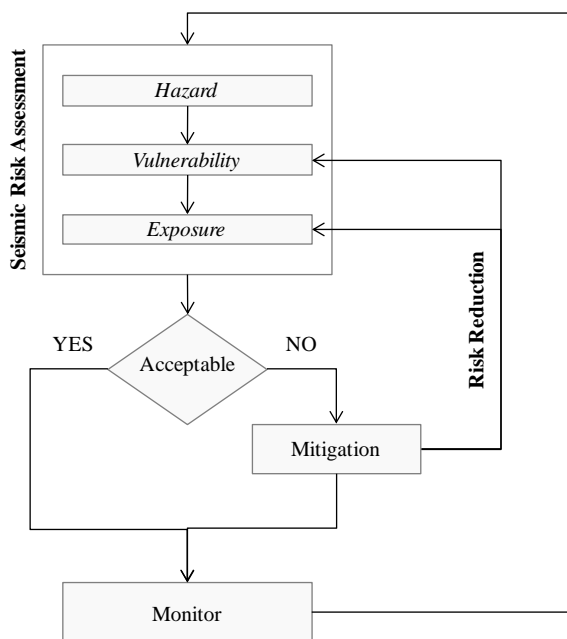


Figure 2.4 Risk management cycle.

Among the strategies acting on exposure it is possible to recall:

- the change of occupancy;
- the development of an effective civil protection system, both in the pre-event phase, through knowledge dissemination, promotion of seismic risk awareness,

etc., and in the post-event phase, by means of emergency management planning, providing pre-defined emergency procedures and plans.

- the development of early warning systems (Iervolino *et al.*, 2011)

Regarding economic loss reduction strategies it is to mention the adoption of insurance policies such as in Turkey, after the 17th August 1999 Kocaeli earthquake, or in Japan, where a national reinsurance scheme is enforced since 1966.

Chapter 3 THE CASE-STUDY BUILDING PORTFOLIO

3.1. Description of the case-study

The procedures for the large-scale prioritization and for the seismic risk assessment presented in this thesis (Chapter 4 to 6) have been applied to a real case study, consisting in a subset of the Italian plants of one of the most important international partners of *AXA Matrix Risk Consultants*. Because of privacy agreement with the stakeholder, the names and geographical locations of these facilities are hidden in this thesis. Each plant will be, therefore, identified by a serial number.

The plant portfolio under investigation is composed of 19 plants for the production of parts for the automotive sector, spread throughout the Italian territory, as can be seen in Figure (3.1).

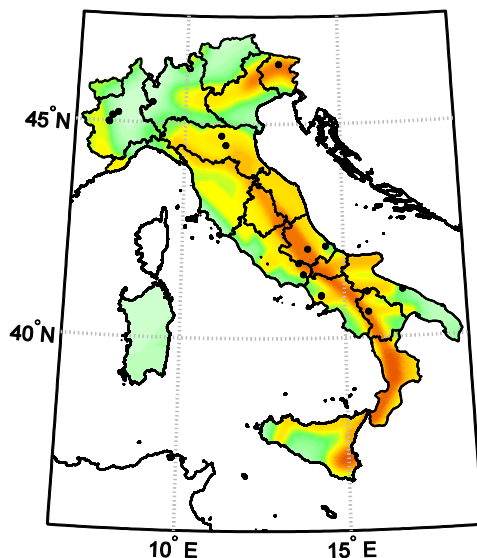


Figure 3.1 Case-study plants represented over the map of PGA with 475 years return period on rock (Stucchi *et al.*, 2011).

For each of the plants composing the case-study portfolio, two kinds of knowledge forms were compiled: an “*Hazard form*”, described in Sect. 3.2, and a “*Knowledge form for industrial manufacturing plants*”, described in Sect. 3.3.

Principal aim of the *Hazard Form* is the characterization of the seismicity of the site, by means of the macroseismic intensity and/or seismic hazard studies with the maximum level of detail available in the Country. Hazard form can be compiled

“offline”, that is to say without any visual survey on site. For Italy, the reference studies for hazard and macroseismic intensity characterization are both provided in the “S1” project funded by Italian National Institute for Geophysics and Volcanology (Istituto Nazionale di Geofisica e Vulcanologia, INGV) and Seismic Risk Office of the Italian Department of Civil Protection (DPC).

Hazard estimates with a return period of 475 years are given both in terms of PGA on rock (Meletti and Montaldo, 2007) and in terms of macroseismic intensity (Gómez Capera *et al.*, 2007; Albarello *et al.*, 2007). The work by Albarello *et al.* (2007), used in this thesis, provides the maximum intensity felt in the past, I_0 , for the whole Italian territory, and macroseismic intensity estimates with an exceedance probability of 10% in 50 years, according to a “site approach” (Albarello and Mucciarelli, 2002) and assuming two different GMPEs (I_{bin} assuming a binomial GMPE, I_G assuming a and a Gaussian one). Table (3.1) reports a ranking of the case-study plants by decreasing PGA with a return period of 475 years on rock, and the macroseismic estimates by Albarello *et al.* (2007).

Table 3.1 Case study plants: PGA on rock and return period of 475 years; macroseismic intensity with return period of 475 years, expressed in terms of I_G and I_{bin} ; maximum seismic intensity felt at the site, I_0 .

Plant ID	PGA [g]	I_G [-]	I_{bin} [-]	I_0 [-]
PLANT-01	0.256	9	9	9
PLANT-02	0.242	9	9	8.5
PLANT-03	0.240	10	10	10
PLANT-04	0.240	8	8	8.5
PLANT-05	0.198	8	8	8
PLANT-06	0.198	8	8	8
PLANT-07	0.191	8	9	9.5
PLANT-08	0.165	7	7	7.5
PLANT-09	0.157	7	7	5
PLANT-10	0.147	7	8	6
PLANT-11	0.143	8	8	7.5
PLANT-12	0.108	7	8	7
PLANT-13	0.082	6	7	6
PLANT-14	0.081	6	7	6
PLANT-15	0.076	7	7	6.5
PLANT-16	0.058	6	6	6
PLANT-17	0.056	6	6	6
PLANT-18	0.046	6	6	5
PLANT-19	0.040	6	7	0

Main objective of the *knowledge form for industrial manufacturing plants* is the reconstruction of the plant layout and the characterization, among the others, of the following parameters: number of structures, main geometric dimensions, structural types, construction materials and exposure. Filling these forms requires at least a visual survey.

During the three years agreement between the *Department of Structures for the Engineering and Architecture* of the *University of Naples Federico II*, Italy, and the *AXA Matrix Risk Consultants*, all the plants have been visually inspected by the author or by field engineers of AXA Matrix.

One of the main difficulty that has emerged from this activity is, certainly, related to the extreme variability of structural types, activities and contents of each structure belonging to different plants. A first classification of the structures that it is possible to encounter in Industry is in:

- building-like structures;
- non-building-like structures.

Building-like structures are typically used as offices or management buildings, workshops, warehouses, or storage structures; non-building-like structures (pipelines, storage silos or tanks, racks, cement kilns, cooling towers, chimneys, etc.) are characterized by layout, structural dimensions and design dictated by the needs of the production, over any other issue.

It is also possible to classify the structures in the manufacturing Industry according to their occupancy, i.e. distinguishing:

- production structures;
- utilities;
- storage structures;
- offices.

Production structures are workshops, or any type of structure (building-like or non-building-like) where large part of the production takes place. They can be considered, therefore, the core of the plant, since the functionality of the whole plant depends on them and most of the exposed values (human lives, contents, activities) are typically located in, or related to, them.

With the term *utilities* all the machineries and apparatuses involved in the production or safety of the plant are, in general, addressed. Typical examples are, in manufacturing industry, energy transformers of pumps for the fire protection system. The structures (typically building-like) built to host such equipments are, therefore, called themselves “utilities”.

Storage structures are all those structures the function of which is to store raw materials, finished or semi-finished products or anything useful for the production or for the use of utilities.

Offices are all those structures not used for the production but for administrative and management purposes.

Other kinds of structure that is possible to observe in manufacturing industry are not considered to be strictly related to production or characterised by a significant exposure (such as recreational facilities, dining areas, locker rooms, parking areas); therefore they are not considered in this study, unless they are part of structures with another use, among those described above.

From the above, the first objective of the knowledge phase is the identification of structures composing the plant for what concerns their occupancy and their main geometrical characteristics.

It is very frequent that industrial structures are characterised by large plan developments and/or that have been constructed in different years, with or without structural joints between different parts of the structure. In fact, they often assume the shape of structural aggregates (e.g. a large workshop). Therefore, one main issue in the knowledge process is the identification of the individual “structural units” composing a structural aggregate, that is to say the single structural entities, separated from the others by structural joints. This is possible by identifying the gaps between the structures, quantifying their size and tracing back the constructive evolution of the building aggregate. This information, in fact, can be used to associate a reference design code to each structural unit and, in the view of a code approach to seismic vulnerability, to obtain information about the nominal seismic capacity of each structure (see Chapter 4). In the following, the term “structure”, if not differently specified, will be used as a synonym of “structural unit”.

Particular effort was dedicated to the characterization of subsoil geotechnical conditions. In 15 of the 19 plants it was possible to gather information about shear wave velocity in the top 30 meters of subsoil under the foundation layer, and associate to each plant the subsoil class according to Eurocode 8 (EC8) (CEN, 2004). In the other cases, prudential assumptions were made on the basis of geological information.

In Table (3.2) the number of structural aggregates and of individual structural units, with specification of their use (for building like structures and silos/tanks only) are reported for each plant of the case-study portfolio. From the previous emerges that the portfolio is made of 58 building aggregates, composed of 140 individual structural units, of which 83 are workshops for production, 29 are offices, 17 are utilities and 11 are storage buildings (Fig. 3.2). It is worth noting that, when storage areas or utilities were included in a structure in which production took place, the structure was

classified as a production one. Besides, in 4 cases silos or tanks for liquid or granular content were part of the plant layout.

Table 3.2 Soil category and structural composition of the case-study portfolio. Regarding storage structures, the first number indicates buildings employed for storage, while the number in parentheses indicates surveyed non-building-like storage structures (tanks, silos).

Plant ID	year of first construct.	PGA [g]	Soil Cat.	Num. of structural aggregates	Num. of structural units	Production	offices	utilities	storage
PLANT-01	1971	0.256	B	3	8	4	2	2	0 (1)
PLANT-02	1988	0.242	C	1	3	2	1	0	0
PLANT-03	1988	0.240	C	2	2	1	1	0	0
PLANT-04	1977	0.240	C	3	14	10	1	0	3 (1)
PLANT-05	1993	0.198	C	6	14	8	2	4	0 (1)
PLANT-06	1993	0.198	C	2	2	1	1	0	0
PLANT-07	1987	0.191	B	3	5	5	0	0	0
PLANT-08	1934	0.165	C	5	15	6	4	5	0
PLANT-09	1973	0.157	D	3	8	4	1	2	1 (1)
PLANT-10	1974	0.147	B	2	6	4	2	0	0
PLANT-11	1988	0.143	B	4	4	3	0	0	1
PLANT-12	2001	0.108	C	1	2	1	1	0	0
PLANT-13	1963	0.082	C	2	7	2	5	0	0
PLANT-14	1968	0.081	B	4	5	2	1	0	2
PLANT-15	1969	0.076	A	7	14	6	2	3	3
PLANT-16	1962	0.058	B	4	14	12	2	0	0
PLANT-17	1919	0.056	B	1	4	4	0	0	0
PLANT-18	1976	0.046	B	3	7	4	1	1	1
PLANT-19	1968	0.040	B	2	6	4	2	0	0
TOTAL:				58	140	83	29	17	11

Use of structures of case-study portfolio

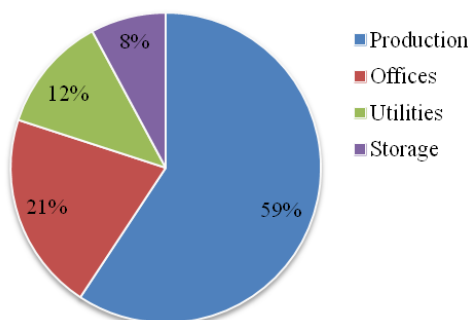


Figure 3.2 Percentages relative to the use of structures of the case-study portfolio.

Referring to the structures used for production, as it can be observed in Figure (3.3), the most part is contributed by precast reinforced concrete (PRC) structures (60% of the total) and the remaining part is composed of steel structures (40%). However, steel structures present, in general, bigger plan dimensions than PRC structures; in fact, the 58% of the whole covered area used for production is relative to steel structures, while the 42% is relative to PRC structures.

Regarding the year of construction, more than one third of the portfolio's structures were built in the '60s and more than the fifty percent of the structures were built before 1980 (Fig. 3.3).

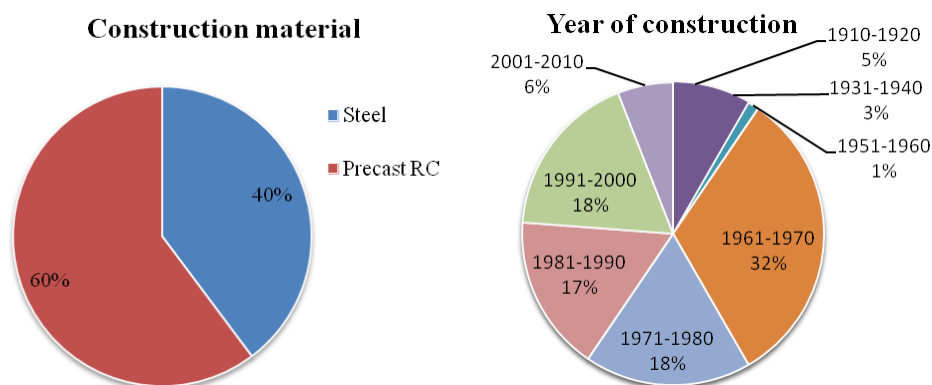


Figure 3.3 Composition of the case study portfolio for what concerns construction material (left) and year of design (right).

With specific reference to the steel structures used for the production, in Figure (3.4) the composition for design year is reported. Except for one structure that is characterized by bracings in one plan dimension, all the structures are moment resisting frames (MRFs), characterized in the 94% of cases by a rectangular shape (the 3% is T-shaped and the 3% L-shaped).

The typologies of the main beam (i.e. the beam in the direction of the moment resistant frame or, when the structure has frames in both the plan directions, the one with the larger span) and of the secondary beam (the one in the orthogonal direction or characterized by the smaller span) are shown in Figure (3.5). In most of the cases the beams are planar lattice trusses, in both the plan directions.

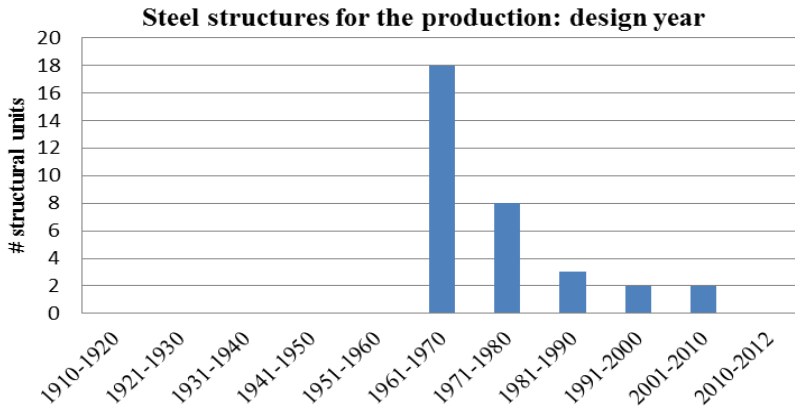


Figure 3.4 Age of design of steel structures used for production

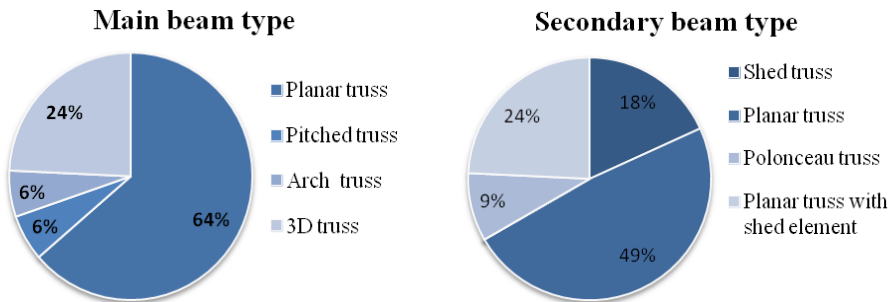


Figure 3.5 Typology of main (left) and secondary (right) beams of surveyed steel structures used for production

Columns types observed in surveyed structures, as summarized in Figure (3.6) were classified distinguishing: battened columns, composite columns created by welded members or plates, single member elements and trussed columns.

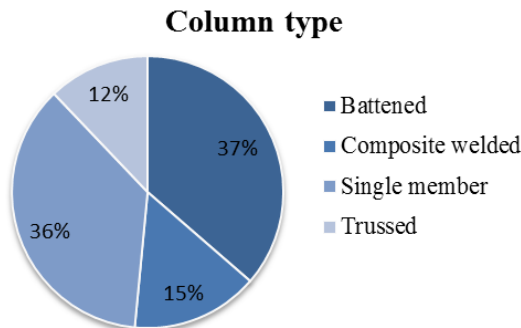


Figure 3.6 Typology of column of surveyed steel structures used for production.

Regarding PRC structures, two structural typologies were observed: workshops with prismatic beams (planar or pitched, with several cross section geometries) and trussed structures. The first is generally used for spans up to 30 meters, while the second is more suitable for spans from 15 to 40 m or more. This latter category of PRC structures was largely used in Italy until ‘70s, while today steel or aluminium structures are preferred for large spans (Capozzi, 2009). The above is reflected by the composition of PRC surveyed structures in terms of age of construction, reported in Figure (3.7). Figure (3.8) summarises the type of beam and of roofing elements observed in the investigated structures. It can be noticed that the 68% of the structures belong to the class of workshops with prismatic beams and the 32% to the one of trussed structures. Regarding columns, all the surveyed structures are characterised by rectangular cross sections, the dimensions of which are summarised in Figure (3.9).

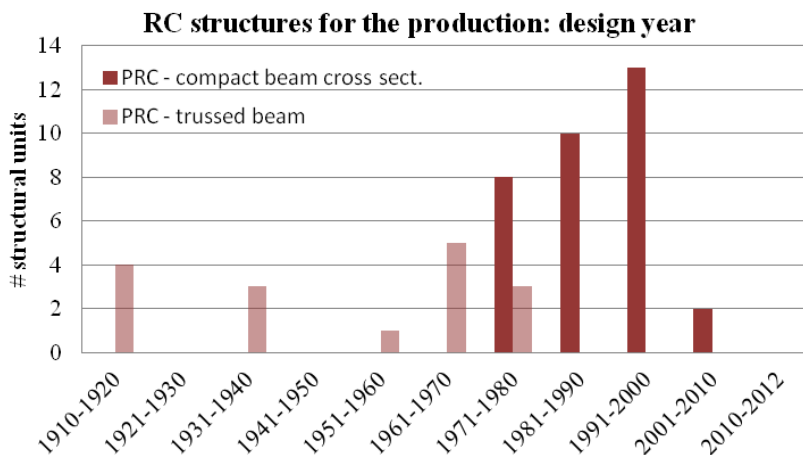


Figure 3.7 Design year of PRC structures used for production.

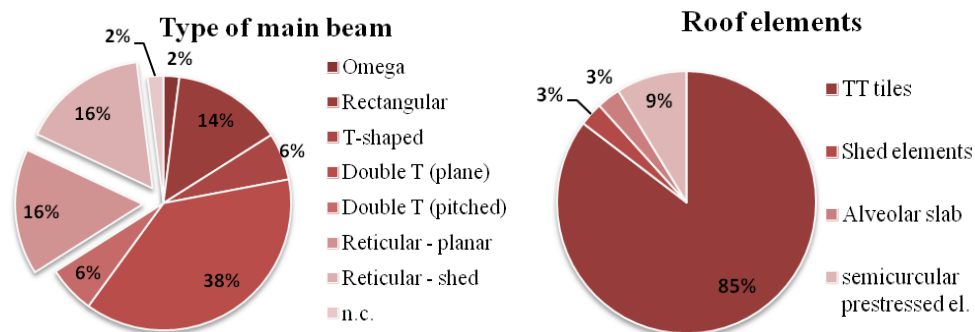


Figure 3.8 Types of main beams and roofing elements of surveyed PRC structures.

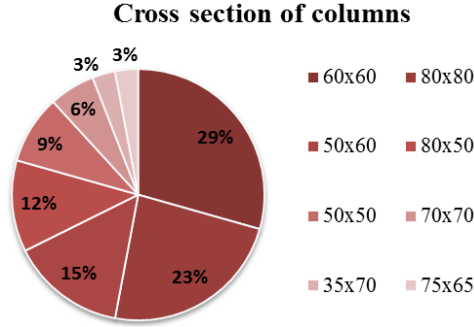


Figure 3.9 Column cross section dimensions of surveyed PRC structures.

The exposure of the production structures of the portfolio can be expressed either in terms of number of occupants and monetary loss (see Sect. 2.3.3). Regarding the former, the exposure of each production structure was assumed equal to the maximum number of occupants in a work shift; regarding the latter, the Property Damage (PD) of each production structure was summed to the Business Interruption (BI) of the whole plant, assuming that the interruption of activity in one production structure implies the interruption of any plant operation. The BI was computed considering both the plant BI (pBI), that is to say the losses undergone by the individual plant in case of a seismic event, and the group BI (gBI), that is to say the losses induced to other plants of the portfolio. These values are function of the typology, cope capacity and resilience of the supply chain of the specific industrial group and, in this case study, were provided by the portfolio manager. In the procedure outlined in Chapter 4, the economic loss (direct and indirect) and the potential for casualties are both expressed normalized by their maximum values. The Occupancy Loss Ratio (OLR) is, therefore, defined as the ratio of the number of occupants of the structure N_{occ} and the maximum number of occupants over the portfolio under consideration (Eq. 3.1). Similarly, the Economic Loss Ratio (ELR) is given by the total economic loss of the plant divided by the maximum total economic loss in the portfolio (Eq. 3.2).

$$OLR_i = \frac{N_{occ,i}}{\max\{N_{occ,i}\}} \quad (3.1)$$

$$ELR_i = \frac{PD_i + BI_i}{\max\{PD_i + BI_i\}} \quad (3.2)$$

These ratios are similar to the Loss Ratio employed in Jeiswal and Wald (2013) for computing economic losses worldwide, on the basis of macroeconomic indicators such as the gross domestic product and real earthquakes losses in the past.

The values of OLR and ELR for the production structures of the portfolio are shown in Table (3.3). From Figure (3.10) it can be observed that the most exposed plants in

terms of number of occupants are characterised by an average monetary loss and are located in the less hazardous sites.

Table 3.3 Number of production structures of case-study plants, ELR and OLR (*computed considering the cumulative occupants of all the structures of the plant).

Plant ID	Num. of production structures	OLR*	ELR
PLANT-01	4	0.50	0.48
PLANT-02	2	0.22	0.43
PLANT-03	1	0.06	0.43
PLANT-04	10	0.67	0.14
PLANT-05	8	0.27	0.43
PLANT-06	1	0.11	0.43
PLANT-07	5	0.11	0.14
PLANT-08	6	0.58	1.00
PLANT-09	4	0.58	0.43
PLANT-10	4	0.44	0.43
PLANT-11	3	0.21	0.43
PLANT-12	1	0.18	0.43
PLANT-13	2	0.18	0.26
PLANT-14	2	0.26	0.43
PLANT-15	6	0.89	0.35
PLANT-16	12	0.78	0.23
PLANT-17	4	0.78	0.42
PLANT-18	4	0.28	0.43
PLANT-19	4	1.00	0.58

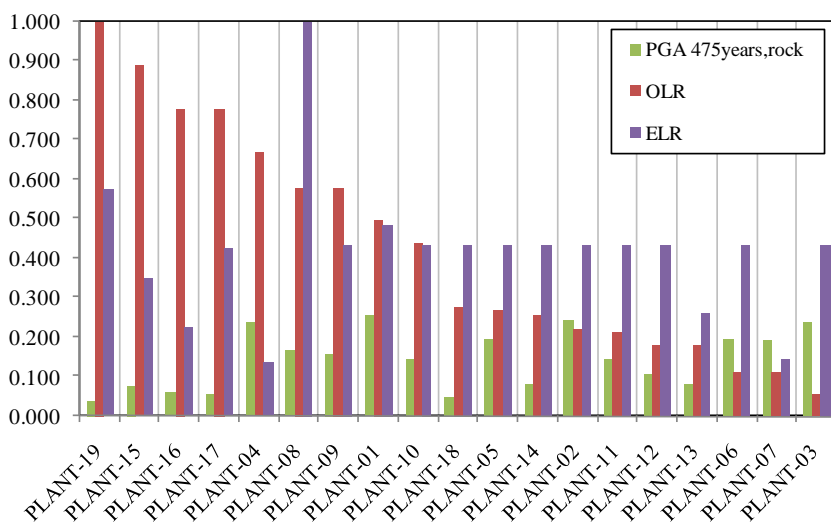


Figure 3.10 Case study plant ranked from left to right in order of decreasing OLR and respective values of ELR and of PGA with 475 year return period on rock.

3.2. Hazard form for industrial plants

As stated in the previous Section, principal aim of the Hazard forms is the characterization of the seismicity of the site where a plant is located, according to the best macroseismic intensity and hazard estimates available. The hazard form was developed specifically for the analysis of the case-study portfolio, therefore specific reference is made to INGV “S1” project deliverables, providing both macroseismic and hazard estimates. Notwithstanding, the structure of the form seems to be suitable also for the application in Countries where studies with a lower degree of accuracy are available. The hazard form, represented in Figures (3.11) and (3.12), are subdivided into different sections, described in the following.

Section1 - Plant location

In this section, data for the identification of the plant are reported, consisting in: name of the plant, complete address, Latitude and Longitude in decimal degrees and year of first construction of the plant. This information, if available, has to match the one included in the knowledge forms, presented in Section (3.3).

Section2 – Proximity to individual seismogenic sources

Typically, near fault (or near source) is the area surrounding an active source in a range approximately equal to the linear dimensions of the source. In the near source, both the shape and the type of seismic waves are considerably affected by the source characteristics, and hence by the faulting mechanism. The presence of near sources can lead to effects, in the case of an earthquake, including, inter alia, forward directivity which can be identified as velocity pulses in recorded ground motion time-histories. GMPEs and current probabilistic seismic hazard analysis are not able to capture such effect well, so that structures with dynamic behaviour in a range of periods related to the pulse period may be subjected to underestimated seismic demand (Chioccarelli and Iervolino, 2010).

Therefore, if specific studies are available, seismogenic sources in the proximity of the site should be identified. In the section 2 of the hazard form this issue is addressed and the identification of individual seismogenic sources (name, distance from the site and rate, if any) is required. Figures of the site location and of near seismogenic sources, if any, can be attached in the form.

For the case-study the INGV Database of Individual Seismogenic Sources (DISS) (Basili *et al.*, 2009) were used. The latter, in its latest release (v. 3.1.1) includes 100 individual seismogenic sources, over 100 composite seismogenic sources, and almost 30 debated seismogenic sources, based on geological/geophysical data and covering the whole Italian territory and some conterminous regions (Fig. 3.11).



Figure 3.11 Individual seismogenic sources according to DISS v.3.1.1 (Basili *et al.*, 2009), on Google earth view, 41°07'19.17''N 1°42'07.86''E, elev.-149m alt 1819.47km, 02/26/2013.

Section3 – Macroseismic Intensity

In this section the available data regarding macroseismic intensity at the site are reported. If macroseismic intensity is available at a site different from the one under consideration (but reasonably close to it), the location can be specified in the field “Reference Site”. For the specific case-study, the work by Albarello *et al.* (2007) was used as a reference for the estimates of macroseismic intensity. As already stated, this study provides macroseismic intensity with an exceedance probability of 10% in 50 years assuming two different GMPEs (I_G assuming a and a Gaussian GMPE and I_{bin} assuming a binomial GMPE), as reported in Fig. (3.12). The same study also provides the number of events felt at the site and the maximum macroseismic intensity felt at the site. This section is completed by the Munich-Re zonation. This is a macroseismic scale elaborated by Munich Reinsurance Company (Münchener Rückversicherungs-Gesellschaft), representing the reference scale in insurance and reinsurance world.

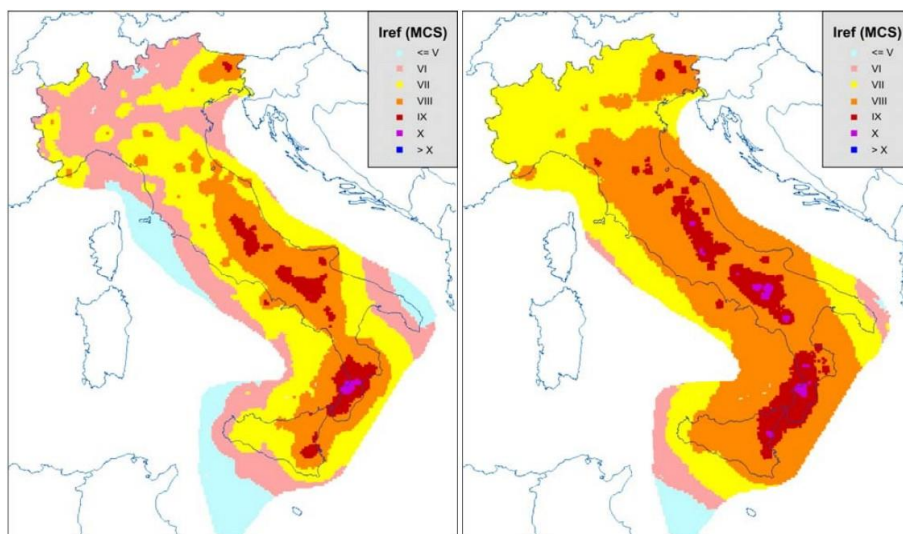


Figure 3.12 Macroseismic Intensity with 10% of probability of exceedance in 50 years employing a Gaussian GMPE (left) and a binomial GMPE (right) (Albarelo *et al.*, 2007)

Section 4 – Seismic hazard

In this section, hazard data are reported according to the most detailed study available. In particular it is required as a mandatory data the PGA on rock with a return period of 475 years obtained from GSHAP project (Giardini *et al.*, 1999). This value can be computed automatically from the tool presented in Chapter 5.

If other values of PGA, relative to different return periods or different studies, are available, they can be inserted in the form as optional data.

Hazard curves, if available, can be reported in this section, taking care to specify the type of curve (rate or probability and the reference time period), the adopted IM, the units, the subsoil category.

For the Italian case-study, the following data were used: the PGA corresponding to 9 return periods (from 30 to 2475 years) on rock (Meletti and Montaldo, 2007) and hazard curves on rock for 11 oscillation periods (Montaldo and Meletti, 2007). Uniform hazard spectra (UHS) for all the given return periods were also computed.

In this section also the current code for seismic design has to be indicated. This information, common to all the plants of the case study portfolio, assumes particular significance in the case of portfolios with structures distributed in different Countries. Finally, the Code-based elastic spectrum is also given.

Section 5 – Disaggregation of seismic hazard

In this section hazard disaggregation at the site is reported, if available. In the case of the plant portfolio under consideration the study by Spallarossa and Barani (2007) was

used for the characterization of the major contribution to the hazard in terms of Magnitude and Distance. This can be useful in the case of DSHA for individuating the reference scenario earthquake(s).

Section 6 – Geotechnical data

In this section the soil category according to EC8 is defined for the subsoil in the facility area. The assumption that this latter is the same for all the structures of the facility is implicitly done, nevertheless, in the case of large plan developments and different subsoil categories in different places of the plant area, the worst category should be indicated herein. This is the reason why the characterization of subsoil is also contained in the Knowledge forms of each individual structure (see next Section). Different kinds of information can be used for the assessment, from the less correlated to seismic wave propagation to the most: stratigraphy with indication of the soil qualitative typology; penetrometric field tests (e.g. cone penetration test, standard penetration test, etc.); laboratory tests (e.g. oedometric test, triaxial cell, etc.); shear wave propagation velocity measurements (e.g. cross hole, down hole, etc.). In the case of plants located in different countries, subsoil would be characterised according to different classifications. In this cases it is possible to obtain the required EC8 classification on the basis of shear wave velocity using conversions such as the one reported in Table (3.4).

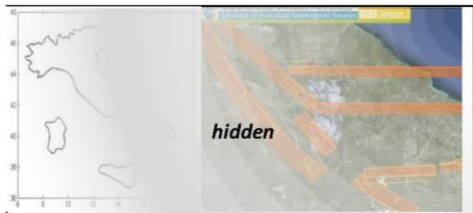
Table 3.4 Comparison of soil classification in modern seismic codes worldwide (Pitilakis *et al.*, 2004).

$V_{s,30}$ (m/sec)	180	360	760	1500
UBC/97 IBC/2000	S_E	S_D	S_C	S_B S_A
GREEK SEISMIC CODE EAK2000	D – C	C B	A	A
EC8 (ENV1998)	C	C B	A	A
EC8 (prEN1998) (Draft4, 2001)	D	C	B	A
New Zealand, 2000 (Draft)	D ($T > 0.6s$ $\Rightarrow V_{s,30} < 200$)	C ($T < 0.6s$ $\Rightarrow V_{s,30} > 200$)	B	A
Japan, 1998 (Highway Bridges)	III ($T > 0.6s \rightarrow V_{s,30} < 200$)	II (I) ($T = 0.2-0.6 s \rightarrow V_{s,30} = 200-600$)	I ($T < 0.2s \rightarrow V_{s,30} > 600$)	
Turkey/98	$Z_4 - Z_3$	$Z_3 - Z_2$	$Z_3 - Z_2 - Z_1$	Z_1
AFPS/90	$S_3 - S_2$	$S_3 - S_2 - S_1$	$S_1 - S_0$	S_0

HAZARD FORM

Form number	1
-------------	----------

Section 1 - Plant Location	
Name	hidden
Address	hidden
ZIP code	hidden
Municipality	hidden
State	hidden
Latitude [°deg]	hidden
Longitude [°deg]	hidden
Plant construction year	hidden



Section 2 - Proximity to individual seismicogenic sources (for Italy: DISS v.3, 2009)			
Sources in the range of 50 km	Name	distance	Rate
hidden	hidden	hidden	hidden

Section 3 - Macroseismic Intensity (for Italy: Progetto S1, 2004)			
Reference site: hidden	Lat [°deg]: hidden	Long [°deg]: hidden	
Macroseismic Intensity with return period 475 years:	IX (Binomial GMPE)	IX (Gaussian GMPE)	
Number of events felt at the site:	35		
Maximum macroseismic intensity observed at the site:	IX-X		
Munich-Re zone:	3		

Section 4 - Seismic Hazard (for Italy: Progetto S1, 2004)			
Reference site: hidden	Lat [°deg]: hidden	Long [°deg]: hidden	
Peak ground Acceleration [g] su suolo A		16 th perc. <input type="checkbox"/>	50 th perc. <input checked="" type="checkbox"/>
84 th perc. <input type="checkbox"/>			
T _R [years]	Exceedance probability in 50 yrs.	PGA [g] on rock	
30	81%	0.0772	
50	63%	0.1014	
72	50%	0.1199	
101	39%	0.1397	
140	30%	0.1611	
201	22%	0.1875	
475	10%	0.2562	
975	5%	0.3280	
2475	2%	0.4449	

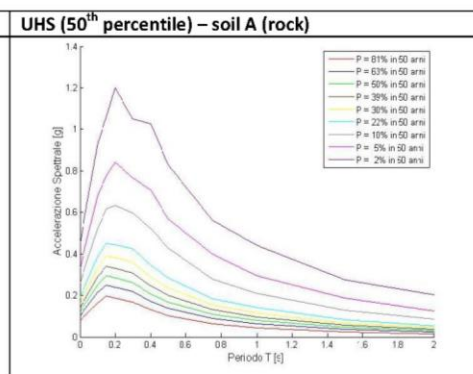
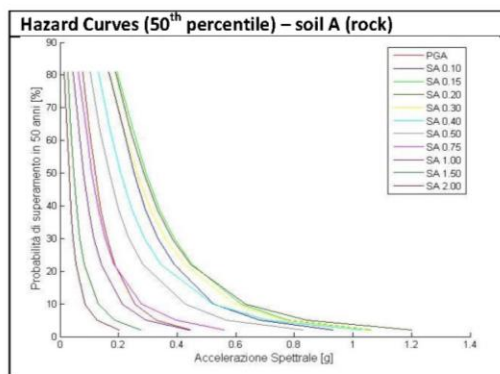


Figure 3.13 Hazard form (1/2)

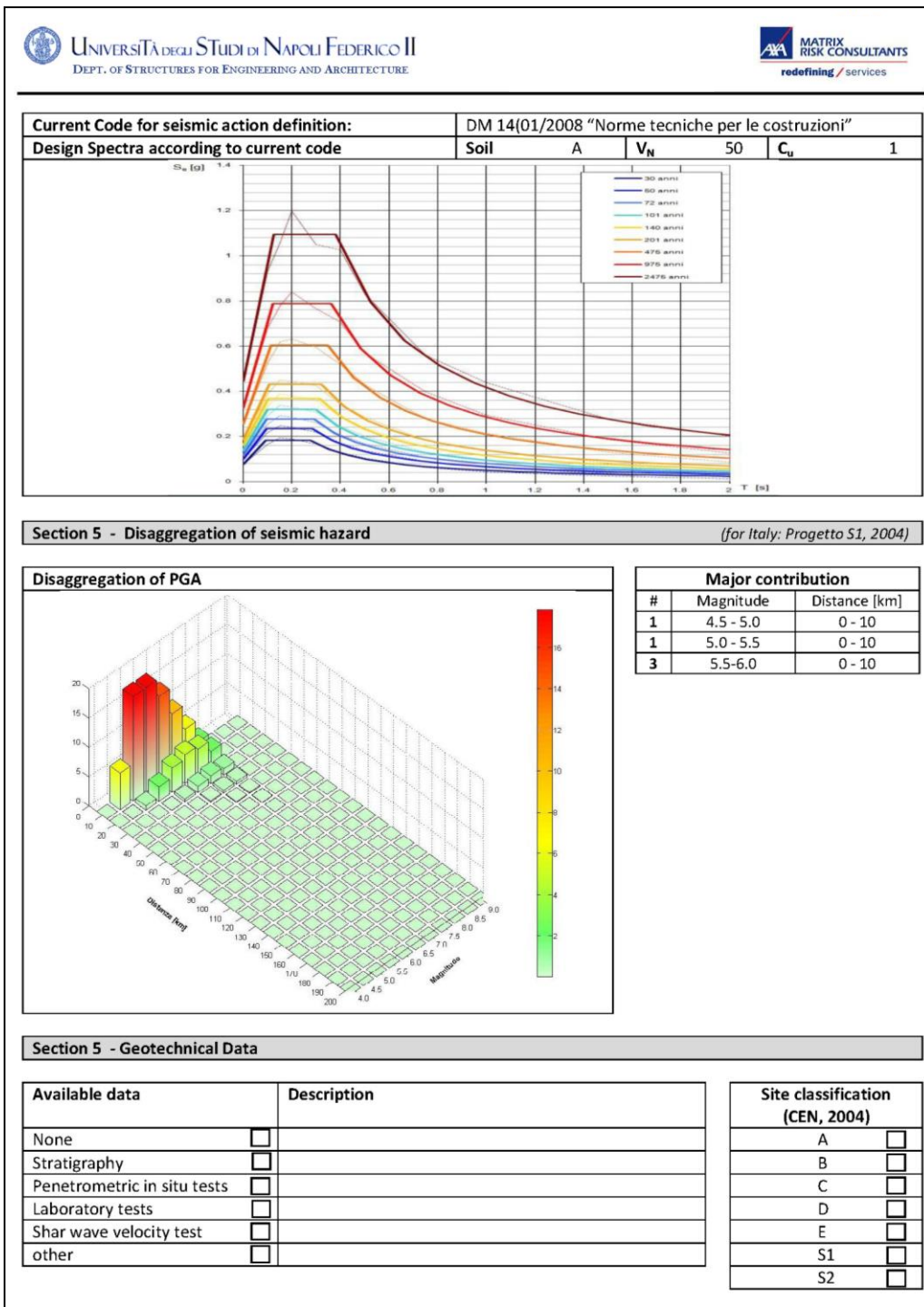


Figure 3.14 Hazard form (2/2)

3.3. Knowledge Forms for industrial manufacturing plants

Knowledge forms were developed in order to investigate the structures of the case-study portfolio and, more in general, to provide tools for achieving the level of knowledge about industrial plants necessary to perform the procedures discussed in this thesis. More specifically, three kinds of knowledge forms were developed:

- plant layout knowledge form;
- building-like structures knowledge form;
- tanks/silos knowledge form.

These forms are aimed at investigating the more typical structures in manufacturing industry; therefore they are not intended for those industrial sectors in which the main structural typology is non-building-like.

For each plant a single *plant layout knowledge form* has to be compiled first, allowing to identify the structural units composing the plant and their design year. Subsequently, for each building-like structure, a *building-like structures knowledge form* is compiled and for each tank or silos a *tanks/silos knowledge form* is filled as well. All the above mentioned knowledge forms require, at least, a visual survey of the structures composing the plant and they were developed to be used by an un-expert subject (e.g. the stakeholder of the plant).

3.3.1. Plant layout knowledge form

The principal objectives of the plant layout knowledge form are:

- the identification of structural aggregates;
- the characterization of each structural unit in terms of main geometrical dimensions and age of design;
- the identification of foundation soil characteristics;
- the characterization of the exposed value in terms of monetary loss for the whole plant;
- the characterization of occupancy and exposure for each structure, expressed in terms of number of occupants.

This form, depicted in Figures (3.16) to (3.17), is composed by the following sections:

Section 1 – General information about the plant

In this section the information needed for the identification of the plant in the portfolio is reported, i.e. the plant name, address and geographical coordinates (in decimal degrees). The number of the corresponding Hazard Form (Sect. 3.2) is also reported.

Section 2 – Information about the compiler

In this section the name, qualification, contacts and signature of the compiler are reported as well as the date of the survey.

Section 3 – Plant Layout

In this section the plant layout is sketched and each building aggregate or tank/silo structure is identified by a progressive number or letter, namely ID (Fig. 3.15) . This ID can be, as an example, composed as follows:

$$\text{buildID} = \text{PL_OCC\#} \quad (3.3)$$

where “PL” indicates the plant name; “OCC” is an abbreviation of the aggregate occupancy and “#” is a progressive number. In Figure (3.15) an example of identification of buildings, aggregates or tank/silo structures is reported. The abbreviations “WS”, “OFF”, “U” and “T” were used, respectively, for addressing workshops, offices, utilities and tanks or silos.

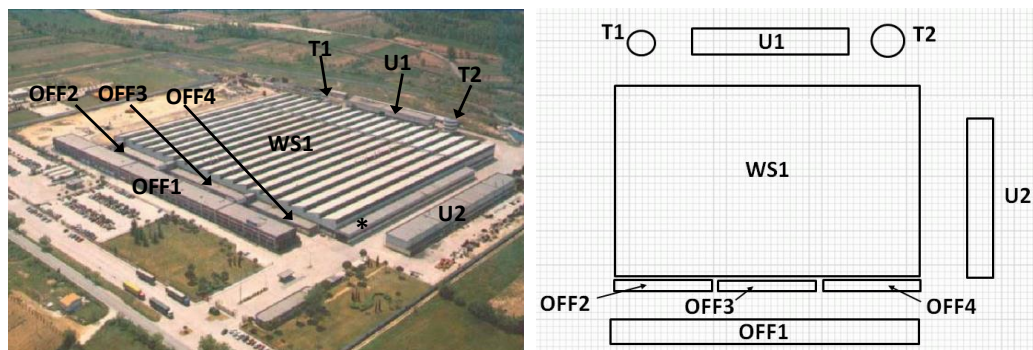


Figure 3.15 Example of identification of structural aggregates. The * in the left panel refers to a structure for loading/unloading finished products not belonging to those under investigation that is, therefore, neglected.

Section 4 – Building aggregate characteristics

In this section each building aggregate or tank/silo structure, identified in the previous step, is characterized in terms of occupancy (production, offices, utilities or storage), activities carried out in it, number of occupants per shift and number of shifts per day.

Section 5 – Topographic and Geotechnical Information

In this section information about topography of the site (plant located in plane, slope or ridge), altitude and geotechnical data are reported. The objective of this latter information is the classification of subsoil according to EC8. The same discussed in Hazard Forms applies in this section.

Section 6 – Exposed Value

Information about exposed value of the whole plant, expressed in monetary terms, are reported in this section. In particular it is necessary to indicate the total Property Damage (PD), that is to say the direct damage related to the loss of all the structures and goods of the plant, and the Business Interruption (BI), possibly subdivided in Plant BI (pBI) and Group BI (gBI).

The information about PD is believed to be available to the stakeholder or the plant manager, since it is commonly used in maximum foreseeable loss scenario for other industrial risks (e.g. fire). On the contrary, the information about BI , and in particular about gBI, is likely to be in the disposal of the portfolio manager.

Section 7 – Notes

In this section any kind of additional information (e.g. plant layout of structure or production lines, supply chain information, etc.), attachments and even problems encountered during the drafting can be reported.



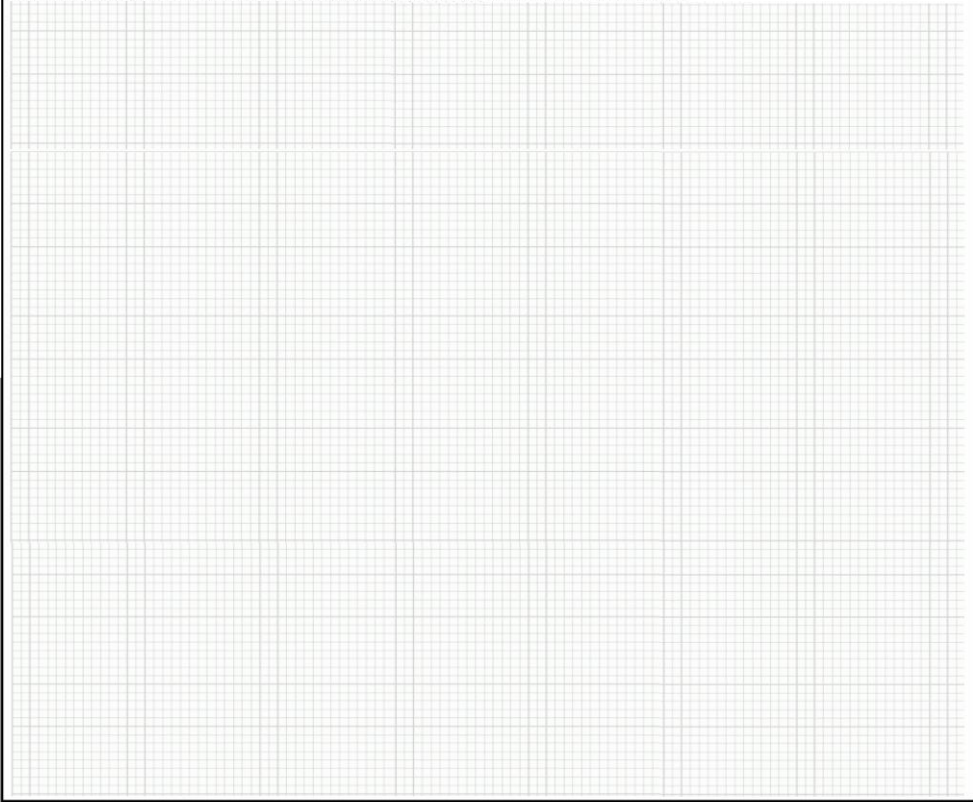
Plant Layout	 PLANT LAYOUT KNOWLEDGE FORM		Plant Layout						
SECTION 1 - General information about the plant		SEZIONE 2 - Informazioni relative al Compilatore							
1a)	Plant Name	2a)	Compiler						
1b)	Address	2b)	Qualification						
1c)	Municipality, ZIP Code	2c)	Contacts						
1d)	LAT / LON [° dec]	2d)	Signature						
1e)	# Hazard Form	2e)	date						
SECTION 3 - Plant Layout									
sketch of plant layout and identify each building aggregate or tank/silo structure by a progressive number or letter (ID)									
									
SECTION 4 - Building aggregate characteristics									
4a)	ID	4b)	occupancy	4c)	description of activities and/or contents	4d)	occup/shift	4e)	shifts/day

Figure 3.16 Plant layout form (1/2).

SECTION 5 - Topographic and Geotechnical Information	
5a) Topography: <input type="checkbox"/> plant located in plane <input type="checkbox"/> slope <input type="checkbox"/> ridge	site altitude: _____ over the sea level
5b) Available information about local geology: <input type="checkbox"/> stratigraphy <input type="checkbox"/> documents about in situ or laboratory tests <input type="checkbox"/> no documentation available	Allegato : _____ Allegato : _____
5c) Foundation soil category according to Eurocode 8 (CEN, 2004) <input type="checkbox"/> subsoil category (A,B,C;D,E,S1,S2) : _____ <input type="checkbox"/> unknown	
SECTION 6 - Exposed Value	
6a) Property Damage Plant property damage (maximum foreseeable loss of the plant) :	_____ units: _____
6b) Business Interruption Plant Business Interruption (pBI): Group Business Interruption (gBI):	_____ units: _____ _____ units: _____
SEZIONE 7 - Note	

Figure 3.17 Plant layout forms (2/2).

3.3.2. Building-like structures knowledge form

Building-like structures represent the most spread typology of structures in manufacturing industry, therefore their knowledge should be, in principle, the most detailed as possible. Nevertheless, the process of acquiring knowledge about the structures of a portfolio could be demanding in terms of time and costs, due to the amount of structures to investigate. Moreover, in some cases, acquiring detailed information could imply the business interruption (e.g. in situ measurements of strengths of construction materials in a production zone) and therefore could be unfeasible or not justified by the actual risk of the structure under investigation. For these reasons “first level” knowledge forms were developed, on the basis of GNDT forms for industrial structures (GNDT,1993) and of the work by Ricci (2010). The proposed survey forms reflect the level of knowledge about the structures of the portfolio required by the procedures dealt in this thesis. As already stated, these forms are aimed at achieving a level of knowledge sufficient to perform a prioritization analysis over the portfolio. Their drafting can be performed by an un-expert subject

and their output is made of qualitative information about structural age of construction, typology and building materials and some limited information about geometry.

The sections composing the first level building-like structures knowledge form are described in the following.

Section 1 – Identification of the building/structural aggregate

This section reproduces the Section 4 of the *Plant layout knowledge form*. This is required in order to ensure coherency between each building form and the plant form. Therefore, the ID of the structural aggregate, occupancy (production, offices, utilities or storage), activities carried out in it and exposure, in terms of occupants, must be reported.

Section 2 – Information about the compiler

The same information reported in the *Plant layout knowledge form* has to be reported.

Section 3 – Main geometry of building/structural aggregate

In this section main geometric dimensions of the structural aggregate are reported both in plan and elevation. The compiler has to identify the plan shape of the aggregate and quantify the main dimensions. Regarding elevation, structures with plan roof have to be distinguished from structures with pitched roof. In both cases main geometric dimensions have to be given. Finally a front view of the structural aggregate must be depicted from the two plan directions.

Section 4 – Individuation of structural units and year of design/construction

In this section individual structural units composing the building aggregate must be identified by means of a progressive number or letter and sketched in the form. The structural unit ID (*StrUnitID*) should include the building ID defined in Eq. (3.1), the acronym “SU” and a progressive number, as reported in the following expression:

$$StrUnitID = buildID_SU \# = PL_OCC \#_SU \# \quad (3.4)$$

An example of identification of structural units composing the workshop “WS1” of Figure (3.15) is reported in Figure (3.18).

In this phase the identification of structural joints and their dimensions is required. Moreover, the age of design or at least, if this information is not available, the year of construction, must be indicated for each structural unit. It is believed that this can be done through the collection of the documentation available in the plant regarding the original design. The identification of the structural unit geometry is completed by the length, the number of bays and the average span length of the single bay in both the plan dimensions.

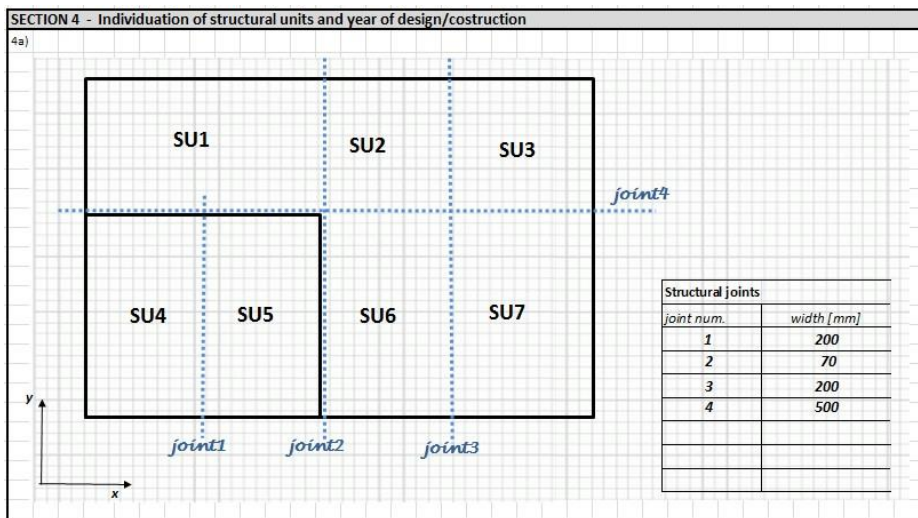


Figure 3.18 Example of identification of individual structural units and relative age of design.

Section 5 – Main structural characteristics

In this section the main characteristics of vertical and horizontal elements are surveyed. It is important to underline that this section of the form was developed in order to be applied to any kind of structural material, and that its aim is uniquely a qualitative characterization of the structures.

Regarding vertical elements, it is first required to indicate the construction material, then to sketch the cross section of columns (if the structure is a frame one) and to indicate the presence of structural walls, cores or vertical bracings, if any. Some qualitative information is given about beam-column joints.

Regarding horizontal elements, beam construction material and type are reported. In the case of steel elements, it is required to indicate if connections are bolted or welded. Information about the slabs is also collected (construction material and thickness of the generic slab and of roof slab), as well as about the presence of roof bracings.

Section 6 – Other documents

In this section any document relative to the design, photo, structural sketch, production layout can be attached to the form or indicated as available at the plant.

Building	 UNIVERSITA' DEGLI STUDI DI NAPOLI FEDERICO II Dept. of Structures for Engineering and Architecture	 MATRIX RISK CONSULTANTS redefining / services	Building																		
FIRST LEVEL BUILDING-LIKE STRUCTURES KNOWLEDGE FORM																					
SECTION 1 - Plant Location		SEZIONE 2 - Compiler information																			
1a) ID (coherent with Layout form) : _____		2a) Compiler _____																			
1b) Occupancy _____		2b) Qualification _____																			
1c) Activities: _____		2c) Contacts _____																			
		2d) Signature _____																			
SECTION 3 - Geometric Data																					
section 3.1) plan data		section 3.2) elevation data																			
<input type="checkbox"/> 3.1.a) rectangular L1 [m] _____ L2 [m] _____	<input type="checkbox"/> 3.1.b) L-shaped L1 [m] _____ L2 [m] _____ L3 [m] _____ L4 [m] _____ L5 [m] _____ L6 [m] _____	<input type="checkbox"/> 3.1.c) T-shaped L1 [m] _____ L2 [m] _____ L3 [m] _____ L4 [m] _____ L5 [m] _____ L6 [m] _____	<input type="checkbox"/> 3.2.a) planar roof n _{floors above ground} _____ n _{underground floors} _____ H _{curr} [m] _____ H _{und} [m] _____ H _{max} [m] : _____																		
<input type="checkbox"/> 3.1.d) C-shaped L1 [m] _____ L2 [m] _____ L3 [m] _____ L4 [m] _____ L5 [m] _____ L6 [m] _____	<input type="checkbox"/> 3.1.e) Z-shaped L1 [m] _____ L2 [m] _____ L3 [m] _____ L4 [m] _____ L5 [m] _____ L6 [m] _____ L7 [m] _____ L8 [m] _____	<input type="checkbox"/> 3.1.f) multiple Z shape L1 [m] _____ L2 [m] _____ L3 [m] _____ n _____ m _____	<input type="checkbox"/> 3.2.b) pitched roof n _{floors above ground} _____ n _{underground floors} _____ H _{curr} [m] _____ H _{und} [m] _____ H _{max} [m] : _____ H _u [m] : _____ α [°]: _____ β [°]: _____																		
view of x side: _____			view of y side: _____																		
SECTION 4 - Individuation of structural units and year of design/costruction																					
4a)																					
			<table border="1" style="width: 100%; border-collapse: collapse;"> <thead> <tr> <th colspan="2">Structural joints</th> </tr> <tr> <th>joint num.</th> <th>width [mm]</th> </tr> </thead> <tbody> <tr><td> </td><td> </td></tr> <tr><td> </td><td> </td></tr> <tr><td> </td><td> </td></tr> <tr><td> </td><td> </td></tr> <tr><td> </td><td> </td></tr> <tr><td> </td><td> </td></tr> <tr><td> </td><td> </td></tr> </tbody> </table>	Structural joints		joint num.	width [mm]														
Structural joints																					
joint num.	width [mm]																				

Figure 3.19 First level building-like structures knowledge form (1/2).

4b) Structural units

Struct. Unit	design year	length,x [m]	length,y [m]	number bays,x	avg. Bay length, x [m]	number bays,y	avg. Bay length,y [m]

SECTION 5 - Main structural characteristics

5.1) VERTICAL RESISTING ELEMENTS

5.1.a) construction material

Cast in place R.C.

Precast R.C.

Masonry

Steel bolted

welded

5.1.c) Load resisting structure

Frame

walls

nucleous

unknown

A[m]: _____ B[m]: _____

A[m]: _____ B[m]: _____

5.2) BEAMS

5.2.a) construction material

Cast in place R.C.

Precast R.C.

Steel

Wood

5.2.b) X direction

unknown (because of: _____)

shape: _____

5.2.c) Y direction

unknown (because of: _____)

shape: _____

section:

view:

section:

view:

5.3) SLABS and ROOF

SLAB OF THE GENERIC STOREY

5.3.a) construction material

Cast in place R.C.

Precast R.C.

corrugated steel sheet

other: _____

unknown (because of: _____)

thickness [cm]: _____

ROOF

5.3.b) construction material

Cast in place R.C.

Precast R.C.

corrugated steel sheet

other: _____

unknown (because of: _____)

thickness [cm]: _____

5.3.c) roof bracings

none

shape: _____

5.3.d) transversal bracings (e.g. between beams)

none

shape: _____

SEZIONE 6 - Other Documents

Num attach.	Type of attachment				acquisition		ref. Section	Note
	Foto	drawing	file	other	attached	available		
					<input type="checkbox"/>	<input type="checkbox"/>		
					<input type="checkbox"/>	<input type="checkbox"/>		
					<input type="checkbox"/>	<input type="checkbox"/>		
					<input type="checkbox"/>	<input type="checkbox"/>		

SECTION 7 - Note

Figure 3.20 First level building-like structures knowledge form (2/2).

3.3.3. Silos/tanks knowledge form

Tanks and silos are certainly two of the most common non-building like structures in manufacturing industry. Several studies in literature have been aimed at the definition of the seismic vulnerability of silos or tanks, especially for those employed in the process industry due to the hazardous materials stocked in them (e.g. Iervolino *et al.*, 2004; Fabbrocino *et al.*, 2005). Notwithstanding, such structures are certainly of primary importance even in manufacturing industry, since they are very often essential to the production (e.g. stocking of raw materials) or to the safety of the plant (e.g. water tanks for fire protection).

For these reasons, forms specifically targeted at the surveying of tanks for liquids at atmospheric pressure or silos for granular content were developed (Fig. 3.21). Pressurised vessels are not addressed at this level of investigation.

For each of tank or silo of the plant, a single form has to be compiled. Similarly to the other forms, they are composed of: two sections regarding, respectively, the identification of the structure inside the plant (*Section 1*) and information about the compiler (*Section 2*), a section (*Section 3*) of general characteristics such as construction material, type of cover (fixed/floating), base anchorage system and type of pipeline connection (rigid/flexible). The form is completed by a section regarding geometric characteristics (Section 4) subdivided into two subsections for tanks and silos. In both cases information about dimensions, average fill ratio, foundation type and dimensions are required, together with indications regarding the eventual connection to other structures.



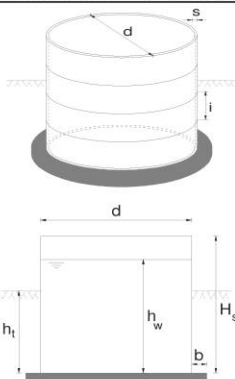
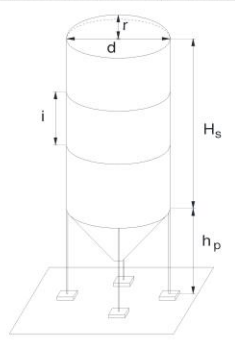

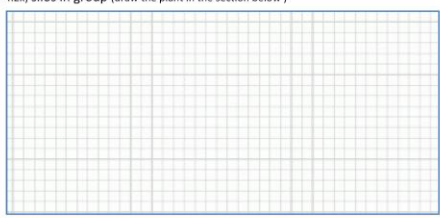
Tank/Silo	 UNIVERSITÀ DEGLI STUDI DI NAPOLI FEDERICO II Dept. of Structures for Engineering and Architecture	 MATRIX RISK CONSULTANTS redefining services	Tank/Silo
TANKS/SILOS KNOWLEDGE FORM			
SECTION 1 - Identification of the structure		SEZIONE 2 - Compiler information	
1a) ID (coherent with Plant Layout Form): _____		2a) Compiler _____	
1b) Content: _____		2b) Qualification _____	
1c) function: <input type="checkbox"/> fire protection		2c) Contacts _____	
<input type="checkbox"/> other: _____		2d) Signature _____	
SECTION 3 - General Characteristics			
3a) Construction Material		3b) Type of cover/roof	
<input type="checkbox"/> Steel <input type="checkbox"/> RC <input type="checkbox"/> Fiber reinforced polymer (FRP) <input type="checkbox"/> Plastic material (PE, PVDF, PP, PVC,...) <input type="checkbox"/> other: _____		<input type="checkbox"/> fixed <input type="checkbox"/> floating	
		3c) base anchorage	
		<input type="checkbox"/> none <input type="checkbox"/> type: _____ note: _____	
		3d) pipeline connection	
		<input type="checkbox"/> flexible connection <input type="checkbox"/> rigid connection	
SECTION 4 - Geometric data			
<input type="checkbox"/> 4.1) Atmospheric pressure tank for liquids, continuously grounded to the foundation			
		4.1a) diameter d [m]: _____ In case of rectangular tank, indicate the plan dimensions A [m]: _____ B [m]: _____	
		4.1b) height of the top from the foundation H _s [m]: _____	
		4.1c) average height of the fill level h _w [m]: _____	
		4.1d) average height of ground covering h _t [m]: _____	
		4.1e) width of the foundation outside the tank b [m]: _____	
		4.1f) thickness s [mm]: _____	
		4.1g) number of segments n : _____	
		4.1h) distance between segments i [m]: _____	
		4.1i) adjacent structures	
		<input type="checkbox"/> isolated <input type="checkbox"/> anchored to other structure: { adjacent structures ID: _____ number/type of joints: _____	
<input type="checkbox"/> 4.2) strutture su appoggi discreti (silos, serbatoi non poggiati direttamente alla fondazione,...)			
		4.2a) d [m]: _____ In case of rectangular tank, indicate the plan dimensions A [m]: _____ B [m]: _____ B [m]: _____	
		4.2b) shaft length H _s [m]: _____	
		4.2c) dome radius r [m]: _____	
		4.2d) average height of the fill level h _w [m]: _____	
		4.2e) thickness of the shaft s [mm]: _____	
		4.2f) number of segments n : _____	
		4.1h) distance between segments i [m]: _____	
		4.2h) legs number: n _{app} [m]: _____ legs height h _p [m]: _____	
		4.2i) adjacent structures	
		<input type="checkbox"/> isolated <input type="checkbox"/> anchored to other structure: { adjacent structures ID: _____ number/type of joints: _____	
<input type="checkbox"/> 4.2j) bracings (draw the section in the section below)		<input type="checkbox"/> 4.2k) silos in group (draw the plant in the section below)	
			

Figure 3.21 Silos/Tanks knowledge form.

Chapter 4 – RISK PRIORITIZATION BASED ON NOMINAL DEFICIT

4.1. Introduction

In this Chapter the “large scale” procedure outlined in Chapter 1 is presented. Such a procedure is aimed at providing aid in risk management and decision making for large structural portfolios, characterized by hundreds to thousands of buildings.

Risk management at a large scale requires low-input methodologies able to provide an, even rough and/or conventional, assessment of the relative seismic risk. In fact, at a regional or national level, or more in general when the portfolio under investigation is composed of hundreds or thousands of buildings, an evaluation of seismic vulnerability by means of analytical methods based on refined mechanical modelling is generally not feasible, due to the amount of information and the computational effort required.

Among the different options for vulnerability assessment of large portfolios, a code-based approach is adopted, i.e. based on the comparison of code requirements at the time of design and current seismic demand (so-called “nominal deficit”). This represent an attempt to define a relative (to the population under investigation), yet quantitative and structure-specific, seismic risk measure for a first sight ranking to identify a fraction of the portfolio deserving deeper investigation.

The evolution of design principles and seismic actions in National codes, renders this kind of approach worth of further investigation. In fact, it is expected that the current seismic demand is larger than any previously enforced; this is due to both the increasing trend of hazard estimates (see Bommer and Abrahamson, 2006 for a discussion) and the evolution of seismic design codes. According to this, the comparison between the current seismic demand and the one enforced at the time of design can be considered a proxy for the seismic performance gap of an existing structure with respect to the current seismic demand.

Despite risk metrics based on “nominal deficit” are based on strong assumptions, they have the advantage of requiring easy-to-retrieve data, at least year of design and location, that can be, reasonably, obtained from census data or directly from the handler of the structure (in the case of large industrial groups, the manager of each plant) so that an “off-line” assessment (i.e. without visual survey) can be performed.

Anyway, if the size of the portfolio and the available resources allow for it, a rapid visual screening could be used for surveying simple structural and site characteristics,

such structural typology, geometry, and subsoil class, that can be used to improve an “off-line” assessment of nominal deficit.

In the following, a review of decision-making frameworks and prioritization approaches is given first and the scientific mainstream of nominal risk indices is discussed (Section 4.2). A proposed approach for risk management is then presented (Section 4.3) and critically discussed with respect to underlying assumptions, critical issues, limitations, and implications (Section 4.4). This approach was developed for the Italian building portfolio case study presented Chapter 3, therefore the evolution of design provisions and seismic hazard classification in Italy is analysed (Sections 4.5. and 4.6).

A prototypal software, namely NODE v.1.1, beta enabling a rapid evaluation of the horizontal performance requirements (due to earthquake and wind) for Italian constructions at any site between 1909 and today, is then introduced (Section 4.7). It allows to assess location-specific code-based design standards, thus to compute nominal risk proxies automatically for large population of buildings.

Finally, the proposed risk management approach was developed with specific reference to the Italian case and applied to the case-study portfolio of structures (Section 4.8) and conclusions are drawn (Section 4.9).

4.2. Review of decision-making frameworks and prioritization approaches

A rational approach to the reduction of seismic risk of building portfolios requires the evaluation of each of the three elements of the risk equation discussed in Chapter 2, i.e. hazard, vulnerability and exposure, and an evaluation of time of intervention and risk management strategies. This could be done, in principle, by means of multiple quantitative loss assessments iterations implementing the chosen mitigation strategies, over the whole building portfolio, according to the procedure discussed in Section (2.2). In the case of large portfolios, the limited amount of resources, in terms of time and costs, for investigating the building stock and assessing the loss, makes risk management based on loss assessment hardly feasible.

For this reason, several risk management procedures were developed in literature providing measures of seismic risk, alternate to the actual loss, and aiding the decision making. These approaches significantly differ from one another, depending on the structure portfolio to which they are applied and to the goals of the analysis. Generally speaking, such frameworks are characterized by one or more of the following:

- a prioritization phase ranking structures in order of risk;
- a multistep approach to vulnerability or hazard assessment;

- minimum capacity levels below which intervention or further analysis steps is required;
- minimum performance objectives for each mitigation strategy;
- time for implementing mitigation strategies.

Depending on the methodology employed for the computation of vulnerability (see Section 2.3), these frameworks can be distinguished, into:

- screening procedures;
- code-based procedures;
- simplified analytical procedures.

Screening procedures employ visual surveys and, in many cases, expert judgment to define a relative measure of vulnerability. A relative measure of vulnerability is also provided by code-based procedures, which employ the provisions enforced at the time of design to define the current vulnerability. Simplified analytical procedures, on the contrary, compute seismic vulnerability on the basis of a mechanical modelling, more or less detailed as a function of the dimensions of the portfolio and the possibility of gathering information about structural characteristics. This approach can be used in risk management framework in order to provide both relative and absolute measures of the vulnerability and, therefore, of the risk.

It has to be noticed that, in case of multilevel frameworks, different approaches to vulnerability assessment can be employed in different steps.

Some of the approaches developed in literature are briefly reviewed in the following.

Risk management frameworks based on solely economic considerations (e.g. Albanesi *et al.*, 1994) are not dealt in the following, as well as methodologies developed with the specific purpose of assessing the damage to structures following an earthquake, in order to guide decision on continued occupancy (e.g. Anagnostopolous *et al.*, 1989).

4.2.1. Screening procedures

A typical field of application or prioritization approaches is the rehabilitation of bridges and hospitals. In most cases, these approaches determine priorities on the basis of a simple screening procedure, aimed at the computation of score-based indices. This is, in general, made by the identification of predefined vulnerability factors by expert judgment and/or by the definition of the importance of the structure (see Section 2.3.2). Vasishth *et al.*, (1995) proposed a seismic prioritization scheme for the Washington State's bridges. The procedure consists in a first ranking of bridges on the basis of their structural typology, from the most vulnerable (bridges with in-span hinges and simply supported superstructure) to the less (multiple columns bridges and those already programmed for retrofitting). Then, a prioritization index is defined as the product of a Criticality Factor and a Vulnerability Factor. The former is a weighted product of

factors depending on the exposure and importance of the bridge in the road network; the latter takes into account hazard, structural deficiencies and remaining service life. The priority ranking obtained by the application of this methodology was used for further elastic and inelastic analyses, followed by retrofitting.

The inspection procedure for prioritization proposed by Chapman *et al.* (2000) for the rehabilitation of bridges in New Zealand, is composed of 11 stages characterised by increasing engineering specialisation, to gradually reduce the inventory size. The first four stages prominently consist in gathering data and individuating structures with higher vulnerability and consequences in the case of collapse.

In the fifth stage an index, namely Seismic Attributes Grades (SAG), is computed as the weighted score of some hazard, vulnerability and exposure parameters. This index is used to define the portion of the portfolio to investigate more deeply in the stages 6 to 8. The stage 9 consists in the identification of structural weaknesses by a specialist bridge engineer survey and the stage 10 is an economic evaluation, including consequences of disruption of the road network and cost of retrofit. Finally, the stage 11 is the collection of all the data in a single ranking.

Similarly, the California hospital rehabilitation programme (Holmes, 2002) consists in the evaluation of a compliance priority rating index, P , defined as the product of a structure deficiency index, taking into account vulnerability, and an essential function exposure, accounting for the presence of critical equipment, contents and number of beds. This approach also provides simple indication about the number of years to retrofit the structure from the time of inspection. This programme was not actually adopted for the retrofitting of the Californian hospitals, but the computation of the P index, in conjunction with information about fault proximity, was employed for the definition of five Structural Performance Categories (SPCs) and five Non-structural Performance Categories (NPCs) for the categorization of hospitals.

Screening procedures based on visual surveys are also available in literature. the Field Evaluation Method (Culver *et al.*, 1975), based on five forms to be filled after visual surveys, regarding vertical and horizontal resisting elements, capacity ratio, intensity level and overall judgement of building seismic safety. This information is then used to classify the building as “good”, “fair”, “poor” and “very poor”.

Another example is the Japanese Seismic Index Method (JBDPA, 1990), based on the definition of seismic performance index, I_S , evaluated by means of a screening procedure, that can be performed at three increasing levels of accuracy. The I_S index is calculated for each storey in every frame direction according to the following expression:

$$I_S = E_0 \cdot S_D \cdot T \quad (4.1)$$

In the previous formulation E_0 , is the basic structural performance, given by the

product between C and F , respectively representing the ultimate strength and the ductility of the building, depending on the failure mode, the total number of storeys and the position of the considered storey. S_D is the structural design index depending on the degree of eccentricity in stiffness and/or mass distribution in plan and elevation. A field survey is needed to define T , that is the time index, accounting for the loss of quality and strength with age due to deterioration, settlements and cracking.

The calculated seismic performance index I_S is compared with the seismic judgement index I_{S0} to determine the degree of safety of the building. I_{S0} represents a storey shear force and is given by

$$I_{S0} = E_S \cdot Z \cdot G \cdot U \quad (4.2)$$

Where E_S is, in the original version of the method, a coefficient taken as 0.6 for the second and third level screening and 0.8 for the first; Z is a zone index used to modify the intensity of the ground motion assumed at the site of the building; G accounts for local effects such as ground-building interaction or stratigraphic and topographic amplification and U is a kind of importance factor depending on the function of the building.

In 1998 a revised version of the Japanese Building Standard Law defined the I_{S0} as the spectral acceleration (in terms of g) at the period of response of the structure in question. This index should be distributed up the height of the structure, and a triangular distribution is suggested.

Preliminary assessment methods based on screening procedures have been proposed in Turkey, too, during last years. Some methods require the dimensions of the lateral load resisting elements to be defined: the “Priority Index” proposed by Hassan and Sozen (1997) is a function of a wall index (area of walls and infill panels divided by total floor area) and a column index (area of columns divided by total floor area); the “Capacity Index” proposed by Yakut (2004) depends on orientation, size and material properties of the lateral load-resisting structural system as well as the quality of workmanship and materials and other features such as short columns and plan irregularities. The Seismic Safety Screening Method (SSSM) by Ozdemir *et al.* (2005) derives from the Japanese Seismic Index Method (JBDPA, 1990).

With specific reference to the Italian context, it is to recall the vulnerability assessment procedure by the Gruppo Nazionale per la Difesa dai Terremoti (GNDT, 1993). This procedure, developed in conjunction with the vulnerability assessment of Benedetti and Petrini (1984) and Angeletti *et al.* (1988), consists in assessment forms, provided for masonry and concrete structures in two levels of increasing details, referred to as Level I and Level II. In particular, the information collected in Level II forms are used for the definition of the vulnerability index, I_V .

The latter is defined on the basis of the scores K_i assigned, after a field survey, to eleven parameters believed to be correlated to the actual vulnerability of the building. The scores are then weighted (W_i) according to the different importance of each parameter:

$$I_V = \sum_{i=1}^{11} K_i \cdot W_i \quad (4.3)$$

In the case of masonry structures I_V ranges from 0 (for low vulnerability) to 100 (for high vulnerability) and the value of PGA expected to cause the collapse is defined according to the following expression (GNDT,1993):

$$PGA_c = \frac{1}{(\alpha_c + \beta_c \cdot I_V^\gamma)} \quad (4.4)$$

where α_c , β_c and γ are parameters calibrated from building performance in past earthquakes. Since the authors believe that the least vulnerable concrete structures are generally less likely to collapse than the least vulnerable masonry ones, in the case of reinforced concrete structures I_V can assume a minimum value of -25 in order to make the values of the index comparable in the two cases. Accordingly, Eq. (4.4) is replaced by this expression:

$$PGA_c = \frac{1}{(\alpha_c + \beta_c \cdot (I_V + 25)^\gamma)} \quad (4.5)$$

Parameters for reinforced concrete structures were obtained by Zonno *et al.* (1999). The GNDT approach was largely used in Italy, for example in 1997 SERGISAI project (SERGISAI Working Group, 1997), in which 13,000 buildings were inspected by means of Level I and II forms and seismic risk map of Italy were developed. Other examples are the LSU-1 project (DPC, 1999) , Di Pasquale *et al.* (2001) and the study by DPC Working Group (DPC, 2000). According to this latter 40,000 buildings were inspected by means of GNDT forms and empirical fragility curves were computed and convolved with hazard data represented as macroseismic intensity. Results of this procedure are, inter alia, annual probabilities of occurrence of given limit states.

In the Catania project (Faccioli *et al.*, 1999), a loss estimation project on the city of Catania, in eastern Sicily, a two-step procedure was followed: the GNDT approach was computed first, then a displacement based vulnerability assessment (Calvi, 1999) was performed.

GNDT forms were also used as a basis for the three level procedure issued in 2003 in Italy for the assessment of strategic buildings, lifelines and of buildings with grave consequences of collapse or important post-earthquake function. According to this

decrease three levels of increasing details were defined, namely Level 0, Level 1 and Level 2. In the Level 0, which can be performed by non-engineers, information about location, main geometric characteristics and occupancy is required. The other two levels require a different level of information and are based, respectively, on linear and non-linear analyses.

Balbi *et al.* (2004), adopted a three-step procedure: a Level 0 procedure based on the construction of a GIS database without any vulnerability assessment; a Level 1 procedure employing the vulnerability evaluation methodology by Giovinazzi and Lagomarsino (2001) aimed at defining vulnerability indices similar to the GNDT ones and, finally, a Level 2 approach similar to the method of Cosenza *et al.* (2005), based on the individuation of likely collapse mechanisms and the analysis of structural models.

More recently, GNDT index was used in Grant *et al.* (2006 and 2007) approach for the definition of times for intervention in Italian public schools, dealt in the following. This approach was enforced in some Italian projects at regional scale, such as the RE.SIS.TO project of Tuscany Region, Italy.

4.2.2. The ATC 3-06 procedure

The ATC 3-06 (ATC, 1978) approach is one of the firstly developed in literature for the risk management of structures, with the exception of historical buildings and monuments. This approach, that can be applied to both single buildings and structural portfolios, as well as to non-structural components, consists of two stages of initial screening, which may be considered as priority ranking, and two successive steps of analysis, with different levels of refinement (Fig. 4.1).

Buildings under investigation are characterized by their relevant seismic zone (1 to 4 from the less hazardous to the most) and by an exposure group, representing building importance. Group III are structures essential for post-earthquake response, Group II are buildings expected to contain a large number of occupants and all other cases belong to Group I. In the first phase of the procedure, buildings are classified on the basis of solely hazard considerations: only the buildings belonging to Zone 4 are passed to the next step of analysis, since it is believed that the buildings located in the less dangerous sites have a sufficient lateral strength due to the design for wind loads. It should be noted, however, that the ATC 3-06 approach was developed before the spread of the concepts of capacity design and, therefore, before the shift of focus from strength to ductility. For this reason, in case of application of such a procedure, at least a qualitative assessment of the structures located in Zones 1 to 3 seems appropriate.

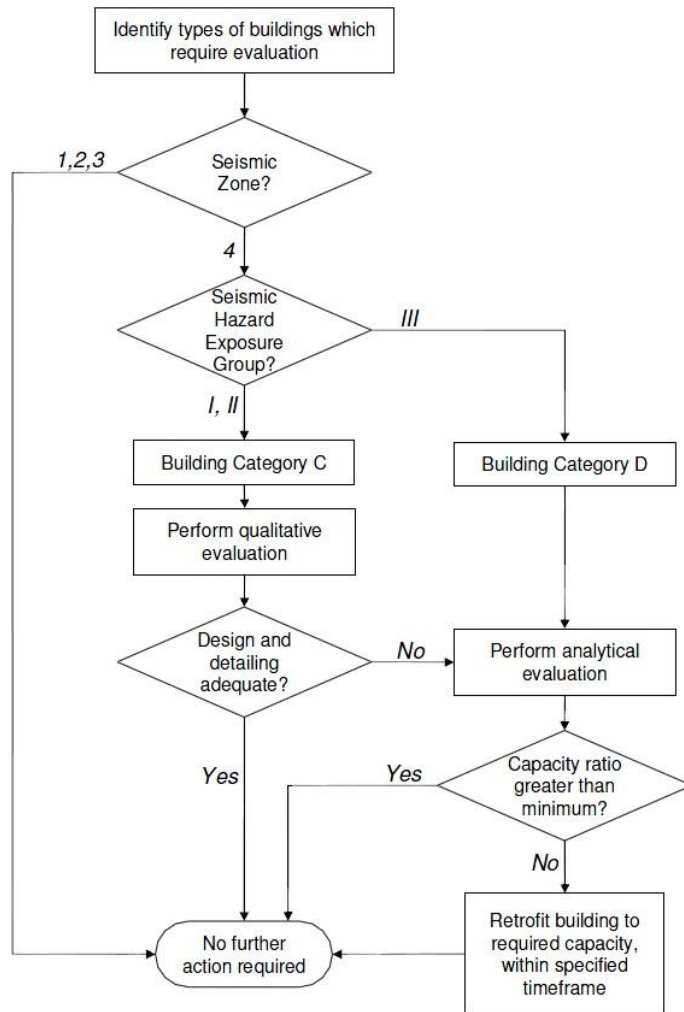


Figure 4.1 ATC 3-06 approach for risk reduction (form Grant *et al.*, 2006 based on ATC, 1978).

The second criterion for selecting the most risk-prone portion of the building portfolio, to be investigated in more detail, is based on the occupancy potential (OP), defined as the ratio of total area of the building (at all floors) and building square meters for occupants ($SMPO$):

$$OP = \frac{\text{total floor area}}{SMPO} \tag{4.6}$$

In the case of industrial structures and of mechanical equipment rooms, ATC 3-06 suggests a value of $SMPO$ equal to 27.9, the same as dwellings, compared to a minimum value of 0.7 in the case of auction rooms and assembly areas, of 7.4 for

hospitals and 4.6 for schools and dormitories. This shows that such an approach is not suitable in the case of industrial buildings, unless occupancy is computed taking into account for the effective exposure in terms of number of occupants and / or value of the contents and activities.

Structures in seismic zone 4 belonging to Group III are classified in Building Category D. They undergo an analytical procedure for the assessment of their seismic vulnerability, that is a force-based approach in which seismic demands are modelled as equivalent static forces. This analytical procedure is carried out with respect to the seismic demand of a new building, with adjustments for in-situ material properties and details that can differ from the requirements in modern design. The strength of the building is determined on a component-to-component basis, and the minimum value is taken as the earthquake capacity ratio r_c .

Regarding structures not located in zone 4 and belonging to Groups I and II (Building Category C), if $OP \leq 100$ only an exterior assessment of non-structural elements is required; if $OP > 100$, a qualitative evaluation of building vulnerability is performed, consisting in the collection of construction drawings, original design calculations and on-site inspections, aimed at enlighten significant structural deficiencies, irregularities likely soft stories and brittle mechanisms (e.g. short-column in RC structures), lack in member connections (e.g. for precast structures). In both cases a further analytical procedure may be required if the design and detailing results are inadequate.

In ATC 3-06 the minimum tolerable ratio between the existing building capacity and the one of a new construction, r_c , is defined as a function of the OP, with minimum values of 0.5. Time for demolition or retrofit is also given, for different building category: for Building Group C it is a function of OP and ranges between 2 and 15 years; for group D it depends on the type of non-conforming elements (primary structural system or non-structural components) and ranges between 1 and 15 years.

4.2.3. *The NZSEE (2003) approach*

Recommendations for prioritising seismic rehabilitation are included in the New Zealand Society for Earthquake Engineering (NZSEE) Guidelines for the Assessment and Improvement of the Structural Performance of Buildings in Earthquakes (NZSEE, 2003). These are a part of an active risk reduction programme enforced by the New Zealand building Act. The approach can be roughly summarised into two kinds of procedures: an Initial Evaluation Procedure (IEP), to be performed by New Zealand Territorial Authorities in order to provide preliminary prioritization for the entire building stock, and a Detailed Assessment Procedure (DAP), performed for the most prone structures resulting from the previous phase by the owner.

As shown in Figure 4.2, the output of the IEP is the assessment of the risk level, defined as the percentage of the required capacity for a new construction. Three risk levels are defined: “low risk”, if the capacity is greater than the 67% of the one of a new structure; “moderate risk”, in case of capacity between the 33% and 67% of the one of a new building and “high risk” for capacity less than 33% of a new design. Low and moderate risks are considerate acceptable, but in the latter case a passive rehabilitation prescription is enforced, i.e. if the owner applies for an alteration of the building or change in use, a detailed assessment is required. In the case of high risk, a DAP procedure has to be performed, consisting in one of the following: force-based assessment, displacement-based assessment or time-history analysis.

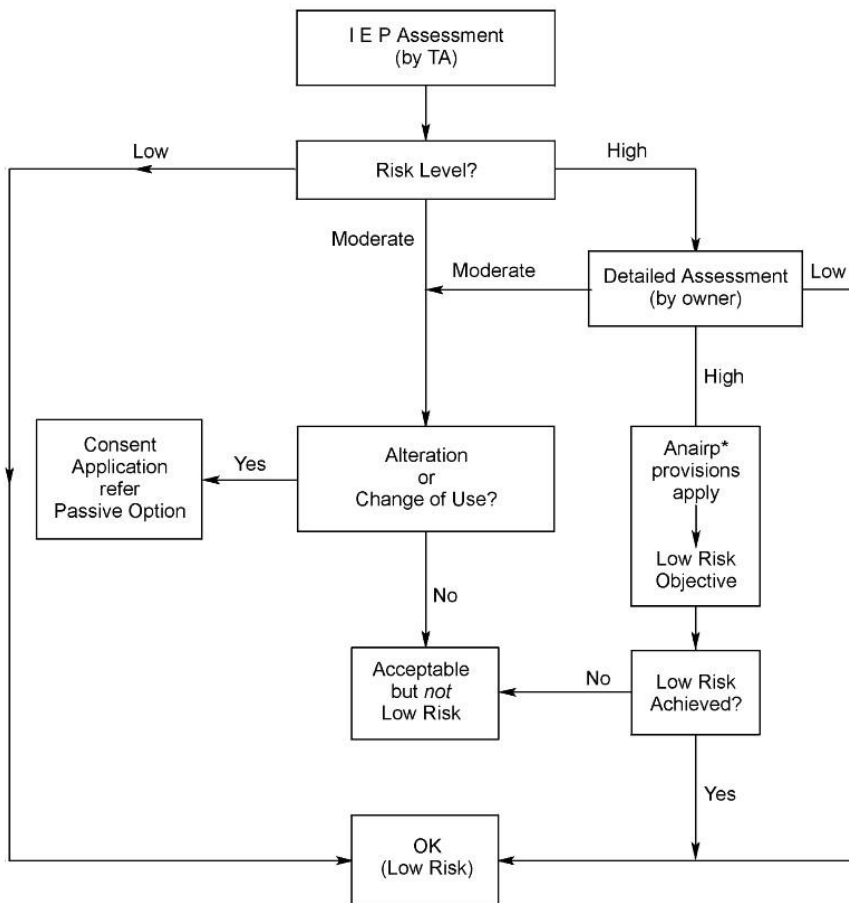


Figure 4.2 NZSEE (2003) active risk reduction programme. TA stands for territorial authority; Anairp for “As Near As Is Reasonably Practicable”. Other acronyms are explained in the text. (NZSEE, 2003)

The Initial Evaluation Procedure represents the actual risk management procedure in the NZSEE approach and it is described more in detail in the following. This is intended to be a simple preliminary screening of the portfolio, performed for the two plan direction of the building under consideration by filling forms provided in the NZSEE (2003) document, namely Tables IEP-1 to IEP-3 of Figure 4.3.

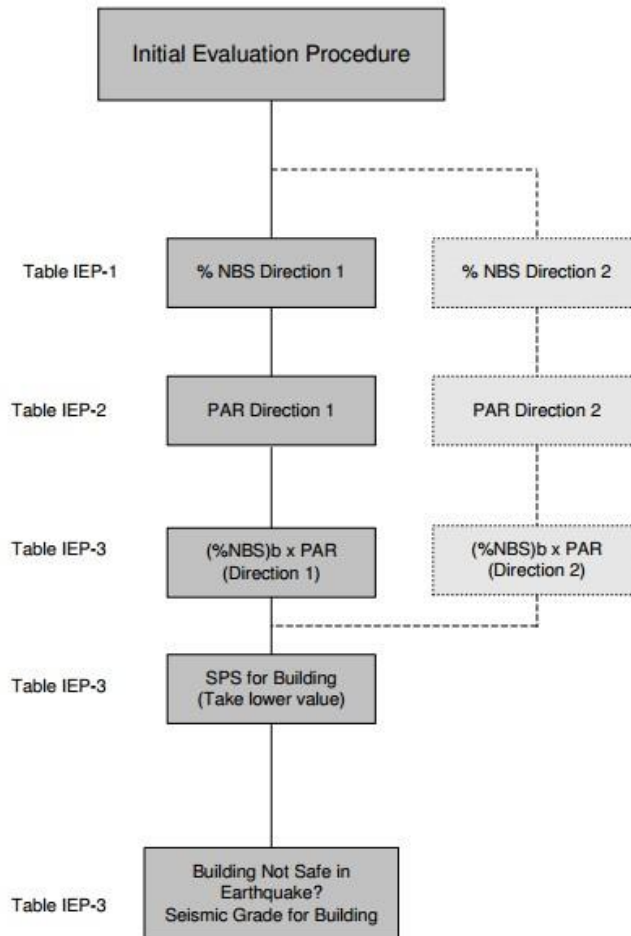


Figure 4.3 Initial Evaluation Procedure (IEP) of NZSEE approach (NZSEE, 2003).

The first step of the procedure is the evaluation of the so-called baseline percent new building standard $(\%NBS)_b$, providing the expected building strength for the appropriate typology and age, reflecting the requirements of the code in place at the time of design and assuming there are no structural weaknesses and perfect code compliance (i.e. a nominal capacity). It is defined as the product of six terms:

$$(\%NBS)_b = (\%NBS)_{gen} \cdot \frac{1}{S_p} \cdot \frac{1}{N} \cdot \frac{1}{Z} \cdot k_\mu \cdot C \quad (4.7)$$

In the previous formulation $(\%NBS)_b$ represents the nominal capacity of the building, obtained from the seismic demand in place at the time of design. Its values are given by the guidelines as a function of the structural fundamental period and the reference design code. S_p represents the so-called structural performance factor and its value is computed as a function of the ductility of the structure. The ratio between $(\%NBS)_b$ and S_p represents a nominal measure of the performance required for the building with respect to requirements for a new one, with no critical weaknesses and complying with code provisions at the time it was built.

The other coefficients of Eq. (4.7) take into account for the presence of near faults (N), seismic zone (Z), return period of the seismic action (C) and ductility of the structure (k_μ).

The second step of IEP is the computation of the Performance Achievement Ratio (PAR), adjusting the baseline capacity in order to take into account structural weakness, pounding potential and site characteristics. The considered structural weaknesses are vertical and plane irregularities and the presence of short columns. These weaknesses are classified as “Severe”, “Significant” or “Insignificant”, to which reduction factors of 0.4, 0.7 and 1.0 are, respectively, applied. The likely of pounding is taken into account through a factor, ranging between 0.4 and 1.0, depending on adjacent building separation, difference in floor alignments and heights. Similar factors, ranging between 0.5 and 1.0, are assigned on the basis of potential for site instability, landslide and liquefaction. The PAR coefficient is given as the product of all the above mentioned factors; its value ranges between 0.013 (if the minimum value is assigned to all the factors) and 1.0.

Finally, in the third step of the IEP, the so-called Structural Performance Score (SPS) is computed for both the plan directions of the building according to Eq. (4.8), the minimum value is assumed as the output of the IEP.

$$SPS = (\%NBS)_b \cdot PAR \quad (4.8)$$

The SPS expresses the percentage of new building strength since, if its value is equal to 100 or greater, the approximate risk relative to new building is equal or minor than one. The SPS index is structured in a form similar to a capacity to demand ratio and it is expressed in percentage of seismic performance required for a new building. In fact, if SPS is minor than 1, the risk of the considered existing building is greater than the one of a new construction; if SPS is minor than 0.67 the structure is potentially an earthquake risk; if SPS is minor than 0.33 the structure is potentially earthquake prone.

As previously discussed, in the last two cases further analyses are needed, performed after knowing building characteristics and details.

On the basis of the *SPS* index, NZSEE (2003) also defines a building grading scheme (Tab.4.1), in order to communicate risk to stakeholders in a more effective way. This scheme can be updated if further information becomes available.

Table 4.1 Grading system adopted in NZSEE (2003).

<i>SPS value</i>	<i>Building Grade</i>	<i>Approximate risk relative to new building</i>
> 100	A+	< 1 time
80 to 100	A	1 to 2 times
50 to 80	B	2 to 8 times
33 to 50	C	8 to 20 times
20 to 33	D	20 to 40 times
< 20	E	> 40 times

Moreover, timetable for further investigation or structural improvements on low grade structures is given depending on the building Occupancy Classification (O_C). In the case of essential building the O_C is taken equal to one; otherwise, for ordinary building it is defined from Figure 4.4, as a function of the Occupancy Load (O_L), i.e. the maximum number of people exposed to earthquake risk during normal functioning of the building, and the Occupancy Intensity (O_I), i.e. the average number of people in 100 m². This latter is defined according to the following equation:

$$O_I = \frac{O_L}{A} \cdot \frac{h_{1w}}{40} \quad (4.9)$$

where O_L is the Occupancy Load, A is the gross floor area expressed in hundreds of square meters, h_{1w} is the number of hours of normal use in one week.

Once the Occupancy Classification is defined, two modification factors are defined: K_1 , accounting for occupancy in the building (values from 1.2 for OC=1 to 0.8 for OC=4) and K_2 , accounting for risk to people outside the building (values from 1.1 in the case of “High” risk to 0.9 for “low” risk). These coefficients allow to define the so-called Prioritized Structural Performance Score (PS) and times for intervention in years (T_c), the possible values of which range between 1 and 20 years:

$$PS = \frac{SPS}{K_1 \cdot K_2} \quad (4.10)$$

$$T_c = \frac{SPS}{5 \cdot K_1 \cdot K_2} \quad (4.11)$$

The NZSEE guidelines emphasise that, while it can be computed after IEP or DEP, the PS coefficient has to be only used for priority analysis and not for the definition of whether the building is safe or not.

Another remarkable aspect is that the SPS values should not be used for the comparison of building in different earthquake zones. This is due to the fact that the SPS retains its interpretation as the ratio of existing building strength to the strength of a new structure, with no explicit consideration of the actual seismic hazard in both the definition of new and existing strengths.

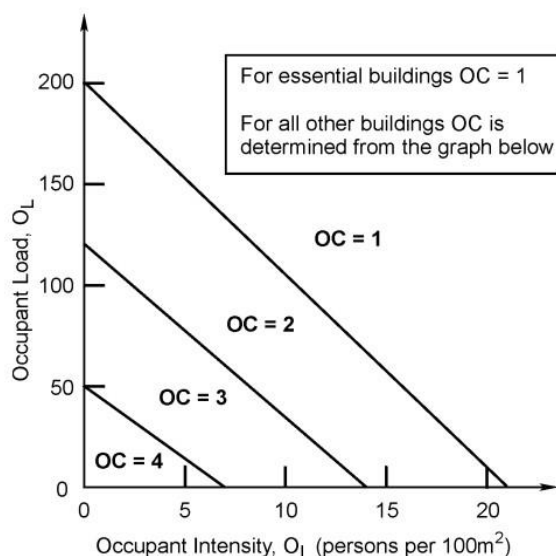


Figure 4.4 Occupancy Classification for ordinary buildings according to NZSEE (2203).

4.2.4. The Grant *et al.*, (2007) approach

Grant *et al.* (2006 and 2007) proposed a prioritization scheme for seismic intervention in school buildings in Italy, providing timescales for retrofitting or demolition. Due to the large amount of structures to be investigated (approximately 60,000), the procedure comprises multiple levels of assessment with an increasing level of detail. Each level aims at reducing the size of the building inventory under investigation for the subsequent step (Fig. 4.5).

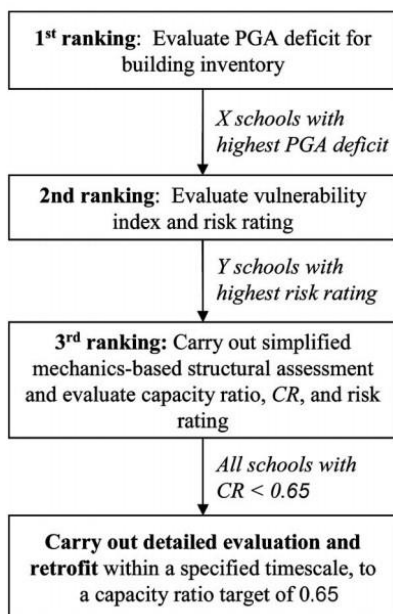


Figure 4.5 Framework of Grant *et al.* (2007) procedure for risk mitigation in Italian school buildings (Grant *et al.*, 2007).

The first level of the procedure is similar to the initial evaluation procedure (IEP) of NZSEE (2003) approach and consists in a code-based assessment of the structure vulnerability. In fact, assuming a uniform and consistent code compliance, building capacity can be assumed to be equal to code demand enforced at the time of design. This latter, converted in PGA, can be compared to seismic demand provided by the most up-to-date available seismic hazard study, that was provided, at the time of the work by Grant *et al.* (2007), by the OPCM 3274 Italian seismic regulation (OPCM, 2003). The $PGA_{deficit}$ is, therefore, computed as follows:

$$PGA_{deficit} = PGA_D - PGA_C \quad (4.12)$$

where PGA_D represent the current seismic hazard, expressed in terms of PGA. The PGA_C term is assumed to be equal to the demand according to the code enforced when the building was designed, rendered somewhat comparable to the actual demand. In fact, since PGA values have been explicitly defined only since 2003, for previous codes the authors define a so-called “effective PGA”, calculated under two strong assumptions, discussed in the following. Firstly, the authors assume that the fundamental period of the building is relatively short, so that it can be considered to lie into the “plateau” of response spectrum; secondly, in the definition of the current seismic demand, they consider it to be inelastic and a constant value of the behaviour

factor⁴ is assumed. The ratio between the plateau ordinate of the current inelastic demand spectrum and the corresponding PGA provides the current maximum spectral amplification factor for which the capacity term is to be divided, thus obtaining the effective PGA. This is equivalent to fitting the actual spectral shape to the seismic coefficient, considered to be a constant, inelastic, spectral ordinate (Fig. 4.6).

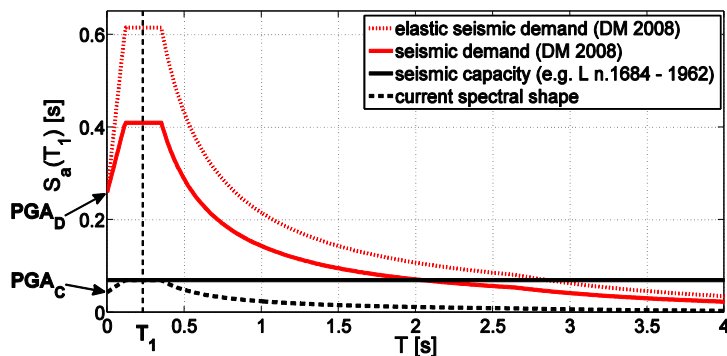


Figure 4.6 Definition of the “effective PGA” (PGA_C) according to Grant *et al.* (2007).

Even if the authors recognize the possibility of assessing different ductilities for different structural systems and different codes through years, they assume a unique building typology (unreinforced masonry) and a constant behaviour factor equal to 3.6. Moreover, in consideration of the particular use of the case-study portfolio (schools), for all post-1984 constructions they assume an importance factor equal to 1.2, resulting in an increase of effective design PGA and, therefore, a decrease of PGA deficit. It is also assumed that all buildings are built on stiff soil, so that site effects can be neglected and that live loads are negligible with respect to dead loads.

Differently from the ATC 3-06 approach, in the case of buildings designed before the introduction of seismic design requirements, the authors assume a PGA_C equal to zero, neglecting the contribution to lateral strength due to gravity design or wind design. This assumption leads to overestimating risk for a large portion of the Italian building stock, due to the evolution of seismic classification code in the Country. The authors, anyway, recognise the possibility of assuming a minimum value of design PGA in the case of pre-code buildings.

As a result of the first screening phase, only a portion of structures subjected to the highest risk, that is to say the largest PGA deficit, passes to the second phase. This

⁴ The latter is also indicated, in Eurocodes, as strength reduction factor R and it is defined as the product of a term related to the ductility of a SDOF system and an overstrength factor.

portion of the building stock has to be defined by the authorities as a function of time, money and engineering personnel available.

The second step of the procedure is based on the evaluation the GNDT vulnerability indices (Benedetti and Petrini, 1984; Angeletti *et al.*, 1988), employing expert judgement and field survey forms and providing a new value of the capacity PGA_C , expressed by Eq. (4.4) and Eq. (4.5). If the vulnerability index and the model parameters of the above mentioned equations (Eqs. 4.4 and 4.5) are considered to be fully deterministic, then a PGA value major than PGA_C will cause the collapse. Under this assumption the annual frequency of collapse can be expressed as the annual frequency of exceedance of a PGA level equal to PGA_C :

$$\lambda[\text{collapse}] = \lambda[PGA_D] \cdot \left(\frac{PGA_D}{PGA_C} \right)^k \quad (4.13)$$

Considering the approximate hazard curve from EC8, according to which the logarithm of PGA and the logarithm of annual frequency of exceedance are related by a linear relationship with a gradient $-k$ (at least in the range of T_R of engineering interest), the hazard curve is completely defined knowing a value of PGA corresponding to a given annual frequency of exceedance λ , and the slope k of the line interpolating all the other points and passing from a reference point (Grases *et al.*, 1992).

Assuming that annual probability of exceedance of PGA_C is approximately equal to the annual frequency of exceedance, the probability of collapse $P[\text{Collapse}]$ can be expressed by the following expression:

$$P[\text{collapse}] = P[PGA_D] \cdot \left(\frac{PGA_D}{PGA_C} \right)^k \quad (4.14)$$

As an example, log-log PGA hazard curve is given in Figure (4.7) for two sites, characterized by different gradients ($k_2 > k_1$), normalised with respect to the same PGA_D value. It is possible to observe that the annual frequency of collapse is greater for the curve with a steeper gradient k_2 .

Gradient of log-log hazard curve was computed in Grant *et al.* (2006) for PGA values from INGV “S1” project (Stucchi *et al.*, 2011) for the whole Italian territory and a k versus PGA relationship was defined. An average value of $k=3$ for the Italian territory was found, that is in good agreement with the value given for European buildings in Eurocode 8.

In the previous formulation (Eq. 4.13) PGA_D is the PGA value from the 475 years hazard map and the $P[PGA_D]$ term is the corresponding annual probability of exceedance, that is approximately equal to 0.21%.

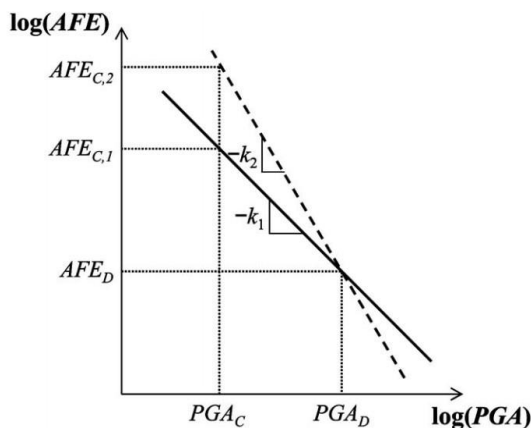


Figure 4.7 Linear log-log hazard curves with gradient $-k_2$ and $-k_1$ (Grant *et al.*, 2007).

Being $P(PGA_D)$ constant for all buildings, a relative measure of probability of failure, that is consistent with the aim of this step of the procedure, i.e. a relative ranking of structures, is obtained as the ratio between seismic demand and capacity, both of them expressed in units of PGA, raised to k , estimated around the return period of interest:

$$Risk\ Rating = \left(\frac{PGA_D}{PGA_C} \right)^k \quad (4.15)$$

Following the distinction made by Di Pasquale *et al.* (2001), the previous formulation is referred to as “individual risk”, that is the risk to which a single occupant of the structure is subjected. Conversely, the “social risk” is obtained by multiplying the previous equation by the number of occupants. Therefore, a general formulation of Risk Rating, taking into account the two above mentioned kinds of risk is:

$$Risk\ Rating = \left(\frac{PGA_D}{PGA_C} \right)^k \cdot N^\alpha \quad (4.16)$$

where α is a coefficient, ranging between 0 and 1. In the former case, the individual risk is computed; in the latter, the social risk. Intermediate values can also be considered in order to obtain a balanced measure of individual and social risk.

A portion of the portfolio with the highest risk rating from Eq. (4.16) is selected, on the basis of the available resources, to be passed to the third stage of the analysis, that is a simplified analytical procedure, based on DBELA (Crowley *et al.*, 2004) and on (Restrepo-Vélez and Magenes, 2004) for concrete structures and masonry structures, respectively. In both cases failure mechanisms and an equivalent linearization of structural response are assumed. The seismic demand is expressed as the inelastic displacement, computed at the effective period and equivalent viscous damping of the

structure. In order to compute the above, information such as number and height of storeys, depth of columns, length and depth of beams, steel grade and adequacy of confinement, is required. The result of the third step is the following Capacity Ratio (CR), similar to the r_c of ATC 3-06 and to SPS of NZSEE:

$$CR = \frac{S_C}{S_D} \quad (4.17)$$

where S_C is the displacement capacity at life safety limit state and S_D is the spectral displacement. The Risk Rating can be defined as:

$$Risk\ Rating = \left(\frac{1}{CR} \right)^k \quad (4.18)$$

Buildings with CR greater than 0.65 can be considered safe, otherwise detailed assessment procedure and subsequent retrofitting or demolition are necessary, according to timescales that are given as a function of the risk rating of Eq. (4.18) and occupancy classes. Moreover, time-dependent hazard from (Peruzza, 2005) is used for the definition of the seismic demand in the cases of identical risk ratings, so that indications of where hazard maps may underestimate immediate risk are taken into account.

Timescales for retrofitting are finally given as a function of the maximum and minimum number of years permitted for intervention and of the maximum and minimum CR considered.

Besides the simplicity and elegance of the method, it can be noticed that in the approach proposed by Grant and his co-workers, no close correlation seems to exist between the nominal index computed in the first phase and the semi-quantitative one employed in the second. Therefore, the main function of the first conventional measure seems to be uniquely to reduce sample size. Moreover, strong assumptions are made about fundamental period, soil condition and behaviour factor, but these seem to be justified by the homogeneity occupancy of the building stock and the necessity of limiting the amount of input data. In fact, under the previous assumptions, the first screening phase does not require inspection and specific studies of the various buildings of the portfolio, but only the knowledge of building geographical location and year of design, while the second ranking employs expert judgment-based indices already available from national research programmes (e.g. SERGISAI, 1997).

4.2.5. The Crowley *et al.*, (2008) approach

Crowley *et al.* (2008) proposed a modification of the approach by Grant *et al.* (2007) and applied the procedure to the scholastic buildings of two Italian regions. In order to make the first two steps of the procedure comparable, the risk rating in the first step

was calculated as in Eq.(4.19), assuming a minimum design PGA of $0.06 g$ for buildings designed in non-seismic zones.

$$PGA_{deficit} = \left(\frac{PGA_D}{PGA_C} \right)^k \quad (4.19)$$

Notwithstanding, the authors noticed that employing the above defined index in the first screening procedure, led to measures of seismic risk coarsely correlated with those obtained in the second step, when the PGA_C value is taken from GNDT approach. Therefore, a new risk rating index was proposed in terms of spectral ordinates, as reported in Equation (4.20). This risk index has proved to be better correlated with the one calculated at the second step of the procedure.

$$S_a(T)_{deficit} = \left(\frac{S_a(T)_D}{S_a(T)_C} \right)^k \quad (4.20)$$

In the previous equations the gradient k of the hazard curve is the one corresponding to the period of oscillation of the building, calculated as reported in Borzi *et al.* (2008).

For masonry buildings, the spectral ordinate corresponding to the capacity $S_a(T)_C$, was obtained directly from the GNDT second level forms (Benedetti and Petrini, 1984), while for reinforced concrete structures it was defined as the seismic design provision in force at the time of construction, multiplied by an overstrength factor, in order to obtain a more realistic assessment of actual strength, named “estimated spectral acceleration”. The authors refer to a minimum overstrength factor of 3.5, based on the findings of Borzi *et al.* (2007) applying it uniformly for all the building stock independently from the design year. This leads, as an example, to an estimated spectral acceleration equal to $0.21 g$ in the case of buildings designed in sites classified as non-seismic, that is the product of $0.06 g$ (the assumed lateral strength for non-seismically designed structures) and the assumed overstrength. Moreover, for building designed according to the current regulatory code, the authors assume an inelastic strength equal to the elastic one, due to the structural overstrength (Mwafy and Elnashai, 2002). Finally, the periods of vibration of the structures are estimated from findings of Borzi *et al.* (2008) and Crowley and Pinho (2004).

4.2.6. The Borzi *et al.*, (2011) approach

More recently Borzi *et al.* (2011) developed seismic risk maps for scholastic buildings, in Italy. The assessment is performed in two phases: in the first one the Italian school building stock, made by masonry and RC structures, is subdivided in 37 classes as a function of level of design (for RC structures only) and number of storeys (for masonry and RC structures) and random populations of buildings are generated for each building class using Monte Carlo Simulation. For each generated building, Simplified

SP-BELA method is used to obtain an approximate bilinear capacity curve. This leads to the definition of the displacement capacity, the vibration period and the viscous damping of an equivalent SDOF system.

For seismically designed RC structures the provisions of the code enforced at the time of design, according to the seismic zone of the site, are used for the definition of base shear coefficient in SP-BELA. This assumption renders this approach similar to the one by Giovinazzi (2005), regarding the capacity definition.

The displacement demand of a given building in the population can be predicted by SP-BELA and compared to the capacity corresponding to different limit states. The ratio of the number of buildings for which the demand exceeds the capacity over the total number of buildings is the probability of exceeding a limit state. The output is the conditional probability of damage, given the occurrence of a seismic event characterized by a given return period.

In the second phase, performed by the authors only for masonry structures, 2nd level GNDT forms are used to update structural capacity on the basis of data available for the specific structure and not computed for each randomly generated building of a class.

The annual frequency of exceedance of a given IM value is computed by the authors under the same assumption of linearity of the hazard curve in the log-log scale as Grant *et al.* (2007) and Crowley *et al.* (2008), but expressed in terms of spectral displacement:

$$\lambda = \lambda_{475} \cdot \left(\frac{S_d(T)}{S_d(T)_{475}} \right)^k \quad (4.21)$$

Where λ_{475} and $S_d(T)_{475}$ are, respectively, the annual frequency of exceedance and the spectral displacement corresponding to the 475 year return period. The authors computed the spectral displacement corresponding to the spectral accelerations at different T_R given in (Stucchi *et al.*, 2011), and the slope of the line passing, in the log-log scale, for the point corresponding to the spectral displacement at 475 years.

The probability of exceedance of a given spectral displacement is obtained considering an homogeneous Poisson model:

$$P = \mathbf{1} - e^{-T_L \lambda} = -e^{-T_L \lambda_{475} [S_d(T)_{475}/S_d(T)]} \quad (4.22)$$

Once probability of exceeding a given spectral displacement and the conditional damage distribution, given a spectral displacement, are known, the failure probability for the considered structural types can be computed and mapped for the whole Italian territory.

Main differences from the second step of Grant *et al.* (2007) approach emerge: the SP-BELA application allows one to define the conditional probability of damage, given a seismic event with a specific T_R occurs, while in Grant *et al.* approach once the second level GNDT index was defined, the capacity was assumed to be deterministic (so that the annual frequency of exceedance of collapse coincides with annual frequency of exceedance of the capacity). The assumption of an annual frequency of exceedance equal to the annual probability of exceedance, made by Grant *et al.* (2007), is neglected in the approach of Borzi *et al.* (2011), whose intent is to compute the unconditional probability of damage, that is the failure probability.

This procedure has, therefore, to be intended more as the application of a loss estimation method than as a risk management framework. It is discussed herein because it was intended by the authors as a validation of the work by Grant *et al.* (2007) and Crowley *et al.* (2008) and because the expression of the annual frequency of exceeding of a spectral displacement given in Eq. (4.21) suggests a nominal index for computing relative risk alternate to the one proposed in previous approaches:

$$Risk\ Rating = \left(\frac{S_d(T)_D}{S_d(T)_C} \right)^k \quad (4.23)$$

Similarly to what discussed in Sect. 4.2.4, the last equation represents a relative risk rating for a given scenario, that is the occurrence of an earthquake with a specific return period. For example, considering 475 years scenario, this is equivalent to assume λ_{475} as a constant through the portfolio and to neglect it in Eq. (4.21).

$S_d(T)_D$ is, therefore, the current seismic demand, expressed as the spectral displacement obtained from the current spectral acceleration spectrum with a return period of 475 years; $S_d(T)_C$ is the displacement capacity that, in a manner similar to Grant *et al.* (2007) approach, could be expressed from the acceleration demand enforced at the time of design, converted into spectral displacement by means of Eq. (4.24) and divided by the spectral reduction factor η , in order to make the two terms comparable.

$$S_d(T) = S_a(T) \left(\frac{T}{2\pi} \right)^2 \quad (4.24)$$

4.3. Proposed risk management procedure

As discussed in the previous Section (4.2), different procedures can be used to define priorities of intervention in portfolios of structures, which mainly differ in the approach followed for computing vulnerability.

Most of these approaches were developed for civil buildings or urban areas, characterized by uniform typologies of structures, for which a uniform level of knowledge was reached through visual surveys or it was already available from previous studies.

In the definition of a prioritization scheme for large industrial portfolios of structures, the following aspects must be taken into account:

- Although the types of occupancy in which it is possible to classify the structures in manufacturing industry are relatively few (see Section 3.1) and a certain repetitiveness can be found in the structural dimensions (for example workshops for the production are characterized by square meshes with dimensions of the order of 10 to 20 meters), a large variety of systems and construction materials can be observed. Thus, despite the large size of the portfolio, the number of buildings for each structural typology could not be such as to justify a specific study. In the opposite case, the available resources for the assessment in terms of time and money could be not sufficient to develop it.
- Structures composing the portfolio of a large industrial group can be located throughout the world. This could cause high difficulties or the total inability in performing visual inspections in all the structures of the portfolio in a timeframe compatible with the time available for the assessment. In any case, reaching a detailed and homogeneous knowledge of the structures is a critical issue.
- The quality and quantity of activities and contents (i.e. the exposure) of the specific individual plant is one of the most important aspects in the definition of priorities for intervention.

As to the knowledge of the writer, the approaches generally applied for prioritizing large portfolios of industrial buildings or for the definition of insurance premiums are still based solely on seismic hazard or on macroseismic intensity. The former, if studies providing hazard in a coherent way across the whole portfolio are available, ignores any information about the vulnerability of the structures; the latter, while considering jointly hazard and vulnerability, retains all the limitations of a qualitative approach to risk, as discussed in Sect. 2.3.2.

The proposed procedure is based on an evaluation of seismic vulnerability of structures

from design code prescriptions (i.e. a code-based approach). The main characteristic which renders this kind of prioritization procedures the most suitable for application to large industrial portfolios is that simplified-mechanics-based approaches are considered to be hardly feasible, because of the large variability in structural typologies and the lack in knowledge about them. At the same time, expert judgment-based methods, because of the worldwide spread of the structures composing the portfolio, might pose a problem of consistency in the judgment, as it would not be possible that all the structures were inspected by the same expert.

The proposed procedure shares with NZSEE (2003) and Grant *et al.* (2007) the assumption that seismic capacity may be considered to be equal to the seismic demand provided by the codes enforced at the time of the design of the structure. Then, the gap between the actual seismic demand and the seismic demand at the time of the design can be considered an indicator of structural performance deficit.

The procedure, outlined in Figure 4.8, is based on two steps, reflecting the available information about the structures composing the portfolio.

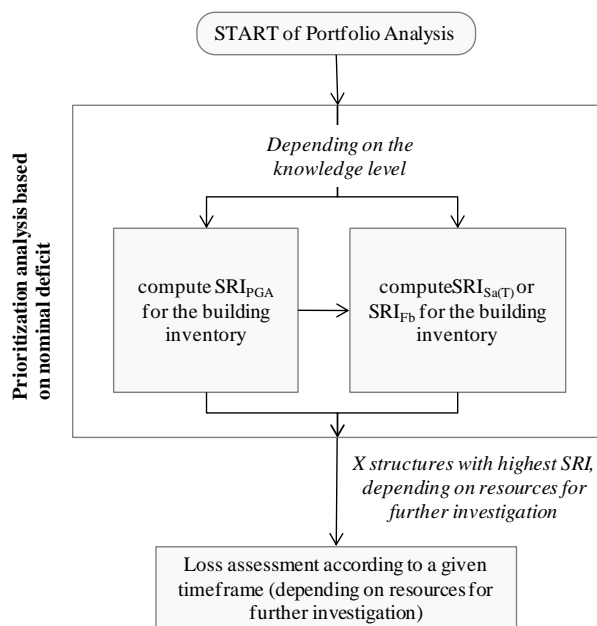


Figure 4.8 Proposed approach for priority ranking in large-worldwide spread portfolios of structures.

The first step is a ranking on the basis of a desk study or a rapid visual inspection of the structures depending on the available resources and portfolio size.

In the first case, extremely poor input data are required: year of design and building location. The nominal index computed in this case is the difference between the PGA

required by the current seismic code requirements or by the most up-to-date hazard study available (PGA_{new}) and the PGA enforced at the time of design (PGA_{old}):

$$NODE_{PGA} = PGA_{new} - PGA_{old} \quad (4.25)$$

It is to underline that the $NODE_{PGA}$ index differs from the one computed in Eq. (4.12), as no modification of the capacity term for taking into account the fundamental period is considered (see Sect. 4.1.4). Moreover, the current PGA is computed taking into account the actual site conditions, if this information is available, otherwise the common assumption of rock subsoil is made through the entire portfolio. This leads to a conservative measure of $NODE_{PGA}$ index.

If a rapid visual inspection is performed, for instance by means of the knowledge forms presented in Chapter 3, information regarding the main geometric characteristics of the buildings, the structural typology and local soil conditions is available. Such information can be sufficient to compute the following nominal deficit index:

$$NODE_{Vb} = V_{b,new} - V_{b,old} \quad (4.26)$$

that is the difference between the current seismic base shear $V_{b,new}$ and the one enforced at the time of design $V_{b,old}$. The aim is, therefore, to quantify the difference between seismic base shears according to regulatory codes enforced in different years: the current seismic demand and the one actually employed by the professional at the time of design.

Two equivalent options are available to compute Eq. (4.26): (i) intending to compare the inelastic performance of the structure (assuming that the older one may represent such behaviour for the existing structure, to follow); (ii) aiming at comparing the elastic demand at the time of construction with the current demand retrieved from elastic seismic hazard.

In the first case, the current base shear may be computed as in Equation (4.27) in which $S_{e,D}(T_{1,new})$ is the elastic seismic demand in terms of spectral acceleration at the fundamental period of the structure, as defined by the current seismic code (or by the most up-to-date hazard study available), q is the behaviour factor which, accounting for ductility and overstrength, allows to transform the elastic acceleration into the design, inelastic, one. For existing buildings its definition is a critical issue (see Section 4.4).

$$V_{b,new} = \frac{S_{e,D}(T_{1,new})}{q} M \quad (4.27)$$

Similarly, the nominal capacity, in terms of base shear, can be expressed as in Eq. (4.28), where $S_{d,C}(T_{1,old})$ is the spectral acceleration determined on the basis of the seismic action at the time of design. In case design spectrum was defined at the time of

design, it is the spectral acceleration at the fundamental period of the structure; otherwise, it is the seismic coefficient (see Section 4.5).

$$V_{b,old} = S_{d,c}(T_{1,old}) \cdot M \quad (4.28)$$

In the previous equations (Eq. 4.27 and 4.28), the M term represents the total mass of the building, obtained considering only dead loads; that is to say that the assumption of negligible live loads, with respect to dead ones, is given. This allows to overcome the assessment of seismic weight, and to neglect its variability over years and building codes. In this manner, it is possible to express the NODE index in the following equivalent form, which is more hazard-friendly (Eq. 4.29):

$$NODE_{Sa,d(T)} = \frac{S_{e,D}(T_{1,new})}{q} - S_{d,c}(T_{1,old}) \quad (4.29)$$

In an equivalent manner, it may be considered that the base shear at the time of design was an elastic one (second point of the previous list) with a known behaviour factor; in such a case NODE may assume the form of Equation (4.30), which may be referred to as an elastic deficit measure ($NODE_{Sa,e(T)}$). The plausibility of this assumption is also remarked by the coefficient accounting for stiffer structures reported in some old structural codes from the '70s and the '80s (e.g. the β coefficient in 1975 Italian seismic code or 1972 Turkish building code), which can be considered a simplified way for considering the inelastic behaviour of different structural systems (see Section 4.5) and, therefore, a sort of “inverse” behaviour factor (Ricci *et al.*, 2011).

$$NODE_{Sa,e(T)} = S_{e,D}(T_{1,new}) - S_{d,c}(T_{1,old}) \cdot q = q \cdot NODE_{Sa,d(T)} \quad (4.30)$$

Beyond their apparent differences, the two indices share the same assumption regarding the nature of the seismic demand given by codes before the introduction of capacity design principles (e.g. OPCM 3274, 2003 for the Italian case) which is considered to be an inelastic seismic demand. Therefore, in order to express capacity and demand in a coherent way, it is possible to employ the behaviour factor for dividing the elastic current demand, as well as multiplying the capacity.

More detailed aspects related to the definition of the fundamental period, the site conditions, the assessment of horizontal strength of structures designed in non-seismic zones and the possibility of iterative application of the proposed procedure are addressed in the following sections.

The second step of the procedure shown in Figure (4.8) is a detailed assessment of the loss due to seismic events. This can be performed according to simplified or detailed analytical procedures, among those dealt in Section (2.3.2), depending on the available resources and the composition of the portfolio. This step is not specifically addressed herein.

An alternate option, suitable for those portfolios characterised by structures for which reliable fragility curves are available in literature, is to adopt the approach to loss assessment presented in Chapter 5. This option was discussed in Section (1.2) and shown in Figure (1.4).

Regarding the selection of the portion of the portfolio deserving deeper investigation, an exposure-based criterion is followed.

The *NODE* index, expressed in terms of PGA (Eq. 4.25), base shear (Eq. 4.26), or spectral acceleration (Eq. 4.29 and Eq. 4.30) is weighted by an Exposure Index (EI). This can be expressed as a joint measure of the number of occupants and of the value of activities and contents, by summing the OLR and ELR normalised exposure measures, defined in Section (3.1) (Eq. 4.31). In fact, since the proposed prioritization scheme produces relative measures of the vulnerability, the EI coefficient provides for a relative measure of the exposure. Moreover, this approach allows to overcome the issue of the definition of the cost of human life.

$$EI_i = OLR_i^\alpha + ELR_i \quad (4.31)$$

Following the approach by Grant *et al.* (2007) and the distinction of individual and social risk by Di Pasquale *et al.* (2001), the OLR is raised to α , that is an individual versus social risk index that can assume values ranging between 0 and 1. In fact it is possible to maximize the social risk posing α equal to 1; conversely, if α is equal to 0, individual risk is addressed.

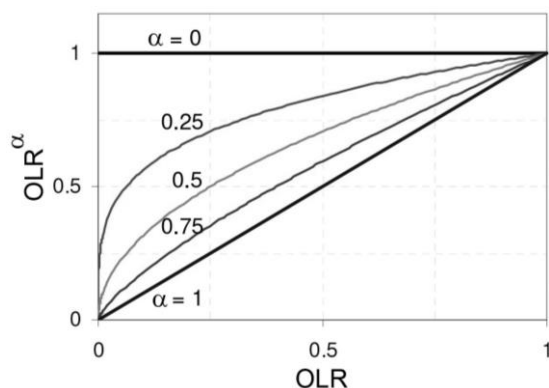


Figure 4.9 Normalised number of occupants raised to α versus normalised number of occupants relationship.

The Seismic Risk Index (*SRI*) is defined for the i^{th} structure of the portfolio as follows:

$$SRI_i = EI_i \cdot NODE_i \quad (4.32)$$

The nominal index of Eq. (4.32) is computed for all the structures of the portfolio and it is normalized with respect to the maximum over the portfolio (Eq. 4.33), so that all the structures are ranked with a risk measure between 0 and 1:

$$\overline{SRI}_i = \frac{SRI_i}{\max\{SRI_i\}} \quad (4.33)$$

The rank obtained according to previous equation represents a relative measure of seismic risk, taking into account exposure, in which the most risk-prone structure can be characterised by a value of SRI equal to one, while a structure with a capacity equal to the current demand and a negligible exposed value is characterised by an SRI equal to zero. The definition of the number of structures to be passed to the second level can be performed considering the actual capacity of the stakeholder or of the portfolio manager in investigating the building stock. This is a function of available resources (e.g. number of engineers, times for investigation) and can be expressed as the number of structures that can be investigated per unit of time. If the time available for investigation is fixed, the number of plants to be investigated is accordingly obtained. The latter is related, due to the normalisation in Eq. (4.33), to the percentage of total exposed value of the portfolio that is further investigated. Conversely, assuming that after the ranking the manager settles to investigate the 80% of the total exposed value in the following step, all the structures with a normalised SRI major than 0.2 must be passed to the next step. The time needed for the development of the subsequent step is obtained accordingly.

4.3.1. Fundamental period and soil conditions

Since the spectral accelerations appearing in Equations (4.29) and (4.30) are proxies for the base shear required by two different codes (the one enforced at the time of design and the current one), it may be considered consistent to compare spectral accelerations corresponding to two different fundamental periods. Under this assumption $T_{I,new}$ and $T_{I,old}$ are, respectively, the fundamental periods of the structure computed according to current code formulation and according to the code in place at time of design. Therefore, when no response spectrum was defined (e.g. for the Italian case, between 1909 and 1975, see Section 4.5) seismic coefficient can be treated as a constant spectral acceleration expressed in units of gravitational acceleration.

Site classification of subsoil according to the current regulatory codes is explicitly considered in the definition of current seismic demand $S_{a,D}(T_{I,new})$. The inclusion of site effect in the current seismic demand, causes that, in the case of better soil conditions (e.g., rock), the nominal deficit assumes the lower possible value for that site (given all other parameters). As it will be discussed more in detail in Section (4.7), the increasing availability in literature of micro-zonation studies, aimed at the classification of subsoil

according to current regulatory codes, makes the explicit consideration of site effect suitable.

The influence of site effect can be explicitly taken into account also in the capacity term. Different ways according to which the past seismic codes and current one take into consideration for site effect could seem to produce a non-coherent computation in the capacity and demand term. Nevertheless, it is remarked that the aim of the approach is to confront two code requirements and assume as seismic capacity the demand actually used by the professional for the design of the structure.

4.3.2. Building designed in non-seismic zones: wind design

For buildings designed for gravitational loads only, i.e. before the inclusion of the construction site in seismic zone, the capacity term, in principle, reduces to zero. In these cases, NODE is equal to the current seismic demand at the site. Although it is widely known that it may be unrealistic to assume that such buildings have no horizontal capacity, it is consistent with the approach to assign, comparatively, the largest deficit to the structures designed without any seismic provisions, as any stakeholder would seldom decide to invest less money to reduce the risk for structures seismically designed in a portfolio rather than structures designed for gravity loads only. Moreover, some may argue that, within the structural class of buildings designed for gravity loads only (e.g., reinforced concrete), significant differences in terms of seismic performance exist, as the minima for elements design render very different the actual vulnerability, especially with respect to the number of storeys (e.g. Polese 2002). It is possible, in principle, to take into account this issue with a careful calibration of the behaviour factors.

Another possible strategy for assessing the seismic capacity of structures designed in non-seismic sites concerns the possibility that the buildings have undergone design for horizontal forces different from the seismic one; e.g. large industrial steel buildings. In order to take into account any prescribed lateral resistance, wind design requirements and their evolution with codes may be also accounted for in the definition of lateral capacity, while the demand term remains the same. In fact, if the geometry of the building is known, it is possible to assess the horizontal capacity in terms of wind base shear, as provided by the code enforced at the time of design. If the mass of the building due to dead loads is given, it is also possible to assess the most demanding action and, dividing the wind base shear by the mass, a corresponding equivalent seismic acceleration can be obtained. For a brief review of the evolution of wind design prescription in Italy, employed for the case-study considered herein, the reader should refer to Appendix A and for a more detailed one to Bartoli *et al.* (2011).

4.3.3. *Updating seismic capacity*

While the proposed methodology is shown as linear in Figure 4.8, it is likely that the practical application would involve several iterative sweeps. This would ensure that the higher risk structures are urgently addressed, while medium risk ones are not completely neglected. Multiple iteration would, moreover, allow stakeholders or portfolio manager to continue in mitigating risk as more resources for investigating larger portions of the portfolio become available and to adjust risk levels at each stage of assessment as more knowledge about seismic demand and capacity is achieved.

Moreover, an effective measure of the seismic capacity can be provided by real seismic events. In fact, in case one or more structures belonging to the portfolio under investigation were affected by a seismic event, the outcome of the verification on continued occupancy⁵ could be used to update the estimate of the seismic capacity of such structures. If the output of the post-earthquake survey classifies the structure as fit for use and the visual inspection shows that the structure has not suffered visible damages to primary structural elements and to significant non-structural ones, it means that its behaviour remained in the elastic field. Therefore, it may be considered that the elastic acceleration registered at the site is less than its seismic capacity. This acceleration, obtained from shakemaps of the affected area, can be used for updating seismic capacity of the structure in the NODE index defined in Eq. (4.29).

4.3.3.1. *The C10 – Comma 10 – v.1.0 software*

On May 20th and 29th 2012 two earthquakes occurred in the Northern towns of Emilia-Romagna region (Northern Italy), characterised by a moment magnitude of 6.0 and 5.8, respectively (estimates by United States Geological Survey). The consequences of these events were 27 casualties, about 400 injured, 15000 homeless and severe consequences in terms of direct losses and, most of all, indirect ones. In fact, the stricken areas constitute one of the most industrialized centers of the national territory, therefore, severe damages have been observed in typical industrial structures (e.g. precast concrete structures, shelves, silos, etc., Magliulo *et al*, 2012), as well as in historical and monumental heritage (Parisi and Augenti, 2013).

These observed damages can be related, from one hand, to the subsoil composition of the Po valley, made of soft alluvial soils, which caused the most of the seismic energy released by the Emilia Romagna earthquakes concentrated in the low frequency range, resulting in large displacement demands up to 15–21 cm on high-period structures

⁵ The decision about continued occupancy after a seismic event is particularly important for industrial buildings since downtime could represent the cause of the largest losses due to business interruption. That decision should represent a balance between the necessity of protect the life of the occupants and the necessity of re-establish the productive activities as soon as possible, if the condition of the structure and the seismic sequence in progress allow it.

(fundamental vibration period greater than 1 s), such as industrial buildings, churches, bell and clock towers.

On the other hand, the affected area was included in the national list of seismic zones only in 2003 and the Nee Italian Building Code (NIBC, CS.LL.PP., 2008) became mandatory for ordinary structures on July 1st, 2009. As a consequence, the majority of existing structures in the affected area were designed only for gravity loads and, in industrial precast reinforced concrete structures, friction connection were largely employed. This caused a loss of the support collapse mechanism for the large part of damaged industrial structures.

Considerable economic losses were observed, related to both property damage and business interruption, estimated by the DPC equal to 13.2 billion Euros (i.e., 17.1 billion USD).

The readiness and the efficiency in the emergency management, coordinated by the Italian Department for Civil protection (DPC), made that Fire brigades carried out approximately 63000 quick usability inspections until July 27, and by August 2012, 39899 usability inspections were performed through DPC forms by teams of experts from several universities, regional institutions and professional associations. Such inspections provided the following statistics about continued occupancy for inspected buildings: 36% fit for use; 17.3% temporary unfit for use; 4.5% partially fit for use; 0.6% temporary unfit for use and to be inspected again; 35.5% unfit for use; 5.5% unfit for use due to external risk (Parisi and Augenti, 2013).

During the immediate post-event the decision about the continued occupancy is under the responsibility of the civil protection department and fire brigades, that can allow the resumption of the normal work activity and make the staff re-entering into the building, or not. Nevertheless, a final judgment about usability must be performed after inspection of a practitioner. This phase usually requires times that, in the case of industrial buildings, could lead to significant economic losses.

For this reasons the Italian Government enforced the decree 74 of June 6th, 2012 (D.L. 74/12, 2012) and the Law 122 of August 1st, 2012 (L. 122/12, 2012) providing indications for the emergency assistance to population, rapid usability decision, resumptions of activities and retrofiting timescales.

According to these documents, in order to make decision about the need for rehabilitation, the following ratio has to be computed:

$$SAr = \frac{\max \left\{ S_{a,e} (T_1)_{1^{st} \text{ event}} ; S_{a,e} (T_1)_{2^{nd} \text{ event}} \right\}}{S_{a,e} (T_1)_{code}} \quad (4.34)$$

where, $S_{a,e} (T_1)_{1^{st} \text{ event}}$ and $S_{a,e} (T_1)_{2^{nd} \text{ event}}$ are, respectively, the spectral acceleration felt at the site during the two events of May 20th and 29th, 2012, as provided by the

INGV shakemaps, and $S_{a,e}(T_1)_{code}$ is the elastic spectral acceleration required by the current seismic regulations (CS.LL.PP., 2008) for the same structures. In case this ratio is larger than 0.7 and no significant damages are observed to structural and non-structural components, rehabilitation is not required. In case of no significant observed damage but the ratio in Eq. (4.34) does not exceed the value of 0.7, the structure need to be verified according to current Italian seismic code.

The definition of a ratio equal to 0.7 signify that the structure actually experienced a significant spectral acceleration with respect to the one provided by the current code for a new building with the same characteristics as the one under investigation.

In order to support the evaluation of the abovementioned ratio, a tool named “*C10 – comma 10 – Strumento a supporto della Legge n.122 del 1 agosto 2012 e del DL n.74 del 6 giugno 2012 – v-1.1 beta*” was developed (Fig.4.10).

This tool provides, for a site located in the area affected by Emilia earthquakes and individuated only by geographical coordinates, the maximum value of spectral acceleration from INGV shakemaps of May 20th and 29th 2012 events. This value is then compared to the elastic acceleration provided by NIBC, obtained from least squares interpolation of data given in (CS.LL.PP., 2008).

Moreover, within the procedures dealt in this thesis, the *C10 v.1.1 beta* software tool was used for updating the seismic capacity of some structures of the case-study portfolio affected by the Emilia 2012 (see Sect. 4.7.3.2).

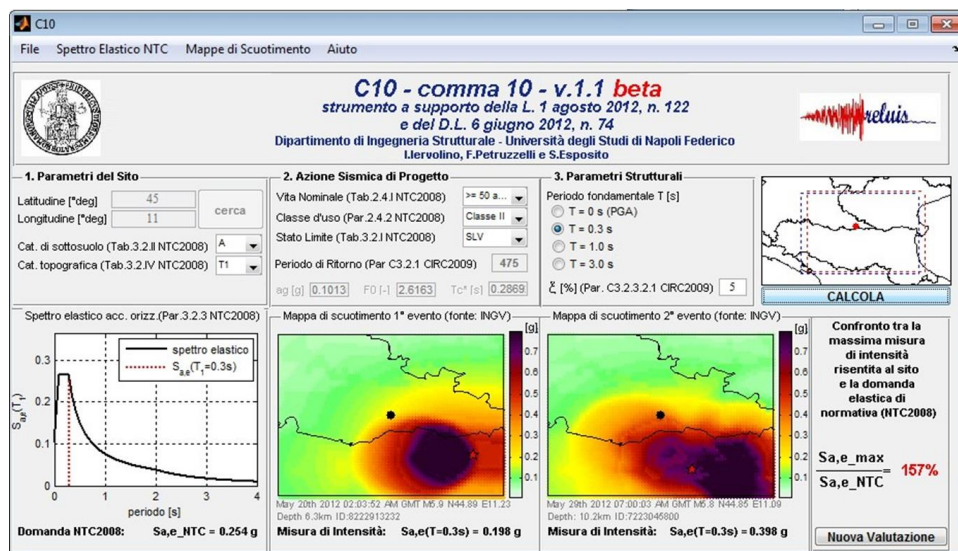


Figure 4.10 C10 – comma 10 – v.1.1 beta graphical user interface.

4.4. Evolution of Italian seismic structural requirements

Italy is considered to be a limited seismicity country, yet of high seismic risk. This is, in fact, repeatedly demonstrated by very large consequences of recent moderate-magnitude earthquakes; e.g., L’Aquila, 2009 (moment magnitude, or M_w , equal to 6.3, 308 deaths, more than 1600 injured and a total cost for reconstruction estimated in about 12.89 billion USD) and Emilia region, 2012 (see Section 4.3.3.1). The high vulnerability of Italian building stock is certainly related to buildings average age, low quality of materials and construction practice and lack in maintenance. Notwithstanding, one of the most relevant sources of vulnerability of Italian building stock is due to the fact that a large portion of structures was designed without any seismic provision or in compliance with obsolete codes, with inherent underestimation of appropriate (according to modern standards) design actions. Figure (4.11) shows the design age for Italian building stock, according to 2001 census data. It is possible to observe that, except for masonry non-engineered structures, a large part of which belongs to cultural and monumental heritage, most of the reinforced concrete and other structural material (e.g. steel) structures was designed between ‘60s and ‘70s, in a period in which, as it will be discussed in the following, only a portion of the Italian territory ranging between the 15% and the 35% was considered to be seismic prone. For these reasons, the knowledge of the evolution of structural seismic provisions in Italy can be indicative, at least in a “large scale” prioritization scheme, of the actual structural vulnerability.

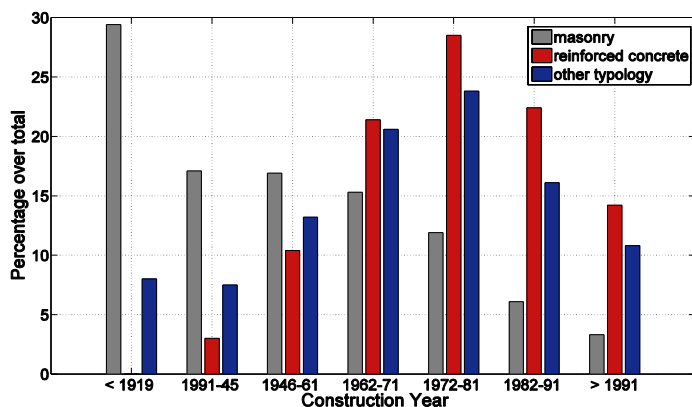


Figure 4.11 Composition of Italian building stock in terms of year of construction, according to 2001 census data (ISTAT 2001)

4.4.1. Early history

Seismic regulatory codes in Italy have undergone a relevant number of changes, enforced, until very recently, mainly as a consequence of catastrophic seismic events. In this section, a few fundamental steps are reviewed, while the reader should refer to

Di Pasquale *et al.* (1999a and 1999b), for a more comprehensive and informative analysis.

The first documented Italian seismic building code was the royal decree (*Regio Decreto*, or RD) no.193 of 04/18/1909 (RD 193/09, 1909), enforced after the Messina Strait earthquake of 1908 (M_w 7.1). It contained instructions to be applied on the most heavily stricken areas, which were also defined as *seismic zones*. In fact, to control seismic vulnerability of new constructions, some limitations about building height and provisions for different structural typologies were given. Although no quantification of horizontal design forces was included, an expert panel recommended to check the building stability under horizontal forces of the order of magnitude of 8% with respect to the weight (i.e., the ratio between the static horizontal force equivalent to the seismic action and the seismic weight of the structure, or *seismic coefficient*, was equal to 0.08).

The first explicit instruction regarding the value of the horizontal seismic base shear was introduced in 1915 with the *Regio Decreto Legge* (RDL) no.573 of 04/24/1915 (RDL 573/15, 1915), after the Avezzano earthquake in the Abruzzo region (M_w 6.9). It provided seismic forces equal to 1/8 and 1/6 of storey weight, for the first and upper levels, respectively. Moreover, it was prescribed to consider vertical loads equal to the sum of dead loads plus the quasi-permanent live loads, increased by 50%, to take into account the vertical seismic action.

The Royal Decree no.2089 of 1924 (RD 2089/24, 1924) prescribed that horizontal and vertical seismic actions were not considered contemporarily acting on the structure, but the values of the mass-proportional horizontal forces remained substantially unchanged.

According to RDL no.431 of 13/03/1927 (RDL 431/27, 1927) a lower level of seismic base shear and less restrictive structural provisions were introduced for sites considered of moderate seismicity. In those zones, belonging to the so-called *second category* or *category II* (with respect to highly hazardous sites, *first category* or *category I*), the seismic action was equal to 1/10 of building weight at each level. The code also prescribed to consider vertical loads equal to the sum of dead loads plus the quasi-permanent live loads, increased by 50% in category I and 30% in category II zone, to take into account the vertical seismic action.

RDL no.640 of 03/25/1935 (RDL 640/35, 1935) imposed to each municipality to develop local building regulations to enforce suitable codes of building practice. On the other hand, it reduced to 40% in category I and 25% in category II the amount of dead and live loads to be considered in vertical seismic action. Moreover, it reduced the horizontal seismic force to 10% and 7% of the seismic weight in category I and II, respectively. The above mentioned seismic weight was computed adding to dead loads

the 1/3 of live loads.

In 1937, according to the RDL no.2105 of 11/22/1937 (RDL 2105/37, 1937) the seismic coefficient for category II was further reduced to 0.05. It can be noticed that the assumption of a constant distribution of forces along building height, established in 1935 and substantially unchanged up to 1975, represents another step backward respect to what stated in previous codes.

The law no.1684 of 12/25/1962 (L 1684/62, 1962) did not bring substantial innovation to the seismic design; however, horizontal seismic forces were assumed equal to 10% and 7% of seismic weight, depending on the seismic zone, and established that vertical seismic action could be neglected, except for cantilever structures.

4.4.2. Modern era

A major step in seismic codes in Italy was the Law no.64 of 02/02/1974 (L 64/74, 1974), still enforced, which gave the administrative framework of seismic regulations in Italy, entrusting the Government with the periodical updating of technical provisions. The *Decreto Ministeriale* (DM) no.40 of 03/03/1975 (DM 40/75, 1975) was the first code issued according to the previous law and introduced relevant changes in Italian seismic provisions: the response spectrum was, in fact, introduced and dynamic or static analyses were given as design options. Horizontal base shear was given as a function of seismic zonation, soil type, structural system, structural fundamental oscillation period, and seismic weight, as reported in the following equation:

$$F_h = C \cdot R \cdot \varepsilon \cdot \beta \cdot W \quad (4.35)$$

where, W is the seismic weight of the building, ε accounts for soil compressibility (ε was equal to 1.00 in the case of “stiff” soil and 1.30 in the case of “deformable” soil), β is a so-called “structure coefficient” accounting for the possible presence of structural walls (β was equal to 1.20 in the case of structural walls and 1.00 in the other cases) and C is the seismic coefficient (0.10 and 0.07 for first and second category, respectively). The R term in Eq. (4.35) defines the spectral shape. It remained substantially unchanged until 2003; its expression was the following:

$$\begin{cases} R = 1 & \text{for } T \leq 0.8s \\ R = 0.862 \cdot T^{-2/3} & \text{for } T > 0.8s \end{cases} \quad (4.36)$$

where T is the fundamental structural period, defined as:

$$T_1 = 0.1 \cdot \frac{H}{\sqrt{B}} \quad (4.37)$$

In the previous formulation, H is the building height and B is the maximum plan

dimension, expressed in meters. Despite the step forward accomplished through the introduction of the spectrum, no indications were given about how the reference seismic action had been defined and how it was transformed in a design spectrum. In other words, the ductility of the system was only indirectly taken into account by means of the so-called structure coefficient β , greater than one for stiffer structures (Ricci *et al.*, 2011). Finally, the fraction of live loads to be considered in the definition of seismic weight was defined as a function of the use of the building and the seismic force defined according to Eq. (4.35) was distributed proportionally to the height of storeys.

Further evolutions of regulatory provisions regarded the introduction of a third seismic category in 1981, through the DM no.515 of 06/03/1981 (DM 515/81, 1981), after the Irpinia-Basilicata earthquake in 1980 (M_w 6.9), corresponding to a C coefficient equal to 0.04, and of an importance factor in 1984, through the DM 06/19/1984 (DM, 1984), equal to 1.2 for relevant buildings and to 1.4 for primary civil protection buildings, amplifying Eq.(4.35). The following Decree of 1986 (DM, 1986), replacing the previous Code, did not introduce any relevant change to seismic actions.

Up to 1996 the only possible design approach was based on admissible stress, that is, conventional elastic analysis at the material level. The DM of 16/01/1996 (DM, 1996a) introduced limit state design and an amplification of seismic horizontal action by 1.5. However, the admissible stress approach, much more familiar to professionals, was still allowed, so that the limit state design was largely disregarded in practice. Moreover, the instruction document related to the 1996 code (*Circolare Ministero LL.PP.* no.65 of 04/10/1997, M.LL.PP, 1997) contained first indications in the direction of capacity design, e.g. detailing in nodal zones to improve local and global ductility.

4.4.3. State-of-the-art and current codes

The 2003 seismic code (OPCM 3274, 2003) and its following modifications (OPCM 3431, 2005) represented the most relevant change in Italian seismic provisions over thirty years. In fact, EC8 approach was acknowledged and a fourth seismic category was introduced; this last change was such that the whole Italian territory, except for the Sardinia region, was considered to be seismically prone. An elastic spectrum with a fixed shape (depending on local geology) anchored to a conventional PGA was introduced. PGA values for the four zones were 0.35 g, 0.25 g, 0.15 g and 0.05 g for category from I to IV, respectively. A site was falling in one of the four categories depending on the PGA, on stiff soil, with an exceedance return period of 475 years, evaluated by means of probabilistic seismic hazard analysis. The elastic spectrum had to be divided by a behaviour factor q to get an inelastic design spectrum. The 2003

code also introduced, for the first time in Italy, capacity design, that is the strength hierarchy and structural regularity principles.

Design base shear was defined as in Eq. (4.38), where λ is a coefficient equal to 0.85 for static analysis, $S_a(T_I)$ is the elastic spectral acceleration (determined on the basis of a standard spectral shape anchored to the mentioned PGA), q is the behaviour factor and g the gravity acceleration.

$$F_h = S_a(T_I) \cdot W \cdot \lambda / (q \cdot g) \quad (4.38)$$

The fundamental period of the structure T_I was calculated as follows:

$$T_I = c_I \cdot H^{3/4} \quad (4.39)$$

where c_I is a coefficient depending on the structural typology; i.e. equal to 0.075 for reinforced concrete structures, 0.085 for steel structures, and 0.05 for any other structural type.

However, despite its major advances, this code release was compulsory only for “strategic” buildings, i.e. those which, in the case of a seismic event, assume civil protection functions or can have significant consequences in terms of losses, while practitioners were still allowed to use the 1996 code in other cases.

The last regulation, i.e. the NIBC (CS.LL.PP., 2008), finally enforced performance-based design criteria (without alternate options for strategic and non-strategic buildings), after L’Aquila earthquake (M_w 6.3) in 2009. As a major change of NIBC, design seismic hazard was defined completely on probabilistic bases as a function of geographic coordinates of the construction site, and no longer on a municipality basis (see following Sect. 4.5). Anyway, this Code became mandatory for ordinary structures on 1st July, 2009. Regarding ordinary buildings in the sites located in zone 4, it allows the use of the admissible stress methodology included in DM 16th January, 1996, but it still requires to take into account the seismic action with the assumption of a degree of seismicity $C = 0.03$.

As a summarizing example, evolutions of code-based seismic actions through the years for L’Aquila downtown site (Lat: 42.36, Lon: 13.41) are reported in Figure (4.12) in terms of seismic coefficient or acceleration response spectrum, if applicable. Note that, since 2003, the spectrum is elastic with 5% damping. Considering that up to 2003 the design was performed assuming an elastic behaviour of the structure and no explicit prescriptions were given in order to take into account the inelastic behaviour of material, structural sections, members and the whole structural organism (except for some prescriptions given in 1996, as stated above), in order to compare the seismic action provided by the codes starting from 2003, it is necessary to reduce the elastic spectrum by the mentioned behaviour factor.

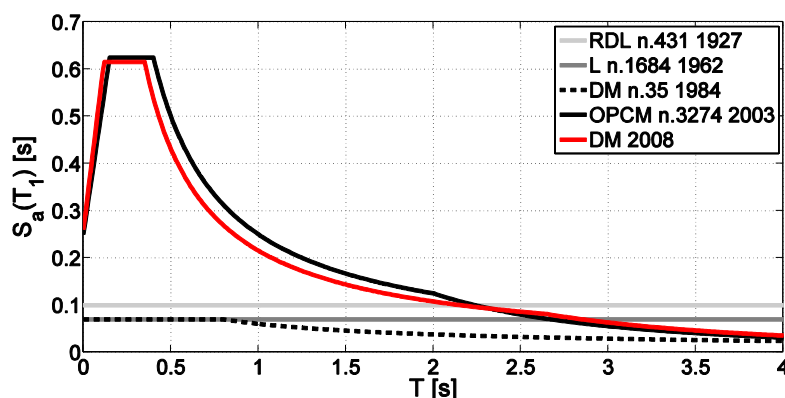


Figure 4.12 Reference seismic demand evolution for L'Aquila site (Lat: 42.36, Lon: 13.41).

4.5. Evolution of seismic classification (design hazard) in Italy

Since 1909, the complex task of mitigating the seismic risk in Italy was entrusted, on one hand, by seismic building codes and, on the other, by seismic classification regulations, defining those portions of the Italian territory to be considered as seismic prone.

For several years the seismic zonation of Italy was defined essentially on the basis of administrative issues, rather than on the implementation of increasing scientific and technical knowledge, although available in the country. Moreover, up to '70s a region was considered to be seismic prone, and therefore included in the so-called *seismic catalogue*, only after the occurrence of a seismic event. This aspect clearly emerges from the Figures (4.13) to (4.18), in which the main steps in the evolution of seismic classification from 1909 to today are shown, reflecting the distribution of earthquakes through Italian territory.

A peculiar, yet relevant, aspect is that, between 1916 and 1936 or 1937 and 1962, several municipalities were *de-classified*, that is, taken from seismically prone to non-seismically-prone zones. This can be only partially justified by the necessity of reconstruction after World War I and II (Di Pasquale *et al.*, 1999a), since it certainly represents one of the most important causes of the current vulnerability of the structures built in these zones.

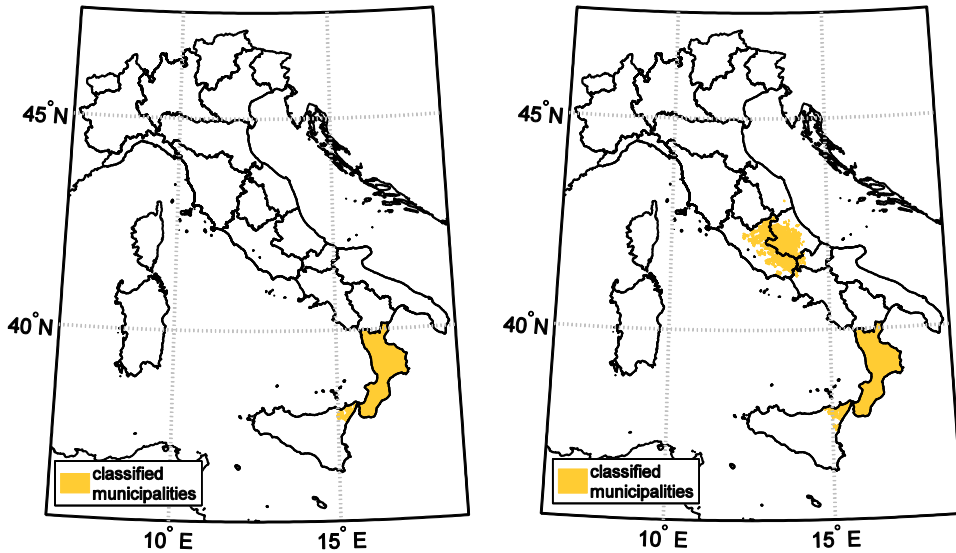


Figure 4.13 Italian seismicity map after year 1909 (left), 1915 (right).

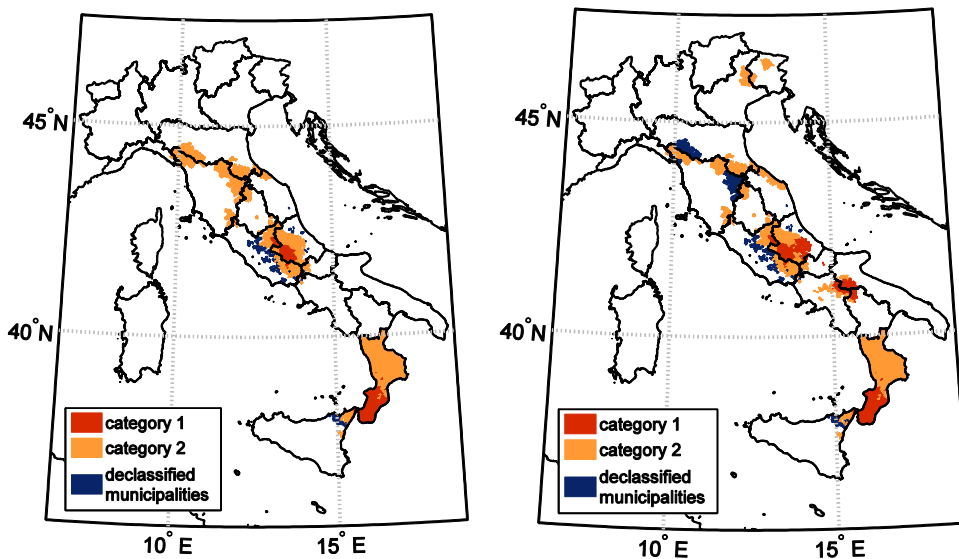


Figure 4.14 Italian seismicity map after year 1927 (left), 1937 (right).

The Law no.1684 of 12/25/1962 claimed that seismic codes should be applied to municipalities subjected to “intense seismic activity”, but until the early ‘80s, this prescription remained substantially unapplied. In 1974, through the Law no.64 of 02/02/1974 (L. 64/74, 1974), it was reaffirmed the need to classify the territory on the basis of “proven technical reasons” and starting from 1980 macroseismic intensities maps were used as a basis for the identification of seismic zones, defined reflecting municipality territory borders. Several decrees aimed at the seismic classification of

territory between 1979 and 1984 were enforced, so that, at the end of 1984, the 37% of municipalities and the 45% of Italian territory was considered to deserve seismic design (Figure 4.16).

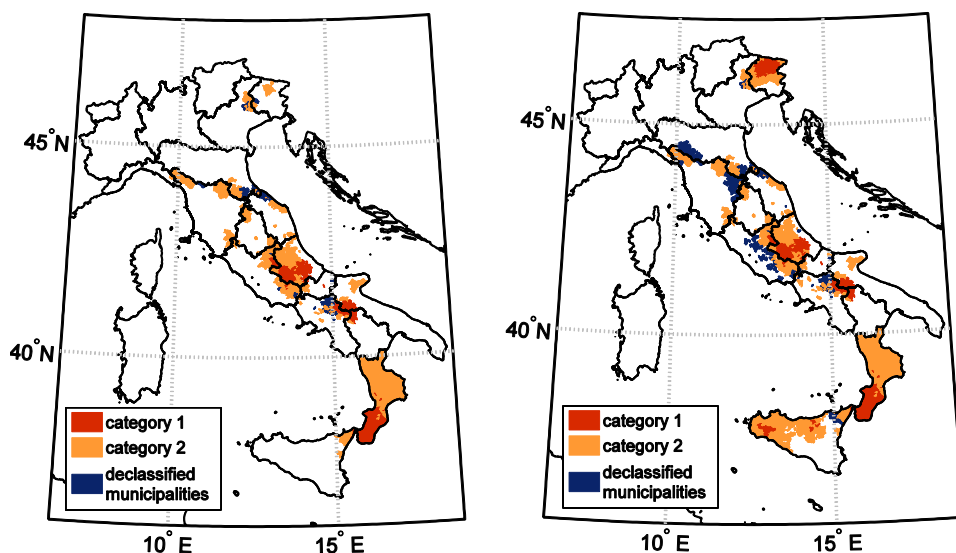


Figure 4.15 Italian seismicity map after year 1962 (left) 1980 (right).

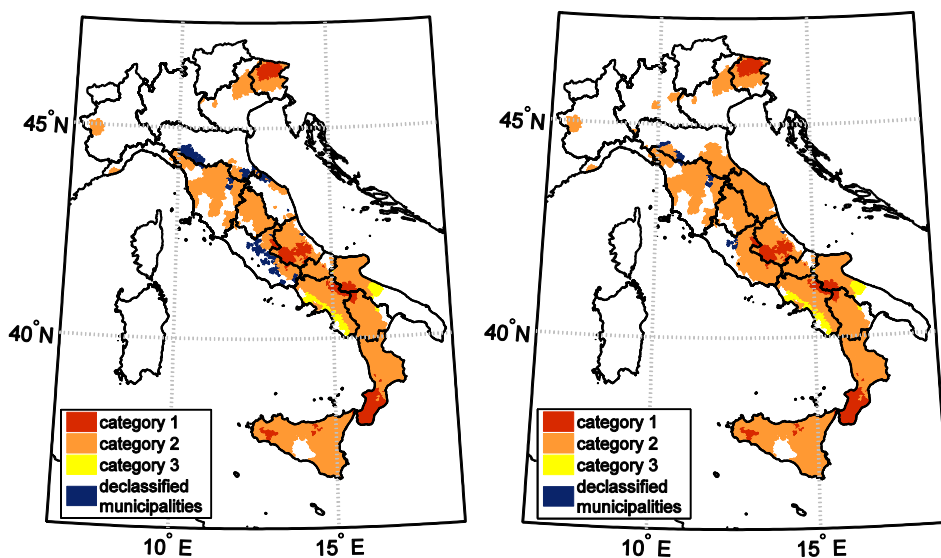


Figure 4.16 Italian seismicity map after year 1981 (left) 1984 (right).

These major changes in the seismic classification were certainly related to the occurrence of the Irpinia and Basilicata earthquake of 1980 (Fig.4.16, left panel), as well as to the conclusion of the “Progetto Finalizzato Geodinamica (PFG)” project by the Italian National Research Council (Consiglio Nazionale delle Ricerche, CNR).

This project produced a hazard map of the Italian territory based on the maximum macroseismic intensity felt at the site in 1000 years, on the expected macroseismic intensity in a period of 500 years and some cost minimisation criteria, that was enforced in the 1984 Code.

Moreover, before this project no real Italian seismic catalogue existed, but different regional (e.g. Carrozzo *et al.*, 1975; Bernardinis *et al.*, 1977) or national ones (e.g. Giorgietti and Iaccarino, 1971 for nuclear plants installation, Carrozzo *et al.*, 1973 or ENEL, 1977 catalog). The PFG project also gave impulse to the creation of a National Seismic Catalogue, the so called PFG catalogue of 1985 (Postpischl, 1985). At the same time the Istituto Nazionale di Geofisica e Vulcanologia (INGV) started the drafting of a national catalogue (ING, 1981), updated in 1995 in the Catalogue of strong earthquakes in Italy (Catalogo dei Terremoti Forti Italiani, CFTI, Boschi *et al.*, 1995).

In the following years, the GNDT produced a map of seismogenic zones (the ZS4 map of 1996, Meletti *et al.*, 2000) and several seismic catalogues (e.g. Stucchi *et al.*, 1993; Stucchi e Zerga, 1994) and in particular the NT4.1, which represents the basis for the compilation of 1996 seismic hazard map (known with the acronym PS4, Slejko, 1996). This elaboration converged into the Global Seismic Hazard Assessment Program (GSHAP, Giardini *et al.*, 1999) but did not produce any significant change in the national regulations for the definition of seismic zones.

In 1998 a work group appointed by the National Seismic Survey (Servizio Sismico Nazionale, SSN) elaborated a proposal for a new classification of the Italian territory, based on a joint evaluation of the Housner intensity with a return period of 475 years, of the peak ground acceleration with an exceedance probability of 10% in 50 years and of the maximum macroseismic intensity felt at the site in the last 1000 years (Slejko *et al.*, 1998). Notwithstanding, this proposal of classification was not implemented in the Codes and seismic classification of Italy remained substantially unchanged from 1984 to 2003 (Di Pasquale *et al.*, 1999b). Another proposal that remained unapplied was the 1999 GNDT-SSN one, differing from the previous essentially for the definition of the employed ground motion prediction equations. In Figure (4.17) the 1996 and 1998 proposal for a new seismic classification of the Italian territory are shown.

In the same year an updated version of seismic catalogue was produced by INGV, GNDT and SSN, namely the Parametric Catalogue of Italian Earthquakes (Catalogo Parametrico dei Terremoti Italiani or CPTI99, GdL, 1999), updated over the years, up to the current version (CPT11, Rovida *et al.*, 2011).

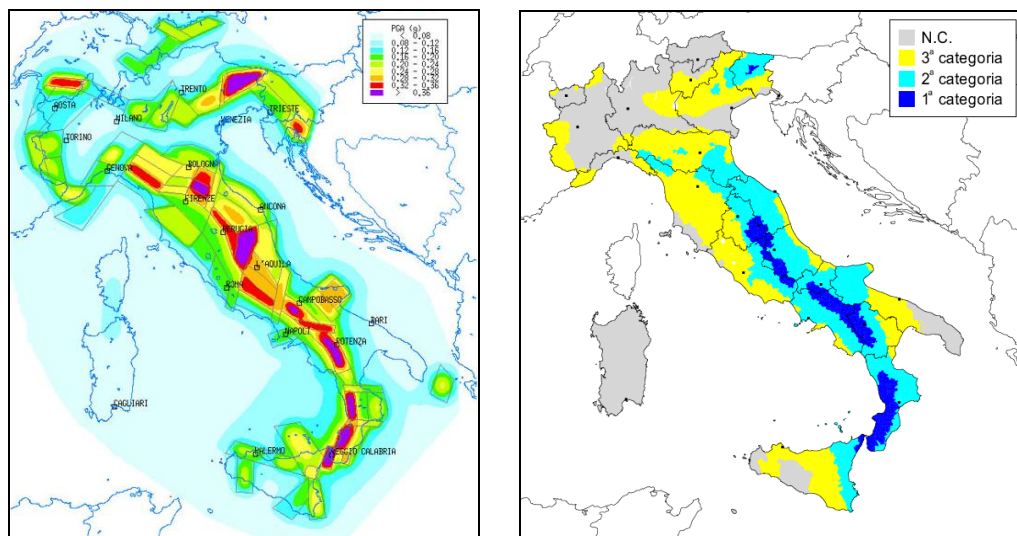


Figure 4.17 1996 SSN (left) and 1998 GNDT-SSN (right) proposals for Italian hazard map.

According to the Decree 112/98 of 1998, the responsibility for the allocation of Municipalities into seismic zones passed to the Regions and Autonomous Provinces. The State was competent only in defining the general criteria for the updating of seismic zones and in enforcing technical standards.

The earthquake in San Giuliano di Puglia, 2002, brought dramatically to attention the lack in updating the seismic classification of the Italian territory, which was still the same as in 1984. In the emergency, the OPCM 3274 (2003) updated the definition of seismic zones enforcing the classification provided by the 1998 proposal and defining, for the first time, a fourth seismic zone 4, characterized by decreasing seismic hazard, replacing the unclassified regions in previous zonations. Therefore, a minimal level a seismic design was ensured for the entire Country (Fig. 4.18), although individual Regions in zone 4 might choose not to adopt the new seismic classification.

Between 2003 and 2004 the regions, with resolutions of the Regional Administrations, enforced the seismic classification included in OPCM 3274, without changes, except for some cases (the Basilicata, Lazio, Campania and Sicily regions and the Autonomous Province of Trento). As already mentioned, the OPCM 3274 also enforced a new seismic design Code, acknowledging the Eurocode 8 and established the criteria according to which a new study of seismic hazard should have been made.

In 2004, the National Institute of Geophysics and Volcanology proposed a new hazard map (called MPS04), prepared according to the criteria of OPCM 3274 and a new seismogenetic sources map (called ZS9). In the following year the INGV and the Italian Civil Protection started the “S1” project (INGV-DPC, 2007), aimed at providing

hazard at different return periods, for several spectral ordinates for the entire Italian territory, except for the Sardinia region (Stucchi *et al.*, 2011).

In 2006 a new Ordinance (OPCM 3519, 2006) adopted the seismic hazard map MPS04 as official reference. Hazard was defined for the first time according to the geographical coordinates and no longer on the basis of municipal boundaries, considering the upper bound value of hazard provided in each of the four zones defined in 2003.

In 2007, a special commission of the Ministry of Infrastructure started a review of the full of matter, which led to the NIBC. According to this code, enforced on 1st July 2010, the INGV “S1” project was acknowledged. Therefore, seismic hazard is currently provided at each point of a regular grid with a 5 km span covering the whole Italian territory (except the Sardinia region) and code elastic spectra are defined starting from uniform hazard spectra computed as a function of the geographical coordinates of the site.

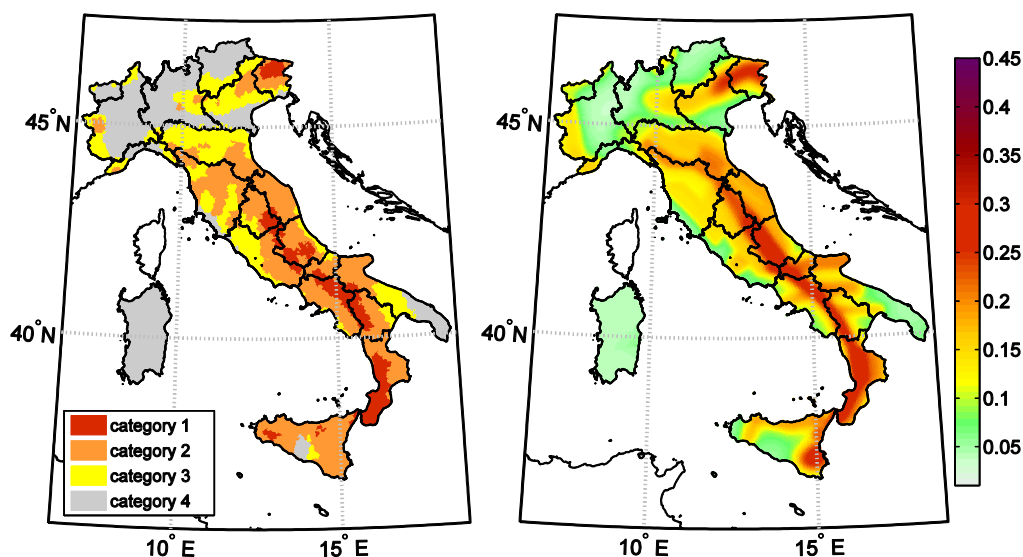


Figure 4.18 Italian seismicity map after year 2003(left) and 2008 (right).

Table (4.2), summarizes the most relevant changes in seismic action computation and classification of the Italian territory, as well as the percentage of municipalities and territory deserving seismic design, between 1909 and 2008 (the latter representing the current situation).

Table 4.2 Summary of the most important changes in horizontal seismic actions and classification of Italian territory, as per regulatory codes. The number of municipalities which changed classification is expressed with respect to the previous code; partially adapted from Di Pasquale *et al.*, (1999a and 1999b).

Code	Horizontal seismic action	Main changes in classification of territory and other relevant issues	classified municipalities	classified territory
R.D. 193 18/04/1909	Undefined	first seismic zonation (367 municipalities)	6%	5%
R.D.L. 573 29/04/1915	$F_h=1/8 W$ first floor $F_h=1/6 W$ other floors	416 municipalities classified as seismic prone	10%	9%
R.D.L. 431 13/03/1927	1st cat: $F_h=1/8 W$ first floor $F_h=1/6 W$ other floors 2nd cat: $F_h=1/10 W$	Introduction of the second category; 951 municipalities changed seismic zone	12%	13%
R.D.L.640 25/03/1935	1st cat: $F_h=0.10 W$ 2nd cat: $F_h=0.05 W$	174 municipalities changed seismic zone	13%	15%
R.D.L. 2105 22/11/1937	1st cat: $F_h=0.10 W$ 2nd cat: $F_h=0.07 W$	Classification and declassification of several municipalities	14%	15%
Law 1684 25/11/1962	1st cat: $F_h=0.10 W$ 2nd cat: $F_h=0.07 W$	Classification and declassification of several municipalities	15%	17%
D.M. 40 03/03/1975	$F_h = C R \varepsilon \beta W$ 1st cat: $C=0.10$ 2nd cat: $C=0.07$	239 municipalities changed seismic zone	17%	20%
D.M. 515 03/06/1981	Unchanged, except for 3rd cat: $C=0.04$	Introduction of the third category; 239 municipalities changed seismic zone	28%	35%
D.M. 19/06/1984	Unchanged except for $I=1.4$ strategic buildings $I=1.2$ crowded buildings	1533 municipalities changed seismic zone	37%	45%
D.M. 16/01/1996	Substantially unchanged	Introduction of Limit State design philosophy. First ductility control prescriptions in its explanatory document.	37%	45%
OPCM 3274 20/03/2003	$F_h=S_d(T_1) W \lambda / (q g)$ zone 1: $a_g=0.35 g$ zone 2: $a_g=0.25 g$ zone 3: $a_g=0.15 g$ zone 4: $a_g=0.05 g$ Performance-based design	All Italian territory classified as seismic prone through the introduction of 4 th seismic category, introduction of performance based design criterion. Non-compulsory for ordinary buildings.	100%	100%
OPCM 3519 28/04/2006	Substantially unchanged	INGV MPS04 map is adopted. Non-compulsory for ordinary buildings.	100%*	100%*
D.M. 14/01/2008 (NIBC)	Substantially unchanged	Introduction of uniform hazard spectrum and definition of seismic hazard on the base of site geographical coordinates. Enforced on July 1, 2009.	100%*	100%*

*Except for Sardinia

4.6. The NODE – NOminal DEficit - v.1.1 beta software

NODE - NOminal DEficit - v.1.1 beta (Iervolino and Petruzzelli, 2011) is a software developed as a prototype to automatically obtain the information required to implement the proposed approach of Section (4.3) and compute some of the indices discussed in Section (4.2) for the Italian territory. Its development was supported in part by the project ReLUIIS 2010-2013, funded by Dipartimento della Protezione Civile (DPM).

NODE v.1.1 beta operates in Mathworks MATLAB® environment and contains the entire evolution of seismic design codes since 1909 up to today (see Sects. 4.5 and 4.5), as well as the evolution of wind design in the same period (see Sect. 4.3.2 and Appendix A), for the whole Italian territory.

The software allows to visualize the evolution seismic classification of the whole Italian territory, associating the municipality boundaries in place at the time of design, according to different census data, provided by ISTAT (i.e. Istituto Italiano di Statistica). Thereby the software allows to easily retrieve, for each Italian site, information about the year of first seismic classification, eventual de-classification, and the entire evolution of seismic and wind design prescriptions. More over the tool includes the calculation of hazard curves on stiff soil for the whole Italian territory, on the basis of INGV data (Stucchi *et al.*, 2011). The gradient k of log-log approximation of hazard curves, for 11 fundamental periods ranging from 0 to 2 seconds, is provided for the Italian territory as useful for the definition of some of the risk indices described above (see Section 4.2),

As an example, in Figure (4.19) a map of k values is shown, obtained from linear regression of median PGA values from INGV study, considering 100, 475, 1000 and 2500 year return period data. It can be observed that k varies significantly throughout Italy with minimum and maximum values of 1.8 and 4.7, respectively. The mean value is equal to 3.07, which confirms EC8 indication, and standard deviation is equal to 0.56. The value of R^2 is wherever major than 0.99, justifying the assumption of linear regression of logarithms in the considered return period range.

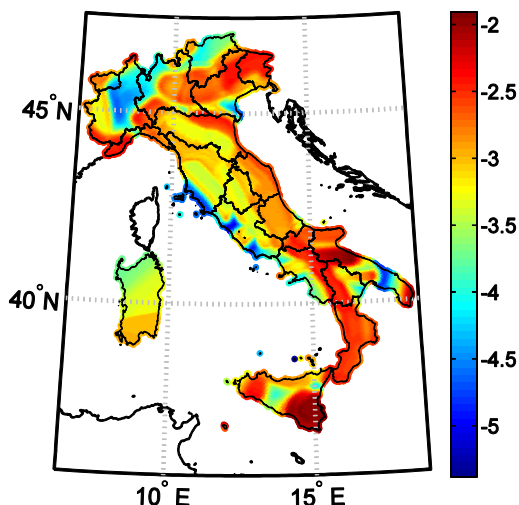


Figure 4.19 Gradient of hazard curve for PGA, obtained from linear regression of logarithms of median INGV data, considering 100, 475, 1000 and 2500 year return periods..

In a similar manner, it is possible to evaluate the slope of hazard curve for other spectral ordinates. Values of mean k , standard deviation and R^2 summarized in Table (4.3) show a significant variation with respect to those defined for PGA. Anyway, these values could be taken with prudence, due to the approximation of probability of exceedance to zero of INGV data for high spectral ordinates, which imposed to consider only three return period of the seismic action (475,1000 and 2500 years).

Table 4.3 Statistics of linear regression of hazard curves for different structural periods, obtained from median INGV data, for exceedance return periods of 475, 1000 and 2500 years.

Spectral Ordinate	mean k	Standard deviation of k	R^2
PGA	3.07	0.56	0.99
$S_a(T_1)=0.10$ s	3.14	0.52	0.99
$S_a(T_1)=0.15$ s	3.09	0.46	0.99
$S_a(T_1)=0.20$ s	2.83	0.41	0.99
$S_a(T_1)=0.30$ s	2.81	0.40	0.99
$S_a(T_1)=0.40$ s	2.57	0.34	0.99
$S_a(T_1)=0.50$ s	2.46	0.30	0.99
$S_a(T_1)=0.75$ s	2.32	0.30	0.99
$S_a(T_1)=1.00$ s	2.27	0.33	0.99
$S_a(T_1)=1.50$ s	2.22	0.33	0.99
$S_a(T_1)=2.00$ s	2.13	0.35	0.99

Another information contained in the *NODE v1.1 beta* software, thanks to the collaboration between the *Department of Structures for Engineering and Architecture* and the *Department of Civil, Architectural and Environmental Engineering* of the *University of Naples Federico II*, Italy is a zonation of site effect for the whole Italian territory, isles included, with a resolution of 1:100,000 (Santo *et al.*, 2013). As it can be seen from Figure (4.20), the tool provides the EC 8 and NIBC subsoil classification, so that the response spectrum at the site can be accordingly modified, in order to take into account site subsoil characteristics in the last 30 meters.

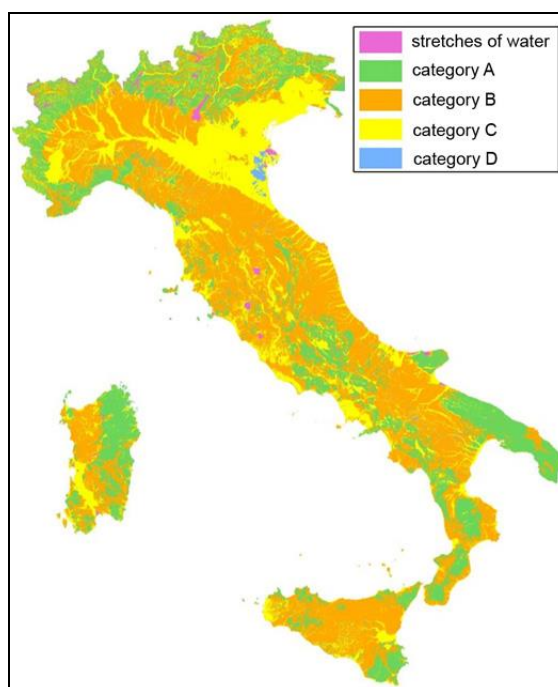


Figure 4.20 Subsoil category according to EC8 and NIBC seismic codes (Santo *et al.*, 2013).

All this information allows to compute automatically, and for large portfolios, the indices discussed in Section (4.2), whose expressions are given below for the convenience of the reader:

- the index defined by Grant *et al.*, (2007), discussed in Section (4.2.4);

$$PGA_{deficit} = PGA_D - PGA_C \quad (4.12)$$

- both the indices defined by Crowley *et al.*, (2008), discussed in Section (4.2.5);

$$PGA_{deficit} = \left(\frac{PGA_D}{PGA_C} \right)^k \quad (4.19)$$

$$S_a(T)_{deficit} = \left(\frac{S_a(T)_D}{S_a(T)_C} \right)^k \quad (4.20)$$

- the proposed $NODE$ and $NODE_{elastic}$ indices, discussed in Section (4.3);

$$NODE_{PGA} = PGA_{new} - PGA_{old} \quad (4.25)$$

$$NODE_{Vb} = V_{b,new} - V_{b,old} \quad (4.26)$$

$$NODE_{S_{a,d}(T)} = \frac{S_{e,D}(T_{1,new})}{q} - S_{d,C}(T_{1,old}) \quad (4.29)$$

$$NODE_{S_{a,e}(T)} = S_{e,D}(T_{1,new}) - S_{d,C}(T_{1,old}) \cdot q = q \cdot NODE_{S_{a,d}(T)} \quad (4.30)$$

- capacity to demand ratios in terms of PGA and spectral acceleration, reported in Eqs. (4.40) and (4.41), similar to the NZSEE (2003) index. The indices below are those calculated in the preliminary screening phase of NZSEE guidelines, except for the coefficients discussed in Section (4.2.3). The meaning of the symbols is the same already discussed for other nominal deficit indices.

$$PGA_{ratio} = \frac{PGA_{old}}{PGA_{new}} \quad (4.40)$$

$$S_a(T_1)_{ratio} = \frac{S_a(T_{1,old})_C}{S_a(T_{1,new})_D} \quad (4.41)$$

The software was developed in order to reflect the quality and quantity of gathered information about the structures of the portfolio under investigation and, therefore, to be suitable for the application in both the first two steps of the proposed procedure for prioritization. In fact, if the information necessary to the definition of fundamental period of the structure is not available, the nominal indices are automatically computed in terms of PGA, that is to say according to Eqs. (4.12, 4.19, 4.25, 4.40). On the contrary, if the available information allows the code-based definition of fundamental period, the computed risk indices are those reported in Eqs. (4.20, 4.29, 4.30, 4.41). It is worthwhile to specify that, according to seismic codes enforced in Italy since 1975 to today (that is to say since the first introduction of the response spectrum), the formulation for the definition of fundamental period required to know only the building dimensions and construction material. This kind of information is believed to be reasonably easy to retrieve from census data and/or rapid visual screening.

The program is operated via the following steps:

1. definition of nominal seismic requirements;

2. definition of parameters for seismic assessment;
3. definition of wind design parameter, if any;
4. assessment of nominal indices.

These steps may be deployed by data entry for each specific structures through the graphical interface depicted in Figure (4.21), as well as loading a spreadsheet with required basic information, for large portfolios.

Step 1 – Definition of nominal seismic requirements

To perform the assessment, it is necessary to enter geographical coordinates of the site or location name. In both cases the software automatically defines the municipality name, used in Italian seismic classification from 1909 to 2008. Once the design year is entered by the user, the seismic maps for design year code and reference year (2009) code are returned (if coordinates are entered, the software returns the exact acceleration for the site according to NIBC, otherwise the value representative for the municipality is returned as that corresponding to the centroid of the polygon defining municipality boundaries). From this step it is possible to immediately check the seismic category for seismic design, the design acceleration, if any, and whether the building was designed for vertical loads only (confront Figure 4.21, box no.1).

Step 2 – Definition of parameters for seismic assessment

After step one is completed, three boxes become editable: the first is relative to the fundamental period; the second to the foundation soil and the last one to the behaviour factor (Figure 4.21, box no.2).

The first box contains those parameters necessary for the automatic computation of the fundamental period depending on the code enforced in the design year. As previously stated, if this information is not available, that is, it is impossible to retrieve building height and/or maximum plan dimension and construction typology, nominal deficit indices can be computed in terms of PGA. This makes year of construction and site location the only strictly necessary data for the assessment.

The second box is relative to the definition of subsoil classification and topographic coefficient, according to NIBC. The NODE software automatically assigns site classification according to NIBC, according to the microzonation study by Santo *et al.* (2013), and a message notifies the user about the automatic attribution of subsoil category, otherwise subsoil category A is considered by default. In any case, the site classification can be modified by the user, if more detailed information is available. The same applies to the topographic coefficient, considered equal to one by default and modifiable by user entry.

The last box allows the definition of a user-defined behaviour factor or the use of a code-based one, for the current seismic demand. Selecting this latter option, a new window appears containing the NIBC approach for the definition of the behaviour factor for a new building and also other parameters that can be changed in the capacity term, according to design year code. The behaviour factor is, by default, equal to 1; this implies that the NODE index equals the elastic-NODE one, as stated by Eq. (4.30). Similarly to the other parameters, the behaviour factor can be modified by the user, and the seismic risk indices are accordingly computed.

Step 3 – Definition of wind design parameter

To, eventually, include the evaluation of the horizontal capacity due to wind design in the assessment, the box “Parameters for wind assessment” must be checked (Figure 4.21, box no.3), otherwise it is possible to pass to the next step. In the first case, a number of parameters appears, according to the wind code enforced at the time of design. These parameters regard essentially geometry of the building, pitch number and inclination, aperture percentage and site altitude (see Appendix A). Other parameters, necessary for the evaluation of wind base shear, are automatically calculated by the software according to the code retrieved by design age information. If the mass of the building is entered, the seismic base shear is also calculated and compared to the wind base shear, in order to assess the most demanding design action among wind and earthquake at the time of construction and quantify the capacity term accordingly.

Step 4 – Assessment of nominal indices

Once the previous steps are performed, by pressing the “Assessment” button (Figure 4.21, box no.4), the software automatically computes the base shears at the time of design and according to NIBC. Switching to the corresponding spectral accelerations, the mentioned nominal deficit indices are computed. In Figure (4.21), these indices are reported in the bottom right corner. The elastic and inelastic demand spectra and the capacity spectrum (where defined, otherwise the seismic coefficient) are always plotted for a visual evaluation of nominal gap. Finally, it is possible to export files with summary of input data and results including response spectra.

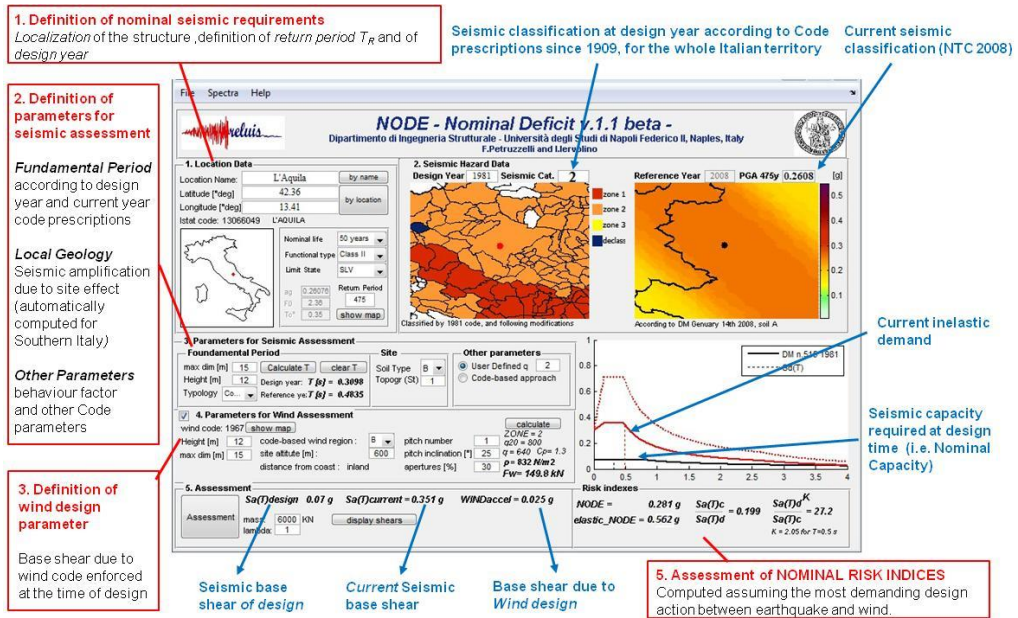


Figure 4.21 NODE – Nominal Deficit - v.1.1 beta graphical user interface.

4.7. Application of the proposed risk management procedure to the case-study portfolio

The risk management procedure outlined in Section (4.3) was applied to the case-study portfolio of Italian plants (see Chapter 3), by means of the *NODE – Nominal Deficit v1.1 beta* – software. The performed operative steps and the knowledge acquisition process are depicted in Figure (4.22). Although presented as alternate options (Fig. 4.8), the case-study was analysed computing NODE index in terms of PGA, spectral acceleration and base shear, as a function of the knowledge achieved in subsequent steps. In fact, a first ranking was performed computing NODE in terms of PGA; then, the plants were surveyed by means of the knowledge forms discussed in Section (3.3) and the NODE index was computed in terms of spectral acceleration and base shear.

It is to recall that the structures taken into consideration in the analysis of the case study portfolio are only those related to the production (83 structural units, distributed in 19 plants). These are identified by an ID composed as follows:

$$STRUCTURE_ID = PL_WS\#_SU\#_MAT_YEAR \quad (4.42)$$

where “*PL*” indicates the plant name; “*WS#*” the workshop or production building or aggregate; “*SU#*” the structural unit composing the aggregate (“#” is a progressive number); “*MAT*” represents the structural material (ST stands for steel and PRC for precast reinforced concrete) and “*YEAR*” is the year of design.

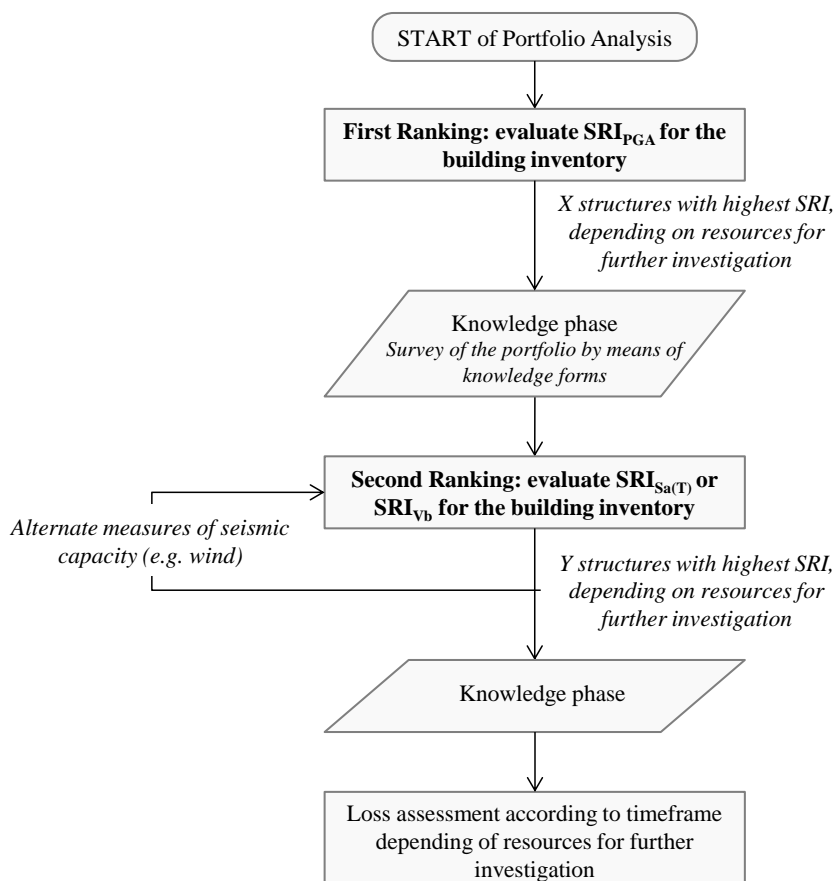


Figure 4.22 Performed procedure for risk management of case-study building portfolio.

Regarding the exposure, the number of occupants and the property damage is an information available for each structural unit; on the contrary, the business interruption is provided only for the whole plant. However, dealing with structures used for production, it seems reasonable to associate the BI loss of the plant to each individual structure, that is equivalent to assume that the interruption of the activities of a production structure causes the downtime of the whole plant. So, for each structure under consideration the OLR and ELR indices (see Section 3.1) were computed. A summary of the characteristics of the analysed structures can be found in Appendix B.

4.7.1. Step 1 –Ranking based on $NODE_{PGA}$ index

As discussed in Section (4.3), in the first phase of the proposed procedure it is possible to compute the $NODE_{PGA}$ index both considering the actual site conditions or not, depending on the availability of information. In the analysis of the case-study portfolio

both the options were explored, therefore, the first step of the procedure was subdivided into two sub-steps: a first one in which the $NODE_{PGA,rock}$ index is computed, assuming a uniform subsoil class (class “A” according to NIBC, i.e. rock) and a second one in which the effective subsoil class of each structure is considered, leading to the definition of the $NODE_{PGA,soil}$ index.

The computation of $NODE_{PGA,rock}$ is intended as a “*desk study*”, therefore the information required for the assessment can be retrieved without any visual inspection of the plant. They are, at least, geographic location and year of design. It is believed that required information is in the availability of the manager of the portfolio or it can be easily requested to the plant manager.

Generally speaking, in this phase, the knowledge about the individual structural units composing each building of the plant (see Section 3.3) could be incomplete. In this case, as a first approximation, the year of design could be the one of the older structure and/or the one of the structure with the larger exposure.

Figure (4.23) shows the $NODE_{PGA,rock}$ index computed for each plant according to Eq. (4.25). On the abscissa of the plot the considered structural units are shown, grouped for plant and ranked in order of descending PGA on rock with 475 years return period. The latter is plotted in black dotted line. The differences in the two ranking above reflect the influence of the original design: 48 of the 83 structures of the portfolio were designed in non-seismic zones, therefore their $NODE_{PGA,rock}$ index coincides with the current seismic demand.

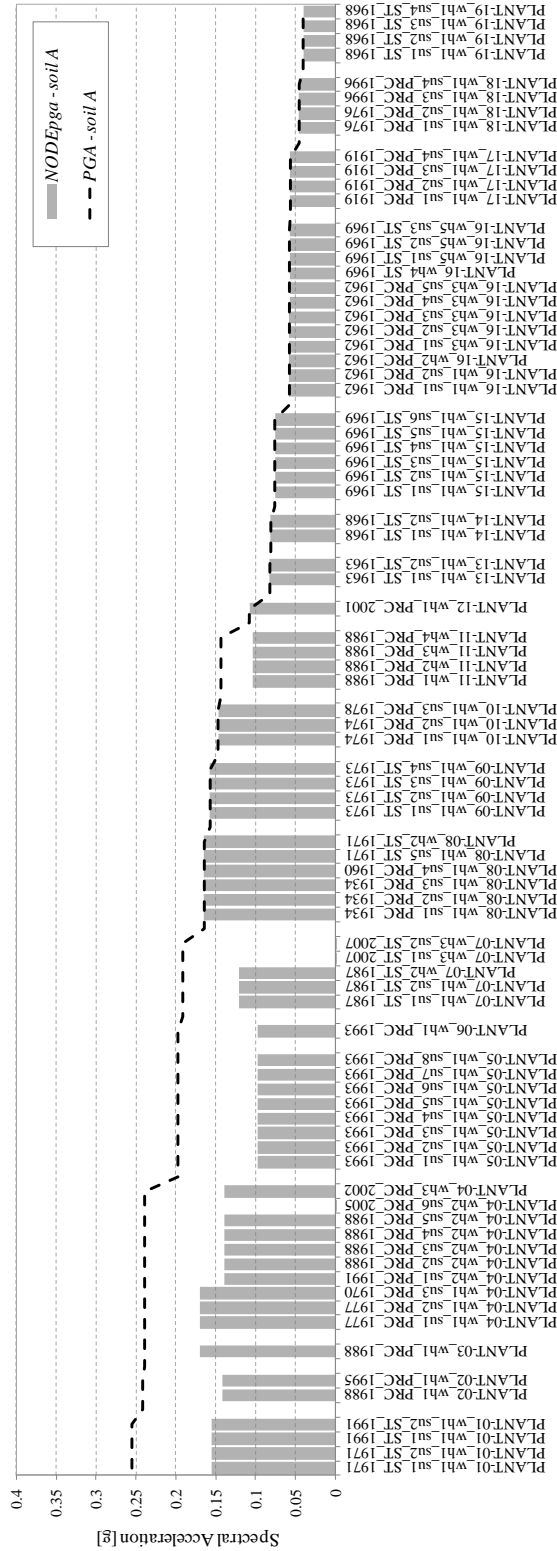


Figure 4.23 Ranking of case-study structures based on $NODE_{PGA,rock}$ (grey bars) and PGA with 475 years return period on rock (black dotted line).

The effect of the exposure can be taken into account, as in Eq. (4.32): multiplying the $NODE_{PGA,rock}$ index by the EI coefficient, that is the sum of the OLR and ELR, the $SRI_{PGA,rock}$ index can be computed.

The results are shown in Figure (4.24), normalised by the respective maximum values: blue bars represent the normalised SRI and the grey ones the normalised $NODE_{PGA,rock}$ index. It can be noticed that some of the plants characterised by high $NODE_{PGA,rock}$ values, such as PLANT-05, PLANT-07 and PLANT-15, as a consequence of their limited exposure, are shifted in a zone of low $SRI_{PGA,rock}$ values. Conversely, other plants climb the $SRI_{PGA,rock}$ ranking, moving from low values of $NODE_{PGA,rock}$ (e.g. PLANT-16 and PLANT-17).

The selection of plants to be passed to the following step can be performed both considering or not the exposure, that is to say referring to the ranking obtained computing $SRI_{PGA,rock}$ or $NODE_{PGA,rock}$, respectively.

The assumption of having limited resources, so that only the 30% of the portfolio can be investigated in an acceptable time by visual inspection, is made for illustrative purposes. This leads to consider a portion of the portfolio deserving a deeper investigation (i.e. passed to the second phase of the procedure) composed by 14 plants over 19; the remaining part is assumed to be characterised by an acceptable level of risk.

Referring to the ranking made in terms of $NODE_{PGA,rock}$ would lead to an acceptable level of risk for the plants from PLANT-15 to PLANT-19 (i.e. plants characterised by the lower grey bars in Figure 4.24).

The ranking made in terms of $SRI_{PGA,rock}$ significantly differs from the previous and the plants that would not be further investigated are: PLANT-07, PLANT-13, PLANT-15, PLANT-18 and PLANT-19 (i.e. plants characterised by a SRI value lower than 0.15, represented by the red dotted line in Figure 4.24).

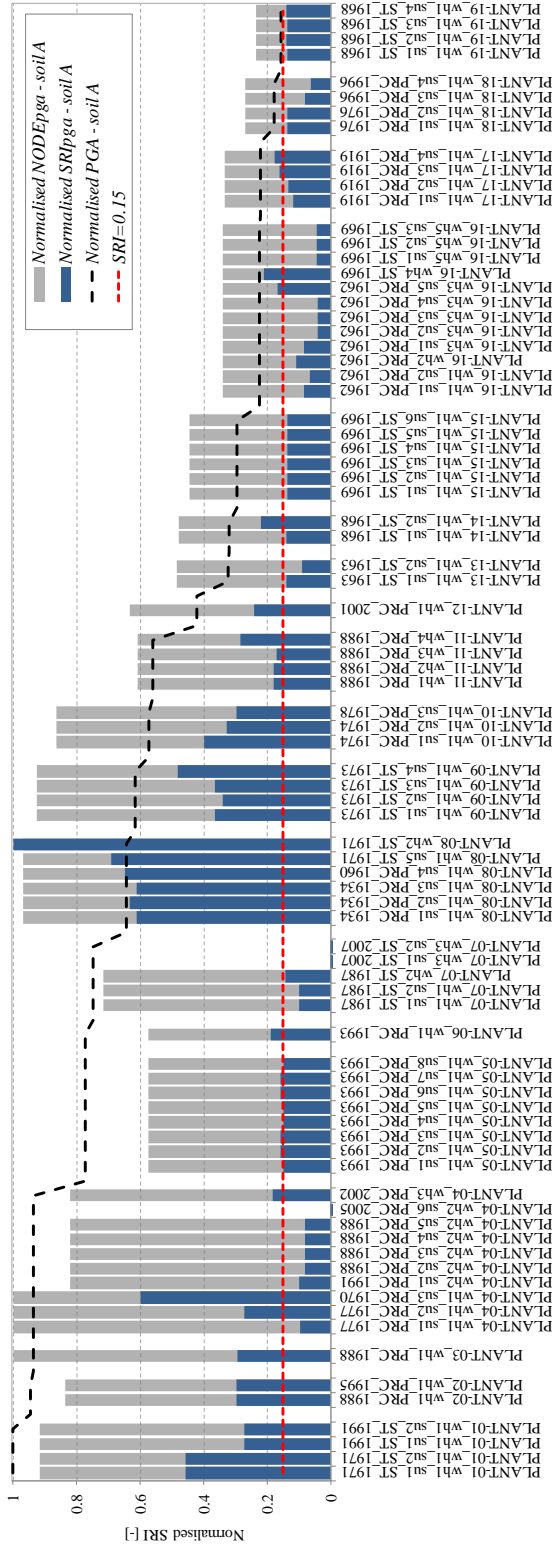


Figure 4.24 Ranking of case-study structures based on normalised $SRI_{PGA,rock}$ (blue bars), normalised $NODE_{PGA,rock}$ (grey bars), and normalised PGA with 475 years return period on rock (black dotted line). Red dotted line refers to the SRI level used for the selection of the 5 less risk-prone plants

If information about subsoil class is available, the $NODE_{PGA,soil}$ index can be computed, according to Eq. (4.25), in which the actual soil class is taken into account in defining both the seismic demand and the seismic capacity (see Sect. 4.2.1). This information could be obtained from micro-zonation studies, could be requested by the portfolio manager to the plant in a desk study, or could be obtained from field survey.

Results are shown in Figure (4.25) where the normalised $NODE_{PGA,soil}$ is depicted in grey and the normalised $SRI_{PGA,soil}$ in green.

Including subsoil class in the assessment causes significant changes in the top of $NODE_{PGA,soil}$ ranking (e.g. the highest risk is observed for the PLANT-09, characterised by a class D subsoil and plants PLANT-01, PLANT-03, PLANT-04 are shifted to the bottom), but no significant changes are observed in low risk structures.

The ranking made in terms of $SRI_{PGA,soil}$ reflects the influence of the exposure on the nominal deficit index-based ranking.

It is worth noting that the five bottom-ranking plants selected on the basis of $NODE_{PGA,rock}$ are the same as those selected according to the $NODE_{PGA,soil}$ (grey bars in Fig. 4.24 and 4.25). The same applies comparing $SRI_{PGA,rock}$ and $SRI_{PGA,soil}$ rankings, as it can be observed from the red dotted lines in Figures (4.24) and (4.25), corresponding to the SRI level below which the risk is considered acceptable.

The above suggests that, for the specific case-study portfolio, the influence of exposure seems to be more pronounced than the one of the soil class, at least in the low risk portion of the inventory. From one of the two SRI rankings (considering or not the effective soil), plants PLANT-07, PLANT-13, PLANT-15, PLANT-18 and PLANT-19 could be considered to be characterised by an acceptable level of risk and they could be not investigated more in detail. However, for illustrative purposes, the following step is performed to all the structures of the portfolio.

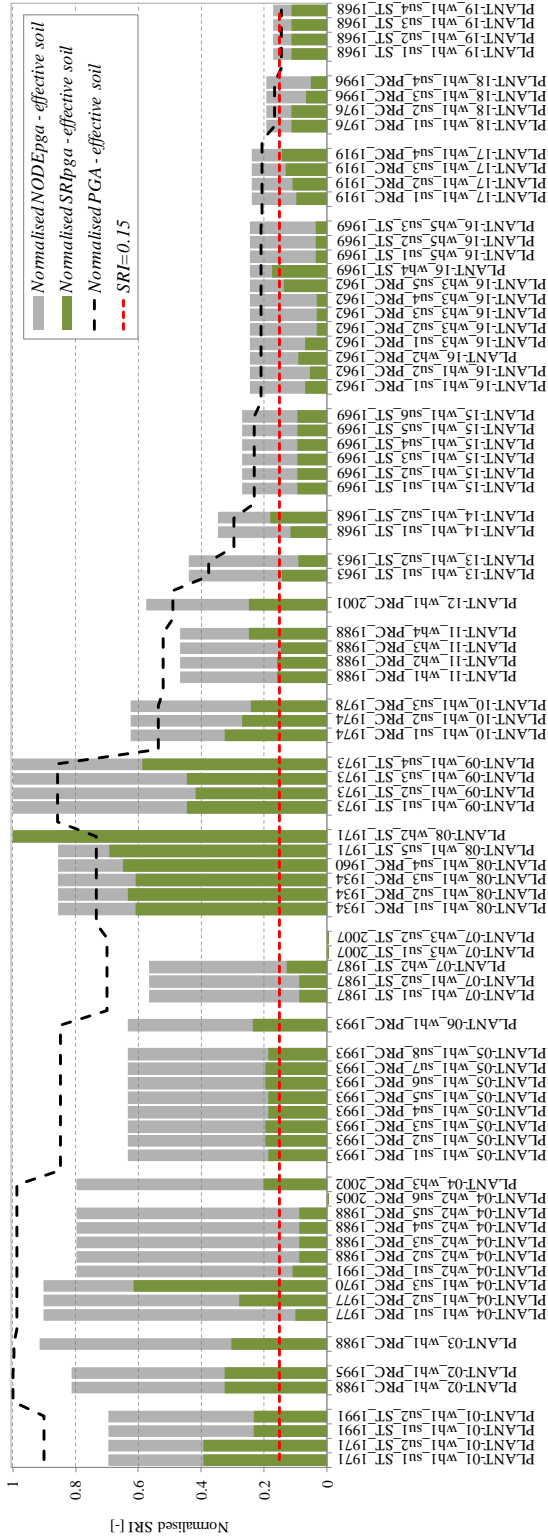


Figure 4.25 Ranking of case-study structures based on normalised $SRI_{PGA,soil}$ (green bars), normalised $NODE_{PGA,soil}$ (grey bars), and normalised PGA with 475 years return period on effective soil (black dotted line). Red dotted line refers to the SRI level used for the selection of the 5 less risk-prone plants

4.7.2. Knowledge phase

The steps described in previous Sections can be performed as a desk study or not. Conversely, the application of the second step requires the identification of individual structural units and the knowledge of their main geometric characteristics. Therefore, the plants composing the portfolio were visually surveyed and “*knowledge forms for industrial manufacturing plants*” presented in Chapter 3 were compiled. For details regarding the level of knowledge achieved and the output of the survey, the reader can refer to Section (3.3).

4.7.3. Step 2 –Ranking based on $NODE_{Sa(T),soil}$ index

The information gathered from the “*knowledge forms for industrial manufacturing plants*” allowed for the definition of the fundamental period of the structures of the portfolio (see Sect. 4.3.1). Therefore, the $NODE_{Sa(T),soil}$ index was computed, according to Eq. (4.29), considering the actual subsoil class for each individual structure.

In order to take into account the ductility and overstrength of existing buildings designed in different years, according to different structural codes, simplified assumptions were made about the behaviour factor q , applying in Eq. (4.29).

Regarding steel structures, if designed before the 1975 (year in which response spectrum and dynamic analysis were enforced, see Section 4.4.2) a q value of 1.5 was assumed; if designed between 1975 and 1996 (year in which first indications about ductility in critical zones were given, see Section 4.4.2) q was taken equal to 2.5 and, finally, if designed after 1996, a q factor equal to 3.5 was assumed. Concerning precast structures, a behaviour factor equal to 1.5 was assumed for structures designed before 1987 (year in which first prescription about mechanical connection of structural elements was given, forbidding the use of connection based on friction); q equal to 2.5 is assumed between 1987 and 1996 and 3.5 after 1996.

It is worth to underline that the values given above represent just an example of reasonable q factors to be applied in prioritization analyses (i.e. for a relative measure of seismic risk).

The results of the second step are shown in Figure (4.26), in which the $NODE_{Sa(T),soil}$ index is represented in gray and the $SRI_{Sa(T),soil}$ in red, except for plants characterised by an acceptable level of risk as resulting from the step 1 (represented in green).

In the $NODE_{Sa(T),soil}$ ranking, the influence of structural dimensions clearly emerges, causing the structures characterised by lower fundamental periods to take place in the most risk-prone portion of the ranking. As an example, the structure *PLANT-04_wh1_su3_PRC_1970*, that is a large PRC structure designed in 1970, places on the

top of the $NODE_{Sa(T),soil}$ ranking, while in the $NODE_{PGA,soil}$ ranking it occupied an average position.

The influence of the construction material on the $NODE_{Sa(T),soil}$ ranking is less pronounced than expected, since the employed code-based formulations tend, in general, to underestimate the fundamental period, in particular for steel structures. As a consequence, very often the fundamental period falls in the constant acceleration branch of the response spectrum. Underestimating the fundamental period is conservative in a force-based approach, as well as in the application of $NODE_{Sa(T),soil}$, leading to an increasing in the demand term. Nevertheless, this tends to reduce the differences in the nominal deficit of steel and PRC structures.

An example of larger fundamental periods due to construction material (steel) and geometric dimensions is the *PLANT-01_wh1_su1_ST_1991*, that is an average size steel building for which the $NODE_{Sa(T),soil}$ is significantly lower than $NODE_{PGA,soil}$. For *PLANT-07*, characterised by recent steel structures, the shifting to the bottom of the ranking is a consequence of larger fundamental periods of its structures and of higher behaviour factors too.

Regarding the ranking in terms of $SRI_{Sa(T),soil}$, it is worth noting that, even if the trend looks similar to the one observed in the previous step, there are cases in which the difference in SRI computed on the basis of $NODE_{PGA,soil}$ or $NODE_{Sa(T),soil}$ leads to significant differences in the two rankings (e.g. *PLANT-02*).

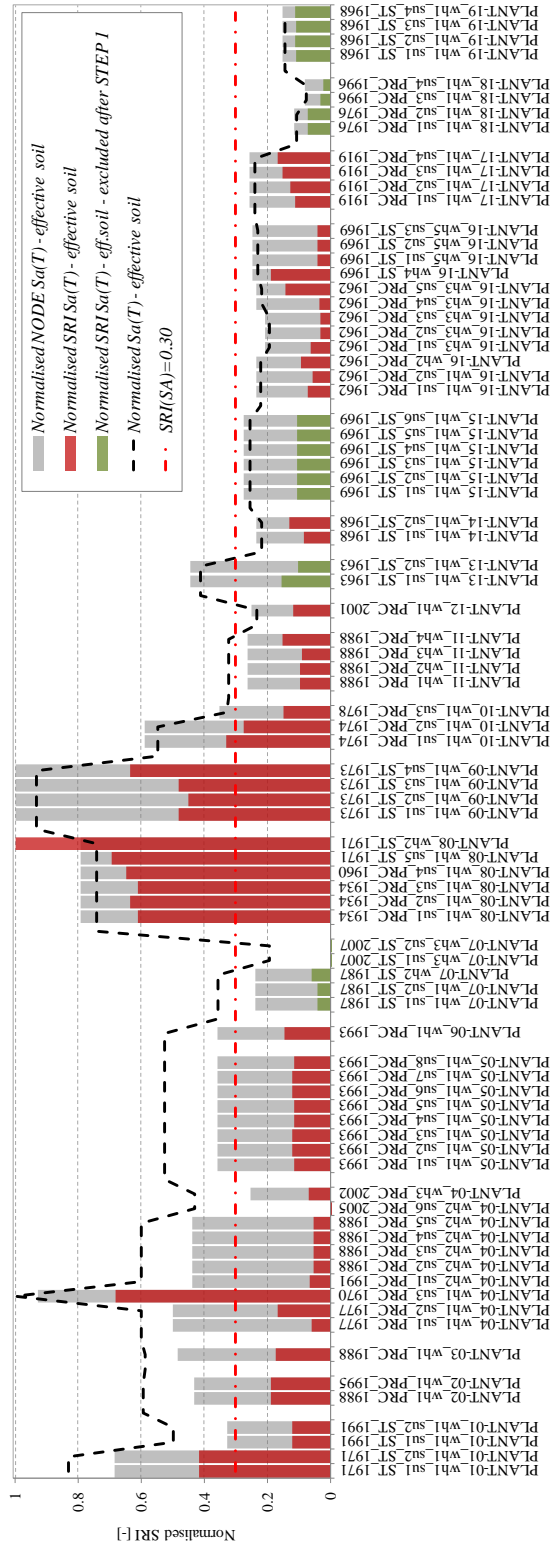


Figure 4.26 Ranking of case-study structures based on normalised $SRI_{Sat(T),soil}$ (red bars for the structures selected after Step 1; green bars for the structures excluded from Step 1), normalised $NODE_{E,Sat(T),soil}$ (grey bars) and normalised spectral acceleration with 475 years return period on effective soil (black dotted line). Red dotted line refers to the SRI level used for the selection of the 5 most risk-prone plants.

4.7.3.1. Seismic horizontal capacity from wind design

As mentioned above, more than the 50% of the structures were not designed for seismic action because at the time of design the site of construction was not included in national seismic catalogues. The achieved level of knowledge is sufficient to compute, by means of the *NODE v.1.1beta* software, the horizontal wind action according to the code enforced at the time of design. Therefore, the most demanding action between earthquake and wind can be defined and, under the hypothesis of perfect code compliance, assumed as the capacity of the structure (see Sect. 4.3.2). This is equivalent to compute the NODE index in terms of base shears (Eq. 4.26).

In doing this, some assumptions are necessary in order to assess the mass of the building and compute the equivalent wind acceleration. In the first level knowledge forms the storey weight is not required as a mandatory data, but it can be obtained referring to the geometrical dimensions and qualitative data surveyed through the form together with the information of Table (4.4), reporting typical weights for structural elements. Moreover, a fixed load accounting for equipments, lifelines and suspended masses of 1.5 KN/m^2 was assumed for all the structures of the portfolio.

Under these assumption, a storey weight ranging between 1.83 and 2.2 KN/m^2 was obtained for steel structures and between 2.5 and 4.2 KN/m^2 for PRC structures.

Table 4.4 Typical weights of structural materials and elements (CEN, 2004; PCI, 2010) .

	structural element	weight
Steel	Steel	77 KN/m^3
	lattice beam (h= 1-5m)	$2 - 8 \text{ KN/m}$
	Corrugated sheet (var. h)	$0.05-0.3 \text{ KN/m}^2$
Precast reinforced concrete	Concrete	25 KN/m^2
	Double pitched beam (h= 1.3 - 2.9 m)	$5.5 - 14 \text{ KN/m}$
	lattice beam (h= 2 - 2.5 m)	$4 - 6 \text{ KN/m}$
	L-shaped cross section beam (h= 0.4 - 1.2 m)	$7 - 17 \text{ KN/m}$
	T-shaped cross section beam (h= 0.4 - 1.2 m)	$7 - 17 \text{ KN/m}$
	I-shaped cross section beam (h= 0.4 - 1.4 m)	$4 - 9 \text{ KN/m}$
	H-shaped cross section beam (h= 0.8 - 1.4 m)	$8 - 12 \text{ KN/m}$
	TT tile roof element (h= 0.3 - 4 m)	$2 - 4 \text{ KN/m}$
	Alveolar slab (h= 0.2 - 0.5 m)	$2.5 - 6 \text{ KN/m}$
Shed roof element (h=1 m)	6 KN/m	

In Figure (4.27) a comparison between the $NODE_{Sa(T),soil}$ obtained both considering and neglecting the wind design for the definition of the horizontal capacity is shown. In approximately the 70% of the cases (58 over 83) the most demanding action at the time of design was the one due to the wind. Of this cases, 10 are relative to structures

located in sites where a seismic code was enforced at the time of design, in the remaining 48 cases the site was not classified. It can be noticed that in some cases, mainly steel structures and structure with large plan developments, a significant reduction of the deficit index is achieved considering wind design. This is the case of PLANT-09 that reduces the nominal deficit of its structures so that it is no more the most risk-prone plant. Similar considerations can be applied to PLAN-16 and PLANT-18, some structures of which reduces their nominal deficit to zero.

Conversely, in the case PRC structures designed in classified sites, the weight of such structures makes the earthquake design, in general, more demanding than wind one (e.g. plants from PLANT-02 to PLANT-06)

From the above, the opportunity of considering wind design in the definition of horizontal capacity emerges. In Figure (4.28) the $NODE_{Sa(T),soil}$ and $SRI_{Sa(T),soil}$ indices, computed accounting for wind design, are reported in grey and red, respectively. The latter nominal measure of seismic risk is the one employed for selecting the structure to investigate with more accuracy in the step 3 of the procedure.

The dotted line in Figure (4.28) corresponds to the SRI level distinguishing those structures to be inspected and analysed more in detail in step 3. The reduction of the portfolio corresponding to this assumption is by the 50% (7 of 14 plants). This level of acceptance was set for illustrative purposes; in practical applications it should be defined by the portfolio manager as a function of the available resources. Notwithstanding, in this example it seems reasonable to set a level major than the SRI value of structures excluded in previous steps.

From all the above, question arises whether considering *NODE* or *SRI* for ranking the structures, that is equivalent to adopt a criterion based on vulnerability and hazard (the *NODE* ranking) or one strongly influenced by the exposure (the *SRI* ranking). As a matter of fact, the two criteria lead to significant differences in the portion of the portfolio selected in each step for further analysis. An example is represented by PLANT-05 and PLANT-13 that, according to *NODE*-based rankings (both in terms of PGA and spectral acceleration) are classified as average risk plants. On the contrary, a ranking based on *SRI* classifies these plants as low-risk prone (Fig. 4.28). An exposure-based criterion seems the more suitable in practical applications and the more effective in taking into consideration for the real potential impact of earthquakes on the assets of the owner of the structure portfolio.

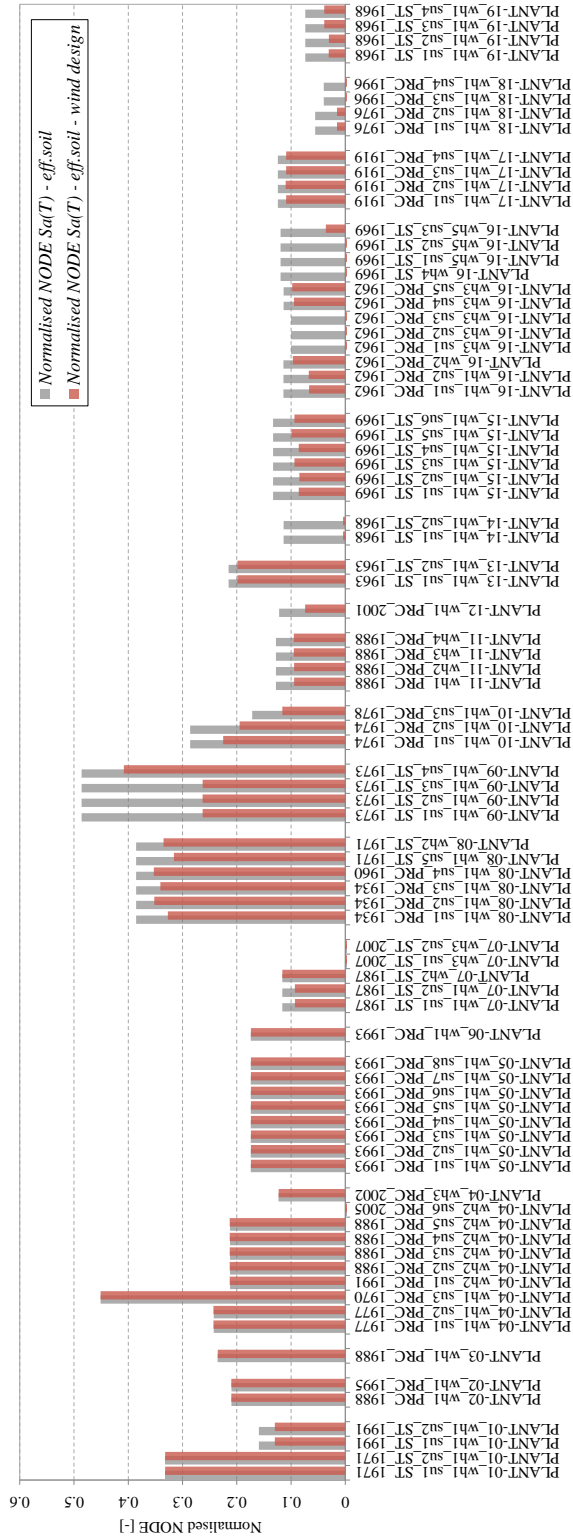


Figure 4.27 $NODE_{Sa(T),soil}$ indices computed considering wind design (red bars) and neglecting it (grey bars) for the case-study structures.

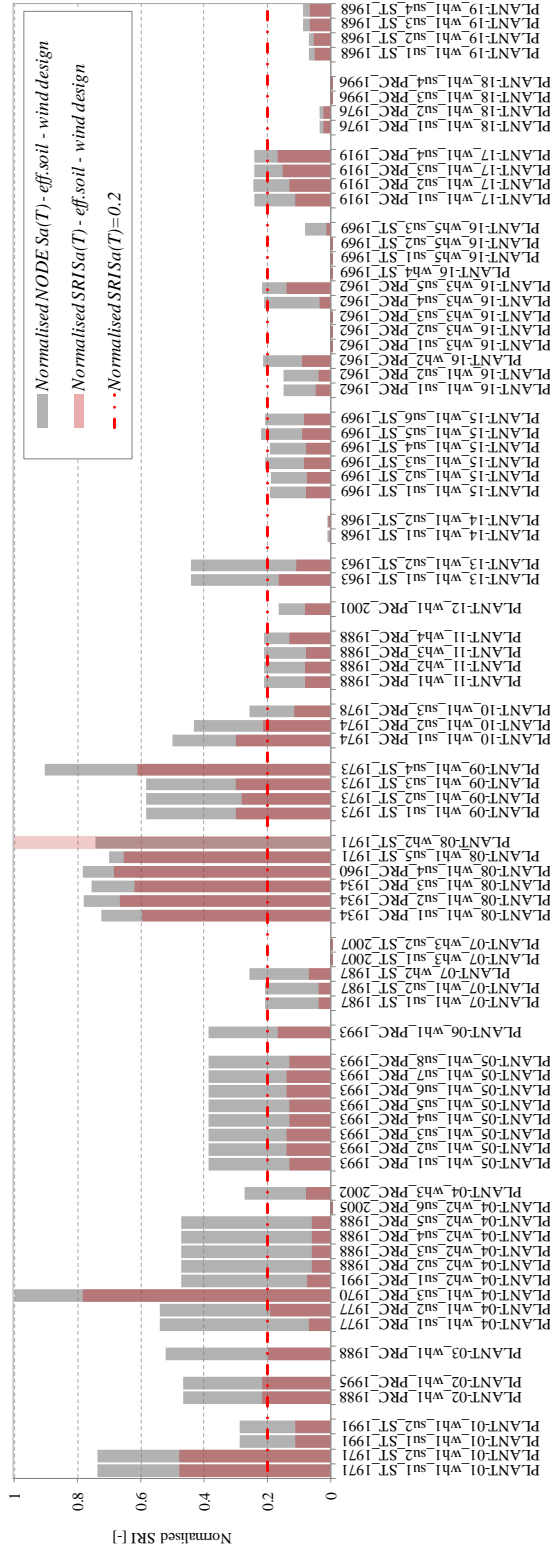


Figure 4.28 Ranking of case-study structures based on normalised $SRI_{Sa(T),soil}$ (light-red bars) and normalised $NODE_{Sa(T),soil}$ (grey bars) accounting for wind design in the definition of the nominal capacity. Red dotted line refers to the SRI level used for the selection of the 5 most risk-prone plants.

4.7.3.2. Updating seismic capacity due to earthquake occurrence

PLANT-08 and PLANT-09 are located in an area affected by the Emilia 2012 earthquake (see Sect. 4.2.3).

The most exposed structures of both the plants (*PLANT-08_wh2_ST_1971* and *PLANT-09_wh1_su4_ST_1973*) are large steel workshops, not designed for seismic action. Moreover, they are characterised by an high exposure, both in terms of number of occupants and monetary value. This led to high ranking position of these plants in all the classifications presented above, except for the one accounting for wind design. In fact, as a consequence of their large plan dimensions, considering the design wind action led to an equivalent acceleration equal to 0.07 g and 0.08g for *PLANT-08_wh2_ST_1971* and *PLANT-09_wh1_su4_ST_1973*, respectively.

The maximum PGA and spectral acceleration at 1 second, $S_a(T=1s)$, felt at the sites in the two events of 20th and 29th May, 2012 was obtained from *C10 – comma 10 – v.1.1 beta* software (see Sect. 4.3.3.1). They are: $PGA=0.027$ g and $S_a(T=1s)=0.046$ g for PLANT-08 and $PGA=0.19$ g and $S_a(T=1s)=0.16$ g for PLANT-09.

The *PLANT-08_wh2_ST_1971* reported no damage and only negligible non-structural damages were observed in *PLANT-09_wh1_su4_ST_1973*. This is believed to be related to the horizontal capacity due to wind design and remarks the opportunity of considering it in the definition of the horizontal capacity in prioritization analyses. Moreover, as discussed in Section (4.3.3), as no significant damages occurred, an updating of the seismic capacity to be employed in the prioritization analysis can be performed. Therefore, assuming as horizontal capacity the maximum between the equivalent acceleration due to wind design and the spectral acceleration observed in the Emilia 2012 earthquake, the risk rating can be updated, as shown in Figure (4.29). As a result, PLANT-08 and PLANT-09 reduce their nominal deficit and their position in the ranking becomes comparable to the one of PLANT-01.

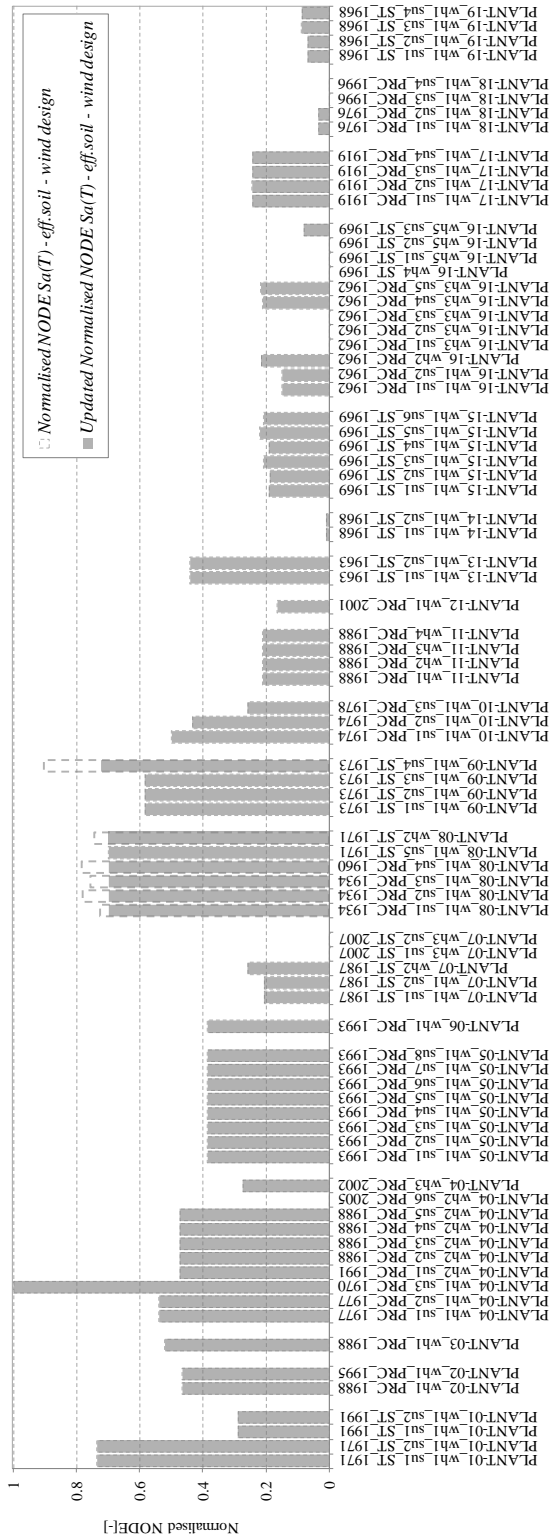


Figure 4.29 Ranking of case-study structures based on normalised $NODE_{SoT(T),soil}$ index (grey bars) updated after Emilia 2012. The ranking obtained before the updating is reported in dashed lines.

4.7.4. Knowledge phase and Step 3 – Loss assessment

The step 3 is a seismic loss assessment of the individual structures. The latter is not specific object of this Chapter and can be performed by one of the analytical approaches discussed in Section (2.3.2) or, if appropriate fragility curves can be allocated to the specific structures of the portfolio, by the procedure outlined in Chapter 5. The knowledge level required for such an evaluation is deeper than the one achieved in previous steps, therefore a knowledge acquisition phase could precede any kind of structure-specific vulnerability and loss assessment.

Finally, it is important to remark that the proposed procedure is intended as a method for driving the knowledge acquisition across the portfolio and focusing the attention to most risk-prone structures with an increasing level of detail. It never can be considered as substitutive of an analytical vulnerability assessment, accounting for the effective mechanical and geometric characteristics of the structures as well defects and deviation from the original design.

4.7.5. Comparison of *NODE* with other indices

A comparison of the $NODE_{Sa(T),soil}$ index with other indices discussed in Section (4.2) is finally performed, by means of the software *NODE v.1.1 beta*. In particular, only those indices sharing with $NODE_{Sa(T),soil}$ the assumptions regarding the code compliance and the force-based philosophy are considered. These are: the “ $PGA_{deficit}$ ” by Grant *et al.* (2007), expressed by Eq.(4.12), and those presented in Crowley *et al.* (2008), expressed by Eqs. (4.19) and (4.20) and referred to as “ PGA_{ratio} ” and “ SA_{ratio} ” in the following.

The index proposed by Grant *et al.* (2007) is quite similar to the one proposed in this thesis. Even if the authors consider (in the definition of the “effective PGA”) a constant behaviour factor and homogeneous subsoil class and fundamental period over the portfolio (see Section 4.2.4), for this comparison the $PGA_{deficit}$ index was computed taking into account the actual subsoil class, the fundamental period of the structure and the behaviour factors discussed in Section (4.7.3). The aim is, therefore, to investigate the effect of considering the “effective PGA”, above all the other aspects (see Section 4.2.4 and Fig.4.6).

In Figure (4.30) the comparison of $NODE_{PGA,soil}$, $PGA_{deficit}$ and PGA_{ratio} is shown. It can be noticed that no substantial differences can be observed in the ranking obtained by means of the first two indices. The $PGA_{deficit}$ takes into account the fundamental period of the structure in the definition of the effective PGA, for this reason some slight differences in the two rankings can be observed for plant from PLANT-01 to PLANT-07. The small difference can be also explained with the formulations adopted for the computation of the fundamental period. This leads to the conceptual difference

between the two indices: while the $PGA_{deficit}$ index represents a comparison of the actual seismic demand with a manipulation of the one enforced at the time of design, the $NODE$ is simply the comparison of the current seismic demand with the one actually employed by the professional in the original design. The latter is the reason for the adoption of code-based formulation for the computation of the fundamental period. The ranking obtained by the computation of the PGA_{ratio} index is substantially different from those described above. This is related to the assumption of a seismic capacity for the structures located in non-classified sites equal to 0.05 g, as needed for indices based on a ratio. This value is relatively high with respect to the average seismic capacity observed in the portfolio. This explains the apparent (due to the normalized plot) shifting to the bottom of the ranking of all the plants except for PLANT-08, PLANT-09 and PLANT-11. Considering the absolute values of the PGA_{ratio} , rather than the normalized ones, the increasing of the deficit ratio for all the plants designed in non-seismic zone is observed, so that they approach the average PGA_{ratio} over the portfolio. For this reasons, it can be argued that the adoption of indices based on a ratio, implying the choosing of a seismic capacity for structures not included in seismic catalogues, deeply influences the ranking and should be carefully evaluated.

In Figure (4.31) the comparison of the rankings based on $NODE_{Sa(T),soil}$ and SA_{ratio} is shown. The index proposed by Crowley *et al.* (2008) clearly contains more information regarding the hazard at the site than the corresponding $NODE$ index. In fact it employs the gradient of the logarithmic hazard curve as a measure of the hazard at the site (see Section 4.2.4). Purpose of the comparison is to observe the impact of this difference in a real case study.

Looking at the Figure, it can be observed that, besides some differences due to the specific k values at the specific site (e.g. PLANT-09) the trends of the two rankings are almost the same, therefore the two indices produce similar scales of priority.

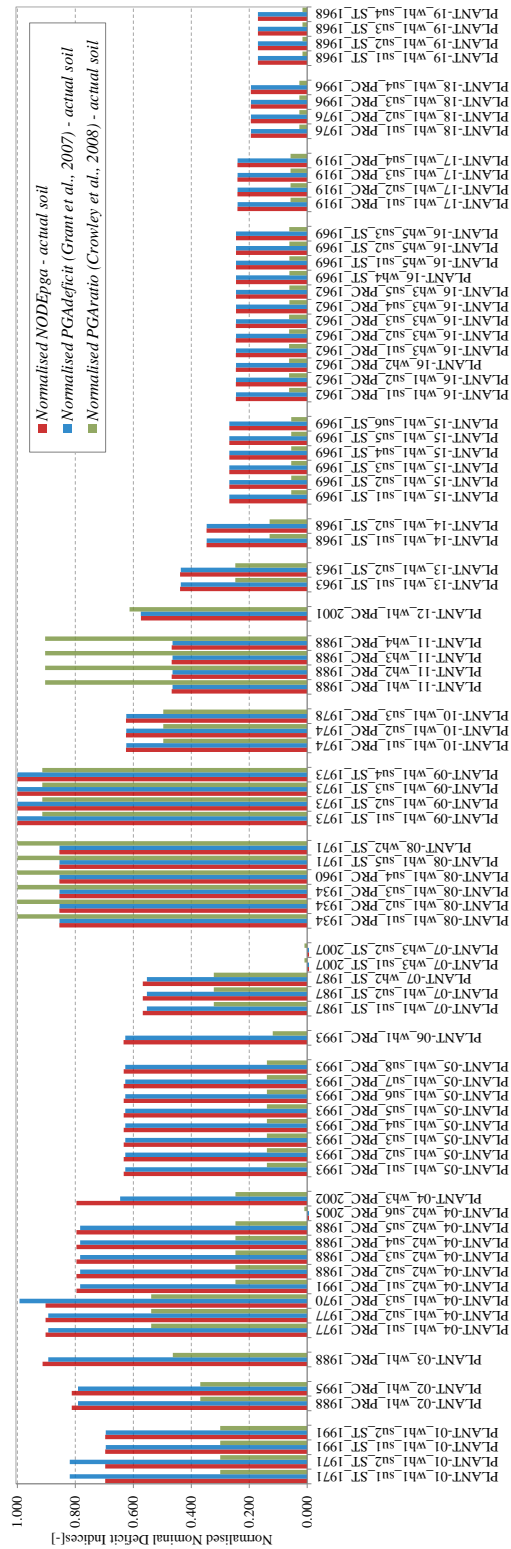


Figure 4.30 Ranking of case-study structures based on normalised $NODE_{pGA,soil}$ index (red bars); $PGA_{deficit}$ by Grant *et al.* (2007) (blue bars) and PGA_{ratio} by Crowley *et al.* (2008) (green bars).

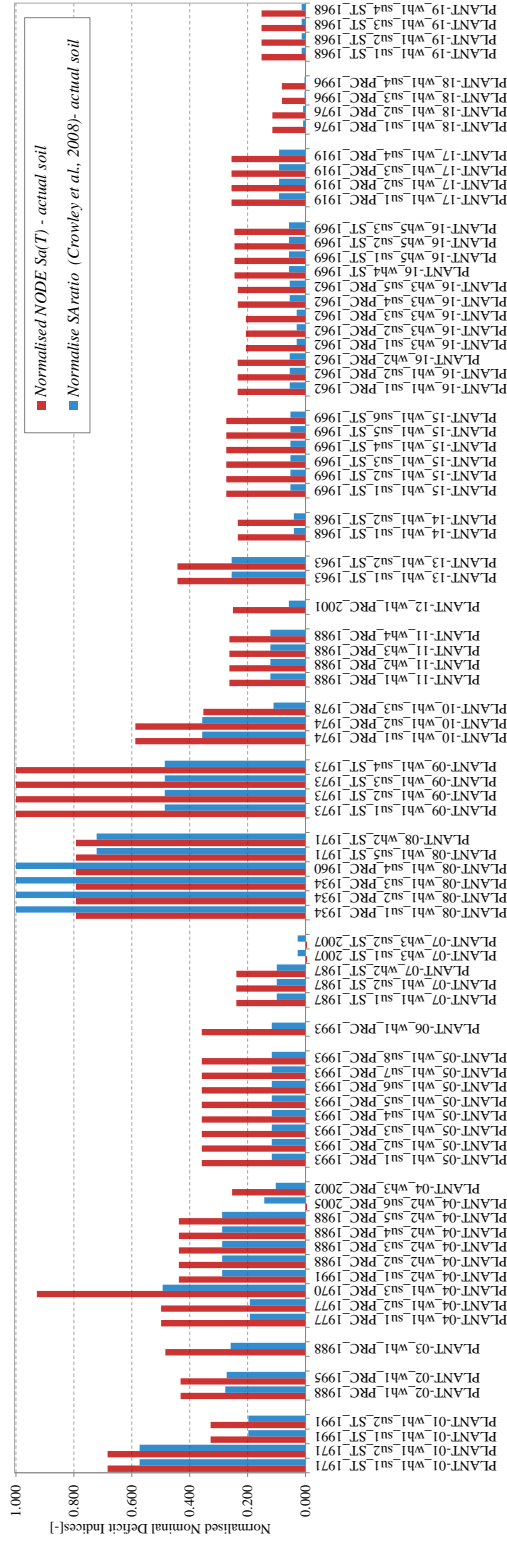


Figure 4.31 Ranking of case-study structures based on normalised $NODE_{PGA,soil}$ index (red bars) and SA_{ratio} by Crowley *et al.* (2008) (blue bars).

4.8. Conclusions

In this Chapter, some prioritization schemes and nominal indexes for the assessment of seismic risk of a building stock have been discussed and confronted with a proposal one. Such procedures and risk metrics were developed in literature because, at large scales, the limited amount of time and resources make a refined assessment of seismic risk unsuitable and the necessity for multi-level approaches arises. These approaches are usually based on a first screening phase, aimed at the selection of the portion of buildings at highest risk, performed as a “desk study” or by rapid visual screening, if any, so that only rough data about the structure are available, such as site localization, year of construction and main geometric dimensions. These information is, in general, just sufficient to assess the seismic risk of a structure in a conventional way, employing nominal indices comparing seismic capacity and demand and assuming that the actual capacity can be considered to be equal to the seismic demand provided by the code enforced at the time of design.

The proposed procedure for the risk management of large structural portfolios is based on the evaluation of nominal deficit indices. This choice is related to the evolution of seismic design provisions, which lead to a generally increasing seismic demand and more restrictive design minima. This is particularly true for the Italian case, for which a comprehensive review of seismic code requirements was produced.

A nominal deficit index called NODE (that can be expressed either in terms of PGA, Spectral ordinates or base shear) was presented and its differences with the other similar indices available in literature were critically discussed. The NODE index was developed with the specific aim of comparing the actual design acceleration employed by the practitioner in the original design to the one provided by the current codes. In doing this, the dynamic behaviour of the structure (through the fundamental period), the site conditions, the behaviour factor and the exposure of the structure are taken explicitly into account. This is due to the necessity to operate with structures that, although typical of the manufacturing industry, can be very different from each other for what concerns structural typologies and dimensions, and that can be dislocated all over the world.

In the proposed prioritization scheme the exposure was accounted by means of relative indices expressing the number of occupant and the monetary loss, normalised with respect to their maximum values. This is coherent with the relative measure of seismic risk provided by a prioritization approach.

Regarding the use of nominal deficit measures, it implies at least some of the following assumptions, which is important to recall when evaluating their applicability:

- compliance with regulatory codes enforced at the time of design, which implicitly means applicability to engineering structures only;
- the methodology needs to define the capacity for those structures in sites not considered as seismically prone at the time of design. This capacity can be assessed, for example, referring to other horizontal design actions, such as wind action;
- live loads are negligible compared to dead loads, in order to confront seismic demand and capacity in a coherent manner and neglect changes in live loads definition over the years;
- the current seismic demand is inelastic and, therefore, the demand at the time of design is considered inelastic, or vice-versa;
- the design demand at the time is assumed to correspond to a known return period of the seismic action.

The definition of the behaviour factor q , or of equivalent measures of ductility and overstrength employed in the described indices, appears as one of the critical aspects of all the described strategies to prioritization. In fact, the current seismic demand is inelastic and one of the strongest assumptions of the approach is that the demand at the time of design may be considered inelastic as well. This is not explicit in the codes pre-2003, meaning that risk indices may not be an absolute measure of performance gap but only give priorities between different structures for which they are applied in a consistent manner.

More in general, the definition of behaviour factors for different code requirements, for example referring to typical structural typologies, materials and construction practice and, most of all, minimum code requirements, should provide useful proxy of actual seismic capacity. It seems appropriate, the adopted q -factor should be lower for buildings designed according to older codes. For example, with specific reference to the Italian case, starting from 1996 detailed requirements for local ductility were enforced, so that, for a building designed according to this code, it seems reasonable to assume larger ductility with respect to a similar structure designed according to an older code. In this way, to a more recent building corresponds a lower value of the nominal deficit. Nevertheless, the evaluation of behaviour factors (both to be applied to current demand or to nominal design base shear at the time of design) is a not yet completely addressed issue and it goes beyond the purposes of this thesis.

Another relevant issue to be addressed is the difference between indices expressed in terms of ratio or difference between demand and capacity. To appreciate an advantage of considering the demand-to-capacity ratio, it is possible to take into consideration two different structures: a first one designed for 0.8 g spectral acceleration and subjected to a modern hazard estimate equal to 1.0 g, and a second one designed for

0.1 g, while it should be 0.3 g according to current standards. Taking the difference, these structures are of comparable risk, but the latter is expected to undergo significantly more ductility demand than the former, which the ratio is able to capture. On the other hand, the use of a ratio imposes the definition of a conventional horizontal seismic capacity to those buildings designed in non-seismic zones, while the difference makes it possible to assume their capacity equal to zero, which, although untrue, may be rational in prioritizing conventional risk in a portfolio.

It can be noticed that, in those cases in which the seismic demand at the time of design was greater than the current one, the discussed risk measures can take values minor than the unity, if defined as ratio, or negative values, if defined as difference. In the case of Italy, this applies basically in the case of design performed after 2003 (see Sect. 4.4); in fact, seismic demands were, according to O.P.C.M. 3274 (2003), generally larger than the current ones.

Given these general assumptions, it is worthwhile to highlight some pros and cons which readily emerge. Regarding the cons:

- All the discussed indices compare seismic performance reflecting different design philosophies behind codes at different ages. In fact, most of older Italian codes is based on admissible stress design which means linear elastic modelling at a material level, without any capacity design principle which underlies current codes, and capacity term of nominal deficit indices;
- on the other hand, the above mentioned indices assume the capacity at the time being inelastic (i.e., the code horizontal force is assumed to be comparable to linear static design of structures nowadays, which may be incorrect and requires to choose a behaviour factor to apply to current seismic elastic demand, which is a not completely solved issue of research and current practice);
- they are a blind prediction based on very poor information, while it is well known that, to assess structural seismic performance of existing structures, they have to be known in large detail (Jalayer *et al.*, 2010; Petruzzelli *et al.*, 2010);
- they do not allow a direct (absolute) estimate of expected loss, yet a comparison of deficit among a portfolio for which the same assumptions can be made;
- any systematic deviation from code requirements is neglected, unless it is conventionally considered by means of coefficients reducing the capacity, as in the NZSEE (2003) approach (see Section 4.2.3);

Regarding the pros apparently there are some, even the strong limitations described:

- these nominal measures of seismic risk are based on very poor information, which, in the most unfavourable cases, may be only the location, year of design, and material/typology, thus applicable at regional scale. Moreover, in many cases, these data are freely available from statistical analysis of building stocks;
- they allow to explicitly account for the evolution of seismic classification of the territory and evolution of codes, which may be reasonably believed to be the main cause of performance deficit, if any;
- being quantitative, they fit with hazard defined at a structural level and may account explicitly for exposure;

Even if the deficit is biased due to inaccurate assumptions they may be useful to rank priorities if they are applied consistently in an homogeneous portfolio.

The problem of assessing the capacity of structures designed in non-seismic sites was also addressed. If the nominal deficit is expressed as the difference between the capacity (i.e. the demand at the time of design) and current seismic demand (Grant *et al.*, 2007 and the proposed NODE index), a zero capacity value, although unrealistic, can be adopted in the methodology, providing consistent measures of the risk index among the analysed portfolio. On the contrary, if the risk index is expressed as a ratio between capacity and demand (e.g. Crowley *et al.*, 2008; NZSEE, 2003), the necessity of define a non-zero capacity arises. In these cases the value of the horizontal capacity can be obtained from literature or from considering wind design requirements and their evolution with codes.

The possibility of updating the seismic capacity after seismic events was also discussed. In fact, in case a structure stricken by an earthquake does not exhibit significant post-elastic behaviour, the spectral acceleration from shakemaps can be used to update the seismic capacity of the structures composing the portfolio. This approach was inspired by the one followed by DPC after Emilia 2012 earthquake. Moreover, a tool named C10 was developed, allowing to easily compute the maximum spectral acceleration from different shakemaps at a site and to compare it to the code requirements for a new structure (located in the same site and analogous to the existing one, under consideration).

In order to implement the proposed procedure, *the NODE software was developed (NODE – NOMinal DEFicit – v.1.1 beta)* (Iervolino and Petruzzelli 2011). This tool allows to compute automatically, and for large portfolios of engineering structures, all of the indices discussed, taking into account for the different information available. In fact, the software contains the site-by-site evolution of seismic hazard since 1909, the corresponding structural code requirements and wind design requirements since the

same year. If the information necessary to the definition of fundamental period of the structure is not available, the nominal indices are automatically computed in terms of PGA; otherwise, they are computed in terms of spectral acceleration.

Moreover, for what concerns the influence of site-effects in modifying the current seismic demand, the site classification according to Italian seismic regulatory Code is automatically provided for the whole Italian territory, including Sardinia and Sicily regions (Santo *et al.*, 2013). This software is believed to be a suitable tool for the rapid analysis of prioritization of a building stock by means of the application of one of the nominal indices discussed in the Chapter, as well as for the realization of National seismic risk maps (e.g. Crowley *et al.*, 2009)

Moreover, it should represent an efficient way for the professional to assess both seismic and wind action at the time of design, in the case of the assessment of an existing building, or, according to NIBC, in the case of a new construction.

NODE v.1.1 beta was used to make a **prioritization analysis of the case-study portfolio** in a framework reflecting the different knowledge levels that it is possible to achieve. From the application of the procedure emerged that more than the 50% of the portfolio was designed in non-seismic zones and that the 70% was designed for wind action.

For all the 83 production structures of the portfolio, visually inspected by means of knowledge forms, the NODE indices were computed in terms of PGA, spectral acceleration and base shear. Exposure was expressed in terms of OLR and ELR ratios (see Section 3.1) for each structure.

Regarding the possibility of performing, in a first approximation, a desk study it seems feasible considering as input data the year of design, the location and the exposure. In fact, this latter term has an impact on NODE deficit computed in terms of PGA larger than the one of soil conditions (that could be known by means of survey).

After a reasonable assessment of the building mass, the capacity deriving from wind design was computed. The case-study analysis confirmed that such an evaluation can be important, especially for industrial portfolios, that are frequently characterized by lightweight and/or large structures for which the wind action could have been the most demanding at the time of design.

Moreover, some of the structures of the portfolio were located in an area affected by the Emilia 2012 earthquake. Therefore an updating of their seismic capacity was performed, assuming that the structures behaved elastically during the earthquakes (no damage was observed after survey). Such structures were both designed for wind actions.

Some of the nominal indices available in the literature were also applied to the case-study portfolio in order to make a *comparison among different nominal deficit measures*.

Only nominal risk indices which are force-based and confronting capacity and demand in a coherent, quantitative manner, were considered. From the comparison of the ranking obtained applying nominal indices from literature and the NODE indices, a general consistency of nominal measures emerges. Nevertheless, the influence of the assumption of a uniform capacity for those structures designed in non-seismic zones was remarked. This suggests that, in practical applications, the use of a constant capacity value obtained, for instance, from literature, should be carefully evaluated.

The author recognizes the opportunity to obtain a relative measure of the probability of collapse based on the assumptions of a deterministic capacity and a linear approximation of the hazard curve at the site, as in the second step of the procedure by Grant *et al.* (2007), as well as in the approach by Crowley *et al.* (2008) and Borzi *et al.* (2008). However, the availability of hazard curves worldwide severely limits the use of such an approach for the purposes and the goals of this thesis.

Finally, it can be concluded that the appeal of the proposed approach, similarly to those available in literature, seems to raise with the size of the population and inversely with respect to the level of detail in which each structure is known. However, if applied consistently over the portfolio, it can provide useful indications for the definition of risk mitigation strategies. In particular, the procedure can individuate those top ranking structures to investigate more in detail and for which a structural analysis is required. This portion of the portfolio is defined as a function of the resources in the availability of the stakeholder for investigating the structural portfolio more in detail.

Chapter 5 – FRAGILITY-BASED RAPID SEISMIC RISK ASSESSMENT

5.1. Introduction

As discussed in Chapter 1, the “meso-scale” procedure, outlined in this Chapter, consists in the explicit computation of the losses by means of the convolution of hazard, fragility and exposure (Fig. 5.1). The outputs of this procedure are failure probabilities for given limit states and estimates of the loss due to earthquake.

The procedure is thought to be applied to the scale of the single industrial plant or groups of industrial installations (tens to hundreds of buildings). In fact, it is believed that, at this scale, it is possible to achieve a level of knowledge about the characteristics of each building under investigation, sufficient to associate a fragility curve to it (or to classes of buildings individuated among the portfolio) selected from those available in literature or computed ad-hoc (e.g., as performed in Chapter 6). Since this procedure requires the knowledge of parameters such as the seismo-resistant system, the construction material, the structural typology, the quality of the main structural details, it is believed it can be applied after a knowledge phase, performed at least at the same level of detail as the one described in Chapter 3.

The application of the procedure presented in the following is independent from the one outlined in Chapter 4; nevertheless, if the size of the building portfolio under investigation is particularly large, a prioritization analysis (Chapter 4) could be necessary. This could reduce the size of the portfolio under investigation and render the knowledge phase affordable.

The use of fragility curves in the computation of seismic risk can be considered a well-established methodology in science and a number of fragility curves are available in literature. Nevertheless, significant differences exist between fragility functions computed in different geographical contexts, reflecting the differences in structural typologies, construction practice and materials. Therefore, several efforts have been aimed at the collection and comparison of available fragility functions. A number of international research projects have targeted, inter alia, the identification or the computation of fragility curves for structural types mostly recurrent in different geographical areas. Recent examples are: the Syner-G (2009) project, for common RC and Masonry building types in Europe; the LESSLOSS (2005) project, for building classes of the Istanbul and Lisbona case-studies; the Risk-UE project (Mouroux and Le Brun, 2006), for the cities of Barcelona, Bitola, Bucharest, Catania, Nice, Sofia and

Thessaloniki. Moreover, collections of fragility curves are, typically, provided in loss assessment frameworks and tools, such as in HAZUS (FEMA, 2001) and SLAT (Bradley, 2009) (for a review of loss assessment tools, the reader could refer to Daniell, 2009).

The wide variability of these curves in terms of employed intensity measure, considered limit states and structural types to which they relate, makes the allocation of a fragility curve (or a set of fragility curves) to a specific structure (or class of structures) a non-trivial task.

Therefore, in order to support the application of the procedure outlined in Figure (5.1), the “*FRAME - Fragility-based Rapid seismic Risk AssessMEnt - v.1.0 beta*” software suite was developed. This is a collection of tools allowing, from one hand, the inventory, the comparison and the harmonization of the wide variety of fragility curves available in literature and, from the other hand, their use in conjunction with hazard estimates and exposure for the computation of the expected losses due to earthquakes.

In this Chapter, a brief review of the main typologies of fragility curves available in literature is performed first (Section 5.2), in order to enlighten the main differences existing in the methodologies employed for their computation, the intensity measures employed and the considered limit states. Subsequently, the *FRAME v.1.0 beta* software suite is presented and each tool composing the suite is described in its main features (Section 5.2). Finally, indications are given about the application of this suite to structural portfolios (Section 5.3)

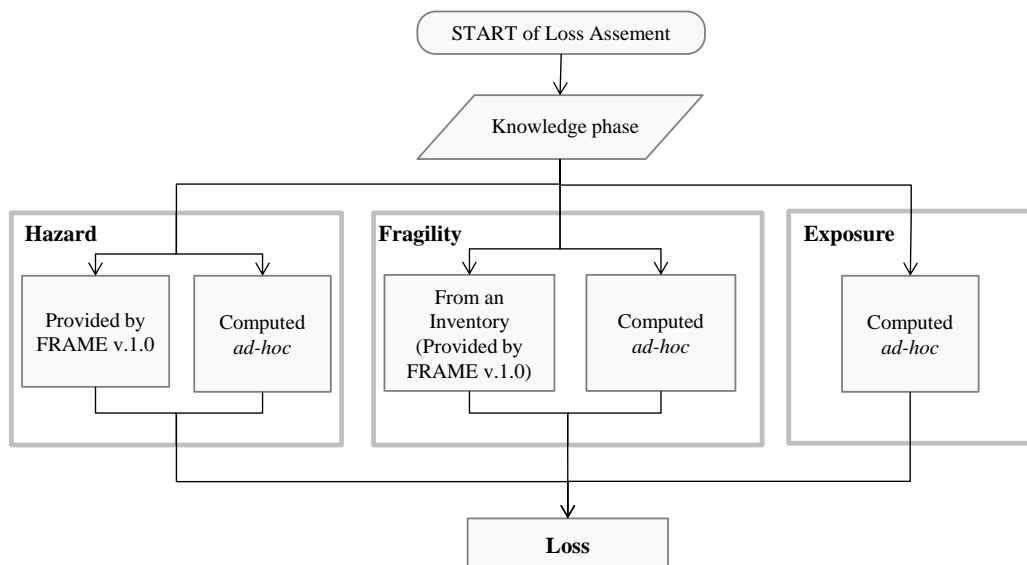


Figure 5.1 Second level procedure for seismic risk assessment

5.2. Review of existing fragility curves

The vulnerability of a structure can be described, in the framework outlined in Chapter 2, by vulnerability curves or fragility curves (Fig. 5.1). Vulnerability curves directly relate the IM to a loss, expressed by a metric among those presented in Section (2.3.3). Therefore, they express the probability of observing a loss level, given a measure of the ground shaking.

Fragility curves describe the probability of exceeding a specific level of damage corresponding to different structural performances (or limit states). Referring to the i^{th} limit state, the fragility curve is expressed by $P[D > C_{LS_i} | im]$, where D is the demand, C_{LS_i} is the capacity corresponding to the considered limit state and im a given value of the IM (see Section 2.2).

Vulnerability functions can be derived from fragility functions, once a relationship describing the probability of loss, given a performance level is provided. Vulnerability functions are not addressed in this Chapter, whereas simple relationships providing the expected loss will be considered (see following Section 5.3).

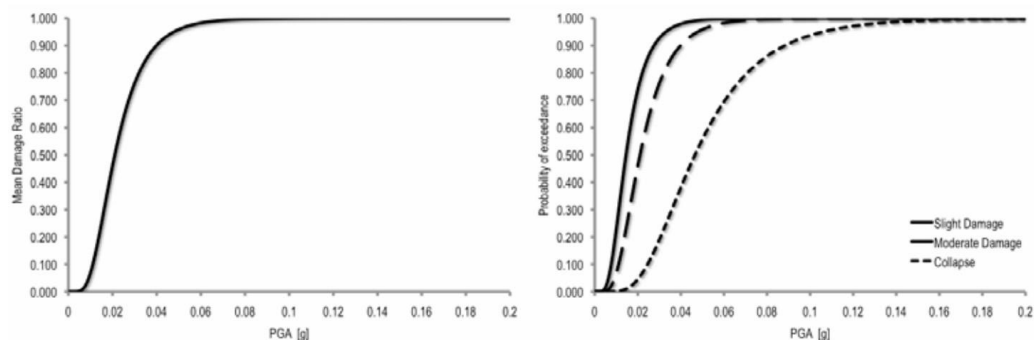


Figure 5.2 examples of: (a) Vulnerability curve; (b) Fragility curve

A comprehensive review of the fragility curves available in literature goes beyond the scope of this thesis. Nevertheless, a brief review of the main methodologies available for the computation of fragility curves and main differences that can be observed in terms of intensity measure employed and limit states considered, is given hereinafter.

5.2.1. Methodologies for computing fragility curves

Different methods can be used for computing fragility curves. According to these, it is possible to distinguish:

- empirical fragility curves;
- expert opinion-based fragility curves;

- analytical fragility curves;
- hybrid fragility curves.

Empirical fragility curves are constructed by the statistical analysis of the observed damage during past earthquakes, collected, in general, by means of post-earthquake survey forms. As discussed in Section (2.3.2), even if a realistic representation of the damage is provided, these curves present the typical shortcomings of a Macroseismic-based approach to vulnerability.

In empirical approaches the damage can be expressed in terms of a macroseismic intensity scale (e.g. ATC-13; Spence *et al.*, 1992; Orsini, 1999) or in terms of an instrumental IM (see next Section). In the latter case, on the basis of ground motion registration at the site or by the use of ground motion prediction equations, it is possible to associate at each observed damage the value assumed by a given IM at the site (eg. Shinghal and Kiremidjian, 1997; Mosalam *et al.*, 1997). In Figure (5.3) examples of empirical fragility curves expressed in terms of different instrumental IMs are given.

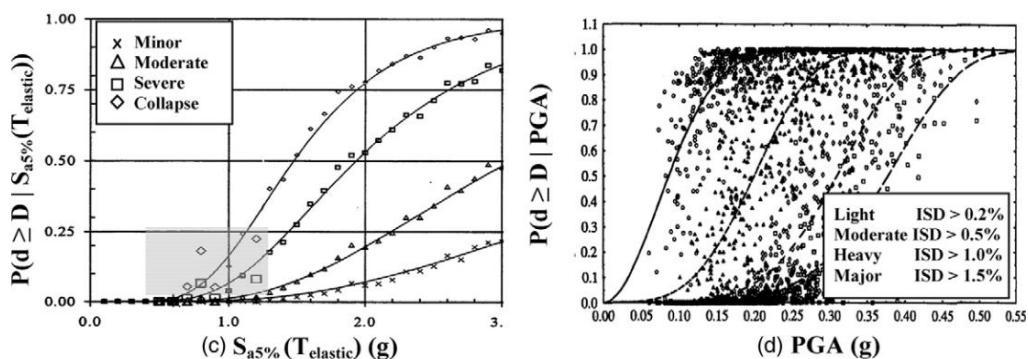


Figure 5.3 (a) Singhal and Kiremidjian (1997) curves for low-rise RC moment resisting frames (points updated with observational data are shown as the larger symbols in the shaded area) using the Park and Ang damage index; Right panel: (b) Mosalam *et al.* (1997) curves for low-rise RC MRF using inter-storey drift values to define damage (adapted from Rossetto and Elnashai, 2003).

Rossetto and Elnashai (2003) developed empirical fragility curves for European reinforced concrete building population, on the basis of 99 post-earthquake damage distributions observed in 19 earthquakes and concerning a total of 340000 RC structures. The combination of data from different earthquakes and locations allowed to cover a wide range of ground motion and to overcome the typical scatter in collected damage data regarding structural characteristics for different building classes. Referring to different earthquakes and, therefore, different seismological contexts,

building heritages and construction practices, the authors defined a new damage scale (called homogenized reinforced concrete scale, HRC, see Section 5.2.3) and employed different GMPEs. Empirical fragility curves were provided considering various parameters for strong ground motion characterization, namely PGA, elastic spectral acceleration and displacement at the fundamental period of the structure and inelastic spectral displacement, as reported in Figure (5.4).

The authors observed that, using spectral displacement, a better correlation to the empirical data was obtained. More recently, Rota *et al.* (2008) proposed continuous fragility curves for Italian buildings, expressed in terms of PGA, obtained by fitting lognormal distributions to damage data evaluated in form of DPMs. More than 91000 damage survey forms from past Italian earthquakes, ESM-98 damage scale and 23 different building typologies were considered by the authors. For each sample (given a building class, a seismic intensity and a damage level) the inverse of the standard deviation of lognormal fitting was used as a measure of the reliability of the single sample.

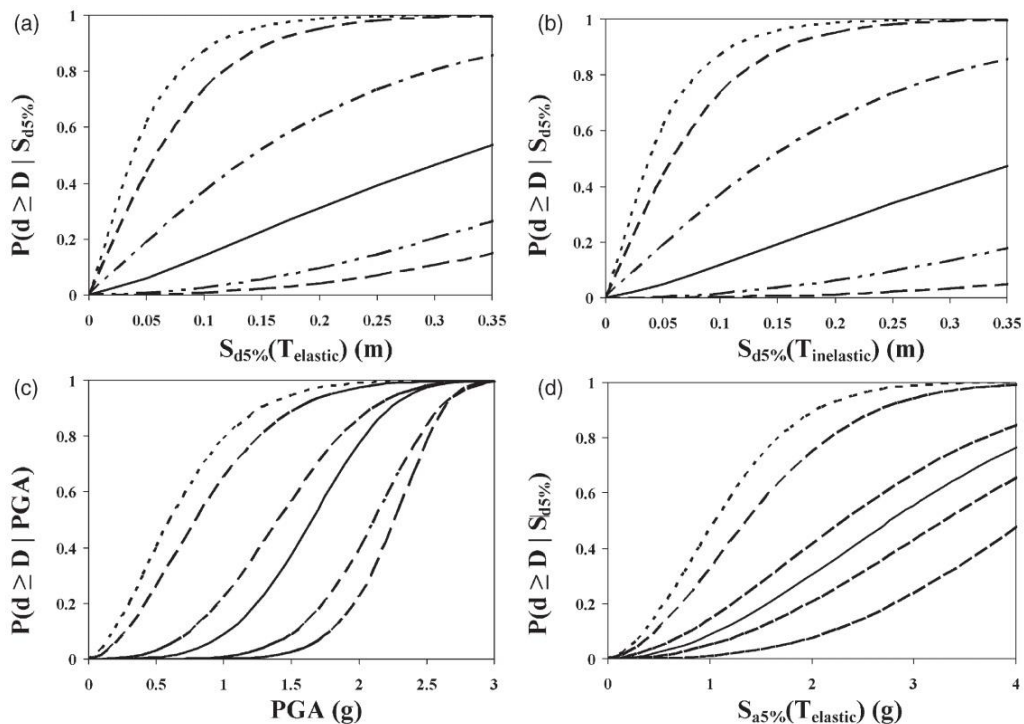


Figure 5.4 Empirical fragility curves for different IMs (Rossetto and Elnashai, 2003)

Those presented were just few representative examples of empirical fragility curves. Other examples are given in (LESSLOSS, 2005; Liel and Lynch, 2009; Sarabandi, 2004).

Expert opinion-based fragility curves are developed from the indications of an expert panel about the mean loss or probability of damage for different structural typologies. These methods, as discussed in section (2.3.2.4), are not affected by the shortcomings deriving from lack in data, but are inevitably affected by the differences in the personal judgment of each expert. Few examples of continuous fragility curves exists in literature (e.g. Kostov *et al.*, 2004), in many cases expert judgment has been employed for computing DPMs (that actually are the discrete representation of a fragility function), as discussed in section (2.3.2.4).

Analytical fragility curves are computed by means of the statistical elaboration of damage distribution deriving from the analysis of structural models, under increasing earthquake intensity. The general flowchart of the analytical computation of fragility curves is illustrated in Figure (5.5):

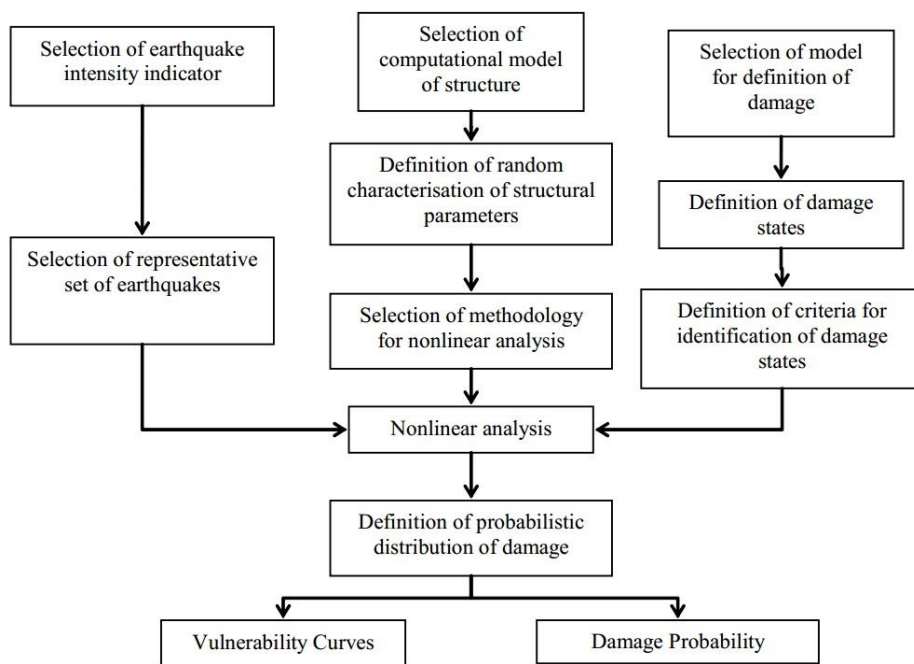


Figure 5.5 Flowchart describing the main steps for the determination of analytical vulnerability functions and DPMs (adapted from Dumova-Jovanoska (2004))

Generally speaking, the analytical computation of fragility curves should properly take into account the uncertainties in both the capacity and the demands and should analyse the structural models in a range of seismic intensity sufficiently wide to investigate the structural performances of interest (that can range from operational limit states to the collapse). The methods for the analytical computation of fragility curves can be classified, as a function of the structural analysis employed, into: (i) non-linear static

analysis-based methods and (ii) non-linear response history analysis-based methods. A further distinction could be made between lumped plasticity models and distributed plasticity (fiber element-based) models. According to non-linear static methods (see Section 6.4.2), the capacity is represented by a pushover curve (representing base shear versus the displacement of a representative point), transformed in an equivalent single degree of freedom (SDOF) system. The demand is usually expressed in terms of acceleration and/or displacement spectrum. In most cases, the definition of the seismic demand is performed according to a capacity spectrum based approach (see Section 2.3.2.2). Examples of the application of non-linear static methods to compute fragility curves can be found in Shinozuka *et al.* (2000), HAZUS (FEMA, 2001), Ricci (2010). The second class of methods of the previous list employs Non-linear response history analyses (RHAs). They represent the best way for propagating record-to-record variability; nevertheless they are time-consuming and computationally cumbersome. Such an approach was employed in this thesis for the analytical computation of fragility curves of a case-study industrial building.

A detailed description of the procedures for computing fragility curves by means of RHAs can be found in Chapter 6.

In most cases, analytical fragility curves are fitted by a probabilistic model. Typically, lognormal model is adopted (Porter *et al.*, 2007). Such a model, characterized by zero probability density at and below zero EDP and fully described by the first and second moments, demonstrated to fit well a variety of structural component failure data (e.g., Aslani 2005, Pagni and Lowes 2006), as well as non-structural failure data (Porter and Kiremidjian 2001, Badillo-Almaraz *et al.* 2007).

In the following some examples of analytical fragility curves developed in literature are given.

Singhal and Kiremidjian (1996) estimated vulnerability curves and DPMs for different RC frames (from Low-Rise, Mid-Rise and High-Rise classes, respectively) through nonlinear dynamic analyses and using the Monte Carlo simulation technique. In this way both uncertainties in seismic demand and capacity were propagated. After performing nonlinear dynamic analyses, for each of the considered level of ground motion intensity, a lognormal distribution of the Park and Ang (1985) damage index was fitted and, once capacity is expressed in terms of Park and Ang index for different limits states, the probability that the demand exceeds the capacity at each level of ground motion intensity was obtained (discrete points in Figure 5.16). Hence, smooth vulnerability curves were obtained fitting lognormal distribution functions to above mentioned probabilities (solid lines in Figure 5.16).

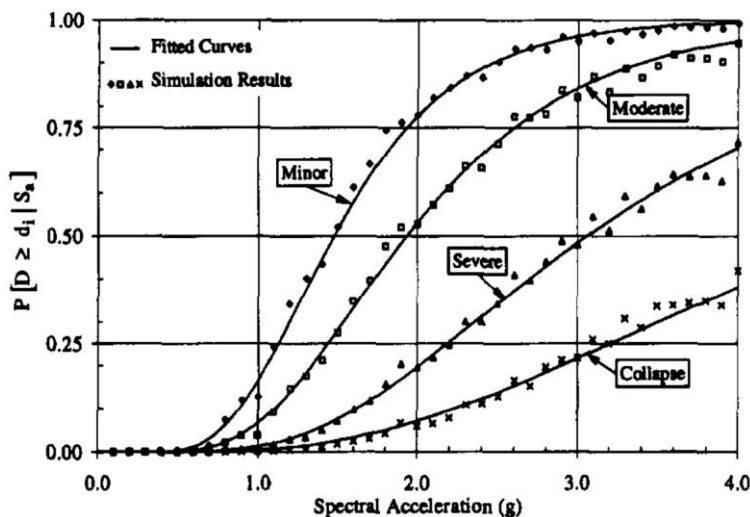


Figure 5.6 Fragility curves for Mid-Rise frames (Singhal and Kiremidjian, 1996)

Rossetto and Elnashai (2005) applied adaptive pushover analyses and capacity spectrum methodology (see Section 2.3.2.2) to European buildings in order to obtain the performance point which was then correlated to a damage state through a damage function calibrated to experimental data (Rossetto and Elnashai, 2003). This procedure was repeated using the acceleration-displacement spectra of many ground-motion records and the variability in the structural characteristics of the buildings was modelled using a response surface method, thus leading to the derivation of analytical displacement-based vulnerability curves.

Dumova-Jovanoska (2004) produced vulnerability curves and damage probability matrices for reinforced concrete buildings built in the Skopje region, employing dynamic nonlinear analysis with a set of 240 synthetic earthquake records. The damage to the structures was measured using the damage index by Park and Ang (1985) and corresponding individual discrete damage states. A normal probabilistic distribution was assumed for the probability of occurrence of damage.

As described above, the computational time needed for analytical methods in general is high. This impacts upon their usability, especially in large scale vulnerability assessments. To reduce the computational effort related to the approaches previously described, simplified analytical models are often used, allowing to perform a large number of structural analyses and to adequately propagate the uncertainties. Some of the simplified analytical approaches available in literature have been presented in Section (2.3.2.2). An alternative to the previous is the adoption of hybrid approaches.

Hybrid fragility curves are based on a combination of different methods for damage prediction. In general, hybrid methods combine analytical modelling and Macroseismic observations of damage in past earthquakes.

Kappos *et al.* (1995, 1998) derived DPMs using a hybrid procedure according to which some DPMs are constructed using vulnerability index procedure and non-linear dynamic analyses are carried out on building models representing different building classes. Such analytical results are included into the DPMs, by means of an empirical correlation between intensity and PGA values at which the accelerograms employed for non-linear analyses were scaled. A correlation is also established between an analytical global damage index obtained from the analyses and the damage expressed as the cost of repair. A total of 120 analyses of typical Greek buildings designed for the 1959 code were run (for 6 structures, 10 ground motions and 2 intensities), and the statistical damage results were combined with the observed damage from the 1978 earthquake in Thessaloniki. A similar methodology is pursued in (Kappos *et al.*, 2010). In (Singhal and Kiremidjian, 1998) the analytical vulnerability curves proposed in (Singhal and Kiremidjian, 1996) for Low-Rise RC frames are updated, based on the observational data obtained on 84 buildings damaged during the 1994 Northridge earthquake, by means of a Bayesian updating technique accounting for the reliability of different data sources. As stated by Calvi *et al.* (2006), the main difficulty in the use of hybrid methods is related to the different sources of uncertainty contained in the analytical and empirical vulnerability curves. In fact, in the first case the sources of uncertainty are defined during the generation of the curves whilst, in the second, the specific sources and levels of variability in the empirical data are not quantifiable.

Calvi *et al.* (2006) suggest that, in order to improve an analytical model through a comparison with an empirical one, it probably would be better to calibrate the former in order to obtain only median values equal to the ones provided by the latter. In this way, the observational data are used to calibrate the analytical model and analytically-derived vulnerability curves, with their sources of uncertainty, are used in the loss model. Therefore, only the uncertainty related to the capacity is propagated and not that related to the ground motion. This ensures that, when fragility curves are used for the assessment of failure probability, the variability in seismic input is not double-counted (in both the hazard curve and in the fragility curve).

5.2.2. Intensity Measure types

Fragility curves express the probability of exceeding a limit state to a given level of ground shaking. Regardless of the methodology employed for their computation, different intensity measures (IM) can be adopted for expressing a level of ground shaking. IMs can be grouped into: (i) empirical (or Macroseismic); (ii) instrumental.

Regarding empirical IMs, different Macroseismic intensity scale can be used for expressing the effect of earthquakes on the physical environment. The first of these scales was introduced by Rossi and Forel in the late nineteenth century and later revised by Mercalli in the early 1900. This classification, initially composed of 10 degrees of intensity (from “not felt” to “destruction”), was subsequently extended to 12 degrees (from “Instrumental” to “Cataclysmic”) by Cancani and later modified by Mercalli, Cancani and Sieberg (MCS intensity scale) in 1930 (Sieberg, 1930). This scale was further modified in the mid of the twentieth Century by Richter (Modified Mercalli Intensity scale, MMI). The MCS scale introduced, for the first time, qualitative indications about the portion of building which suffer a certain level of damage. This kind of information was kept in all subsequent intensity scales, such as the Medvedev-Sponheuer-Karnik one (MSK) (Medvedev and Sponheuer, 1969) . The MSK scale was revised in 1976 and 1981 and was superseded by the European Macroseismic Scale in 1998 (EMS-98) (Grüntal *et al.*, 1998) which is characterised by a greater degree of detail than the previous one. According to it, six vulnerability building classes are defined (A to F, as reported in Figure 5.7) and for each class a qualitative description (“few”, “many”, “most”, as reported in Figure 5.8) of the portion of building suffering a given level of damage (1 to 5, as reported in Figure 5.9) is provided, as a function of the seismic intensity level, ranging from V (the onset of structural damage) to XII.

	Type of Structure	Vulnerability Class					
		A	B	C	D	E	F
MASONRY	rubble stone, fieldstone	○					
	adobe (earth brick)	○	—				
	simple stone	—	○				
	massive stone		—	○	—		
	unreinforced, with manufactured stone units		—	○	—		
	unreinforced, with RC floors			—	○	—	
	reinforced or confined				—	○	—
STEEL REINFORCED CONCRETE (RC)	frame without earthquake-resistant design (ERD)			—	○	—	
	frame with moderate level of ERD			—	○	—	
	frame with high level of ERD				—	○	—
	walls without ERD			—	○	—	
	walls with moderate level of ERD				—	○	—
	walls with high level of ERD					—	○
STEEL	steel structures				—	○	—
WOOD	timber structures			—	○	—	

Figure 5.7 Vulnerability classes according to EMS-98 scale (Grüntal *et al.*, 1998)

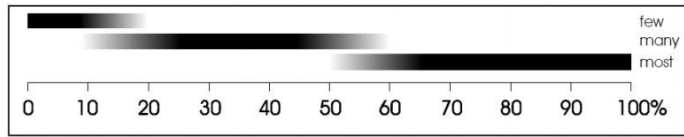


Figure 5.8 Definition of quantities according to EMS-98 scale (Grüntal *et al.*, 1998)

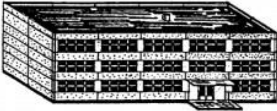
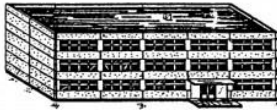
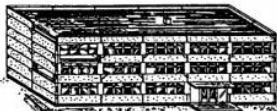
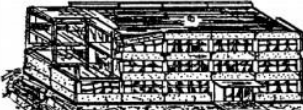
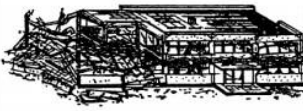
Classification of damage to buildings of reinforced concrete	
	<p>Grade 1: Negligible to slight damage (no structural damage, slight non-structural damage)</p> <p>Fine cracks in plaster over frame members or in walls at the base. Fine cracks in partitions and infills.</p>
	<p>Grade 2: Moderate damage (slight structural damage, moderate non-structural damage)</p> <p>Cracks in columns and beams of frames and in structural walls. Cracks in partition and infill walls; fall of brittle cladding and plaster. Falling mortar from the joints of wall panels.</p>
	<p>Grade 3: Substantial to heavy damage (moderate structural damage, heavy non-structural damage)</p> <p>Cracks in columns and beam column joints of frames at the base and at joints of coupled walls. Spalling of concrete cover, buckling of reinforced rods. Large cracks in partition and infill walls, failure of individual infill panels.</p>
	<p>Grade 4: Very heavy damage (heavy structural damage, very heavy non-structural damage)</p> <p>Large cracks in structural elements with compression failure of concrete and fracture of rebars; bond failure of beam reinforced bars; tilting of columns. Collapse of a few columns or of a single upper floor.</p>
	<p>Grade 5: Destruction (very heavy structural damage)</p> <p>Collapse of ground floor or parts (e. g. wings) of buildings.</p>

Figure 5.9 Damage grades for reinforced concrete buildings according to EMS-98 scale (Grüntal *et al.*, 1998)

While the above mentioned IMs do not require any instrument to be quantified (but visual surveys and questionnaires), instrumental IMs are analytical values computed from recorded accelerograms. Examples of typical IMs are: the peak ground acceleration, a spectral acceleration or displacement, peak ground velocity and so on.

From the above, a large variability of IMs emerges and several efforts have been aimed at developing suitable conversion formulae from one Intensity measure to another. In Table (5.1) an example of conversion of one Macroseismic intensity scale into another is reported (Musson *et al.*, 2010).

Table 5.1 Comparison of Macroseismic intensity scales (Musson *et al.*, 2010).

RF	EMS-98	MCS	EMS-98	MMI 56	EMS-98	MSK	EMS-98	JMA-96	EMS-98
								0	1
1	1	1	1	1	1	1	1	1	2 or 3
2	2	2	2	2	2	2	2	2	4
3	3	3	3	3	3	3	3	3	4 or 5
4	4	4	4	4	4	4	4	4	5
5	5	5	5	5	5	5	5	5L	6
6	5	6	6	6	6	6	6	5U	7
7	6	7	7	7	7	7	7	6L	8
8	7 or 8	8	8	8	8	8	8	6U	9 or 10
9	9	9	9	9	9	9	9	7	11
10	– ^a	10	10	10	10	10	10		
		11	11	11	– ^a	11	11		
		12	– ^a	12	– ^a	12	– ^a		

A number of study exists in literature regarding the conversion between empirical and instrumental IMs.

Conversion equations aimed at providing intensity measure from an instrumental IM (typically the PGA) are named Ground Motion to Intensity Conversion Equation (GMICEs). Examples are those employed for the computation of shakemaps in terms of Macroseismic intensity (Wald *et al.*, 1999). Conversely, Intensity to Ground Motion Conversion Equations (IGMCEs) are generally employed in historical earthquake studies, that is to say when only Macroseismic intensity is available. These formulations should be applied to the specific geographical context for which they have been tailored. Moreover, their inversion is not allowed. An exception to this is represented by the Faenza and Michelini (2010) GMICE, based on orthogonal distance regression (Syner-G, 2009). An extensive study about conversion formulae and their validation, to which the reader should refer for details, is the one performed by Cua *et al.* (2010) on behalf of GEM1 and GEM projects.

5.2.3. Limit states

In the PBEE approach (see Section 2.2), fragility curves describe the probability of exceeding pre-defined limit states corresponding to given structural performances. More in detail, the limit state is defined as the threshold separating two damage conditions. For example, in the case of three limit states, four damage state are accordingly defined (one of which could also be the absence of damage), as represented in Figure (5.10).

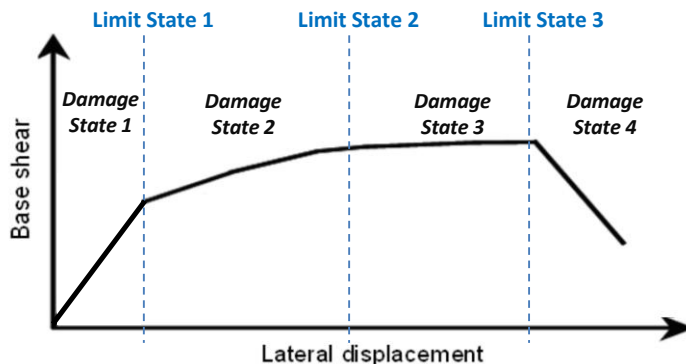


Figure 5.10 Example of Limit States and Damage States.

The definition of damage states and limit states depends on the scale employed for measuring the damage. In empirical approaches, the damage states are expressed in terms of the Macroseismic scale employed in the assessment; in analytical approaches, damage states are defined in terms of mechanical properties of the building (e.g. displacements or drifts). Different damage scales have been defined in Literature such as the ATC-13 (ATC,1985) scale, The Vision 2000 (SEAOC, 1995), the EMS98 (1998), the HAZUS99 scale (FEMA, 2001), the FEMA 356 (ASCE, 2000), the HCR scale (Rossetto and Elnashai, 2003).

A comparison of some of the abovementioned scales is performed in (Rossetto and Elnashai, 2003), summarized in Table (5.2).

Table 5.2 Comparison of damage scales (Rossetto and Elnashai, 2003).

HRC	HAZUS99	Vision 2000	EMS98	ATC-13
None	No damage			
Slight	Slight damage	Fully operational	Grade 1	Slight
Light		Operational		Grade 2
Moderate	Moderate damage	Life Safe	Grade 3	Moderate
Extensive	Extensive damage	Near Collapse		Grade 4
Partial Collapse		Collapse	Major	
Collapse	Collapse			

5.3. The “*FRAME – Fragility-based rapid seismic Risk AssessMEnt - v.1.0 beta*” software suite

The FRAME v.1.0 software suite is composed of different tools, developed in Mathworks MATLAB® environment, with the following purposes:

- performing a rapid evaluation of seismic risk, worldwide applicable;
- providing an inventory of existing fragility functions that can be easily managed and expanded;
- allowing the comparison and manipulation of fragility curves and the identification of the most suitable to describe the seismic performance of a specific structure or structural type;

Each of the previous tasks is accomplished by a specific tool. In fact, the FRAME software suite is composed by the following tools:

The *FRAME Main tool* is the main program, from which the other tools can be accessed. It allows the input of the data required for the assessment and provides the output. Regarding the Input data, they are: (i) hazard data, (ii) fragility curve, (iii) loss data. Depending on the hazard data provided, the tool returns different outputs. This tool is described in Section (5.3.1).

The *FRAME Manager tool*, described in Section (5.3.2), allows the user to manage fragility curves, defining a new fragility curve according to a taxonomy, modifying existing curves and collapsing or expanding the adopted taxonomy.

The *FRAME Comparison&Conversion tool*, allows to compare fragilities in order to compute statistics, convert intensity measures and manage limit states. It is described in Section (5.3.3)

The *FRAME Filter tool*, allowing the user to perform search queries for selecting fragility curves (Section 5.3.4) ;

In Figure (5.11), the tool composing the suite are illustrated, together with the main function of each one, the input data and outputs.

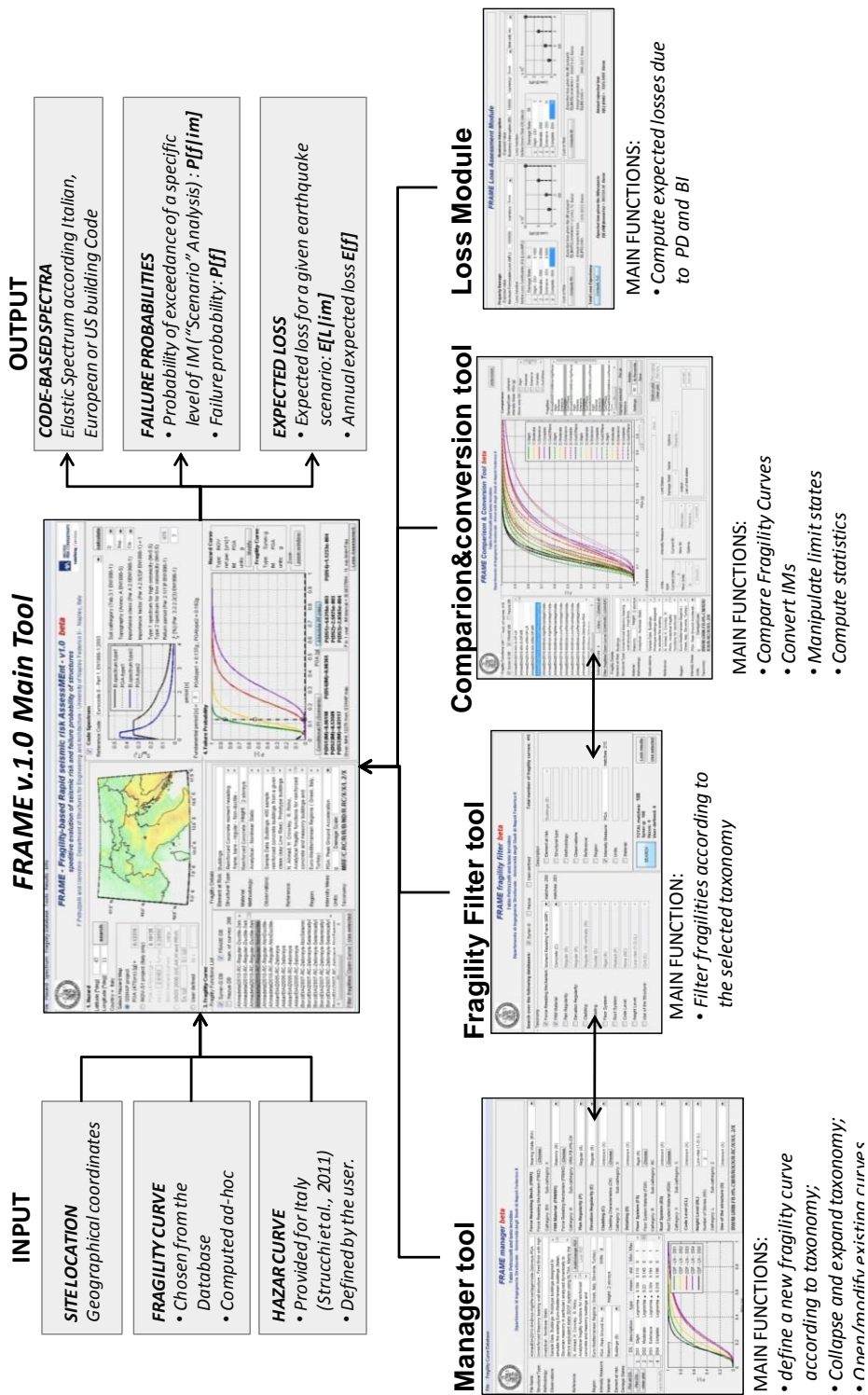


Figure 5.11 The FRAME - Fragility-based rapid seismic Risk AssessMEnt - v.1.0 beta software suite.

The suite includes different datasets of hazard and fragility. Regarding the hazard, the FRAME suite includes:

- the GSHAP hazard map (Giardini *et al.*, 1999), providing worldwide the PGA with a return period of 475 years on rock, in the following referred to as PGA_{GSHAP} ;
- the hazard curves from INGV “S1” project (Stucchi *et al.*, 2011) (see Section 4.5), provided at each point of a regular grid with a 5 km span covering the whole Italian territory (except the Sardinia region);
- the USGS 2008 (Petersen *et al.*, 2008) hazard maps providing the 2% in 50 years probability of exceedance of 0.2 and 1.0 spectral acceleration, for US 48 Conterminous States, Alaska, Hawaii, Puerto Rico or US Virgin Islands.

Regarding the fragilities, the curves obtained from the following studies are included or are currently under inclusion in the software:

- Syner-G (2009a and 2009b), providing fragility curves for RC and Masonry structures in Europe.
- the HAZUS @MR4 (FEMA, 2003) fragility curves for structures in the US.

Currently the FRAME tool includes 415 fragility curves. The possibility of including a user-defined hazard curve or fragility curve is provided by the software suite.

5.3.1. FRAME v.1.0 Main Tool

The main objective of the software suite is to provide the expected annual loss, employing fragility curves chosen from a database or computed ad-hoc, and the best hazard estimates available at the site. Therefore, the functions of the main tool are:

- computing automatically the seismic hazard or defining new one;
- associating to the building a fragility function or defining a new one;
- computing seismic risk;

The tool allows to work with two different levels of information about hazard, reflecting in the output provided by the program.

If no hazard curve is available, a so-called “*Conditional P_f* ” (or “*scenario*”) analysis is performed. It provides a conditional probability of failure, that is the probability of exceeding a pre-defined limit state (or a set of limit states, as defined by the fragility curves), given a scenario earthquake. This latter is identified by the chosen IM at the site, corresponding to a given return period, $IM=im^*$. Therefore, according to this analysis, the $P[D > C_{LSi} | im^*]$ is computed, that is the probability of that the demand exceeds the capacity corresponding to the i^{th} limit state, given the im^* .

The probability of being in the i^{th} -damage state is, (see Section 5.2.3):

$$P[DS_i | im^*] = P[D > C_{LS_i} | im^*] - P[D > C_{LS_{i+1}} | im^*] \quad (5.1)$$

Since the tool includes the GSHAP hazard map, this kind of approach is always feasible worldwide, providing $P[DS_i | PGA_{GSHAP}]$.

The loss measure computed in this analysis is $E[L|im^*]$, that is the expected loss, given the im^* scenario. It can be computed, in the hypothesis that the expected loss given that the structures is in the i^{th} limit state is independent from im^* , as follows:

$$E[L | im^*] = \sum_i E[L | DS_i] \cdot P[DS_i | im^*] \quad (5.2)$$

If a hazard curve is available (defined by the user or, for the Italian territory, automatically provided by the tool), a so-called “**Absolute P_f** ” (or “**Risk**”) analysis is performed, providing the annual failure probability for each considered limit state, as reported in the following equation (see Section 2.2):

$$P_{f,i} \approx \int_{im} P[D > C_{LS_i} | im] \cdot |d\lambda(im)| \quad (5.3)$$

In this case, considering the probability of the structure to be in one particular damage state $P[DS_i]$, the tool provides the expected loss:

$$E[L] = \sum_i E[L | DS_i] \cdot P[DS_i] \quad (5.4)$$

Figure (5.12) summarizes the two possible analysis and the relevant outputs.

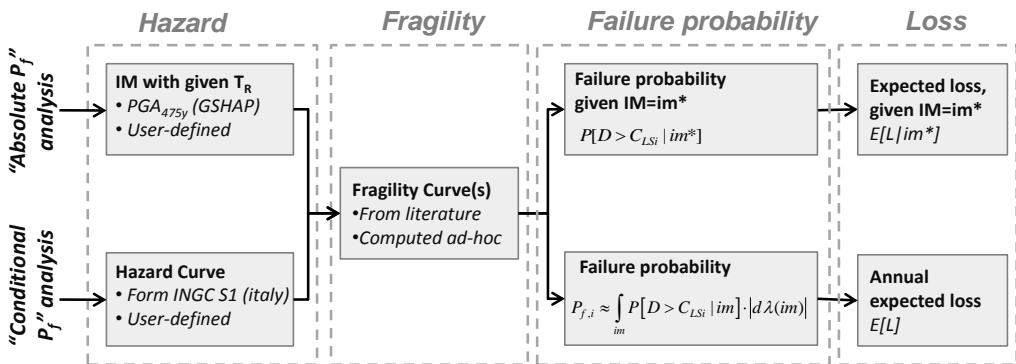


Figure 5.12 “Conditional P_f ” analysis and “Absolute P_f ” analysis analysis performed in FRAME v.1.0.

In Figure (5.13) a screenshot of the Graphical User Interface (GUI) of Frame main tool is reported. It operates by means of the steps described in the following.

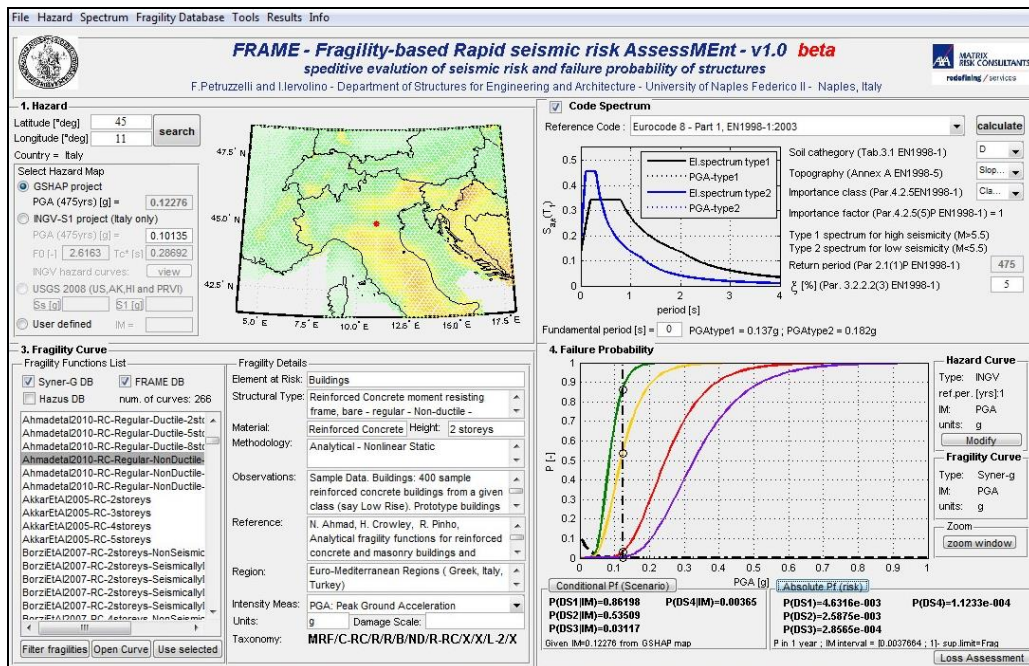


Figure 5.13 FRAME – Fragility-based rapid seismic Risk Assessment – v1.0 beta main GUI.

Step 1 – Hazard definition

The top left side panel refers to the hazard: the user can insert the geographical coordinates of the site and the software will automatically compute the PGA with 475 years return period or rock, from the GSHAP hazard map. If the facility is located in the US, Alaska, Hawaii, Puerto Rico or US Virgin Islands, besides the GSHAP PGA value, the low period (0.2s) and high period (1.0 s) spectral accelerations according to the 2008 USGS map are computed.

If the facility is located in Italy, in addition to the GSHAP PGA value, the PGA with 475 years on rock, according to CS.LL.PP (2008), is shown.

These values can be employed in a “conditional P_f ” approach. If more than one IM value is available at the site (e.g. in Italy), the user is requested to select one. Accordingly to the user choice, the hazard map is plotted in the left-top panel.

In any case, the input of a specific $IM=im^*$, with a given return period, is allowed.

In case of Italian sites, the button “INGV hazard curves” becomes active. If pushed, a window appears allowing the computation, at the site under investigation, of hazard curves for INGV data (see Section 4.5). If this option is pursued, the computed hazard curve is plotted in the bottom right panel of Figure (5.13) and a “Absolute P_f ” analysis can be performed, proceeding to steps 3 and 4 (to follow).

Step 2 (optional) – Computation of elastic Spectrum

The top right panel of the FRAME v.1.0 GUI (Figure X.X) refers to the computation of elastic spectrum. The tool allows to compute the elastic spectrum according to the following national and international code standards: Italian Building Code (CS.LL.PP, 2008); Eurocode 8 (CEN, 2004) and International Building Code (IBC, 2012) and ASCE 7-10 (ASCE, 2010) provisions.

Although not strictly necessary to the procedure (reason why the panel is inactive, by default), the computation of elastic spectrum could be useful in order to define the $IM=im^*$ to be employed in a “Conditional P_f ” analysis. In fact, if the fragility curve selected in the next step is expressed in terms of a specific spectral ordinate and/or the local soil conditions at the facility site are known, the computation of the elastic spectrum can provide the $IM=im^*$ accounting for the abovementioned aspects, in a code-based approach. It is to mention that, the tool checks the coherency of the requested spectrum with the hazard selected in the previous step. Therefore, it not possible to compute Italian elastic spectrum for a facility outside the Italian National borders (being the Italian spectrum defined with transition periods depending on gridded data), while it is possible to compute the EC8 and IBC2012 elastic spectra worldwide. In fact, EC8 elastic spectrum is anchored to the hazard at the specific site only by the PGA value, that is provided worldwide by the GSHAP map. Regarding the IBC2012 spectrum, if the site is located in a zone where the USGS map is available, its computation does not require any assumption. Conversely, the Spectral accelerations at high and at low periods are assumed, respectively, equal to the PGA from GSHAP map and 2.5 times the PGA from GSHAP map.

Step 3 – Selection of the fragility curve(s)

The left-bottom panel of Figure (5.13) presents a list of the fragility curves available in the database. Selecting one record of the list, the main characteristics of the curve, such as structural type, construction material, geographical region, units, damage scale and the adopted taxonomy are shown. The taxonomy allows to summarize the main characteristics of the buildings and actually its definition is a key issue for the classification and the inventory of fragility curves. It will be discussed in Section (5.3.2). In order to facilitate the search through the database, in section it is possible to “Filter” the database by means of the FRAME Filter tool, presented in Section (5.3.4). That reported is only a part of the information associated to each single record, to which the user can access selecting one record and pushing the “Open Curve” button. This remands to the FRAME Manager tool, described in Section (5.3.2).

Once a curve is selected, that is to say it is assigned to the structure under investigation, by pushing the “Use Selected” button, it is plotted in the fourth panel and superimposed to the hazard curve, if any (see Section 5.3.1.1).

Step 4 – Assessment of failure probability

In this step, the failure probability related to each limit state (defined by the fragility curve set employed) is computed, according to the type of analysis performed (“Conditional P_f ” or “Absolute P_f ” analyses).

For each i^{th} limit state, in the case of a “Conditional P_f ” analysis, $P[D > C_{LSi} | im^*]$ are provided, while in the “Absolute P_f ” analysis the failure probabilities $P_{f,i}$ are computed. The results are shown in the bottom right panel of the GUI, reported in Figure (5.13). The dashed line in the Figure represents the im^* values used for “Conditional P_f ” approach and the circles represent the correspondent $P[D > C_{LSi} | im^*]$.

Step 5 – Loss assessment

As it concerns loss assessment, it is possible to use the previous probabilities to compute the “cost of risk”, that is reported in Eq. (5.2) and Eq. (5.4) for the two cases of “Conditional P_f ” and “Absolute P_f ” analyses, respectively. The assessment is performed both in terms of Property Damage (PD) and Business Interruption (BI).

To perform the assessment in terms of PD, the maximum foreseeable loss (MFL) of the structure under consideration is required. The latter can be, as discussed in Section (2.3.3), the total property value of the structure or the replacement cost.

Moreover, it is necessary to associate a k_i coefficient (minor than one) representing the fraction of MFL associated to each damage state DS_i .

It is to note that the ensemble of k_i coefficients actually represent a function allowing to transform the fragility curve into a vulnerability curve (see Figure 5.2)

Under this hypothesis the expected loss, for the i^{th} damage state, is:

$$E[L_{PD} | DS_i] = MFL \cdot k_i \tag{5.5}$$

therefore, Eqs. (5.2) and (5.4) can be rewritten as follows:

$$E[L_{PD} | im^*] = MFL \cdot \sum_i k_i \cdot P[DS_i | im^*] \tag{5.6}$$

$$E[L_{PD}] = MFL \cdot \sum_i k_i \cdot P[DS_i] \tag{5.7}$$

Regarding the expected loss related to the business interruption (BI), the same approach as the one discussed for PD is pursued. The main difference is that the MFL is substituted by the loss due to business interruption in one time unit (Unit Business Interruption, UBI) and the k_i coefficients are substituted by n_i , representing the length

of downtime (expressed in the same time unit as UBI) for any damage state. This leads to the following equations for the two kinds of analysis:

$$E[L_{BI} | im^*] = UBI \cdot \sum_i n_i \cdot P[DS_i | im^*] \tag{5.8}$$

$$E[L_{BI}] = UBI \cdot \sum_i n_i \cdot P[DS_i] \tag{5.9}$$

Such calculations are performed in FRAME v.1.0 in the Loss Module, accessible by pushing the “Loss Assessment” button on the extreme bottom-right of the Main GUI. In Figure (5.14) the Loss module is shown. It allows to insert the MFL and UBI values, to choose the currency and the time unit; the k_i and n_i coefficients are inserted by the user in the two tables in Figure (the number of rows of which is equal to the number of damage states) and Eqs. (5.6) to (5.9) are computed.

The tool finally provides the “Total Loss Expectancy” (TLE), computed as the sum of the expected losses due to PD and BI, in both the “Conditional P_f ” and “Absolute P_f ” approaches.

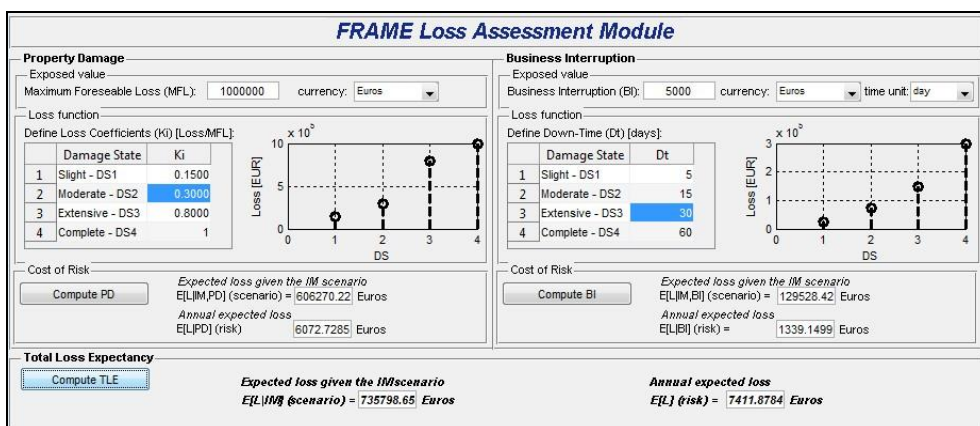


Figure 5.14 FRAME v.1.0 beta loss assessment module

Step 5 – Saving/exporting results

The FRAME v.1.0 tool allow to save the hazard maps (both as image or gridded data), the elastic spectra (In MS Excel format), the plots and the computation of failure probabilities and expected losses. A log file can be compiled in “.txt” format.

5.3.1.1. Hazard curves from INGV data or by user entry

In case the site of the facility under investigation is located in Italy, by pushing the “INGV hazard curve” button, the window reported in Figure (5.15) opens, allowing to compute and manipulate the hazard curve provided by INGV. In particular, the 16th,

50th and 84th percentiles of the INGV hazard curves, expressed in terms of spectral acceleration for eleven fundamental periods (from 0 s to 2.0 s) can be computed. The uniform hazard spectra are also shown and they can be overlapped to code-based ones (from CS.LL.PP, 2008).

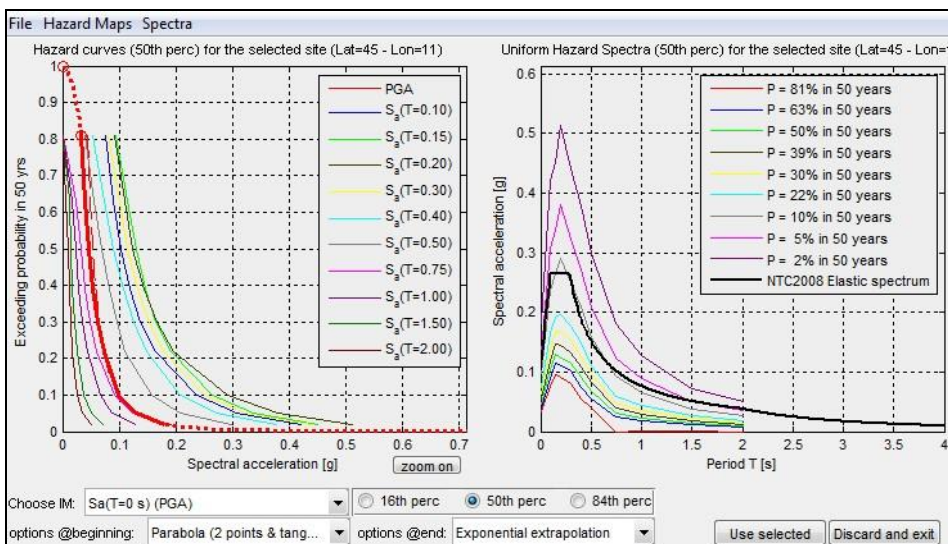


Figure 5.15 INGV hazard curves and UHS computation in *FRAME v.1.0 beta*.

Hazard curves are provided by INGV in terms of probability of exceedance in 50 years therefore, in order to compute the expected annual loss, the FRAME tool automatically converts them in terms of annual probability of exceedance. Moreover, the higher and lower probability values provided by INGV are, respectively, 0.81 and 0.02. In order to broaden the range of spectral acceleration for the computation of failure probability, different options for the extrapolation of the hazard curve at higher probability values (i.e. in the range of low IMs) and at lower probability values (i.e. in the range of high IMs) are allowed by the tool. In particular, if $S_a^{P=0.81}$ is the lower P value of the spectral acceleration provided by INGV, the extrapolation at low IM values ($S_a(T) < S_a^{P=0.81}$) can be performed: (i) considering $P=0$, that is equivalent to not extrapolate the curve and it is the default option; (ii) considering $P=1$ for all $S_a(T) < S_a^{P=0.81}$; (iii) considering $P=0.81$ for all $S_a(T) < S_a^{P=0.81}$; (iv) considering a linear extrapolation to the point (IM=0;P=1); (v) considering a parabolic extrapolation (different sub-options are provided in order to superimpose conditions on the tangents at the initial and final point of the parabola); (vi) a third-degree polynomial (eventual values of $P > 1$ are truncated). Regarding the extrapolation at high values of IM ($S_a(T) > S_a^{P=0.02}$), the

possible options are to: (i) assume $P=0$; (ii) assume $P=0.02$; (iii) extrapolate by means of an exponential function fitted to the points provided by INGV.

Regardless the site location, it is possible to employ a user defined hazard curve. This option is available from the FRAME main window, in the “hazard Curve” panel, at the bottom right corner. Once the “modify” button is pushed, the window represented in Figure (5.16) appears; it allows to define, import (from excel or from a previously created curve) and export hazard curves. In this window, besides the numerical data of the curve, the user has to define: the intensity measure adopted; the units; the reference period to which the curve is defined and whether the defined curve is expressed in terms of rate of exceedance or probability of exceedance. In any case, the tool allows the conversion from probability of exceedance to frequency of exceedance, as a function of the time period provided.

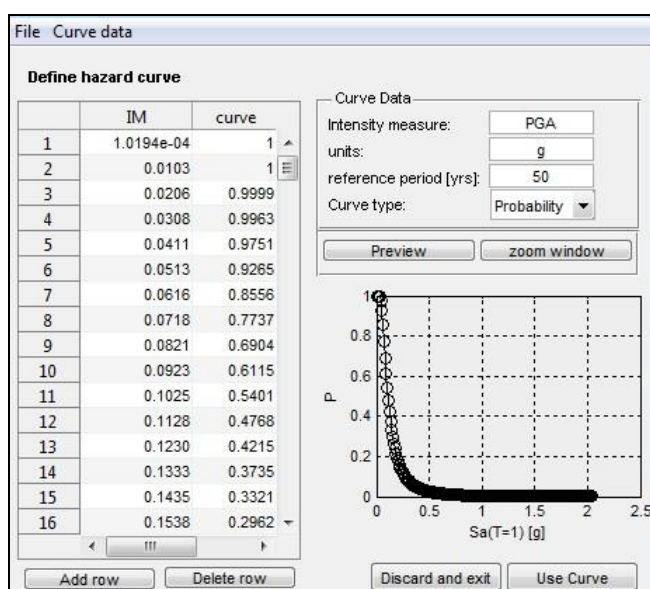


Figure 5.16 Input of a user defined hazard curve in *FRAME v.1.0 beta*.

5.3.2. Managing Fragility functions: the *FRAME Manager tool*

The allocation of a fragility curve, or a set of fragility curves, corresponding to different limit states to the structure under investigation is the key step of the procedure previously outlined. For this reason, the FRAME Manager tool was developed with the aim of storing, visualizing and managing existing fragility curves as well as adding to the inventory new curves computed *ah-hoc* or available in literature.

A relevant issue in managing fragility curves (or, more in general, dealing with building inventories) is the adoption of an appropriate Taxonomy, according to which

classify fragility curves (or buildings). The adoption of a given taxonomy is equivalent to the individuation of those relevant elements used for distinguishing one fragility curve (class of building) from another. Therefore it is indispensable for classifying fragility functions and filtering the database in order to select only those matching some search criterion.

An appropriate taxonomy should be:

- flexible: i.e. collapsible and expandable so that it can be adapted to the adding or removing of fragility curves to the inventory;
- detailed: so that relevant elements that allow to distinguish one building class to another are not neglected
- hierarchical: so that an indication is given about those elements of the taxonomy more important in order to classify fragility curves.

Among the available taxonomies in literature, it was adopted a taxonomy practically coincident with the one adopted in Syner-G project (Syner-G, 2009a), consisting in eleven categories (the same of Syner-G project plus the eleventh that is the “occupancy”). A hierarchy is used for some categories where additional information might or might not be available. For example, the construction material is a mandatory information (cat.2) but it is optional to specify the strength class of the concrete (sub-category 2). In Figure (5.17), the adopted taxonomy and an example of the possible values of a category (CAT.2) and a sub-category (SUB-CAT2) are reported.

Each possible value of each category and subcategory is expressed by an ID, when no value is given, because unknown, the “X” ID is reported. A fragility curve is, then, defined using the label of each parameter within a given category, separated by a slash; subcategories are separated by the category to which they refer by a dash, as reported in Eq. (5.10)

$$\begin{aligned} \text{Taxonomy} = & \text{cat1} / \text{cat2} - \text{subcat2} / \text{cat3} / \text{cat4} / \text{cat5} - \text{subcat5} / \dots \\ & \dots \text{cat6} / \text{cat8} - \text{subcat8} / \text{cat9} / \text{cat10} - \text{subcat10} / \text{cat11} \end{aligned} \quad (5.10)$$

Therefore, as an example, *MRF / C – RC / IR / R / B / D / R – RC / X / X / M – 5 / X* refers to a moment resisting frame (MRF), made by reinforced concrete (C-RC), irregular in elevation (IR), regular in plan (P), bare (B), with ductile details (D), rigid floor made by reinforced concrete slab (R-RC) and mid-rise (M) with 5 floors.

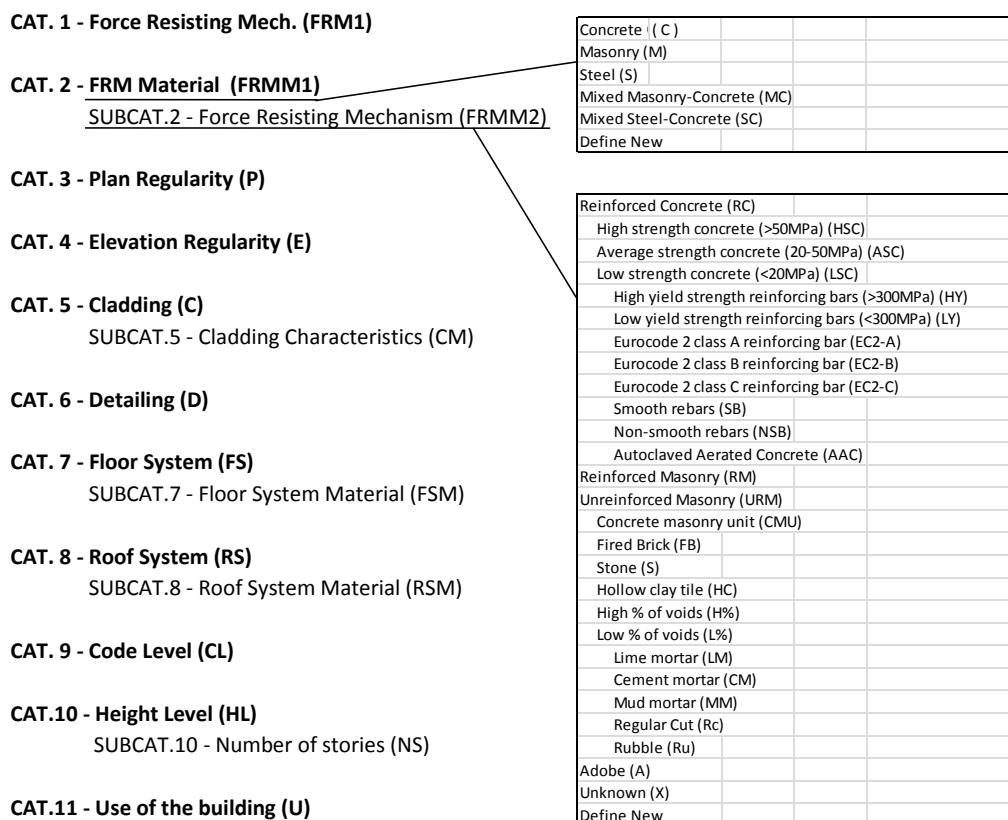


Figure 5.17 Adopted Taxonomy

In Figure (5.18) the main GUI of the *FRAME Manager tool* is reported. The tool allows to define a new curve, to open an existing one and to modify it. As it can be observed from Figure (5.18), the left side of the window is dedicated to the description of the main parameters of the curve and its definition. Some of the data included in this section are: the name of the file in the database, the structural type, the methodology employed for the computation of the curves (see Section 5.2.1), the intensity measure (Section 5.2.2), the units and the adopted damage scale. The box in the left side of the windows allows the input of the fragility curves for the considered limit states. The tool was developed to deal with: (i) lognormal, (ii) normal and (iii) empirical fragility curves. In the first two cases the probability distribution of exceeding a given damage state is defined by means of its two moments. In case of empirical distributions, they can be defined by user entry or importing a spreadsheet.

The right panel of the *FRAME Manager tool* window is, conversely, dedicated at the definition or the expansion/collapse of the taxonomy. In fact, for each category, a value among those available can be assigned to the specific case (or eventually removed) or a

new one can be defined. Finally the Frame Manager allows to store into the database the curve created/modified.

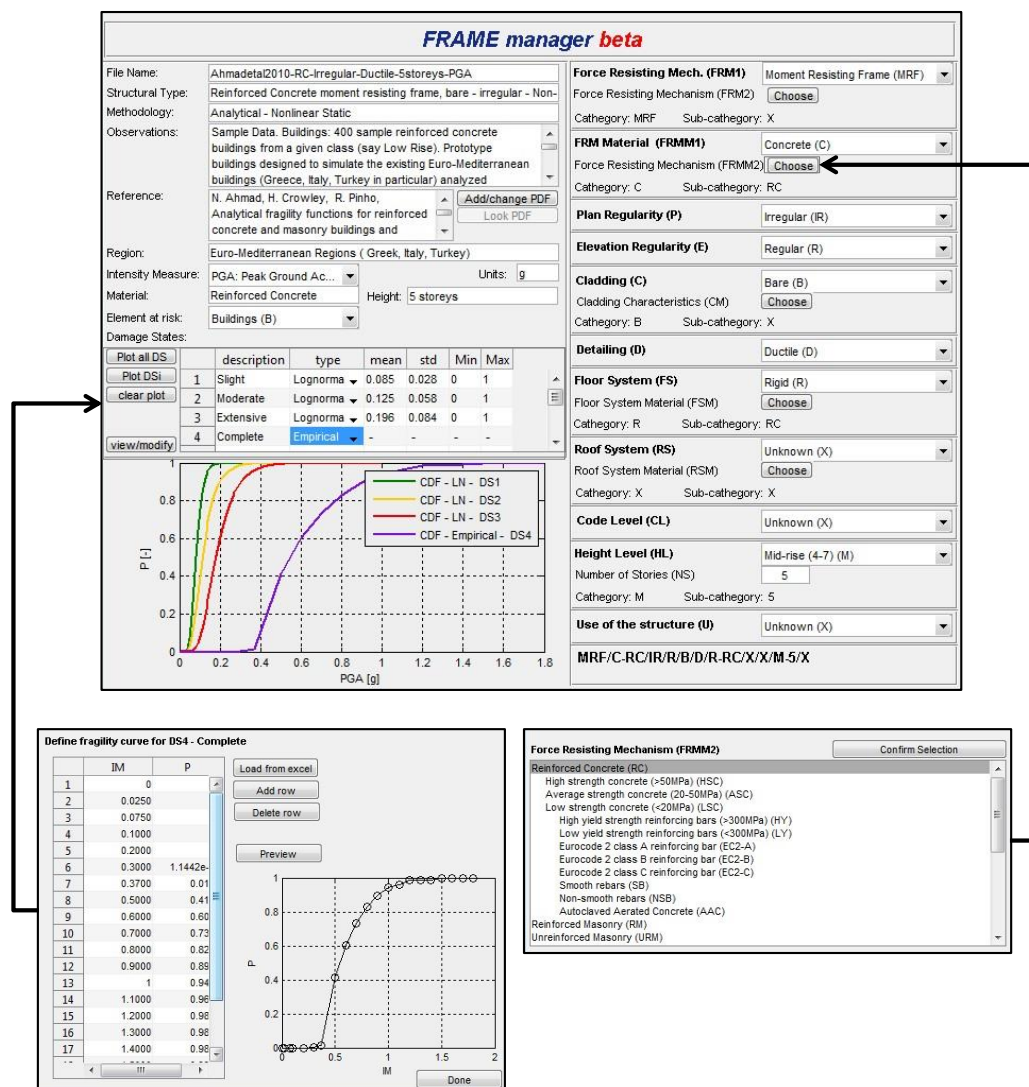


Figure 5.18 FRAME Manager tool GUI (top) and windows allowing the input of empirical fragility curves (bottom-left) and taxonomy (bottom-right)

5.3.3. Comparison, homogenization and conversion of Fragility functions: the FRAME Compare&Conversion tool

One main issue concerns the possibility of comparing the fragility curves, that are characterized, as discussed in section (5.2), by a large number of adopted IMs and limit states. The FRAME Comparison and Conversion Tool was developed with the aim of:

- comparing fragility curves and computing statistics;
- modifying the set of curves relevant to a single building, converting the intensity measures or modifying the considered limit states.

In Figure (5.19) the GUI of the *FRAME Comparison and Conversion tool* is reported. It is composed of a *selection panel* (on the left side), a *plot panel* (on the centre), a *comparison panel* (on the right side) and a *conversion panel* (on the bottom side).

From the *selection panel*: (i) the database of available curves can be explored and the main characteristics of a selected curve can be viewed by simply selecting one record from the list; (ii) the inventory can be filtered (see Section 5.6) in order to show only a portion of interest (pushing the “Filter Fragilities” button); (iii) a selected curve can be opened in the FRAME Manager (see Section 5.4) in order to be viewed in detail or modified (pushing the “Open Curve” button).

Furthermore, if more than one record is selected by the checkmark and the button “Compare” is pushed, the *comparison panel* activates, allowing to perform the first point of the previous list. If only one record is selected and the button “Convert” is pushed, the *conversion panel* activates, allowing to perform the second point of the previous list. These functions are presented in the following subsections.

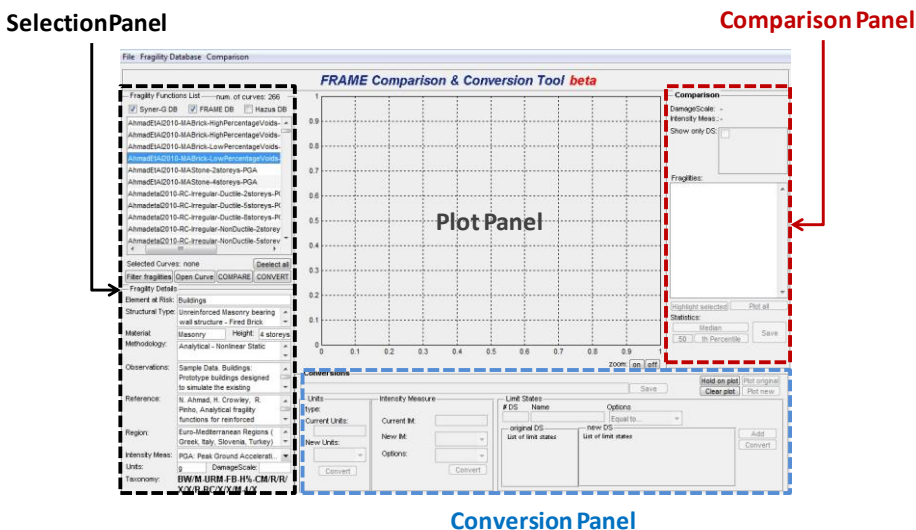


Figure 5.19 FRAME Comparison&Conversion tool GUI.

5.3.3.1. Comparing fragility curves

Once a set of curves is selected from the inventory, the tool checks the coherency of their intensity measures, units and number of considered damage states. If the coherency check is not passed, a window appears, allowing the user to remove from the list of the considered fragility curves those expressed in a non-coherent IM and/or

unit. These could be converted as described in the next sub-section. Regarding the damage states, the user can select the number and type of damage states to compare by simply clicking on them, thus selecting a set of fragility curves to compare, characterized by the same number of damage states.

In Figure (5.20) the ensemble of coherent fragility curves for the comparison is shown. From the comparison panel, it is possible to select only some specific limit states and show them in the plot panel, highlight one curve among the others and perform statistics.

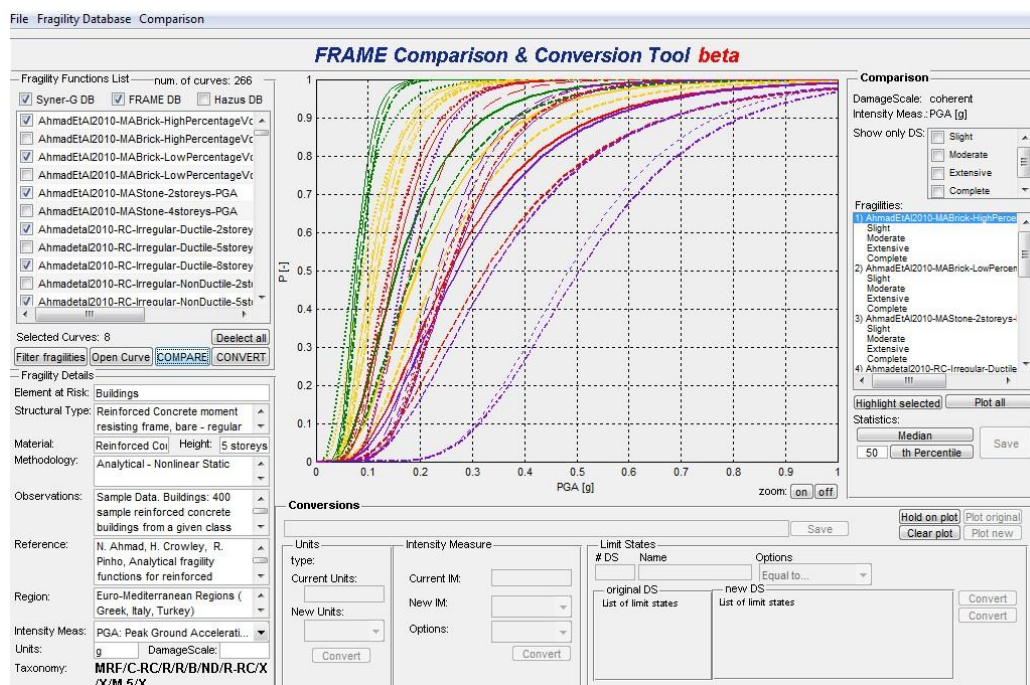


Figure 5.20 *FRAME Comparison & Conversion tool* GUI showing the comparison of an ensemble of fragility curves selected from the inventory.

To this regard, different approaches for the computation of a given percentile of the selected set of curves were followed. These options are accessible from the menu of the tool.

The first option is based on the evaluation of the distribution of the probability of exceedance, conditioned to a given IM level. In fact, at each IM level, it is possible to fit a distribution of exceedance probabilities from the ensemble of curves, as shown in Figure (5.21). The choice of a statistical model is performed computing the Log-likelihood for the following models: Normal, Lognormal, Weibull, Exponential, Beta, Gamma. As it can be observed from the top left panel in Figure (5.11), the tool

provides, for each IM stripe considered, the computation of the log-likelihood for the abovementioned models and the plot of the chosen distribution for the specific IM level. The mean of the log likelihoods above all the considered IM levels provides an indication of the statistical model that “on the average”, on the full IM range, best fits the distribution of the probability of exceedance, given IM. In most cases, the best fitting model, as observed also in Syner-G (2009a), is the Beta one.

The second option is similar to the one proposed by Bradley (2010). considering that all the curves under investigation are homogeneous (e.g. all lognormal), the median $\mu_{\ln(IM)}$ and standard deviation of the logarithms $\sigma_{\ln(IM)}$ of each fragility curve are used to fit a lognormal bivariate model, the mode of which is used for computing the median fragility curve of the ensemble under consideration.

A third option, similar to the previous one, is to fit a univariate statistical model (chosen by the user on the basis of log-likelihoods provided by the tool) to the medians and standard deviations of the fragility curves under consideration. From both the distributions the mode value is obtained and used to compute the median fragility curve for the ensemble of under consideration.

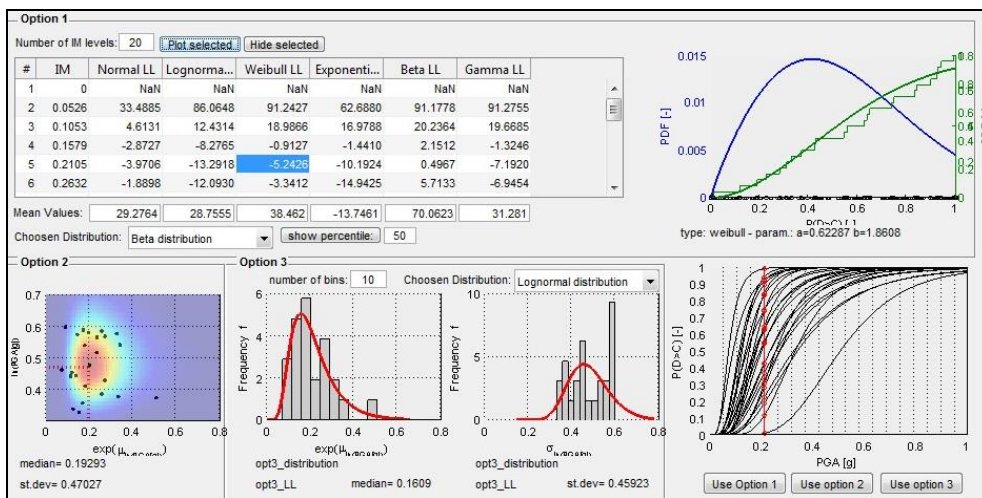


Figure 5.21 FRAME Comparison & Conversion tool: different options for computing statistics.

It is to mention that the computation of the percentiles of the ensemble of curves is performed, by defaults, by means of this first option, assuming a Beta distribution for the exceeding probabilities, given IM.

The fragility curve corresponding to a given percentile can be, finally, saved. In fact, by pushing the “save” button, the FRAME Manager tool opens, allowing the user to add to the curves all the information he believes it is important to store.

5.3.3.2. Converting fragility curves

If a single record is selected in the “selection panel”, by pushing the “convert” button the specific set of curves is plotted and the following options become available:

- units conversions;
- IM conversions;
- limit States manipulation.

Regarding the first, the tool automatically recognizes the kind of intensity measure and the unit employed, proposing the relevant conversions. Regarding the conversions between IMs, as discussed in section 5.2.2., different relationships exist. In the tool the following GMICEs and IGMCEs are implemented: Faenza and Michelini (2010); Margottini *et al.*, (1992); Wald *et al.*, (1999b); Murphy and O’Brien (1977); Sorensen *et al.* (2008); Tselentis and Danciu (2008). Faenza and Michelini (2010) and Wald *et al.* (1999b) also provide for the conversion from PGV to Macroseismic intensity scales. The tool performs a check of coherency in the damage scale defined in the fragility curve and the one to which the conversion formula is related. Regarding the conversion of spectral acceleration to PGA (and vice versa), and the conversion from spectral displacement to PGA (and vice versa), in a first approximation, the spectral shape from IBC,2012 was chosen in order to operate the previous conversions. Regarding the conversion from PGV to PGA, the Bommer and Alarcon (2006) approach was followed in order to estimate the $S_a(T=0.5 \text{ s})$ and, then, by means of the IBC 2012 spectral shape (ICC, 2012), the PGA.

Finally, the managing of limit states is performed allowing the user to define new ones that can be: (i) equal to one original limit state, (ii) the mean between two limit states; (iii) the median of all the limit states and (iv) the mean of all the limit states .

In Figure (5.22) a plot of the GUI of the *FRAME Comparison&Conversion tool* is reported, showing the manipulation of limit states. In fact, in the Figure, the original limit states (LS) were five, represented with dashed lines. By means of the tool three limit states were created (represented with solid line): the first is the mean between the LS_1 and LS_2 ; the second is the mean between LS_3 and LS_4 and the third is equal to the original LS_5 .

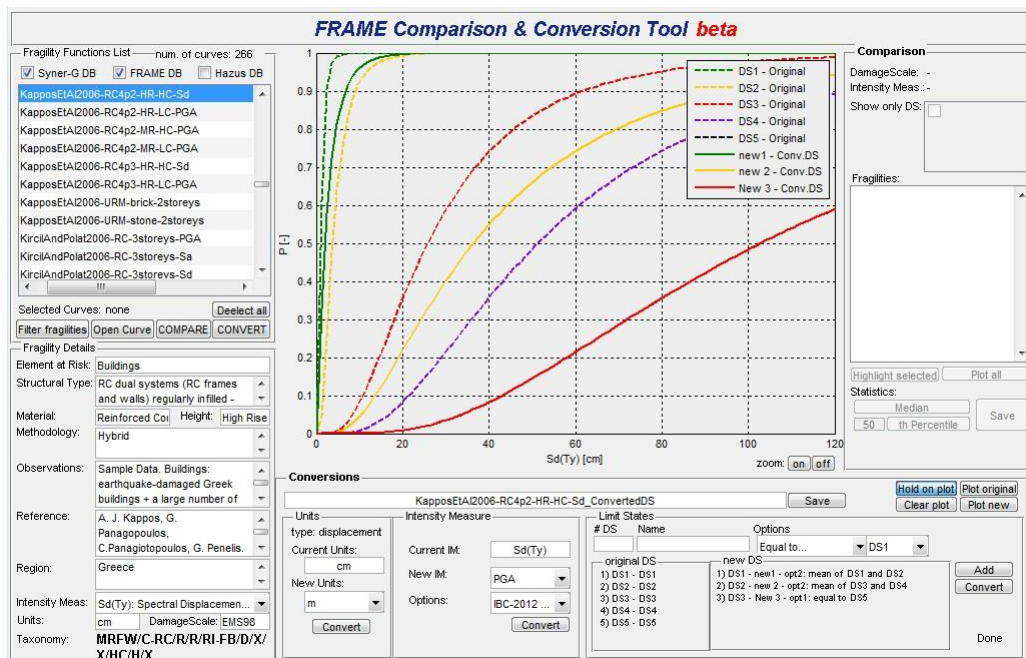


Figure 5.22 *FRAME Comparison & Conversion tool* GUI showing the manipulation/homogenization of limit states.

5.3.4. Filtering fragilities: the *FRAME Fragility Filter tool*

Managing an inventory of fragility curves also requires to perform search queries, in order to select a portion of the inventory with a specific taxonomy. Therefore the *FRAME Fragility Filter tool* was developed and included in each one of the previously described software. The *FRAME Fragility Filter tool* GUI is shown in Figure (5.23).

In the top of the GUI it is possible to select the databases in which the search has to be performed; the bottom portion is subdivided vertically into two panels. The left panel reproduces the adopted taxonomy, therefore the user can select one or more categories specifying, for each one, the value to search for. Next to each category, the number of matches is shown. The right panel reports the ensemble of additional descriptive information that characterizes each fragility curve. A search can be performed specifying one or more words to search for in descriptive fields.

Pushing the “search” button, only the curves matching contemporarily all the criteria defined above are selected.

FRAME fragility filter beta

Search over the following databases: Syner-G Hazus User-defined Total number of fragility curves: 266

Taxonomy		Description	
<input checked="" type="checkbox"/> Force Resisting Mechanism:	Moment Resisting Frame (MRF) matches: 137	<input type="checkbox"/> Element at risk:	Buildings (B)
<input checked="" type="checkbox"/> FRM Material	Concrete (C) matches: 185	<input type="checkbox"/> Structural type:	
<input type="checkbox"/> Plan Regularity:	Regular (R)	<input type="checkbox"/> Methodology:	
<input type="checkbox"/> Elevation Regularity:	Regular (R)	<input type="checkbox"/> Observations:	
<input type="checkbox"/> Cladding:	Regular in fill vertically (RI)	<input type="checkbox"/> Reference:	
<input type="checkbox"/> Detailing:	Ductile (D)	<input type="checkbox"/> Region:	
<input type="checkbox"/> Floor System:	Rigid (R)	<input checked="" type="checkbox"/> Intensity Measure:	PGA: Peak Ground Ac... matches: 215
<input type="checkbox"/> Roof System:	Flat (F)	<input type="checkbox"/> Units:	
<input type="checkbox"/> Code Level:	None (NC)	<input type="checkbox"/> Material:	
<input checked="" type="checkbox"/> Height Level:	Low-rise (1-3) (L) matches: 89	TOTAL matches: 33 Syner-g: 33 Hazu: 0 User-defined: 0	
<input type="checkbox"/> Use of the Structure:	Civil (C)		

SEARCH Look results
Use selected

Figure 5.23 *FRAME fragility filter* tool.

5.4. Conclusions

In this chapter, the so-called "meso-scale" procedure was presented. Its principal objective is the evaluation of the expected loss for seismic events, considering the separate contribution of hazard, vulnerability and exposure. This procedure is designed to be applied to the scale of tens to hundreds of buildings.

The main step of the procedure is the assignment of a fragility curve to the structure under investigation. Given the wide variety of fragility curves available in literature, a study of the main differences existing in terms of methodologies employed for their computation, their intensity measures and considered limit states, was performed first. In order to manage such a number of fragility curves and to implement the proposed procedure worldwide, the *FRAME – Fragility-based seismic Risk Assessment - v.1.0 beta* was developed.

The tool allows to manage and manipulate an inventory of fragility curves, converting their intensity measures and units. The Syner-G project and Hazus project fragility curves were included into the software, as well as the possibility of defining a new, user-defined, one.

The software also allows to compare fragility curves, after checking their coherency in terms of intensity measure and number of considered limit states, allowing to define mean and confidence intervals from a given set of fragility functions. This is performed searching the best-fit distribution of the probability of exceedance, given an intensity measure level. The definition of new limit states from existing ones is also possible, as well as the conversion of one intensity measure into another. Regarding this former aspect, the use of both conventional code-based spectrum shape and of real earthquake

spectra is possible. Moreover, the definition of fundamental period (necessary for some intensity measure conversion, such as the one from PGA to spectral acceleration or displacement) can be performed, for different structural typologies, according to several empirical or numerical formulations.

Moreover, the inclusion in the software of seismic hazard at the global scale, from the GSHAP project, makes it possible to use fragility curves for computing the probability that a specific measure of intensity is exceeded in a given period of time. With specific reference to the Italian context, the inclusion of the curves of seismic hazard referred to project DPC-INGV S1, allows to characterize the probability of exceeding a specified limit state. The software also includes the American hazard map from USGS, as well as the possibility of defining a user-defined hazard curve for the chosen intensity measure.

The inclusion in the software of a loss module allows the rapid assessment of seismic risk worldwide, expressed as the expected loss, given a scenario earthquake. The latter is represented by the PGA with 475 year return period, obtained from the GSHAP hazard map. If a hazard curve is available (i.e. the facility is located in Italy or a user-defined hazard curve is provided), the expected annual loss is computed.

The risk metrics described above are believed to be useful to the stakeholders for the comparison of annual revenues with annual expected losses and the and implementation of risk management strategies over the structural portfolio. In Insurance such measures of seismic risk could represent an aid in computing premiums worldwide.

It is believed that this software could represent a valuable contribution to the spread of quantitative procedures for the assessment of seismic risk and an instrument for the rapid evaluation of risk for relatively large building portfolios. Moreover the possibility of comparing fragility functions developed for the same structural typology, by different authors, for different geographical contexts, under different assumptions, can represent a valid instrument for the vulnerability of classes of buildings.

Chapter 6 –SEISMIC RISK ASSESSMENT OF AN INDUSTRIAL STEEL BUILDING

6.1. Introduction

At the scale of the single building (“*site-specific*” scale, Chapter 1), the most reliable way for computing seismic risk is through an analytical assessment of the structural fragility.

Steel structures represent a large part of the industrial building stock of many countries, but the analysis of their seismic vulnerability have been subject of relatively little investigation with respect to other types of existing structures and a lack in fragility curves developed for this specific structural typology can be observed in literature.

This is due to the fact that such structures are, in general, relatively lightweight and, in most cases, designed for wind actions. Nevertheless, assessing the seismic performance of industrial buildings is fundamental for the estimation of the possible consequences of earthquakes, in terms of direct damage and/or business interruption. Furthermore, the seismic analysis of existing industrial steel structures presents some peculiar modelling aspects that are worth of further investigation (Petruzzelli *et al.*, 2011a and 2012a).

Therefore, in order to investigate the abovementioned aspects and provide fragility curves and failure probabilities to be employed in loss estimations, the analysis of the seismic response of an existing industrial steel building is presented in this Chapter.

Generally speaking, it is known that assessing the seismic performance of existing structures is a task quite different from the seismic design of new constructions. One essential aspect is that both the geometry and the mechanical properties of the existing structure are generally known to only some limited extent. Such uncertainty directly affects the risk assessment and it must generally be considered along with variability of seismic structural demand. On the other hand, the process to acquire knowledge about an existing structure is known to be expensive and, in the case of industrial facilities, not always feasible, since it could require business interruption.

In the Chapter, this issue is addressed after a description of the case-study building (Sect. 6.2). Then, some modelling aspects, peculiar of existing steel structures, are critically discussed (Sect. 6.3). In this context, an especially relevant issue for existing structures is the need for the models to capture all failure modes, especially those reflecting brittle behaviour.

In case of single-storey structures the typical column-sway plastic mechanism deserves special attention, because sensitivity to P-Delta effects is frequently large due to the low redundancy of the structural system.

Moreover, in case of old existing steel structures it is frequent to encounter partial-strength connections, the contribution of which to the system inelastic response cannot be neglected. Modelling those connections may be not a straightforward task; the reason is twofold: (i) modelling the inelastic response of low-ductile failure modes is generally more difficult because of strength and stiffness degradation and (ii) the geometry of existing connections may differ significantly from the standard detailing for which research results and code information are available. In case of existing industrial steel buildings, such undesired failure modes may also involve the roof structure, the design of which is generally dominated by gravity and, eventually, wind loading. In fact, seismic actions may not rule the design, while in the case of strong ground motion, peak force demands to roof elements may exceed the design values, possibly leading to roof collapse. Roof failure modes are generally characterized by low-ductility (e.g., when failure is due to connections) and significant structural consequences (e.g. when a statically determined truss is transformed into a mechanism after failure of any element), implying possible large losses. In addition, in the case of industrial steel buildings, the roof structure may generally be a complex three-dimensional system, the dynamics of which may involve modes of failure different from those relevant to horizontal rigid floor diaphragms, suggesting the need for a complete three dimensional (3D) structural modelling. The response of 3D models is therefore investigated in comparison with simpler two-dimensional (2D) ones, allowing identifying and predicting different collapse modes. The analysed structural models, their basic linear elastic dynamic properties and their static non-linear response are analysed in Section (6.4).

The assessment of seismic risk is dealt in Section (6.5). Methodological issues relevant to seismic hazard, selection of ground motions and dynamic analysis, accounting for both peak and residual drift in the range of large displacements, as well as local force demands to roof members, are discussed.

The Results of wide-range Multi Stripe Analyses (MSAs) are presented in Section (6.6). Fragility curves for the analysed three-dimensional and two-dimensional models are provided. The latter are employed, in conjunction with the hazard computed at the facility site, to estimate failure probabilities for typical structural performances.

6.2. Case-study structures

The case-study building is the main workshop structure of one of the most risk-prone plants of the case-study portfolio, as resulting from the prioritization analysis

performed in Chapter 4. For reasons of Company policy, the name of the plant and the location of the industrial facility are hidden.

An aerial view of the case study industrial facility is shown in Figure (6.1). It is composed of one large workshop building with overall plan dimensions of 252 m (X -direction) and 192 m (Y -direction) and some structures for utilities and offices.

As it can be observed in Figure (6.1), three small reinforced concrete structures, adjacent to the southern portion of the workshop building, exist. These structures, used as offices, have been neglected in the analysis, since it was supposed that, during seismic action, their behaviour doesn't significantly influence workshop building's response.



Figure 6.1 Aerial (left) and close-up (right) view of the whole facility

Figure (6.2) schematically illustrates that the case-study workshop building is composed of four building structures, built in different years, separated each other by gaps. The white area in the figure refers to the older structure, built in 1971 and separated into two portions by a longitudinal joint parallel to the direction X . In 1979 these two portions were enlarged with no separation between the new and old constructions (light grey shaded area in Figure 6.2). Considering that additions were built using the same materials and structural dimensions as those of the previous 1971 structures, these will be referred to as “1971/79” structures. Finally, the most recent parts were built in 1991, as indicated by the dark grey shadow in Figure (6.2).

Both the 1971/79 and the 1991 structures were designed according to old seismic codes, with significant underestimation of design seismic intensities with respect to current design seismic actions based on probabilistic hazard at the site (CS.LL.PP., 2008). As widely discussed in Section (4.4), Codes and Standards used for the design of the existing structures were largely based on the Allowable Stress method without any account of Limit State and Capacity Design principles. The expected consequence is that no control was taken of the location of plastic zones, which may therefore involve also relatively brittle failure modes (further discussion to follow).

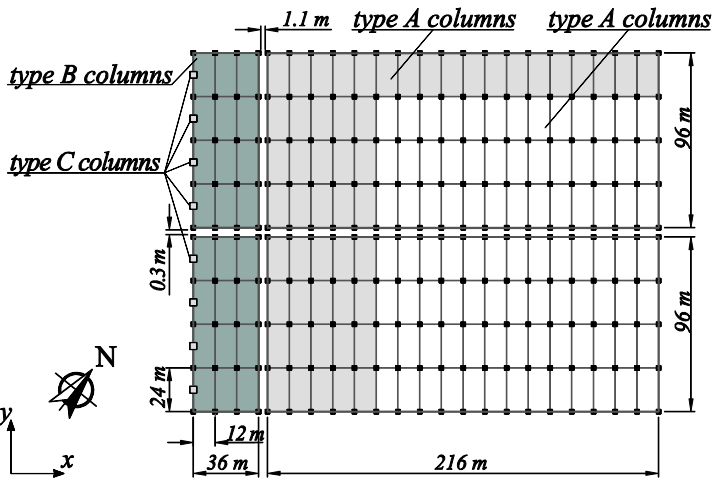


Figure 6.2 Schematic drawing illustrating different portions of the case-study building.

The design seismic action was, for both the portions, equal to $0.10 g$, while current hazard estimates (CS.LL.PP., 2008) provides a PGA with 475 years return period, on rock, equal to $0.26 g$. Full original design drawings were available for the most recent portion of the structure, the one built in 1991, while original design drawings were only partially available for the 1971/79 portion. This information was completed by means of visual surveys.

Parts made in different years have the same structural plan layout (columns spaced at $12 m \times 24 m$ in the two main directions X and Y) and a similar roof structure. The latter is made of shed-type trusses in direction X and Pratt trusses in direction Y . One full cross section of the roof structure in the X -direction, as given in the original design drawings, is shown in Figure (6.3). The cross-section intersects the frames belonging to the portions of 1979 and 1991 (i.e. one of the top-side frames in Figure 6.2). The separation joint between the 1979-portion and the 1991-portion is visible in the cross-section of Figure (6.3). The lower frame on the right-end of the cross section indicates a secondary minor structure built adjacent to the main industrial building for stocking and transferring finished products.

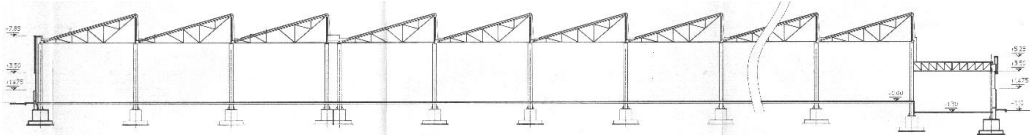


Figure 6.3 Full structural cross section in the x -direction

Single-bay structural cross sections of trusses in directions *X* and *Y*, as recorded in the original design drawings, are reproduced in Figures (6.4, 6.5 and 6.6).

Figures (6.4) and (6.5) show typical cross sections of roof trusses for internal frames in the direction *X* and *Y*, respectively.

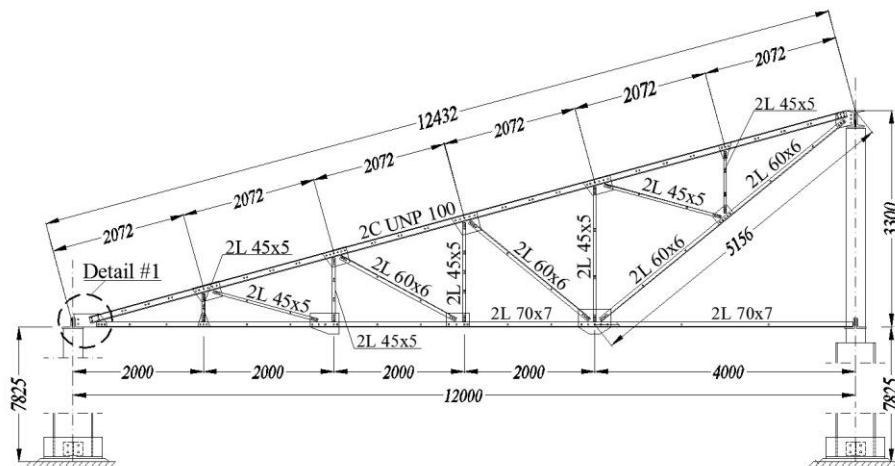


Figure 6.4 Single-bay structural cross-sections of trusses in direction *X*.

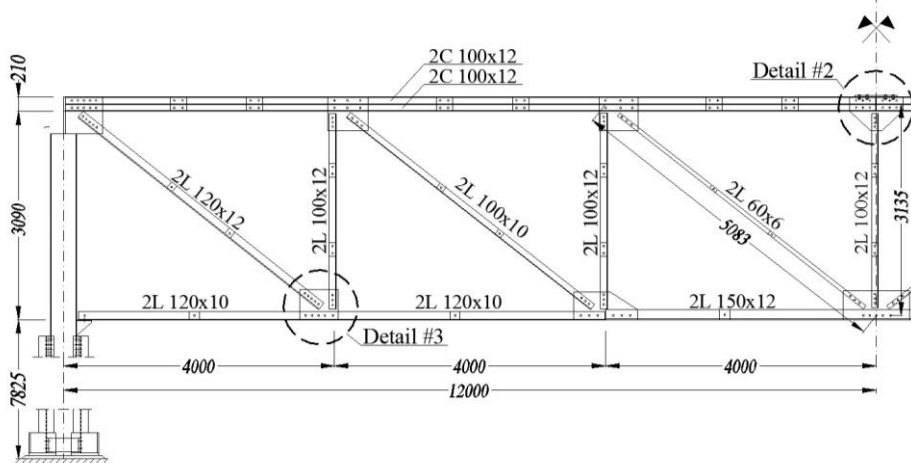


Figure 6.5 Single-bay structural cross-sections of main frame trusses in direction *Y*.

Figure (6.6) shows a cross section of the truss located onto the west-side perimeter frame highlighted in Figure (6.2). Such a perimeter frame is characterized by additional columns as respect to other frames and a smaller free length of columns because the corresponding roof truss is at a smaller height. A sample of some details of roof elements is illustrated in Figure (6.7). As mentioned, detailing (bolts pitch, hole-to-bolt diameter tolerance, etc.) follows outdated Italian regulations about the design of steel structures (DM, 1996a; CNR, 1985).

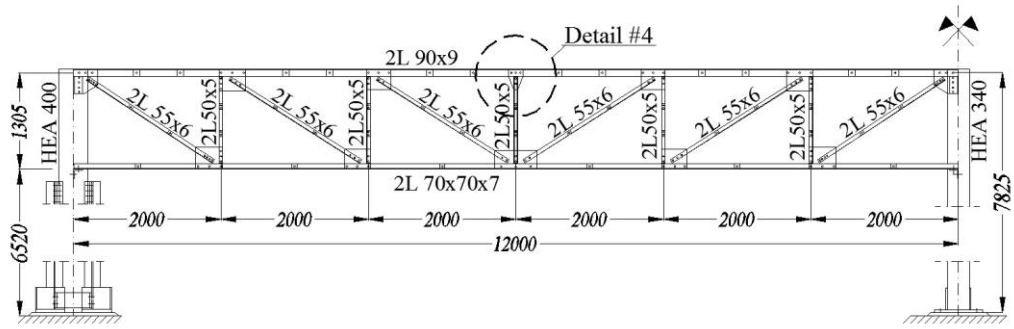
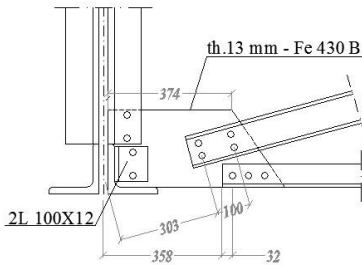
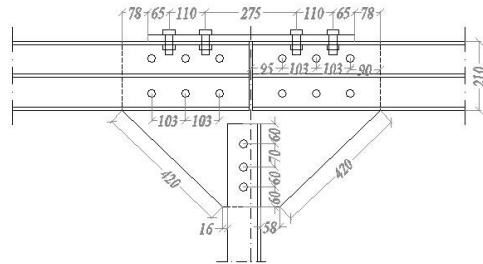


Figure 6.6 Single-bay structural cross-sections of trusses of the perimeter frame in direction Y

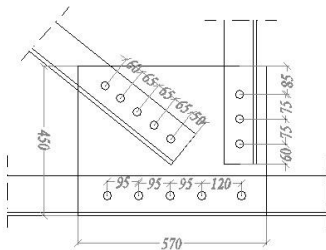
a) Detail #1



b) Detail #2



c) Detail #3



d) Detail #4

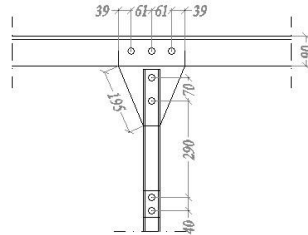


Figure 6.7 Close-up view showing roof gusset plate connections.

The roof structure is completed by in-plane sub-horizontal X-bracing and minor elements supporting the roof panels.

The roof structure is designed to sustain the live-load due to machineries, stairs, and any other minor structure or mechanical component needed for the industrial works. The characteristic live-load was assumed equal to $(0.3 + 1.57 = 1.87) \text{ kN/m}^2$ as in the original design drawings. The 0.3 kN/m^2 contribution is due to the minimum equipment predicted at the time of the design while the additional 1.57 kN/m^2 is considered for possible subsequent added equipments and minor structures. These are used as characteristic values of live-loads in this assessment process. Based on the information given in the original design drawings, the roof structure weight is assumed to be equal

to 0.37 kN/m^2 . Characteristic values of snow and wind loads at the building site are equal to 1.06 and 0.8 kN/m^2 , respectively.

Vertical resisting members, which are both sustaining the roof structure and resisting horizontal forces, are composite batted columns. In the portions of the structure built in 1971/79, composite columns are made of two IPE 360 shapes, reinforced on the flanges with 15 mm thick plates and coupled together by battens consisting of plates welded to the flanges (Fig. 6.8a). A HEA 240 profile is welded at the top-end of the batted column in order to connect the roof trusses. These composite columns will be hereafter referred to as columns of *type A*, the plan location of which is indicated in Figure (6.2). In the 1991 building, the main columns, referred to as *type B* (Fig. 6.2), are also composite members, obtained by bating IPE 600 shapes. Battens of *type B* columns were obtained by cutting pieces from hot-rolled profiles with HE A 500 cross-section and bolting their flanges to the web of the main column members, as shown in Figure (6.8b).

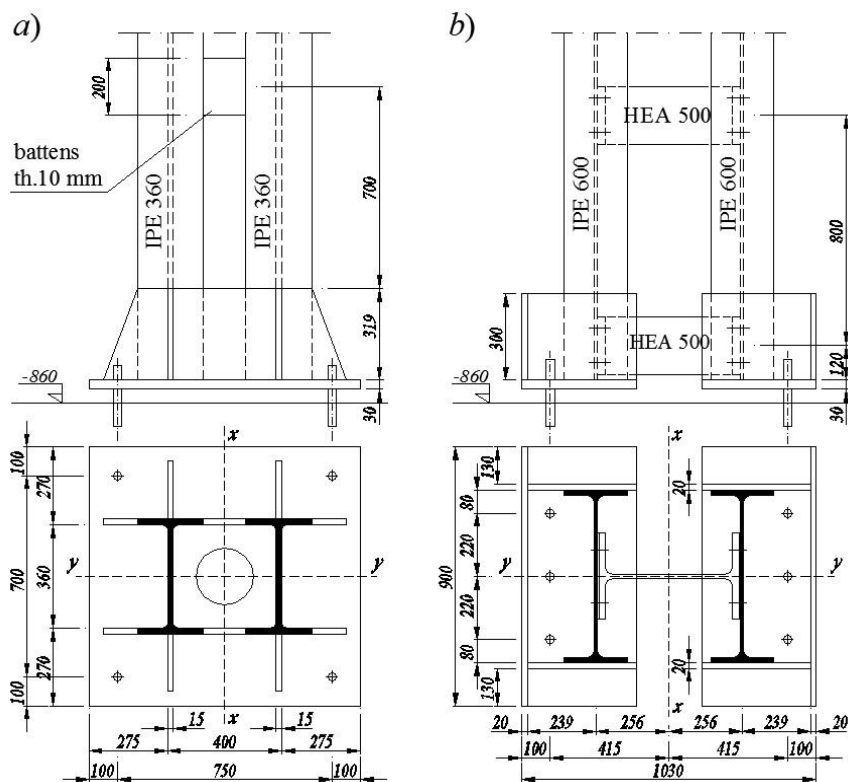


Figure 6.8 Columns and base connections: (a) type A column, (b) type B column.

A hot-rolled HE A 400 shape is placed at the top-end of the column (+7.825 m), connecting the latter to the roof. Flanges of the HE A 400 shape are connected to the web of the composite column members by means of bolts, as made for battens (Fig. 6.9a). In addition to the above, there are also columns consisting of a single hot-rolled HE A 340 shape (*type C*, Fig. 6.9b), located at the left-hand side perimeter frame shown in Figures 1b and 2c. These *type C* columns are located in the middle of each main span, the length of which is therefore reduced to one-half (12 m) of the value in other frames parallel to the direction *Y*.

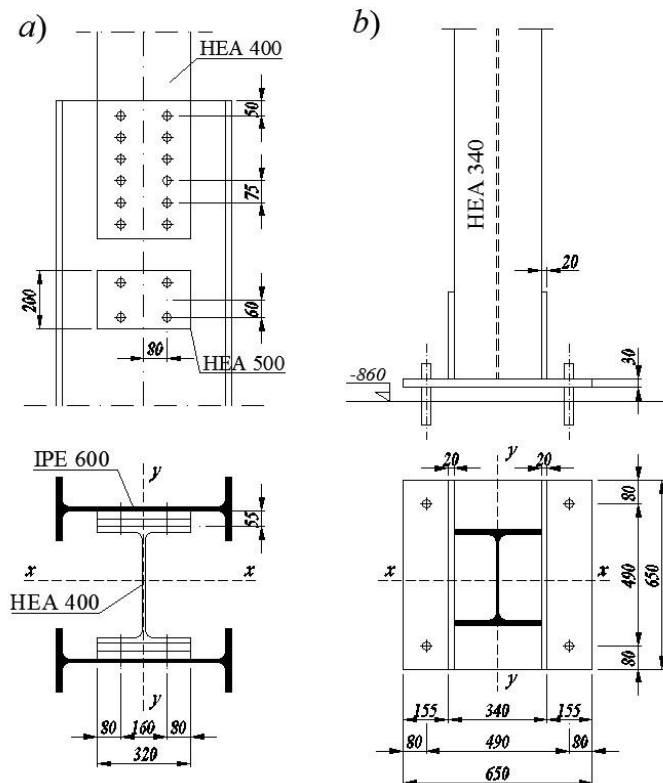


Figure 6.9 (a) details at the top of type B columns; (b) columns and base connections of type C columns.

Figures (6.8) and (6.9) also show details of the connections to the foundation for different types of columns. For *type A* columns, the connection is provided by a single 20 mm thick steel plate, anchored by bolts (diameter or $\phi = 30$ mm) to the reinforced concrete (RC) foundation (Fig. 6.8a). For *type B* columns, the connection is constituted of two separate 30 mm thick steel base plates, each one anchored to the foundation by means of three bolts ($\phi = 30$ mm) (Fig. 6.8b). The connection of *type C* columns to the foundation, similarly to other types, is made by a steel plate (thickness $t = 30$ mm) and

anchor bolts ($\phi = 30 \text{ mm}$) (Fig. 6.9b). In each of the cases described above, base plate stiffeners with thickness varying between 15 and 20 mm were used.

Based on the available information, the building foundations are made of isolated reinforced concrete footings. Original design documents indicate that the soil can be assumed as *class B* according to the current Italian seismic code. Soil type *B* is a quite stiff soil, which is characterized by average shear wave velocity in the first 30 m of depth from ground surface ($V_{s,30}$) in the range 360 m/s to 800 m/s. Soil-structure interaction is expected to be not significant for such soil conditions and it was neglected in the analysis.

6.2.1. Knowledge about material strengths

An important issue in the analysis of existing buildings concerns the acquisition of an adequate knowledge about geometry, mechanical properties and structural defects, characterizing the as-built state of the structure (Jalayer, 2011). In particular, the characterization of material strengths plays an important role in the assessment of the performance of existing constructions (Monti and Alessandri, 2008; Franchin *et al.*, 2008).

On the other hand, the process of acquiring knowledge about an existing structure is known to be expensive, because of: (i) on-site geometrical surveys, (ii) drawing out material specimens, (iii) carrying out material tests in the laboratory, (iv) characterizing the response of existing structural and non-structural components, eventually by means of laboratory tests. Besides, such as-built data collection may also require temporary business interruption. In fact, the relatively limited standardization of resisting systems of steel industrial structures may worsen this issue with respect to some other, more repetitive, structural typologies. Therefore, a compromise between accuracy of the analysis and costs is generally sought, in order to be able to reach unbiased conclusions about the structural performance with the minimum possible effort to warrant tolerable confidence.

Generally, expected average material properties are used to evaluate the seismic strength and to estimate the seismic deformation demand. According to the current Italian seismic code (CS.LL.PP., 2008), the expected average values of yield strength are about 1.10-1.20 times the characteristic values, depending on the steel grade. No information is provided by the code about average-to-characteristic strength ratio of bolts, which are considered non-dissipative elements for the design of new structures. However, as shown in the next Sections, in the case study structures as-built column base connections are partial-strength. Column base connection failure occurs with a mixed failure mode involving failure of bolts in tension. Therefore, a necessary (but cautious) choice was to use the characteristic strength of bolts in the calculation of

column base connection strength. Considering that large uncertainty of demand is expected due to the type of ground motion (GM) used in the analyses, that steel strength is, in general, characterized by a low dispersion (Da Silva *et al.*, 2009) in order to be consistent with the use of characteristic values of bolt strength, it was decided to use always the characteristic values of material strength. While this assumption is conservative for evaluating global displacement demand, it may be not acceptable to evaluate the hierarchy of strength at local level. To exclude the occurrence of some failure modes (e.g. failure of base plate welds or failure of column battens), thus simplifying the global analysis model, peak values of column base strength were estimated using commonly adopted material and strain-hardening factors with a total assumed overstrength factor equal to about 1.3. According to the original design documentation characteristic values of the material properties are as follows: yield stress of members $f_{ym} = 235 \text{ MPa}$; yield stress of column base plates $f_{yp} = 275 \text{ MPa}$; yield stress of roof gusset plate connections $f_y = 355 \text{ MPa}$; grade 8.8 for bolts; grade C20/25 (CEN, 2005) for concrete.

6.3. Structural modelling

6.3.1. General issues

The modelling of an existing building should be able to capture all the possible failure modes that may affect the structure. In fact, while the design of new structures is performed according to modern codes, in order to prevent the occurrence of undesirable failure modes (i.e. low ductility or brittle modes), in case of existing structures, the design could have been made without any explicit control of the available ductility or capacity design principles. This situation may be exacerbated in case of single-storey industrial steel buildings, the design of which is frequently driven by gravitational loads or wind actions.

The main failure modes that can affect an existing steel building (Petruzzelli *et al.*, 2011b), such as the case-study one, can be: (1) global instability (i.e. sidesway) collapse; (2) local failure modes; (3) out-of-plane buckling of members or trusses of the roof structure; (4) pounding of adjacent buildings. The main modelling issues regarding the above failure modes are dealt in the following.

In particular, the global instability of the structure, dealt in Section (6.3.2), is related to the sensitivity of the structure to P-Delta effects and to the modelling of plastic hinges and hysteresis cycle at the bases and at the top sections of columns.

Local failure modes can affect both the main roof trusses or column elements and their connections. In particular the failure of column battens would cause a brittle failure mode, nevertheless, in the specific case-study, it was checked that the battens are able

to sustain the maximum internal actions corresponding to the peak column shear force associated with flexural strengths at the top and bottom ends. Consequently, composite columns were treated as linear elastic elements, taking into account the increase of shear elastic deformability due to the discontinuous and flexible web connections (CEN, 2005). Similarly, the welds connecting the columns to the foundation plates were verified to sustain the flexural strength of the column.

Therefore, in Section (6.3.3) the problem of local failures is addressed with specific reference to the roof elements, the failure of which, due to the statically determined structure, may lead to the collapse of the whole roof structure.

Regarding the out-of-plane buckling failure, it can be observed for both roof members and frame trusses. This issue, dealt in Section (6.3.4), is related to the deformability of the roof diaphragm and to the adoption of three-dimensional or two-dimensional models.

It is finally to remark that pounding of adjacent frames was not explicitly modelled, because the peak displacement deriving from the analysis of individual frame models (Section 6.6) showed that relative joint displacements would never be large enough to close the existing gap prior to the occurrence of global frame collapse.

6.3.2. Sidesway collapse

A relevant modeling issue regarding the sidesway collapse is the representation of the hysteresis response of plastic zones, especially with reference to cyclic degradation phenomena.

Single-storey buildings are low-redundancy structural systems, for which P-Delta effects may play a significant role. Consequently, adequate attention should be given to the evaluation of the risk of a sidesway global collapse due to excessive drift demand. One important parameter determining sensitivity to global (storey) P-Delta effects is the ratio θ between the story weight and the product of the story initial first-order stiffness and height. The influence of the parameter θ on the collapse behaviour of frames subjected to ground motions was proved by former experimental tests on small scale specimens (Vian and Bruneau, 2003). Similar tests on small scale specimens with non-degrading plastic zones have also shown that a good estimate of the drift capacity at collapse is obtained by the displacement corresponding to zero lateral strength from a pushover analysis (Kanvinde, 2003). However, all subsequent investigations have clearly proved that degradation of plastic zones is an essential factor to be taken into account in order to predict accurately the sidesway collapse of frames (e.g. Rodgers and Mahin, 2003, Lignos *et al.*, 2008, Suita *et al.*, 2009, Della Corte *et al.*, 2002, Ibarra and Krawinkler, 2005). The rather extensive parametric study presented by Ibarra and

Krawinkler (2005) demonstrates the importance of a probabilistic framework in the assessment of the collapse behaviour of frames allowing consideration of variability of response due to both ground motions (frequency content) and system parameters uncertainty. Parametric studies (Ibarra and Krawinkler, 2005, ATC, 2005) have led to a distinction between in-cycle (post-elastic negative stiffness) and cyclic (i.e. between subsequent cycles) strength degradation (Fig. 6.10).

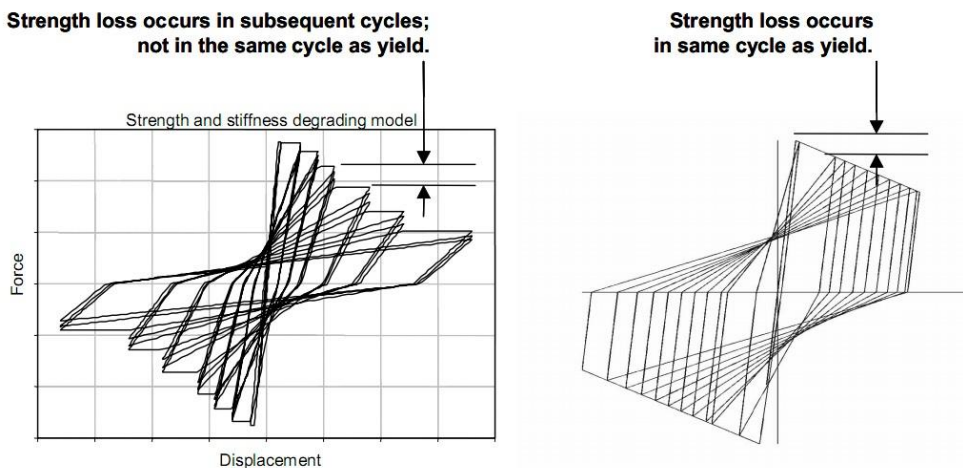


Figure 6.10 Cyclic (left) and in-cycle strength degradation (right) (ATC, 2005).

Such studies have shown that in-cycle strength degradation, such as the one due to P-Delta effects, has a much more pronounced effect on the evaluation of seismic response than cyclic strength degradation, especially for flexible structures. It is also to note that the development of accurate models representing the hysteretic response of plastic zones generally involves significant efforts, even in case of standard geometries for which several experimental test results are available in the technical literature. Additionally, in the specific case studies, column base connections of *type B* are characterized by a very special geometry for which there are no experimental test results available, according to the Author's knowledge. Though the response can be qualitatively predicted (e.g., pinching of hysteresis loops and cyclic strength degradation is expected) quantification of the actual response is difficult. Therefore, the cyclic moment-rotation response of column base connections was approximated by the Pivot hysteresis model (Dowell *et al.*, 1998) involving pinching of hysteresis loops but no cyclic degradation. The moment-rotation response of flexural plastic hinges in hot rolled members was approximated by an elastic-perfectly plastic model. In Figure (6.11) the hysteresis model for column *Type B* is shown. The procedure followed to

obtain the monotonic moment-rotation relationship relative to the hysteresis model in Figure (6.11) is described in the following sub-Section.

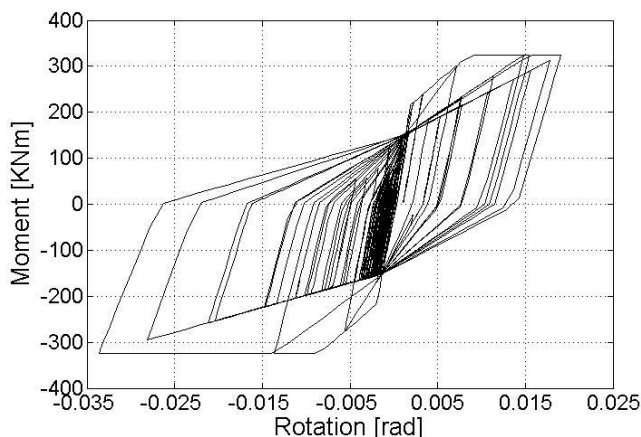


Figure 6.11 Cyclic moment-rotation response of type B column base connection.

6.3.2.1. Modelling of Column Base Connections

Current seismic codes (e.g., CEN, 2005) do not allow inelastic deformations to take place into connections because of the generally smaller ductility capacity of such elements, unless specific test results can be used to characterize capacity. In case of existing steel structures, the end member connections may be partial-strength and flexible and their modelling is challenging with respect to new constructions.

The methodology employed in Eurocode 3 (EC3) (CEN, 2005) for the definition of moment-rotation relationship of joints is the so-called *component method* (Faella *et al.*, 1999; Jaspart, 2000). The method, based on plastic analysis and on the individuation of equivalent T-stub models in tension and compression (Sokol and Wald, 1997), allows to compute the overall moment-rotation response of the connection through the analysis and the assembly of simpler components. It was proved the method provides reliable estimates of the actual flexural behaviour of column base plates (Wald *et al.*, 2000), if the geometry of the connection allows to consider T-stub models to be valid. As an example, Figure (6.12) reports some allowed and not allowed geometries, according to EC3. It can be observed that the component method requires that anchor bolts are located inside a portion of the base plate as wide as the flange of the vertical member (shaded area of Figure 6.12).

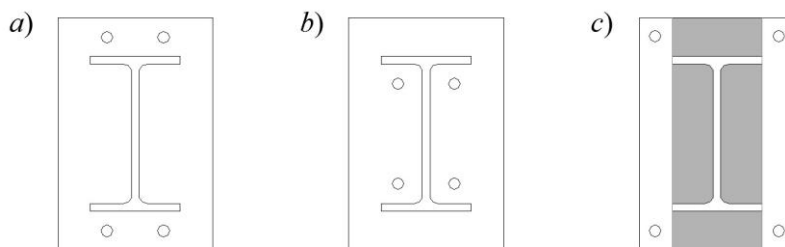


Figure 6.12 Allowed (*a* and *b*) and not allowed (*c*) connection geometries for the application of T-stub model.

Figure (6.13) reports the scheme for computing flexural strength M_{Rd} and initial stiffness $S_{j,ini}$ of column base connection according to EC3. The tensile strength T is computed as the minimum between the contribution due to end plate in bending, $F_{T,pl,Rd}$, and the one due to column web in transverse tension $F_{T,wc,Rd}$; the compressive one; C , on the contrary, is the minimum between the contribution due to column flange and web in compression $F_{C,fc,Rc}$ and the one due to concrete in compression $F_{C,pl,Rd}$. According to EC3, the tensile strength and the compressive one are located, respectively, under the anchor bolts and under the compressed flange of the vertical element. The compressed part of column web is, in general, neglected.

On the basis of the initial rotational stiffness and flexural strength values, the EC3 allows to derive the moment-rotation relationship of the connection for both the cases of small eccentricity (the connection is fully compressed or fully tensed) and large eccentricity (the connection is partially compressed/tensed).

Such a relationship is composed of three main branches: a first elastic one, up to $2/3$ of the flexural strength M_{Rd} ; a post-elastic branch, between the $2/3$ of M_{Rd} and M_{Rd} and, finally, a perfectly-plastic branch, up to the rotational capacity. It is to mention that, since EC3 is dedicated to the design of new structures, it implicitly assumes that, in case all the requirements given at material, cross-section and element levels are met, the connection has a sufficient rotational capacity. Therefore it does not provide any indication about the determination of the rotational capacity.

Moreover, since EC3 is dedicated to analysis under static loads, it gives information as to how calculating the flexural strength for a given eccentricity of the axial force ($e_d = M_{Ed}/N_{Ed}$, M_{Ed} and N_{Ed} = design values of bending moment and axial force respectively) and not at increasing eccentricity levels, as it is reasonable to observe in case of seismic loads. In order to overcome this shortcoming, an iterative procedure computing the tangent stiffness of the moment-rotation relationship, at increasing eccentricity levels, is presented in the following.

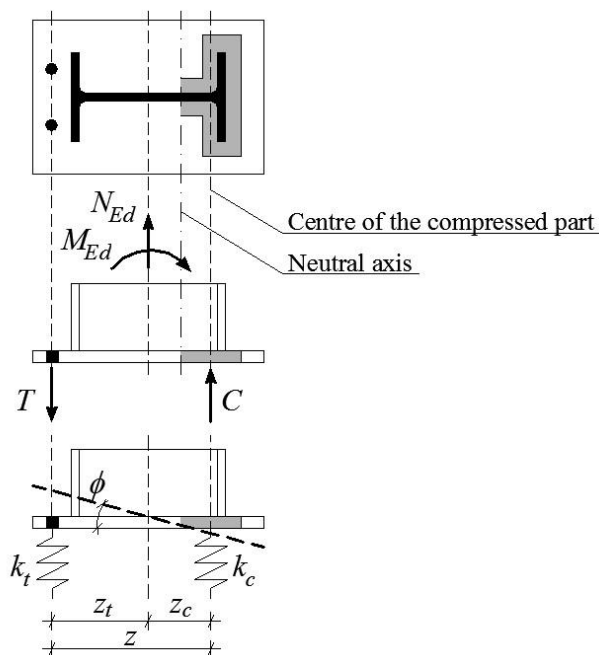


Figure 6.13 Component method according to EC3 (CEN, 2005).

Column base connections of existing structures very often differ in geometry respect to standard types, therefore some adaptations and extrapolations of the approaches developed for new structures are needed.

The modelling approach followed for the case study column base connections is described in the following sub-Sections. Evaluation of stiffness and strength of connections was essentially based on adaptations, deemed reasonable and prudential, of EC3 rules (EC3 part 1-8; CEN, 2005) (Petruzzelli *et al.*, 2011a). Description of models will start with the most simple type encountered in the examined structures (*type C*), followed by the more complex cases (*types A* and *B*).

Type C connections

Type C column base connections (Fig. 6.9b) represent a widely used design solution. However, Figure 6.9b shows that the vertical stiffening plates and the location of anchor bolts make such a connection different from the standard type presented in the Eurocode 3 (EC3). In the case of bending about the weak axis ($x-x$) of the column section, it is believed that the resultant of compression can be placed at the centroid of the stiffening plate welded to the flanges of the column. The resultant of tension is, as from the regulatory approach, placed under the row of bolts (Fig 6.14a).

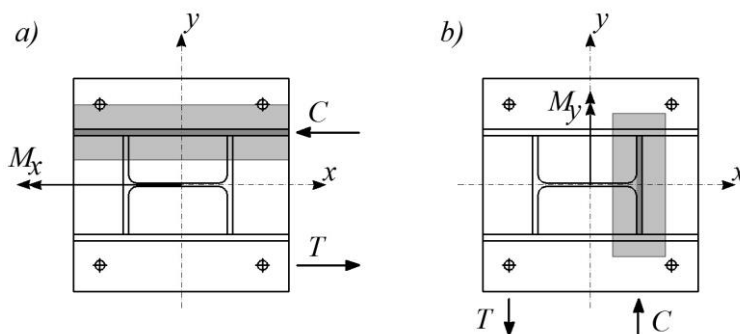


Figure 6.14 Tensile and compressive strengths in *type B* column base connection: (a) bending about *x-x* axis; (b) bending about *y-y* axis.

As regards the determination of the compressive strength of the concrete (see EC3, Sect. 6.2.6.9 and 6.2.5), it is determined according to the model of equivalent T-stub in compression as follows:

$$F_{C,f_c,Rd} = f_{jd} \cdot b_{eff} \cdot l_{eff} \quad (6.1)$$

where f_{jd} is the bearing strength of the joint, accounting for concentrated concrete resistance (CEN, 1992); the product b_{eff} and l_{eff} is the effective area of the equivalent T-stub in compression. The effective width b_{eff} is computed as follows:

$$b_{eff} = t_{sp} + 2 \cdot c \quad (6.2)$$

where t_{sp} is the thickness of the stiffening plate. In the previous equation c represents the additional bearing width, as defined by EC3:

$$c = t_p \cdot \left[f_y / (3 \cdot f_{jd}) \right]^{0.6} \quad (6.3)$$

where t_p is the thickness of the base plate and f_y the yield strength of the T-stub flange. The contribution to the compression resistance provided by the column flange and web in compression (see EC3 Sect.6.2.6.7) was neglected, due to the presence of stiffening plates welded to the column flanges. Regarding the tension resistance of the connection, it is possible to observe a single row made of two bolts, widely spaced one another. The contribution due to the bending of the base plate derives from the identification of the minimum yielding pattern. In the specific case a local non-circular yielding pattern was observed, affecting the neighbourhood of the bolt and the external edge of the base plate. No prying forces develop for the specific case, therefore the tensile strength of the connection T is obtained as follows:

$$T = \min \left\{ \frac{2M_{pl,Rd}}{m}, \sum F_{t,Rd} \right\} \quad (6.4)$$

in which, $M_{pl,Rd}$ is the flexural strength of the base plate, $F_{t,Rd}$ is the tensile strength of an anchor bolt and m is the distance between the centroid of the bolt and the stiffening plate, reduced by the width of the weld of the stiffening plate.

In the specific case the failure of the equivalent T-stub in tension is due to the yielding of base plate and failure of anchor bolts. The value of the tension resistance is much lower than that in compression; this identifies the tensile side of the connection as the weak element.

With regards to the rotational stiffness, it is computed according to EC3, by the dimensionless stiffness coefficients (EC3 Sect.6.3.2) k_{13} for the concrete in compression; k_{15} for the base plate in bending and k_{16} for the anchor bolts in tension. On the basis of the above, the moment-rotation relationship can be obtained at a given level of the design eccentricity. Nevertheless, in the case of seismic actions it is reasonable to assume that the axial force remains approximately constant and equal to the value produced by the seismic combination of gravitational loads ($N_{G,s}$), while the bending moment will grow significantly due to horizontal seismic forces. To account for this, the maximum value of the eccentricity e_{max} that the connection may sustain (i.e., the eccentricity inducing failure of the weakest connection component) was determined first. Given the symmetry of the connection, the possible limit equilibrium conditions are shown in Figure (6.15) for bending about the weak column axis.

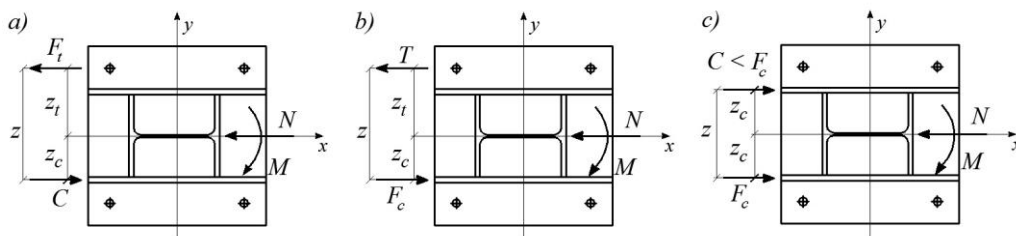


Figure 6.15 Limit equilibrium conditions: (a) “large” eccentricity and tension failure; (b) “large” eccentricity and compression failure; (c) “small” eccentricity and compression failure.

Panels *a* and *b* of Figure (6.15) illustrate the case of “large eccentricity”, where failure may be due to either excessive tension (F_t , case *a*) or excessive compression (F_c , case *b*). Panel *c* of Figure (6.15) represents the case of “small eccentricity,” where the connection is fully compressed. Using formulations of EC3, the bending strength corresponding to each of the failure modes shown in Figure (6.15) can be computed for

any value of the axial force. The flexural capacity of the connection, M_{Rd} , is the smallest value among the three modes of failure, corresponding to the acting axial force $N_{G,s}$, as shown in Figure (6.15).

Once the maximum eccentricity, $e_{max} = M_{Rd} / N_{G,s}$, has been calculated, the moment-rotation relationship can be obtained for any given value e of the eccentricity in the range $(0, e_{max})$. The connection tangent stiffness for the real loading conditions (varying bending moment with constant axial force) is then assumed equal to the derivative of the moment-rotation relationship obtained for the given value of the eccentricity e . Henceforth, the moment-rotation response of the connection for a varying eccentricity can be obtained. This calculation procedure is shown in the following Figures (6.16) and (6.17).

In Figure (6.16) the moment-rotation response of the connection, except for the perfectly-plastic branch, is shown for any given value of the eccentricity in the range $(0, e_{max})$.

To low values of eccentricity (both the sides of the connection compressed, i.e. small eccentricity), low values of flexural capacity correspond. As eccentricity increases, the flexural capacity increases as well, up to a maximum value of 380 KNm that is observed for an eccentricity of 325 mm . Beyond this value, the strength of the connection tends to decrease and to draw asymptotically the value of M_{Rd} corresponding to maximum eccentricity.

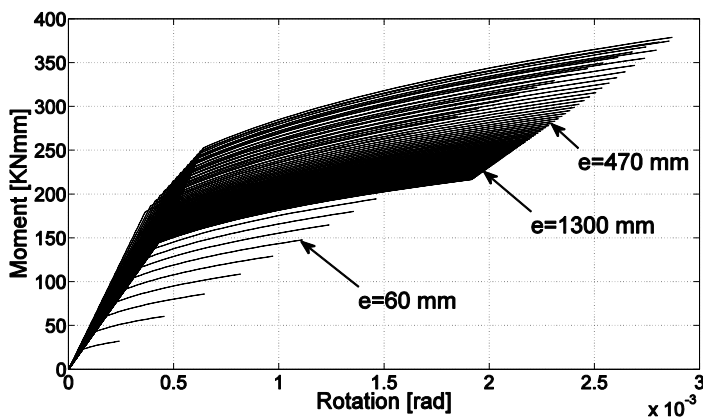


Figure 6.16 Moment-rotation relationships for different values of eccentricity

In order to obtain the moment-rotation relationship for varying eccentricities, a MATLAB® procedure was implemented, so that for each moment-rotation curve corresponding to a given value e^* of the eccentricity, automatically computes the

tangent stiffness value corresponding to a bending moment $M^* = N_{G,s} \cdot e^*$, as shown in Figure (6.17).

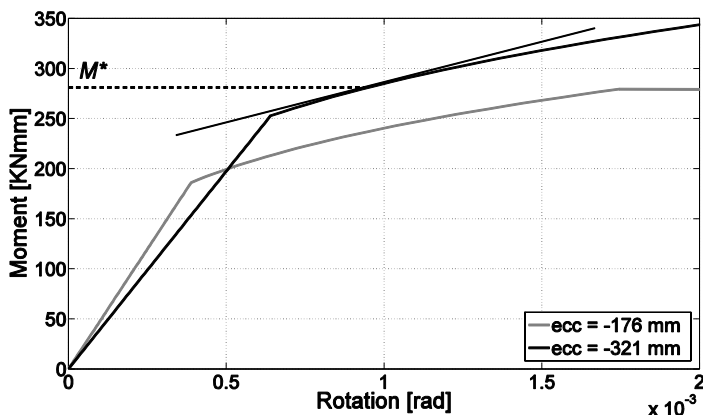


Figure 6.17 Tangent stiffness computed at $M^* = N_{G,s} \cdot e^*$.

The moment-rotation relationship of type C column, for bending about the $x-x$ axis, is, therefore, obtained by forward approximation. The values of the initial rotational stiffness and of the flexural strength of the connection are, respectively, $S_{ini} = 3.71 \cdot 10^5 \text{ KNm}$ and $M_{Rd} = 220 \text{ KNm}$

In Figure (6.18) the moment-rotation response for a varying eccentricity is illustrated. Limit values of rotational stiffness and strength provided by EC3 for classifying connections are also shown in Figure (6.18) by dashed lines. It can be seen that the specific connection is rigid and partial-strength.

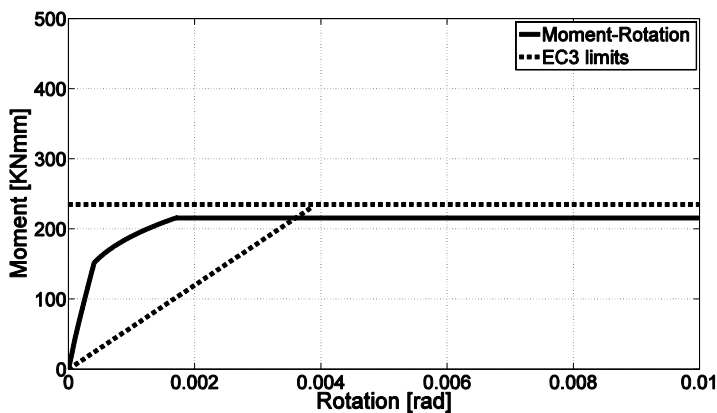


Figure 6.18 Moment-rotation relationships for type C base plate at increasing values of eccentricity, in the case of bending about the $x-x$ axis.

In a way similar to the one described above, the moment-rotation relationship of the *type C* column was obtained for bending about the *y-y* axis (Fig. 6.14*b*).

The main differences regard the characterization of the basic components of the connection. In fact, the compressive strength of the connection is calculated assuming that the compression resultant is located below the flange of the column, neglecting, for cautionary, the presence of the stiffening plates (Figure 6.14*b*).

Regarding the characterization of the equivalent T-Stub in tension, it is possible to observe that the presence of stiffening plates makes it impossible to detect an actual row of anchor bolt, and avoids the formation of yielding patterns involving both the anchor bolts. Therefore, for each single bolt a T-stub in tension is considered (Fig. 6.19), the web of which is the portion of the stiffening plate comprised between the column flange and the plate edge.

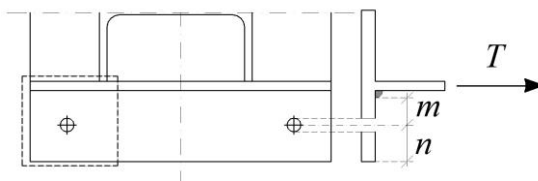


Figure 6.19 Considered T-stub in tension.

Under these assumptions, prying forces develop and the tensile strength of the connection is computed as follows:

$$T = \min \left\{ \frac{4M_{pl,Rd}}{m}, \frac{2M_{pl,Rd} + n \cdot \sum F_{t,Rd}}{m + n}, \sum F_{t,Rd} \right\} \quad (6.5)$$

The meaning of the symbol of Eq. (6.5) was already explained in the text; *m* and *n* considered in the specific case are shown in Figure (6.19).

The moment-rotation relationship for increasing eccentricity was obtained in a similar manner to that described for bending about the *x-x* axis. The values of flexural strength of the connection and of the initial rotational stiffness are, respectively, $M_R = 195 \text{ KNm}$ and $S_{ini} = 3.41 \cdot 10^5 \text{ KNm}$. Also in this direction, the connection can be characterized as rigid and partial strength (Fig. 6.20).

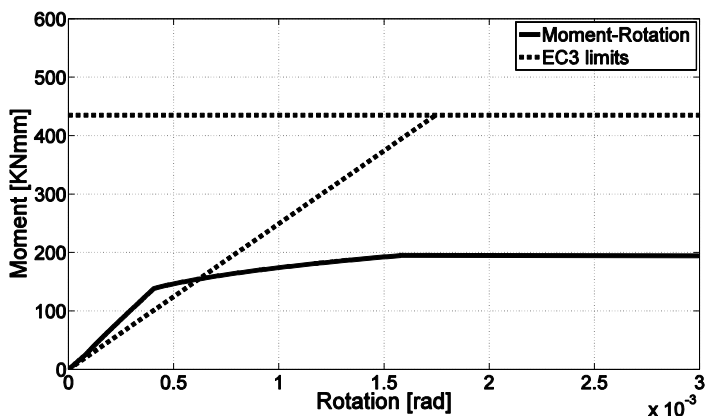


Figure 6.20 Moment-rotation relationships for type C base plate at increasing values of eccentricity, in the case of bending about the y-y axis.

Type A connection

In order to obtain the moment-rotation for increasing eccentricity for the *type A* connection, a procedure similar to that previously described for the connection of *type C* has been implemented.

The main difference with the previous case concerns the determination of the tensile strength of the link (Fig. 6.21a and 6.21b). In fact, the presence of stiffening plates placed in continuation of the web and of the column flanges and of bolts in the four corners of the base plate does not allow to identify any equivalent T-stub in tension. Therefore a nonlinear field plate, perforated in correspondence of the bolt, has been modelled (Fig. 6.21c), in order to calculate the tensile force acting on the single bolt necessary to yield the base plate. The axial stiffness was computed as the value of the axial force to the bolt producing a unit axial displacement of the plate. In the specific case, the obtained values of axial stiffness and tension resistance are rather similar to those that would be obtained by considering an equivalent T-stub in tension characterised by a flange width equal to the size of the angle portion of the plate. Regarding the equivalent T-stub in compression, the compressive strength was located under the stiffening plates, as reported in Figure (6.21a)

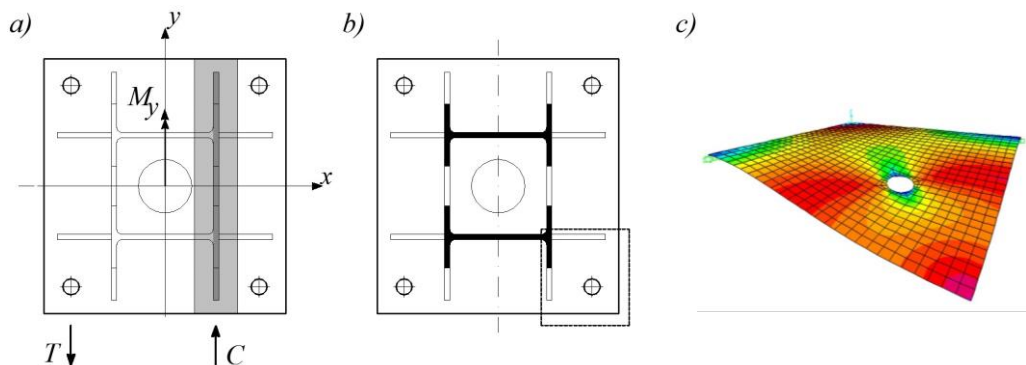


Figure 6.21 (a) tensile and compressive strengths in *type B* column base connection; (b) T-stub in tension; (c) characterization of tensile strength of the base plate through FEM modelling of the base plate portion marked by dashed box in panel *b*.

In Figure (6.22) the moment-rotation relationship for the *type A* connection is represented, for what concerns bending about *x-x* axis. The flexural strength and the rotational stiffness of the connection are, respectively, $M_R = 345\text{KNm}$ and $S_{ini} = 7.25 \cdot 10^5\text{KNm}$. It can be observed that the connection is rigid and partial-strength. Due to the almost symmetric geometry, the response for bending about the *y-y* axis is rather similar, therefore it is not reported.

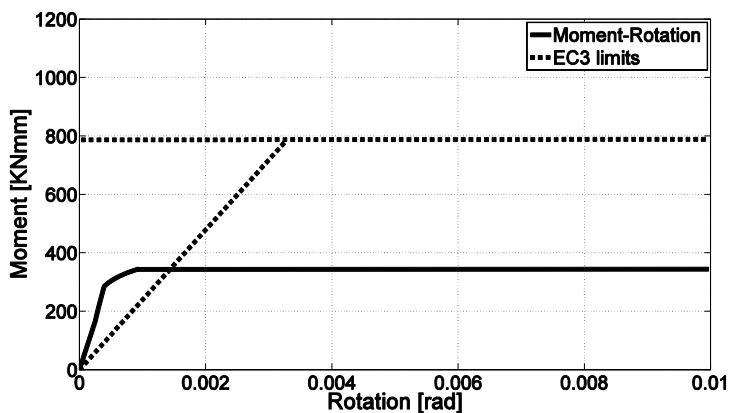


Figure 6.22 Moment-rotation relationships for type A base plate at increasing values of eccentricity, in the case of bending about the *y-y* axis.

Type B connection

Type B column base connections are significantly different from the standard type covered by EC3, because of: (1) presence of two different base plates under vertical members; (2) anchor bolts located outside the flanges of the column member; (3) presence of stiffening plates welded to the flanges of the column members and on the edge of the base plate. A decomposition of the total connection response into individual contributions was then pursued (Fig. 6.23). The total bending moment and the axial force acting at the base of the composite columns were decomposed into contributions due to single column members and transmitted to the corresponding base plates. Such contributions include both an axial force (N_t or N_c) and a bending moment (M_t or M_c) for each of the two profiles and corresponding base plates. Axial forces are assumed to be centred at the single profile web axis, both in tension and compression. Consequently, two springs are used to characterize each base plate connection, one for translations (response to the axial forces, N_t or N_c) of stiffness $k_{\Delta t}$ or $k_{\Delta c}$ and one for rotations (response to the bending moments, M_t or M_c) of stiffness $k_{\phi t}$ or $k_{\phi c}$.

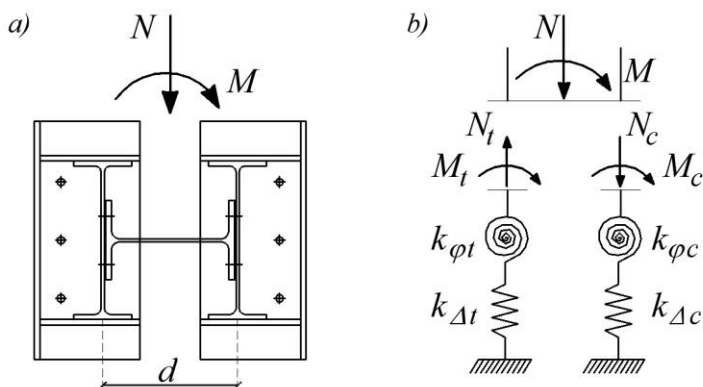


Figure 6.23 Decomposition of connection response into separate contributions.

Taking into account the overall symmetry of the connection formed by the two plates, the total rotational stiffness is obtained by assembling the individual contributions, according to Eq. (6.6). Note that the individual spring stiffness was calculated on the basis of the schemes illustrated in Figure (6.24).

$$k_{\phi} = k_{\Delta t} \cdot \frac{d}{2} + k_{\Delta c} \cdot \frac{d}{2} + k_{\phi t} + k_{\phi c} \quad (6.6)$$

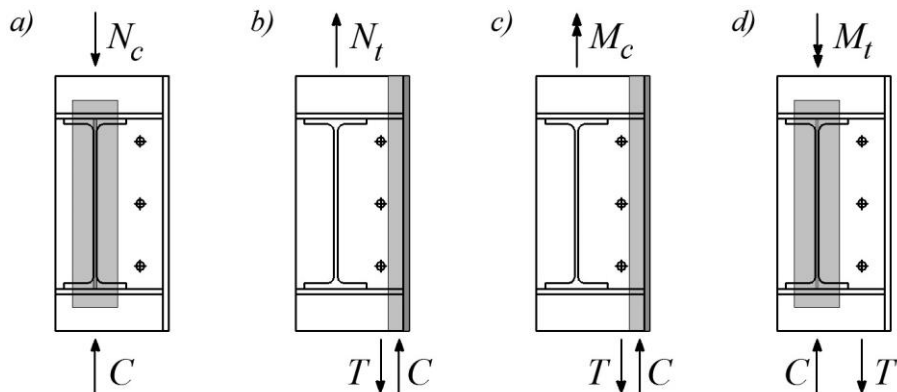


Figure 6.24 Individual contributions to connection response.

Panels *a* and *b* of Figure (6.24) show the schemes for the evaluation of the translation stiffness of the springs in compression (k_{Δ_c}) and tension (k_{Δ_t}), respectively. Panels *c* and *d* of Figure (6.24) complete the illustration of the schemes for evaluating the rotational stiffness, with reference to contributions from bending moments associated with the individual column members (k_{φ_c} and k_{φ_t}).

The first contribution (Fig. 6.24*a*), that is the one of base plate in compression, is computed assuming that the base plate connection reacts with an equal and opposite force also located at the web centreline. The stiffness contribution to Eq. (6.6), was computed from k_{13} coefficient defined in EC3.

For tension forces, (i.e. base plate in tension, panel *b* of Figure 6.27) it is considered that the plate connection reacts with both a resultant force and a bending moment. In the specific case, accounting for the additional bearing width c defined by the EC3, would lead to an effective width such that the anchor bolts would be compressed. Therefore, the compression center was evaluated assuming a rectangular (*stress-block*) distribution of stresses at the contact of the steel plate and concrete foundation. Regarding the equivalent T-stub in tension, a circular yielding pattern involving the three bolts is observed and prying forces develop. By simple equilibrium conditions, the flexural strength of the base plate under tension is computed as the minimum between:

$$M_{\Delta,1} = \frac{T \cdot z}{1 + z_c/e} \quad (6.7)$$

$$M_{\Delta,2} = \frac{C \cdot z}{1 + z_T/e} \quad (6.8)$$

where z is the lever arm between T and C ; z_C and z_T are the distances of the center of the plate from C and T , respectively. The stiffness contribution in this scheme is due to the rotational stiffness of the plate, considering the corresponding eccentricity of the applied force. It is to mention that, while the computation of the compressive stiffness coefficient can be performed according to EC3 approach (k_c in figure 6.25), for the definition of the tensile stiffness k_t (Fig. 6.25), the base plate portion comprised between the column web and the stiffening plates was modelled as a rectangular plate restrained on the four edges, in a manner similar to the one described in Section (6.3.2).

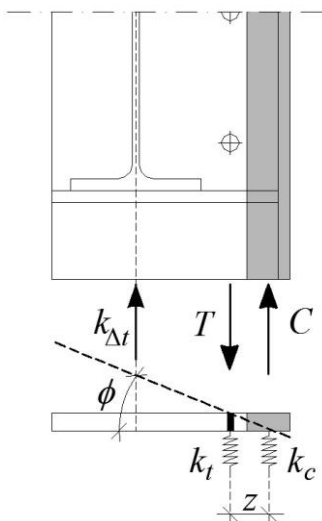


Figure 6.25 Determination of $k_{\Delta t}$ according to panel *b* of Figure (6.24).

Once the axial stiffness values of Figure (6.25) are known, the axial force applied to the column web that produces a unit axial displacement is:

$$k_{\Delta t} = \frac{-k_c \cdot x - k_t \cdot x + k_t \cdot z}{1 - x} \quad (6.9)$$

where x is the distance between the rotation center of the plate and the compressive strength C .

In the calculation of this contribution, the decompression phase should be considered when the gravity induced axial force is larger than the tension due to the total column bending moment. However, in the analysis of seismic response this initial phase generally has a role for only small earthquake intensity, when the system behaviour is elastic. At a larger seismic intensity inducing appreciable inelastic deformation, the use of a secant stiffness corresponding to the decompression phase is generally acceptable. Besides, it is also noted that this contribution to the total stiffness given by Eq. (6.6) is

rather small, as it may be argued by the small lever arm of the reacting forces shown in Figure (6.25).

The case of base plate under M_c action (Figure 6.24c) is similar to the previous one for what concerns the definition of the tension resistance (T) and the compression resistance (C), as well as of stiffness coefficients. The main difference is the absence of an eccentric force acting on the column web centroid, therefore the flexural strength in this scheme is:

$$M_c = \min \{T \cdot z, C \cdot z\} \quad (6.10)$$

The rotational stiffness is computed as the value of the bending moment causing an unit rotation of the plate:

$$k_{\phi,c} = k_t (z - x) z \quad (6.11)$$

The case of base plate subjected to a bending moment M_t (Figure 6.24d) can be reduced to the case of base plate subjected to a force with infinite eccentricity, as dealt in EC3. It seems reasonable to assume that the resulting compression C is placed beneath the column web, neglecting the contribution to the equivalent T-stub in compression flange due to the stiffening plates. Similarly, the tensile strength T of the plate and of the bolts can be obtained as previously discussed for scheme reported in panel a of Figure (6.24). The flexural strength and the rotational stiffness are reported in the following equations.

$$M_t = \min \{T \cdot z, C \cdot z\} \quad (6.12)$$

$$k_{\phi,t} = \frac{E \cdot z^2}{\left(\frac{1}{k_c} + \frac{1}{k_t} \right)} \quad (6.13)$$

Figure (6.26) shows the moment-rotation curves obtained for *type B* connection, assuming a EC3-type relationship. Limit values of stiffness and strength according to EC3 are also shown by dashed lines. It can be seen that the connection is partial-strength and semi-rigid.

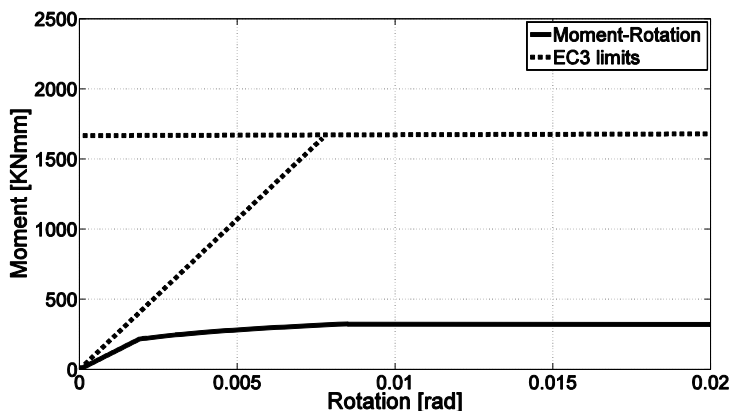


Figure 6.26 Moment-rotation relationships for *type B* base plate.

6.3.3. Roof failure modes

The roof structure of single-storey industrial steel buildings is frequently made of trusses, where failure may occur either in the form of member buckling or connection failure. Such failure modes are generally characterized by low ductility capacity, especially in case of partial-strength connections. Furthermore, a local failure mode may propagate at a global level in case of statically determined roof structures where failure of any element may transform the structure into a mechanism. The examined case studies are examples of such a type. The serious damages consequent to roof collapse have been frequently observed in the past; one well documented case of roof collapse due to failure of gusset plate connections yet not induced by earthquake actions was presented by Brencich (2010). Therefore, failure of roof elements was taken into account by a cautious approach. Generally, if the failure of an element takes place, then an explicit assessment of the corresponding deformation demand must be carried out in order to check whether the deformation capacity is exceeded. Alternatively, the force demand must be evaluated for those elements which are considered to have low ductility and for which the force capacity is required to be not exceeded. The second approach was followed in the case studies; the results are shown in Section (6.6.2).

6.3.4. Two-dimensional versus three-dimensional modelling

The behaviour of single-storey steel buildings is generally affected by the roof deck diaphragm, which is almost always comprised of a thin-walled cold-formed trapezoidal sheet. The shear flexibility of such deck diaphragm is not negligible, generally leading to an increase of the building period of vibration (Tremblay *et al.*, 2004). Analysis models including a flexible diaphragm have been proposed (Jain and Jennings, 1985,

Tena-Colunga and Abrams, 1996, De Matteis *et al.*, 1999). However, it has also been proved that nonstructural components may reduce appreciably the period of vibration as respect to predictions based on a model including the steel deck only. Consequently, investigations concerning the effect of nonstructural components have been carried out (Mastrogiuseppe *et al.*, 2008). It is noted that the contribution of nonstructural components may be difficult to be quantified in practice because of the different materials which may have been used and for which scarce data and information about the mechanical behaviour may be available. On the other hand, a typical practice in the design of single-storey steel buildings consists of neglecting the stiffening contribution of the roof deck diaphragm and to use roof braces to distribute horizontal actions among frames. Such roof braces were found in the examined case study structures and they significantly stiffen the roof structure. However, roof braces are characterized by high slenderness which may lead to buckling for relatively low levels of seismic intensity. Whether roof braces buckle, the coupling of response of parallel 2D frames obviously reduces and the system response approaches the one of isolated 2D frames. In the case study, this aspect is investigated considering for the 1991 structure both three-dimensional modelling and bi-dimensional one. In the three-dimensional modelling all the structural elements are considered, including the bracing elements but the latter are assumed to behave elastically. The two-dimensional models are obtained extracting two single frames from the structure, each one subjected to vertical loads derived from an analysis of the three-dimensional model for gravitational loads. The analysis of response of the 3D model with elastic braces and of the 2D frame model allows identifying boundaries to the real structural response, which is expected to be intermediate to the above two limit cases because of early brace buckling and consequent degradation of the coupling effect. In addition to the above comments, consideration has to be given to the feature of a 3D model to explicitly and automatically capture buckling of the roof structure. 2D models are unable to represent out-of-plane buckling of the corresponding roof elements and they therefore may be missing important information about the possible failure modes of the structure. Out-of-plane buckling modes are sensitive to end-restraint conditions. Members of roof trusses are commonly modelled as perfectly pinned at their ends when in-plane structural analysis is to be carried out. This is generally motivated because the truss response is dominated by axial forces: neglecting bending moments removes one source of stiffness and strength thus resulting into conservative global response assessment. However, out-of-plane end-restraints may be essential in case of transverse vibrations of plane trusses: releasing transverse end moments may result in such a case into an unstable structure. The importance of such modelling of roof joints was investigated by analysing two alternative 3D models: (i) a model where releases were

included for only in-plane moments while leaving continuous joints for out-of-plane flexure (labelled as “partially continuous”) and (ii) a model where all roof joints were assumed to be fully continuous (labelled as “fully continuous”).

Results from analyses of 3D models are subsequently also compared with those from 2D models, which have the advantage to be much lesser cumbersome from the points of view of the computational time and effort. In the 3D model the roof bracing elements were assumed to be linear elastic but with P-Delta effects activated. Therefore, the 3D model is able to capture elastic buckling but it is not able to capture inelastic buckling or failure of connections which must be checked separately based on peak force demand.

6.4. Analysed Structural Models

The structural models schematically illustrated in Figure (6.27) were considered. Four two-dimensional (2D) frame models were analysed, one per direction (X and Y) for each of the structures built in 1991 and 1971/79 (see also Figure 6.2). Additionally three-dimensional (3D) models were developed for the 1991 building, analysed only for earthquakes acting along the direction Y . As stated in the previous Section (6.3.4), two alternative 3D models were analysed by changing the type of roof member joints: (i) a “partially continuous” model, in which in-plane moments are released, while continuous joints are considered for out-of-plane flexure; (ii) a “fully continuous” one, in which all roof joints were assumed to be continuous for both in plane and out of plane bending.

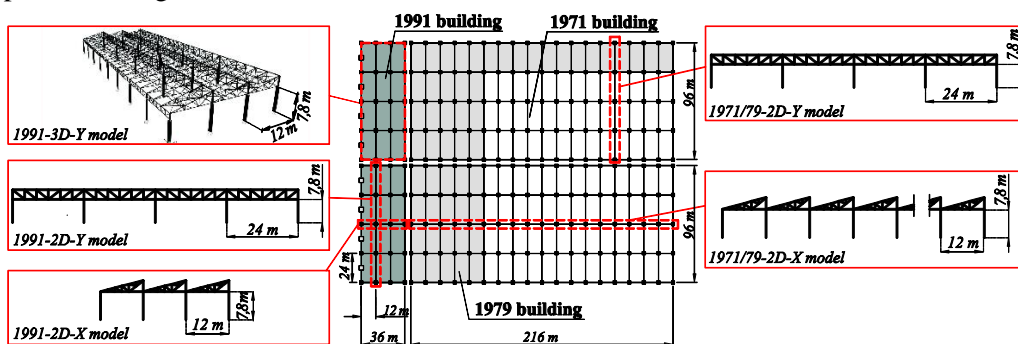


Figure 6.27 Structural models for 1991 and 1971/79 portions of the case study buildings.

In Figures (6.28) and (6.29) the 3D model and the 2D models of the 1991 portion are shown. In all the considered models, non-linearity has been concentrated at column bases, to simulate non-linear response of connections, and at sections located on the top of columns immediately below the connection with the roof trusses. All other

members are assumed to behave elastic, with P-Delta effects taken into account. Though buckling is not explicitly modelled, roof truss members and transverse truss bracings are checked against buckling. The event of buckling of any member is then tracked and recorded in order to consider limits of validity of the numerical model. Similarly, the onset of local failure modes due to failure of roof members is checked after the analysis based on peak force demand. Results from analyses of 3D models are also compared with those from 2D models, which have the advantage to be much lesser cumbersome from the points of view of the computational time and effort.

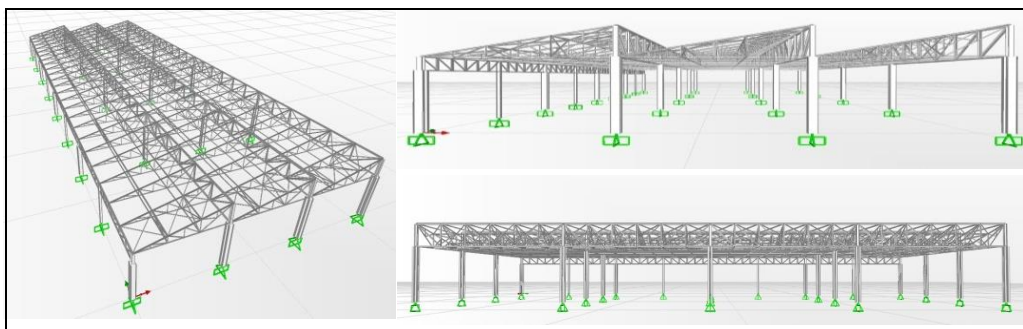


Figure 6.28 Aerial views of a 3-dimensional finite element model (1991 portion).

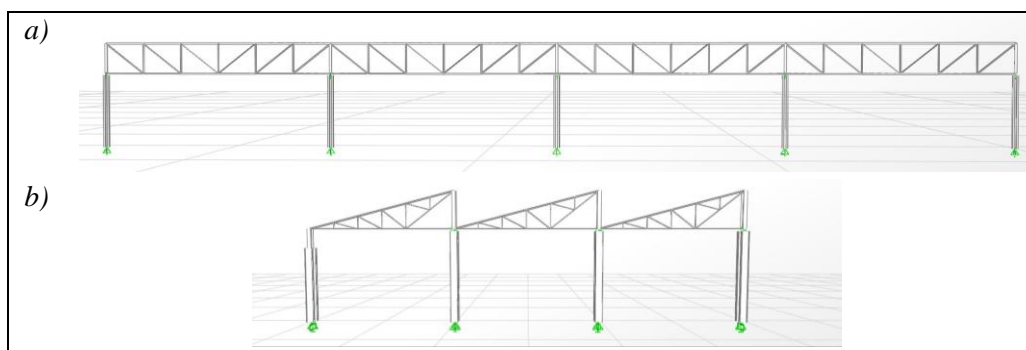


Figure 6.29 Bi-dimensional model of one central frame extracted from the 1991 structure in Y - (a) and X -direction (b).

Structural models schematically illustrated in Figure (6.27) are analysed by means of modal analyses (MA), static nonlinear analyses, frequently referred to as pushover analyses (PAs), and dynamic nonlinear response history analyses (RHAs).

MA and PA were used as preliminary analyses to the RHAs. In fact, MA provides some main elastic properties of the structures, needed for hazard estimates and for the selection of ground motions to be employed in RHA.

PA is a very convenient tool to evaluate the global structural capacity, especially for single storey buildings. Using demand spectra in combination with PA curves is a well-established simplified method of analysis (e.g. ASCE, 2000, ATC, 2005). However, PA curves are not used in this thesis with this purpose because of two reasons: (i) static nonlinear analysis is generally reliable whether the structure is in a stable range of behaviour, i.e. far from collapsing (ATC, 2005); (ii) this study is aimed at the definition of fragility curves and framed within a general probabilistic framework of performance assessment, where RHA is still the most rigorous tool to quantify uncertainty of demand predictions reflecting record-to-record variability.

PA curves are used in this study only to compare the response of different structures and to investigate whether such a comparison can anticipate results from comparison based on RHAs. The results of MA and PA are described in the following sub-Sections. Results were obtained using lumped plasticity finite element models, analysed by means of SAP 2000 v.14 (Wilson, 2002).

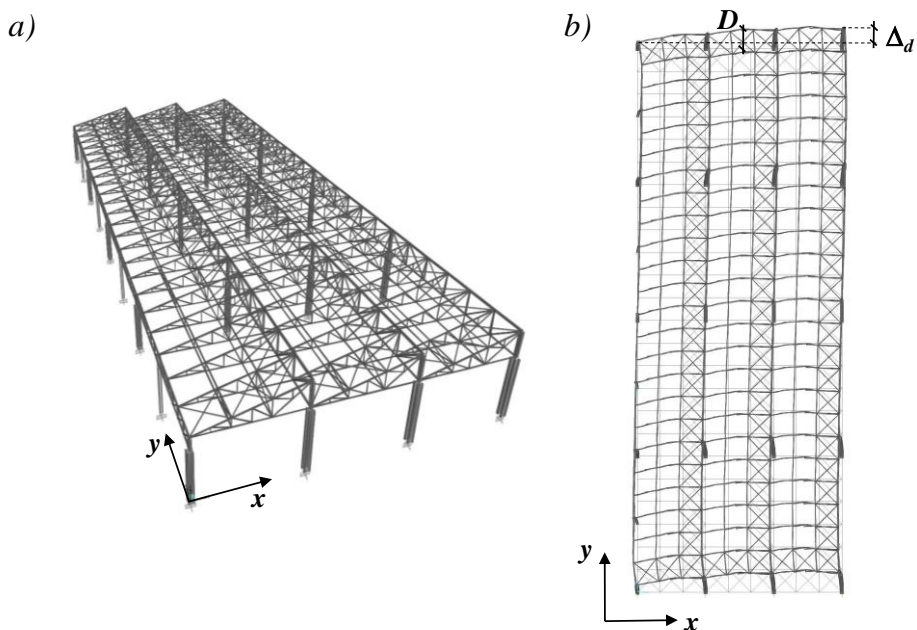
6.4.1. Basic linear properties

The fundamental periods of vibration (T_1) and the corresponding effective (participating) mass ratios ($M_{\text{eff}}/M_{\text{tot}}$) are summarised in Table (6.1) (second and third columns) for the examined structural models.

The first mode of vibration of the 1991-3D-Y models is characterized by a prevailing translation in the direction Y with non-negligible difference between displacements of different frames. As it can be observed from Figure (6.30), the peak value of the difference between displacements of the two perimeter frames in the loading direction Y (Δ_d) was equal to about 60% of the displacement evaluated at the center of mass (D). Therefore, there is significant flexibility in the transverse connection between parallel 2D frames. It is important to note that even if the global response of the 3D model is dominated by the Y -direction translation of frames, nodal masses do also exhibit displacement components in the transverse X and vertical Z directions. Such displacement components will reveal to have important consequences on the 3D model inelastic response under strong earthquakes, because transverse joint displacements can activate significant local P-Delta effects in roof members, an aspect which is further discussed in Section (6.6.1).

Table 6.1 Summary of structural characteristics of the examined models.

Structural model	T_1 (s)	$M_{\text{eff}}/M_{\text{tot}}$ (%)	α_e	δ_d/δ_y	R_{max}	$S_{a,y}$ (g)	$S_{a,\text{collapse}}$ (g)
1971/79-2D-X	1.60	100	0.129	2.98	5.21	0.07	0.38
1971/79-2D-Y	1.60	99	0.061	2.61	7.64	0.09	0.71
1991-2D-X	0.98	100	0.051	2.56	7.44	0.13	0.95
1991-2D-Y	1.03	100	0.038	1.48	8.09	0.20	1.65
1991-3D-Y <i>fully continuous</i>	0.98	91	0.043	6.90	12.7	0.32	3.99
1991-3D-Y <i>partially continuous</i>	1.00	91	0.045	6.95	12.5	0.31	3.92

**Figure 6.30** Three-dimensional structural model of the 1991 building portion (a) and deformed shape according to the first mode (b).

6.4.2. Static non-linear response

PA analyses were firstly used in earthquake engineering by Gulkan and Sozen (1977) and Saiidi and Sozen (1981) as displacement-based seismic assessment methods, and by Krawinkler (1995) as procedure for seismic design. PA represents an estimation of the evolutionary response of structures that could be obtained by means of non-linear

dynamic analyses at increasing ground motion intensity levels. Different PAs can be performed, as regards the applied lateral load pattern (i.e. force- and displacement-based procedures); the control strategy (i.e. force- and displacement-controlled procedures); number of vibration modes accounted for (single- versus multi-mode procedures) and load pattern evolution (non-adaptive versus adaptive procedures). One of the most important aspects to be taken into consideration is the possibility of a PA of considering three dimensional effects. The problem was addressed by several researchers with regards to the torsion of rigid diaphragm structures (e.g. Kilar and Fajfar, 1996 and 2001; Penelis and Kappos, 2002; Meireles, 2006).

As previously discussed, in the specific case, because of the absence of a rigid floor diaphragm and of the relative position of the centre of stiffness and of masses, no torsion of the whole roof structure is observed in the first modal shape, but significant differences in the displacements of each frame in the Y -direction. Considering that the effective mass related to the first mode is, in all the structural models, major than the 90% of the total mass, single-mode non-adaptive PAs were performed under displacement control, accounting for the (in-plane) flexibility of the floor system by varying the position of the control node. Generally, the location of the control node has insignificant effect on the PA curve at large displacements, i.e. when a plastic mechanism is activated. But the in-plane diaphragm flexibility may have a non-negligible effect on the elastic phase and on the transition-to-plastic phase of response. In the examined single-storey buildings, the control node was always located at a height (h) equal to the top of composite columns. The exact in-plan location of the control node was instead moved in order to obtain lower and upper bounds to PA curves (Petruzzelli *et al.* 2012a and Della Corte *et al.*, 2013)

In particular, for two-dimensional frames, the control node was located in the extreme corners and in the centre of the frame; for three-dimensional models, it was located at the extreme corners of the perimeter frames and at the centre of the roof deck. The analyses were conducted in both the direction of the seismic action, for a total of 36 structural analyses. In Figure (6.31) the ensemble of pushover curves obtained from the translation of the control node is shown. On the abscissa of the Figure the absolute value of the displacement is reported, apart from the one due to gravitational loads.

It can be observed that, as expected, the variation of the position of the control node has a significant effect for most deformable structures, such as the 1971/79-2D-X one. In other cases, its effect is negligible. Moreover, analysed structures strongly differ one another for what regards the maximum base shear and the slope of the post-peak branch. The latter, as mentioned in Section (6.3.2), is strictly related to the sensitivity of the structure to the P-Delta effect.

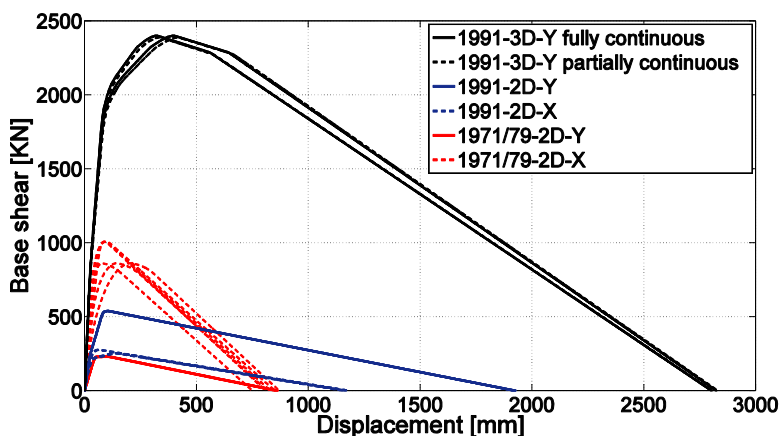


Figure 6.31 Ensemble of pushover curves accounting for different positions of the control node.

A comprehensive discussion about the role of P-Delta effects and consequent strength degradation on the seismic collapse behaviour of structures is reported by ATC [2005]. ATC guidelines introduce a couple of parameters to evaluate sensitivity to global collapse from static non-linear analyses: one parameter called α_e is the ratio between the slope of the strength degrading branch and the initial stiffness; the second parameter is the ductility (Δ_d/Δ_y) available before strength degradation takes place. The above mentioned parameters are depicted in Fig. (6.32) together with the equivalent linearization procedure proposed in ATC (2005).

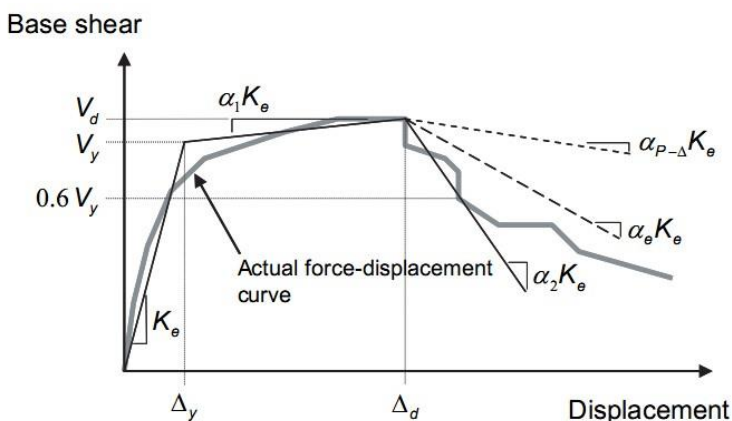


Figure 6.32 FEMA 440 (ATC,2005) procedure for equivalent linearization of pushover curve and simplified verification of sensitivity to dynamic instability due to strength degradation.

The ATC (2005) document deals with the general case of cyclic and in-cycle strength degradation, therefore the α_e is obtained as the sum of the contribution due to P-Delta effects ($\alpha_{p,\Delta}$ in Figure 6.32) and the one observed after the PA analyses due to cyclic degradation (α_2).

The two parameters α_e and Δ_d/Δ_y are combined into Eq. (6.14) in order to evaluate the maximum strength ratio $R_{max}=S_{a,collapse}/S_{a,y}$ corresponding to global collapse in a sidesway mode ($S_{a,collapse}$ and $S_{a,y}$ are the spectral accelerations leading to collapse and to first significant yielding, respectively).

$$R_{max} = \frac{\Delta_d}{\Delta_y} + \frac{|\alpha_e|^t}{4} \quad (6.14)$$

In Eq. (6.14), t is a coefficient given by the following equation:

$$t = 1 + 0.5 \ln(T) \quad (6.15)$$

where T is the fundamental period of the structure.

The ATC document clarifies that the previous equation, representing a simplification of the one by Miranda and Akkar (2003), was obtained using SDOF systems and should be used only for the identification of cases where dynamic instability should be further investigated using response history analyses and not as an accurate measure of the lateral strength required to avoid dynamic instability in MDOF structures.

Values of both α_e and Δ_d/Δ_y , as well as the corresponding R_{max} , will be reported in the following and predictions from PAs will finally be compared with those from RHAs.

Values of significant parameters from PA curves are reported in Table (6.1) for each of the examined structures. Parameters α_e and Δ_d/Δ_y (ATC, 2005) were evaluated using a tri-linear approximation to the real PA curve obtained through a procedure slightly different from the ATC method. Indeed, ATC guidelines are relevant to PA curves characterized by an abrupt loss of strength at a peak force, a consequence of the type of plastic hinge modelling. There was not such an abrupt loss in the assumed models and the following similar procedure was used to obtain the substitute tri-linear PA curve (Fig. 6.33): (a) a point (B) was individuated on the PA curve corresponding to a displacement beyond which strength degradation follows a practically linear path; (b) an elastic-perfectly-plastic initial branch (OAB) was substituted to the real PA curve based on the equal-energy approach. It is noted that the last column in Table 1 is the product of $S_{a,y}$ and R_{max} , which can be considered the spectral acceleration at collapse, $S_{a,collapse}$, predicted from PA results.

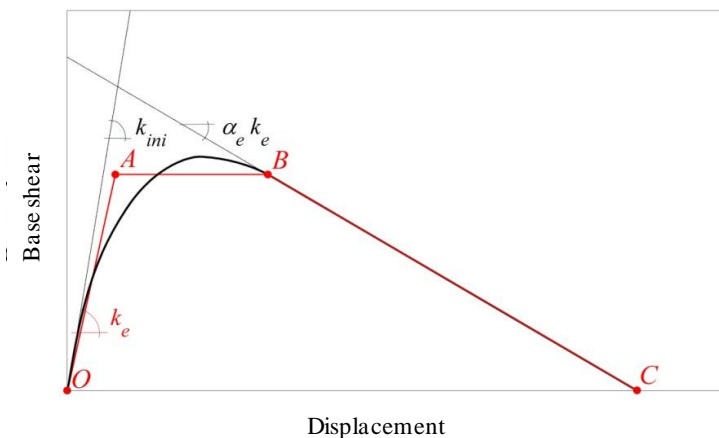


Figure 6.33 Implemented procedure for equivalent linearization.

Results of PAs are presented also in terms of normalised response curves, where the base shear force is divided by the effective structure weight and the column top displacement is divided by the corresponding height on foundations. This normalisation allows comparing the response characteristics of different structures when they are in their stable range of behaviour, i.e. before entering a strength-degrading branch due to P-Delta effect (in fact, the normalization produces equal strength degradation branches for all the curves).

Figure (6.34) shows normalized pushover curves which were selected from the ensemble obtained by moving the control node. They are the PA curves characterized by the larger values of the parameter R_{max} .

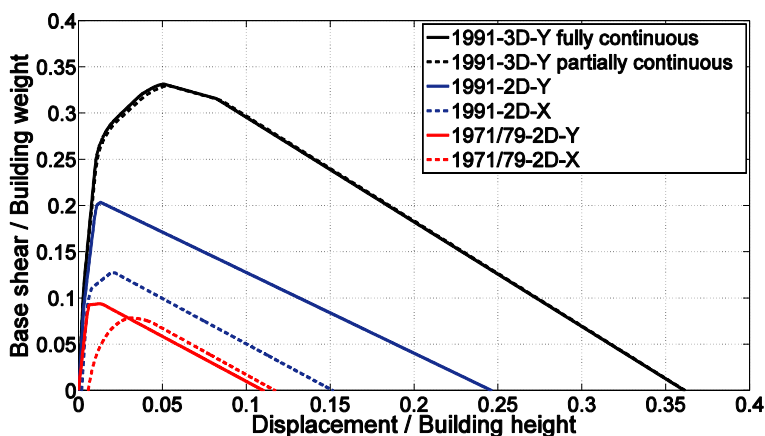


Figure 6.34 Normalised pushover curves for the considered structural models.

Based on the PA results shown in Figure (6.34) and Table (6.1), the following conclusions can be drawn:

- Due to the smaller normalized initial stiffness and strength (Fig. 6.34), the 1971/79 building is expected to exhibit larger displacement demand than the 1991 portion, while the building response remains stable in the plastic range. At large displacement demand, P-Delta effects take a significant role, and they have a more pronounced influence on the 1971/79 building than on the 1991 building (because of the larger α_e). However, the structural model 1971/79-2D-Y also shows ductility before strength degradation (Δ_d/Δ_y) larger than the corresponding 1991-2D-Y model. Consequently, values of R_{max} for the 1971/79-2D-Y and 1991-2D-Y structures are close each other, while the R_{max} for the 1971/79-2D-X frame is much smaller than the value obtained for the 1971/79-2D-X frame. Values of $S_{a,collapse}$ reported in the last column of Table 1 clearly shows the larger vulnerability of the 1971/79 structures to global collapse than the 1991 structures.
- Considering the two different directions of a given portion of the building, the direction X appears to be the most dangerous for both buildings, because of the larger period of vibration and smaller $S_{a,y}$ and R_{max} .
- Comparing the Y-direction response of the 3D and 2D models of the 1991 building shows that the models are characterized by (approximately) the same period of vibration (Tab. 6.1), while the (normalized) strength of the 3D model is larger than the corresponding value for the 2D frame. This difference is basically due to the perimeter frame on the west side (Fig. 6.2) which is stiffer than internal frames originating plastic redistribution and consequent apparent hardening in the PA curve. Table 1 shows that the value of R_{max} for the 3D models is independent of the modelling option for roof joints, while it is largely smaller than the value obtained from the 2D analysis. Consequently, the 3D model is expected to exhibit a better response from the point of view of global sidesway collapse based on PA results, as confirmed by the values of $S_{a,collapse}$ shown in the last column of Table (6.1).

6.5. Analysis methodology

As discussed in Chapter 2, seismic risk assessment can be performed referring to a given number of pre-defined structural performance objectives. The performance objectives considered in this thesis are the three limit states frequently adopted within the PBEE framework (Cornell and Krawinkler, 2000), namely, immediate occupancy (IO), life safety (LS) and collapse prevention (CP) (FEMA, 2000). These performance

objectives are identified in this study by taking into account the uncertainty in ground motion, while structural capacity is assumed to be deterministic (Petruzzelli *et al.*, 2012b). For any given limit state, the annual probability of failure (P_f), that is the probability of being in or exceeding a given limit state, is computed as follows (see Section 2.2):

$$P_f \approx \int_x P[\text{failure} | x] \cdot |d\lambda(x)| \quad (6.16)$$

where IM denotes the chosen ground motion intensity measure and $P[\text{failure}/x]$ is the fragility, i.e. the annual probability that the demand exceeds the capacity at the considered limit state, for a given level of the intensity measure $IM = x$. In the analysis of the case study, as already stated, the spectral acceleration at the first period of vibration and 5% damping ratio, $S_d(T_1)$, is used as intensity measure. Such an approach, based on a scalar measure of seismic intensity, is fully justified in case of a SDOF structure, which is an acceptable approximation to the case studies from the point of view of global response (see Sect. 6.4.1). The $|d\lambda(x)|$ term in Eq. (6.16) is obtained from a probabilistic seismic hazard analysis for the site of interest. In the case study, $|d\lambda(x)|$ is obtained from a hazard curve computed *ad-hoc* for the specific geological conditions at the site of the facility. In fact, although the Italian Seismic Code (CS.LL.PP., 2008) provides seismic hazard for a dense grid covering the country (see Sect. 4.5), such information is only available for site class A (rock), which does not correspond to the local geological condition of the facility. The same source model considered to develop the official Italian seismic hazard was employed. The procedure and data are the same as in Iervolino *et al.* (2011), where details may be found regarding GMPE employed and seismogenic sources' parameters.

The uncertainty in the seismic demand (record to record variability) was propagated by means of non-linear RHAs performed on real acceleration records, selected on the basis of a procedure reflecting the hazard at the site.

In fact, a deaggregation of the seismic hazard has been performed, at different return period of the seismic action, in order to individuate the Magnitude and focal distance mostly contributing to the seismic hazard at the site. Then, in order to assure the coherency between the records to employ in RHAs and the hazard at the site, different sets of real ground motion records were selected from the European Strong-motion Database (ESD) and the Italian Accelerometric Archive (ITACA), having magnitude and focal distance from the site in the range of values obtained by the deaggregation procedure. For the purposes of the analysis each record of each set is scaled in order that the elastic spectral acceleration at the fundamental period of vibration is equal to the target intensity level.

The computation of the structural fragility ($P[\text{failure}/x]$ in Eq. 6.16), is performed on the basis of a Probabilistic Seismic Demand Analysis (PSDA), performed assuming as EDP either a displacement or force quantity. Peak transient roof drift ratios, residual drifts as well as peak positive and negative force demand to members and connections are considered as EDPs. Regardless of the EDP being used, non-linear structural response can be affected by dynamic instability at large demand levels. This dynamic phenomenon needs to be properly considered in a probabilistic framework.

These issues will be addressed in the following subsections, starting from the analysis of the seismic response in terms of peak transient drift. Subsequently, the inclusion of residual drift in the assessment of the failure probability is presented. Finally, the assessment of local demands to roof members and local failure probabilities is addressed.

6.5.1. Assessment in terms of peak transient drift

Alternative non-linear dynamic analysis procedures, using real ground motions records, can be used to make a probability-based seismic assessments. They can be carried out both on the full range of ground motion intensity measures of interest and also for a limited range of IM levels. In fact, according to the classification made in Jalayer (2003), to which the reader should refer for a detailed description of the non-linear demand estimation approaches, these methods can be classified into *narrow-range* and *wide-range*, based on the range of IM and EDP values for which they provide demand estimations.

Among the wide range methods “multi-stripe analysis” (MSA) and “incremental dynamic Analysis” (IDA) (Vamvatsikos and Cornell, 2002) can be performed.

The first is a procedure according to which structural analyses are performed for a set of record, or different sets of records, scaled to a given level of IM. The output of a typical MSA analysis is shown in Figure (6.45a). At each IM level, the conditional probability distribution of EDP, given IM can be computed.

Incremental Dynamic Analysis is, in essence, the re-compilation of the results of multiple-stripe analysis into a collection of random entities known as the IDA curves (Jalayer, 2003). According to this procedure, each ground motion record of the considered set is scaled to multiple IM levels and the resulting EDPs are calculated. The IDA curve connects the resulting EDPs corresponding to each ground motion record, as shown in Fig. (6.45b). A strict relationship exists between the mean IDA curve (from a set of records) and the pushover curve; that is why it is also known as *dynamic pushover analysis*.

Wide range methods provide the best way for a probabilistic assessment at different performance levels but they require, in general, a significant computational effort. In

order to reduce this effort, single-stripe (SSA) (Figure 6.45c) and double-stripe (DSA) analyses were defined in literature and applied to case-studies (e.g. Cordova *et al.*, 2000; Jalayer *et al.*, 2009) providing an assessment for a single limit state. Among the narrow-range methods it is also to be mentioned the “Cloud” analysis, a procedure in which the structure is subjected to a set of ground motion records with different IM values, without any scaling procedure. The name of the method reflects the typical output of the analysis, reported in Figure (6.45d). In order to treat the output of a cloud analysis, a statistical model for the EDP has to be defined. In most cases a lognormal model of EDP is considered, by means of a conventional linear regression (using least squares), applied to the “cloud” response in the natural logarithmic scale (Cornell, 1996). Even if the range of IM investigated by means of a Cloud analysis could be wide, a probabilistic model, fitting the EDP response in a wide range of IMs is, in general, unfeasible. This is the reason why this method is used, in general, for the definition of structural response for a given IM level and it is defined as a narrow-range method.

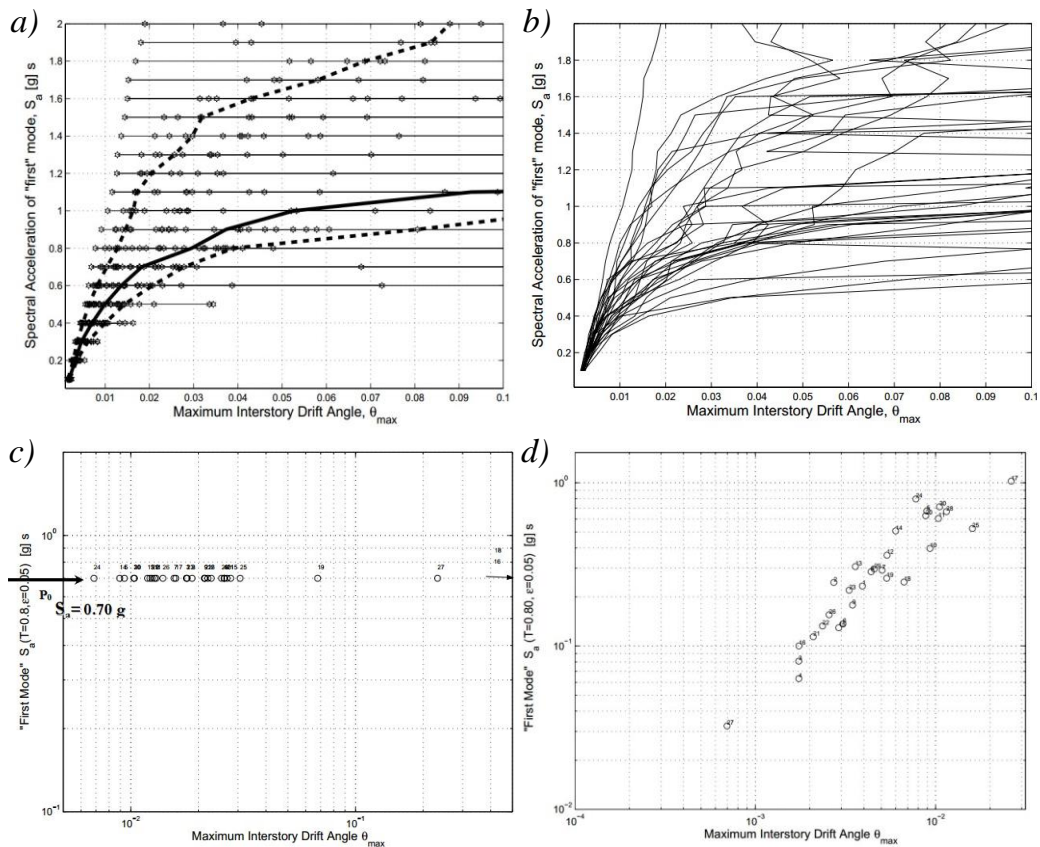


Figure 6.35 Typical output of non-linear dynamic analyses: (a)MSA analysis; (b) IDA analysis; (c) SSA analysis; (d) Cloud analysis. (Jalayer, 2003).

As mentioned in the previous section, the case study building is analysed at different performance levels by means of RHAs performed on different sets of records, selected on the basis of a deaggregation analysis of the hazard at the site.

Therefore, a wide-range MSA is performed for each structural model presented in Section (6.4).

At high values of the chosen IM, the output of a RHA could be not credible or, in effect, unavailable. This may occur when the EDP resulting from the analysis exceeds a threshold of validity of the mechanical model, or when the numerical non-convergence of the solution algorithm employed in the analysis is observed.

In the following, it is assumed that both the situations can signal the overall lack of stability of the structure, i.e. no distinction is made between the so-called *dynamic instability* and *numerical instability*. These cases of extreme dynamic displacement response will be referred to as “collapse cases”. Anyway, it was already stated that global sidesway collapse is only one of the possible collapse mechanisms that can affect existing buildings.

Two main issues are related to the onset of dynamic instability:

- the individuation of the output of an analysis as a collapse case, or, equivalently, the definition of the EDP value beyond which the analysis result is a collapse case;
- how to deal with collapse cases in probabilistic assessment of structural performance.

The first issue can be addressed in different ways, depending on the performed analysis. In case of IDA, global dynamic instability for each ground motion record can be individuated both according to an IM-based criterion and an EDP-based criterion (Vamvatsikos and Cornell, 2002) or as the point where the local slope of the IDA curve decreases to a certain percentage (e.g. the 20% of the initial stiffness in FEMA-350; FEMA, 2000) or, on the limit, the point where an IDA curve becomes horizontal.

In case of MSAs, the definition of the EDP value beyond which the analysis result has to be considered as a collapse case is needed. A generally employed limit of validity of structural models is a transient drift equal to $\delta_U = 10\%$.

Regarding the dealing with collapse cases in a probabilistic framework (second point of the previous list), one possible approach is the one proposed by Shome and Cornell (2000), according to which the collapse cases are included as separate contributions for calculating failure probabilities, by means of the following equation:

$$P[\text{failure} | x] = P[\text{failure} | x, NC] \cdot P[NC | x] + P[\text{failure} | x, C] \cdot (1 - P[NC | x]) \quad (6.17)$$

According to the previous equation, the $P[failure/x]$, i.e. the conditional probability of failure given the intensity measure $IM=x$, is decomposed in two contributions: the first contribution is due to non-collapse (NC) cases; the second contribution is due to the collapse (C) cases.

The conditional probability of failure, given that collapse has occurred and that the intensity measure $IM = x$, $P[failure/x, C]$, is equal to one, whichever the limit state and the IM are. The $P[failure/x, NC]$ can be expressed by a lognormal distribution function. According to these hypotheses and assuming the peak transient drift (δ_p) as EDP, Equation (6.19) can be re-written as follows:

$$P[failure | x] = \Phi_{\delta_p | IM=x, NC}^{Comp} \left(\frac{\ln(\delta_{p,f} / \delta_p)}{\sigma_{\ln(\delta_p)}} \right) \cdot P[NC | x] + (1 - P[NC | x]) \quad (6.18)$$

where $\Phi_{\delta_p | IM=x, NC}^{Comp}$, providing the probability of conventional failure given that no global collapse occurred due to dynamic instability, is the standard complementary cumulative normal distribution, δ_p is the median of peak drift demands, $\sigma_{\ln(\delta_p)}$ is the standard deviation of the logarithms, and $\delta_{p,f}$ is the peak drift limit to conventional failure. $P[C/x] = (1 - P[NC/x])$ and $P[NC/x]$ are computed as the number of collapse and non-collapse cases, respectively, over the total number of records (i.e., thirty in the specific case study) at each IM level. However, it should be noted that the lognormal model (defined for any δ value) may be not perfectly appropriate as, factually, it should not apply for values $\delta_p > \delta_U$ (recall that these data were not used to determine the parameters of the lognormal distribution). In fact, a truncated model (if data support such a choice) should be used, meaning that the lognormal term at the right hand side of Equation (6.21) should be divided by one minus the exceedance probability of δ_U it provides.

Fragility curves for all the considered structural models were computed according to the procedure outlined in Eq. (6.21), as it was checked that the truncation does not lead to significantly different results. Alternatively, maximum likelihood estimates of the distribution parameters, according to a censored data sample, may also be used.

Figure (6.48) summarizes what stated above: grey dots represent the result of individual RHAs; the vertical dashed lines represent the peak drift limitation for the considered structural performances ($\delta_{p,IO}$, $\delta_{p,LS}$, $\delta_{p,CP}$ for the IO, LS, CP limit state, respectively) and the one used for the individuation of collapse cases (δ_U). The latter limitation divides the range of EDPs in two regions: a non-collapse one ($\delta < \delta_U$) and a collapse one ($\delta > \delta_U$). The black solid line and the dash-dotted lines represent,

respectively, the median and the median plus and minus a standard deviation of non-collapse cases, obtained assuming a lognormal distribution. It can be observed that, at increasing levels of the IM, the median curve tends to become vertical, as a consequence of the increasing number of records for which global collapse is observed. At the same time, the standard deviation of the non-collapse cases distribution could reduce at increasing IM levels, nevertheless the fitted probabilistic model becomes less reliable, as a consequence of the reduction in the number of non-collapse cases. This aspect is, anyway compensated by the $P[NC/x]$ term of Eq. (6.21) which reduces the contribution of non-collapse cases to $P[failure/x]$, at high IM levels.

In Figure (6.36) the lognormal complementary cumulative distribution function (CCDF) of non-collapse cases is represented in red, for a given IM level (e.g. $Sa(T1)=1.6 g$). The solid red line is the one obtained if the abovementioned truncation of the lognormal distribution of non-collapse cases is made in the region of $\delta_p < \delta_U$; the dashed line is the one obtained according to a non-truncated model. As it can be observed from the Figure, the two assumptions produces negligible differences. The shaded area in Figure (6.36) represents the probability that the demand exceeds the capacity at the CP limit state, given that no collapse occurred, that is the $\Phi_{\delta|IM=x,NC}^{Comp}$ term of Eq. (6.21), computed assuming $\delta_{p,f} = \delta_{CP}$.

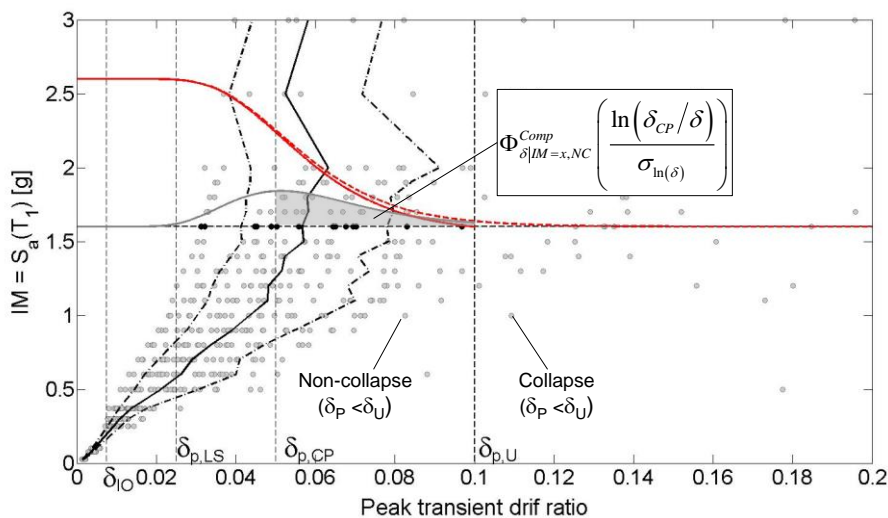


Figure 6.36 Result of MSA analysis and computation of $P[failure|x,NC]$.

Finally, it is to mention that an alternate option for computing fragility curves (i.e. $P[failure/x]$), employed in Jalayer *et al.* (2007), is based on the assumption that:

$$P[failure|x] = P[IM^{failure} \leq x] \tag{6.19}$$

where $IM^{failure}$ is the IM value in correspondence to which Capacity equals the Demand (i.e. conventional failure occurs). Assuming that $IM^{failure}$ is a random variable distributed according to a given model (the authors assume a log-normal one), the fragility curve can be computed from the corresponding CDF. This approach has the advantage to be insensitive to the occurrence of large demands due to non-converged analysis. Notwithstanding, for the case-study, the adoption of such an approach might have made necessary to adopt high IM scale factors in order to force all records to intersect the vertical line individuating the capacity. Moreover, fragility curves obtained according to this approach are essentially equivalent to those obtained by fitting probability distribution of EDP at any given level of IM (Jalayer *et al.*, 2007), therefore Eq. (6.21) was used in the analysis of the case study.

6.5.2. Assessment in terms of peak transient and residual drift

Residual (or permanent) deformations play an important role in defining the performance of a structure and can have significant economic consequences. In fact, assessing the residual deformations of structures, in the event of a major earthquake, is a fundamental step in the definition of the technical feasibility and of the cost effectiveness of strengthening solutions.

First indications about the residual deformation of SDOF systems were given by Mahin and Bertero (1981). Years later, MacRae and Kawashima (1997) enlightened the role of the post yielding stiffness ratio in influencing the amplitude of residual deformations. These observations were later confirmed by Borzi *et al.* (2001). Pampanin *et al.* (2002) demonstrated that the residual deformations and their dispersion strongly depend on the seismic intensity, hysteretic behaviour and post yielding stiffness ratio.

Regarding MDOF systems, few studies exist addressing residual deformations, such as those by Gupta and Krawinkler (1999); Pampanin *et al.* (2003 and 2006); Medina and Krawinkler (2003). In the last study four structures with different floor number were analysed by means of RHAs and increasing dispersion of residual drifts was observed for increasing seismic intensities.

Extensive numerical analyses were carried out by Garcia and Miranda (2005) to propose an empirical relationship to evaluate the ratios of residual displacement demand to the peak elastic displacement demand for SDOF systems. Moreover, it was observed by the authors that residual displacement ratios exhibit larger levels of record-to-record variability when compared to peak inelastic displacements.

Uma *et al.* (2006), on the basis of the work by Pampanin *et al.* (2002) proposed the adoption of performance objectives for the design analogous to the performance design

objective matrix by Vision 2000 (SAOC, 1995), but in terms of both peak and residual deformations.

More recently, Uma *et al.* (2010) proposed the use of a bivariate lognormal probability density functions of peak transient and residual drift in order to characterize the joint occurrence of residual and maximum deformations within a chosen performance domain. This leads to the definition of fragility curves representing the probabilities of achieving or exceeding different maximum-residual performance levels.

In this thesis an approach analogous to the one by Uma *et al.* (2010) was performed for the definition of fragility curves (presented in Section 6.6.3.2) accounting for the joint distribution of both the peak transient drift (δ_p) and the residual drift (δ_r). Moreover, the possibility of considering two different joint distribution of the abovementioned EDPs, that is a non-truncated one and a truncated one, was explored and described in the following. At each IM level, the result of a RHA can be expressed by the bin (δ_p, δ_r) that has to respect the following conditions: (1) the residual drift cannot assume values greater than the peak drift; (2) until the system behaviour remains elastic, the residual drift must be equal to the drift due to gravitational loads. Therefore, as illustrated in Figure (6.37), at a given IM level, the possible values of (δ_p, δ_r) bins can lie, until the system behaves elastically, on the line $\delta_r = \delta_G$ and, after the onset of plastic deformations ($\delta_p \geq \delta_l$), in the shaded area, the boundary of which is the $\delta_p = \delta_r$ line. In the case study, δ_l is assumed as the drift corresponding to the yielding of the first plastic hinge, for each structural model (Della Corte *et al.*, 2013).

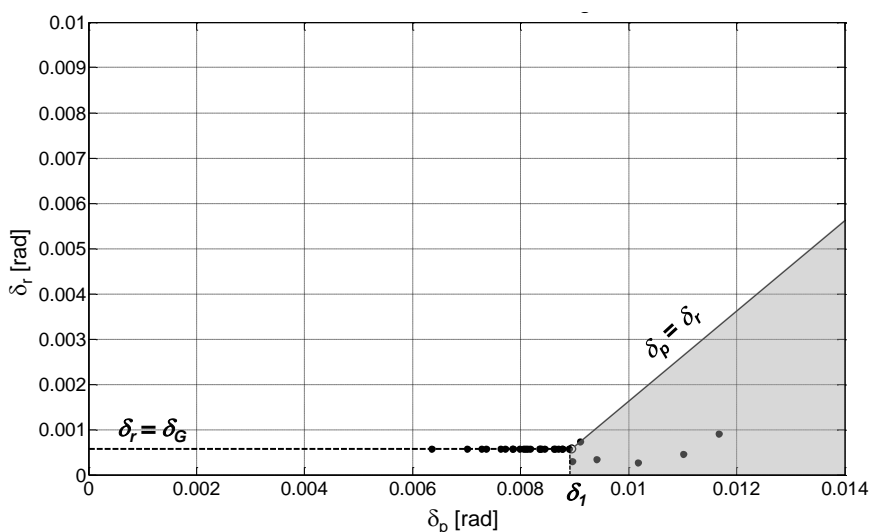


Figure 6.37 Peak transient (δ_p) - residual drift (δ_r) values at $S_d(T_1)=0.2 g$ for the *fully restrained* 1991-3D-Y model. δ_G is the drift due to gravitational loads; δ_l is the drift corresponding to the yielding of the first plastic hinge of the model.

It should be noted that, in order to account for global dynamic instability (dealt in the previous Section), a limitation of both peak transient and residual drift has to be considered. In the case-study it was adopted, for residual drift, a superior limit equal to the peak one, therefore the shaded area of Figure (6.37) extends up to 0.10 rad both for δ_p and δ_r .

EDPs values at increasing levels of the IM are represented in Figure (6.38), for the *fully restrained* 1991-3D model, in the range of non-collapse cases (δ_p and δ_r minor than 0.10 rad).

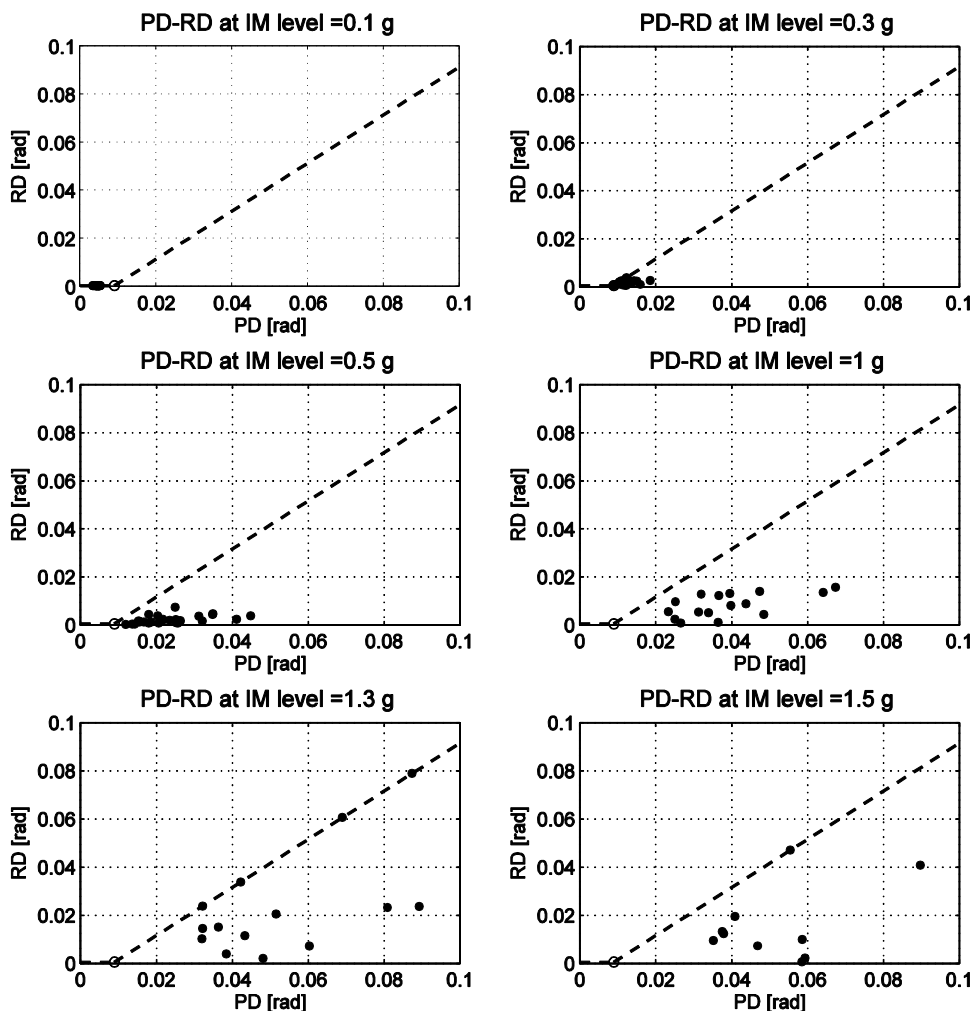


Figure 6.38 Peak transient-residual drifts at given IM levels for the *fully continuous* 1991-3D model, analysed in direction Y . Each point refers to the output of a RHA for which no dynamic instability occurs.

It can be observed from Figure (6.38) that, at low intensity levels, the EDPs are fully distributed along the $\delta_p = \delta_R$ line; conversely, at higher intensity levels, the residual drift can assume values different from δ_G . It can be also noted that at high levels of intensity the number of represented (δ_p, δ_r) bins tends to decrease, due to the onset of dynamic instability.

These cases are treated according to Eq. (6.17). In fact, the $P[NC/x]$ term of Eq. (6.17) is computed as the number of cases for which the peak transient drift exceeds $\delta_U = 0.10$ rad over the total number of RHA performed at the considered IM level. A bivariate distribution of the EDPs can be assumed for computing the $P[failure/x, NC]$.

The possibility of employing two kinds of joint probability distributions of the EDPs was investigated: (i) a non-truncated lognormal bivariate distribution, similar to the one by Uma *et al.* (2010), which does not account for the limitation of the possible values of (δ_p, δ_r) bins illustrated in Figure (6.37); (ii) a truncated one, which, conversely, takes into account it.

Therefore, according to a non-truncated model, the non-collapse cases are used for fitting a bivariate distribution of peak transient and residual drifts which extends without any limitation about possible values of the two EDPs. Under this hypothesis, the $P[failure/x, NC]$ is given by the joint conditional probability of exceeding a given value of peak transient drift ($\delta_p = \delta_{p,f}$) and of residual drift ($\delta_r = \delta_{r,f}$), given IM. This can be expressed as follows:

$$\begin{aligned}
 P[failure | x, NC] &= P[\Delta_p > \delta_{p,f} \cup \Delta_R > \delta_{r,f} | x, NC] = \\
 &= 1 - \int_0^{\delta_{p,f}} \int_0^{\delta_{r,f}} f_{\Delta_p, \Delta_r}(\delta_p, \delta_r | x, NC) d\delta_p d\delta_r
 \end{aligned} \tag{6.20}$$

Eq. (6.20) represents the complementary cumulative distribution function (CCDF) of $f_{\Delta_p, \Delta_r}(\delta_p, \delta_r | IM)$, given the IM level. $f_{\Delta_p, \Delta_r}(\delta_p, \delta_r | IM)$ is the bivariate distribution of the EDPs. In the previous formulation, $\delta_{p,f}$ and $\delta_{r,f}$ are the (deterministic) drift limits associated to the conventional failure conditions, for peak transient and residual drift, respectively. In Figure (6.39) the lognormal bivariate distribution of peak transient drift and residual drifts $f_{\Delta_p, \Delta_r}(\delta_p, \delta_r | IM)$ is shown, for the *fully continuous* 1991-3D model and a given IM level (Fig. 6.39a). Black dots refer to the (δ_p, δ_r) bins (analysis result) and black dashed lines refer to capacity limits in terms of peak transient and residual drift ($\delta_{p,f}$ and $\delta_{r,f}$, respectively). In Figure (6.39b), the contour plot of the lognormal bivariate distribution is shown; grey marks refer to the realizations of the (δ_p, δ_r) used for computing the $P[failure/x, NC]$ through numerical simulation.

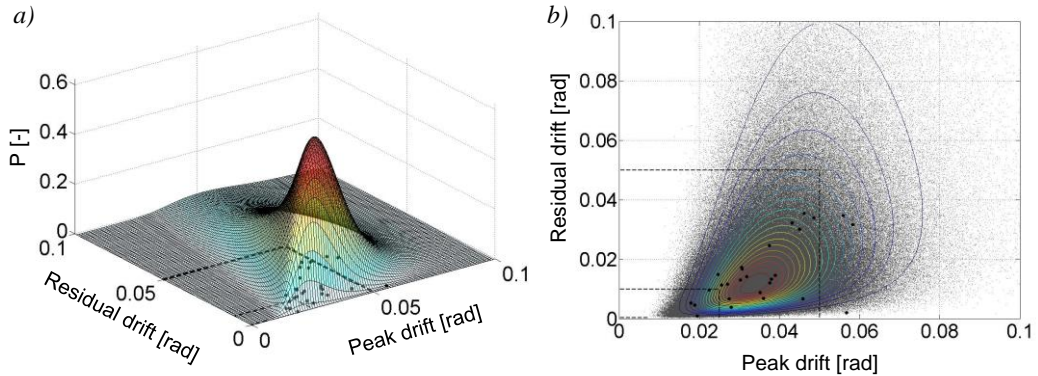


Figure 6.39 Joint lognormal probability density function of the EDPs, given the IM level, for non-collapse cases.

On the contrary, according to a truncated model, the non-collapse cases are used for fitting a lognormal bivariate distribution, the domain of which is truncated to the shaded area represented in Figure (4.37), extended up to a peak transient drift equal to 0.10 rad . Such a truncated bivariate function is normalized so that the volume under the curve is one. In Figure (6.49) the truncated and normalized bivariate distribution of the EDPs is shown for the same model and intensity level as the ones shown in Figure (6.39). The limits of the domain used for truncating the bivariate distribution of the EDPs, given that no global collapse occurred, are reported in red-dashed line in Figure (6.40).

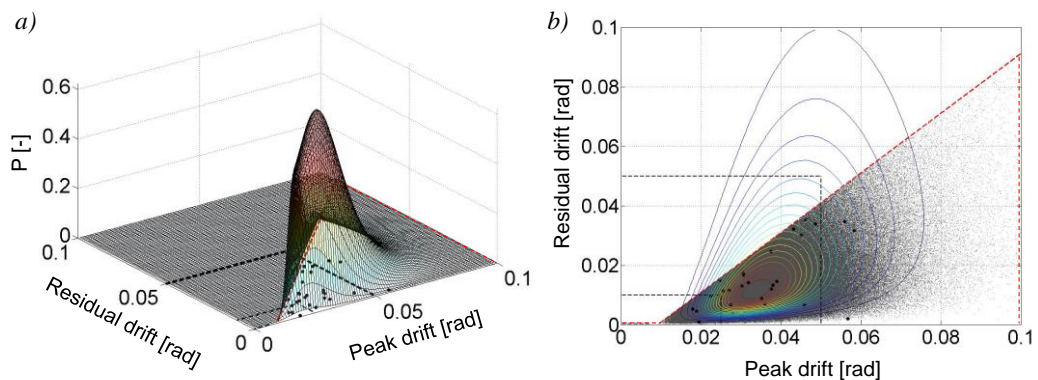


Figure 6.40 Truncated joint lognormal probability density function of the EDPs, given the IM level, for non-collapse cases.

In order to compute the $P[failure|x,NC]$ term of Eq. (6.17), i.e. the joint conditional probability of exceeding a given value of peak transient drift ($\delta_p = \delta_{p,f}$) and of residual drift ($\delta_r = \delta_{r,f}$), given an IM level, three possible cases can occur:

- at the investigated IM level the structure behaves elastically, i.e. $\delta_p < \delta_1$ and the (δ_p, δ_r) values lie on the line $\delta_r = \delta_G$. In this case, $P[failure|x,NC]$ is provided by the univariate CCDF distribution of the peak transient drift:

$$\begin{aligned} P[failure | x, NC, elastic] &= P[\Delta_p > \delta_{p,f} | x, NC, elastic] = \\ &= 1 - \int_0^{\delta_{p,f}} f_{\Delta_p}(\delta_p | x, NC, elastic) d\delta_p \end{aligned} \quad (6.21)$$

where $f_{\Delta_p}(\delta_p | IM)$ is the PDF of the peak transient drift.

- at the investigated IM level, the structure is in the range of plastic deformations, i.e. $\delta_p \geq \delta_1$ and all the (δ_p, δ_r) values lie in the shaded area of Figure (6.37). In this case:

$$\begin{aligned} P[failure | x, NC, plastic] &= \\ &= P[\Delta_p > \delta_{p,f} \cup \Delta_r > \delta_{r,f} | x, NC, plastic] = \\ &= 1 - \int_0^{\delta_{p,f}} \int_0^{\delta_{r,f}} \bar{f}_{\Delta_p, \Delta_r}(\delta_p, \delta_r | x, NC, plastic) d\delta_p d\delta_r \end{aligned} \quad (6.22)$$

Where $\bar{f}_{\Delta_p, \Delta_r}(\delta_p, \delta_r | x, NC, plastic)$ is the JPPDF of the peak transient and residual drift with a truncated domain (Figure 4.46) and a normalised volume;

- at the investigated IM level, the structure is in the transition zone between elastic and plastic deformations. This is the case depicted in Figure (6.37), in which (δ_p, δ_r) are distributed both on the line $\delta_r = \delta_G$ and in shaded area. In this case, representing a generalization of the previous two, the abovementioned probability can be computed as follows:

$$\begin{aligned} P[failure | x, NC] &= P[\Delta_p > \delta_{p,f} \cup \Delta_r > \delta_{r,f} | x, NC] = \\ &= P[\Delta_p > \delta_{p,f} | x, elastic] \cdot P_{elastic} + \\ &+ P[\Delta_p > \delta_{p,f} \cup \Delta_r > \delta_{r,f} | x, plastic] \cdot P_{plastic} \end{aligned} \quad (6.23)$$

where $P_{elastic}$ is the probability of observing elastic behaviour, that is the number of cases for which $\delta_p < \delta_1$ over the total and $P_{plastic}$ is equal to $(1 - P_{elastic})$, or the number of cases for which $\delta_p \geq \delta_1$, over the total. According to

what stated in Section (6.5.1) for the assessment in terms of peak transient drift, the $P[\Delta_p > \delta_{p,f} | x, elastic]$ term should be obtained normalizing the $f_{\Delta_p}(\delta_p | x, NC, elastic)$ function so that the area under the curve is equal to one. Anyway, such an approach is necessary only in a limited number of cases, since it regards only the IM levels in which the transition from an elastic behaviour to a plastic one occurs.

Results deriving from the application of the described approaches to the computation of fragility are reported in Section (6.6.3.3).

6.5.3. Assessment in terms of local force demands

As previously described, 2D models do not consider possible out-of-plane buckling and connection failures of roof elements. Therefore, from each RHA, the maximum and minimum force demands to roof elements are computed, in order to check whether the buckling or the connection capacity is exceeded. The results are processed in a way similar to the one discussed for sidesway collapse, that is a MSA is performed for each structural member, providing the peak force demand to the member at increasing intensity measure levels. The records determining global collapse in terms of drift (peak transient drift exceeding 0.10 rad) were excluded from the calculations shown in the following (see Section 6.6.2.2 and 6.6.3.4).

It is worth noting that considering failure of any roof member and/or connections may pose serious problems of roof collapse, due to the statically determined structural scheme and the potentially brittle nature of these phenomena. Moreover, if not properly accounted for, it could undermine the results obtained in terms of global structural behavior. The capacity to each member is computed, according to Eq. (6.24), as the minimum axial force considering the following failure modes:

- member Buckling $N_{R,c}$
- tension failure of the net cross section, $N_{R,yt}$
- bolt shear failure, $N_{R,bv}$
- bolt bearing failure, $N_{R,bf}$
- failure of gusset plates in tension, $N_{R,ct}$
- failure of gusset plates in compression, $N_{R,cc}$

$$N_{cap} = \min \{ N_{R,c}; N_{R,yt}; N_{R,bv}; N_{R,bf}; N_{R,ct}; N_{R,cc} \} \quad (6.24)$$

The probability of observing a local failure to each member, is obtained, in the frequentistic approach, as the ratio of the number of ground acceleration records inducing a demand larger than the capacity and the total number of records.

6.6. Analysis Results

6.6.1. Seismic Hazard and Record Selection

As stated in Section (6.5), hazard curves were developed for soft soil, which is considered a conservative proxy for soil site class B (CS.LL.PP., 2008), the actual site class of the facility (Iervolino *et al.*, 2011). In Figure (6.41) the seismic sources considered in the hazard analysis and the site (triangle) are shown (these are the same of the official Italian hazard map). In Figure (6.42) the resulting hazard curves in terms of exceedance probability in 1 year of the spectral acceleration at 1 s and 1.6 s (the fundamental periods of the structures of the workshop building, Table 6.1) are reported.

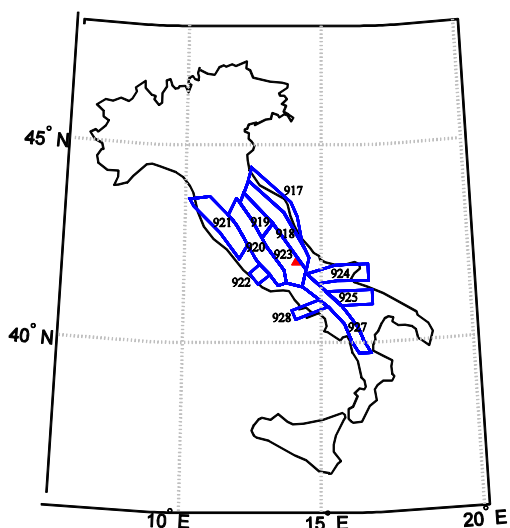


Figure 6.41 Seismic sources affecting the hazard at the site (courtesy of E. Chioccarelli).

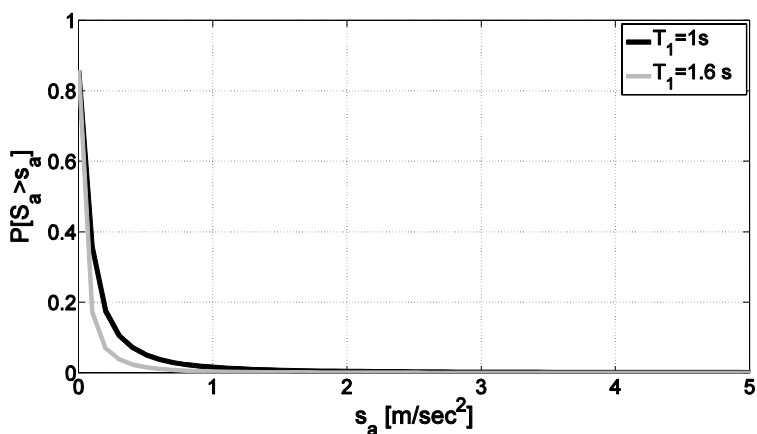


Figure 6.42 Exceedance probabilities for soft soil in 1 year, for the spectral acceleration at 1 s and 1.6 s.

To assure consistency between records and hazard at different intensity levels, four basic intervals of spectral acceleration corresponding to return periods of 50, 475, 975, 2475 years, were considered. At each level of intensity, deaggregation of seismic hazard has been preliminarily carried out. Deaggregation, in terms of Moment magnitude and focal distance, is shown in Figures from (6.43) to (6.46) for the reference return periods. Deaggregation has been obtained by using the same software of Iervolino *et al.* (2011), leading in all the analysed cases to a distribution with a single mode; i.e., one source zone dominates the hazard for the site.

Once the intervals of magnitude and distance contributing to the seismic hazard have been calculated for each intensity level, record selection was carried out searching, via the REXEL software (Iervolino *et al.*, 2010), for accelerograms recorded during earthquakes having magnitude and focal distance from the site in the range of values obtained by the deaggregation procedure. In Table (6.2) the magnitude (M) and distance (R) corresponding to each return period, the hazard for I_s spectral acceleration and the database in which REXEL has searched for records, are reported

Table 6.2 Selection criteria for records consistent with disaggregation of seismic hazard at the facility site. Different sets of records were considered at four different levels in which intensity has been divided.

T_R [yr]	$S_a(T_1=1s)$ [g]	R [km]	M	Database
50	0.10	0 – 20	5 – 6	ITACA
475	0.30	0 – 30	5.3 – 6.5	ITACA
975	0.37	5 – 25	6 – 7	ESD
2475	0.50	0 – 40	6 – 7.5	ESD

From Table (6.2), it can be seen that different magnitudes and distances characterize earthquakes producing different levels of spectral accelerations (second column of Table 6.2) associated to different return periods (first column of Table 6.2)

Sets of 30 records have been selected from the European Strong-motion Database (ESD) and the Italian ACcelerometric Archive (ITACA) for each pre-fixed level of intensity. In Figures from (6.47) to (6.50), the acceleration spectra of the set corresponding to different return periods are given. The fundamental records characteristics are also given for the return periods of interest in Appendix C.

In the range of spectral accelerations identified by two subsequent levels in Table (6.2), the acceleration records found for the lower bound level have been used, by scaling accelerations until the upper bound acceleration level of the range has been reached.

The structural models presented in Section (6.4) were analysed in a range of IM sufficiently wide to push the structure to collapse. Table (6.3) reports, for each structural model, the number of IM levels employed and range of IM investigated.

It may be worth noting that 2D-models were analysed for $S_a(T_1)$ between 0.025 and 3 g, with 24 levels of variation of $S_a(T_1)$. The smaller range of $S_a(T_1)$ in case of a 3D models was due to the larger computational efforts in comparison with the 2D models. In the case of *partially continuous* 1991-3D-Y model, the investigated range of $S_a(T_1)$ is narrower than the one employed for the *fully continuous* model. As it will be discussed in the following (Sect. 6.6.1), this limitation in the range of values of $S_a(T_1)$ is due to the differences in the failure mechanism of the two models.

Table 6.3 Summary of the performed analysis for each structural model.

Structural model	n_{levels}	$S_a(T_1)_{\text{min}}$ [g]	$S_a(T_1)_{\text{max}}$ [g]
1971/79-2D-X	24	0.025	3
1971/79-2D-Y	24	0.025	3
1991-2D-X	24	0.025	3
1991-2D-Y	24	0.025	3
1991-3D-Y “ <i>fully continuous</i> ”	20	0.025	1.8
1991-3D-Y “ <i>partially-continuous</i> ”	12	0.025	1

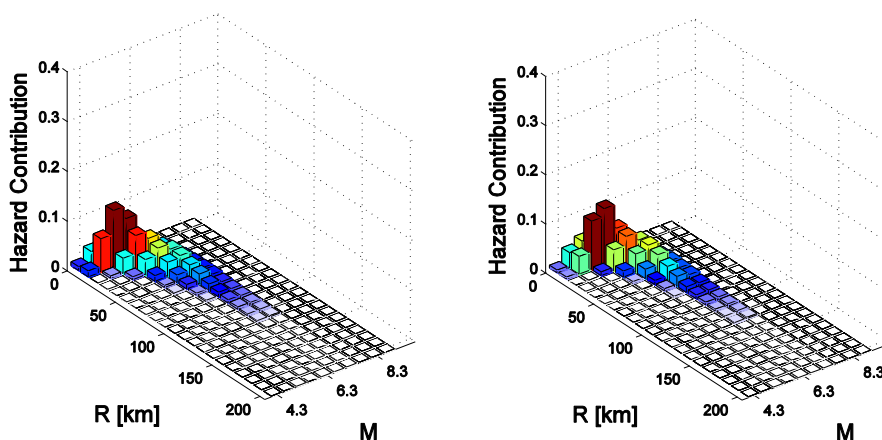


Figure 6.43 Seismic hazard deaggregation of $S_a(T)=1.0$ s (a) and 1.6 s (b) at the building site for 50 yrs return period.

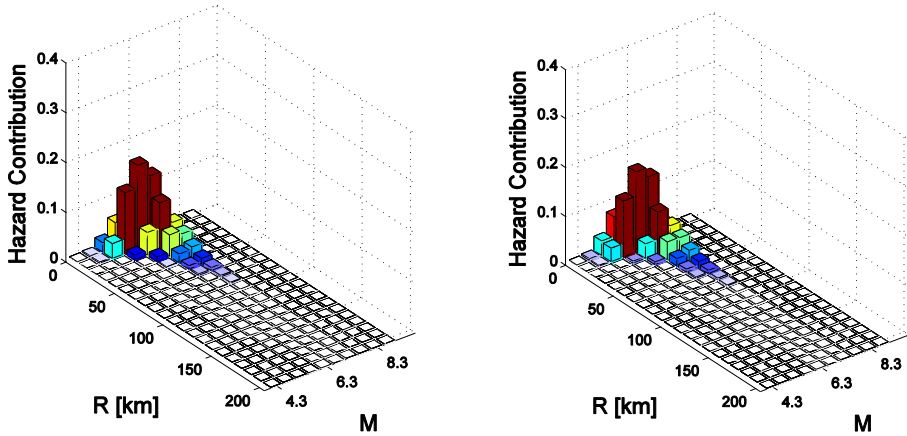


Figure 6.44 Seismic hazard deaggregation of $S_a(T)=1.0$ s (a) and 1.6 s (b) at the building site for 475 yrs return period.

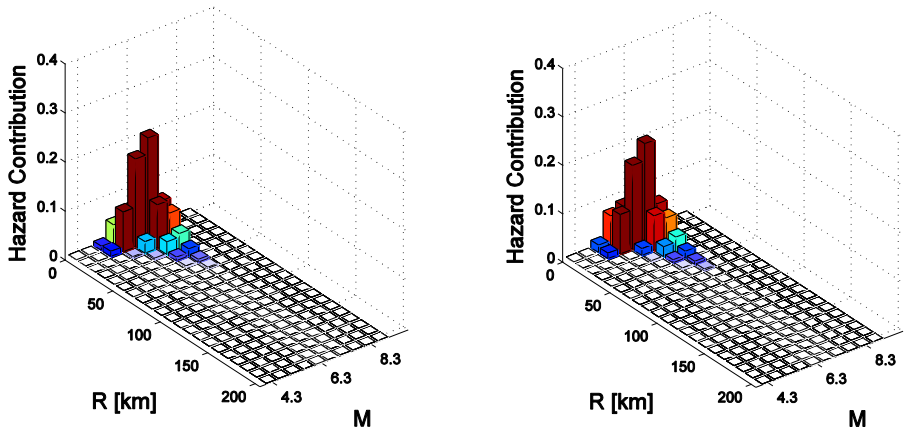


Figure 6.45 Seismic hazard deaggregation of $S_a(T)=1.0$ s (a) and 1.6 s (b) at the building site for 975 yrs return period.

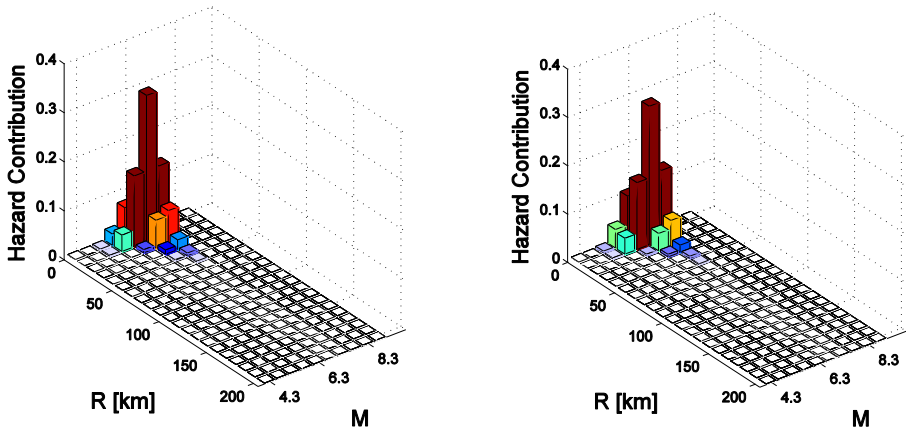


Figure 6.46 Seismic hazard deaggregation of $S_a(T)=1.0$ s (a) and 1.6 s (b) at the building site for 2475 yrs return period.

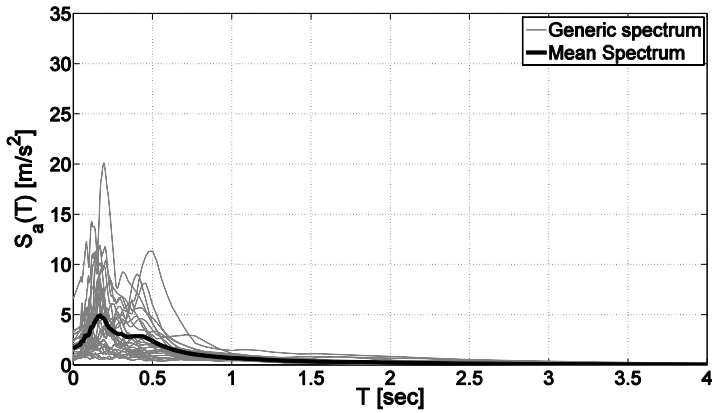


Figure 6.47 5% damped pseudo-acceleration response spectra of selected accelerograms for TR=50 years.

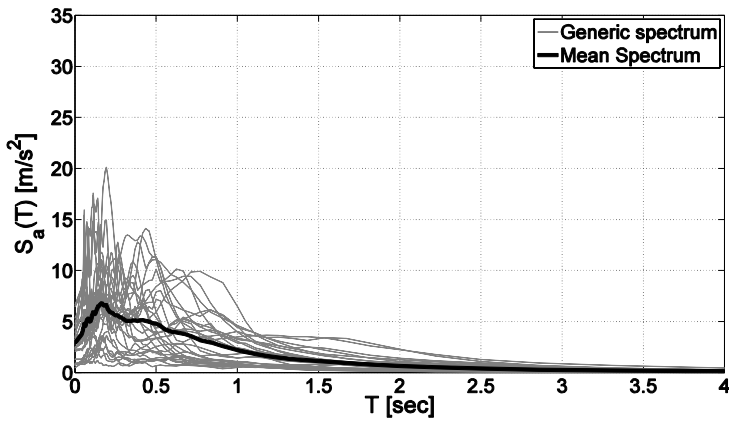


Figure 6.48 5% damped pseudo-acceleration response spectra of selected accelerograms for TR=475 years.

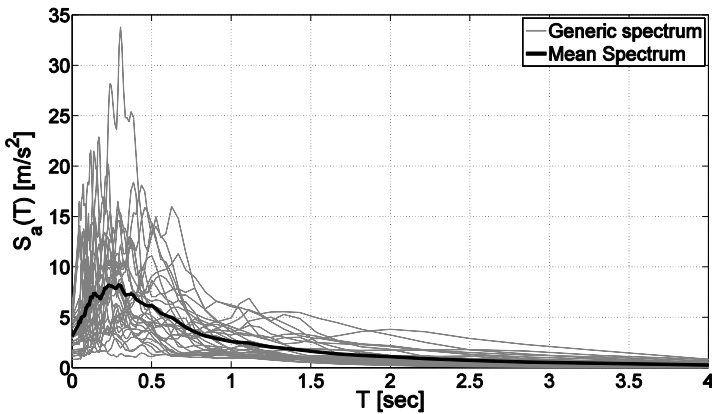


Figure 6.49 5% damped pseudo-acceleration response spectra of selected accelerograms for TR=975 years.

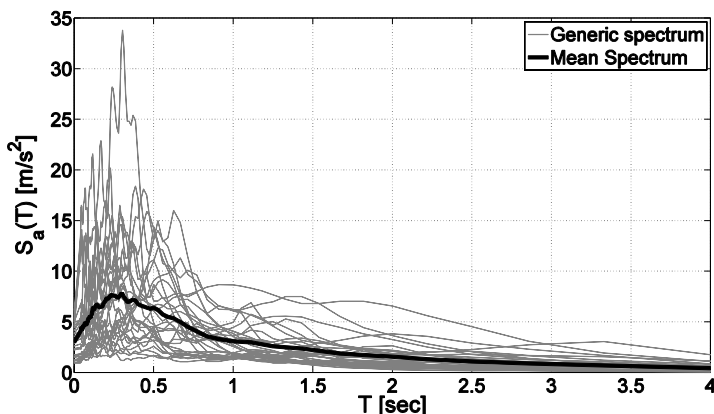


Figure 6.50 5% damped pseudo-acceleration response spectra of selected accelerograms for TR=2475 years.

6.6.2. Seismic demands

6.6.2.1. Peak transient and residual drift demands

Results of the RHAs are summarized hereafter by showing the relationships between the assumed IM (i.e., spectral acceleration at the fundamental period of each structure and 5% damping ratio) and the selected engineering demand parameters (EDPs). It is worth noting that the results shown hereinafter are valid under the assumption that no local failures occur. As mentioned, the possibility of observing the instability of the connection failure to roof elements will be checked after the analysis.

The chosen EDPs were peak transient and residual roof drift ratios. Dealing with structural models characterized by deformable roof structures, the drift assumed for the analysed models is the ratio of the maximum displacement among those at the top column end and the corresponding height on the ground. Figures from (6.51) to (6.56) shows results in terms of drift ratio demand to the four 2D structures for all the selected earthquake intensities and GMs. Both peak transient (full dots) and residual (empty dots) drift demands are shown. Counted median drift demands are also illustrated with solid line (transient) and dashed line (residual).

Horizontal dash-dotted lines are also reported in Figures (6.51) to (6.54), representing the spectral accelerations at collapse predicted from PA results and ATC guidelines (Table 6.1).

Figures (6.51) and (6.52) allow comparing the response of the 1971/79 frames, in the X and Y directions respectively. It is noted that the X -direction frame is characterized by an appreciable (non-zero) value of the drift under gravity loads (i.e. for $S_a(T_1)=0$). This is due to the asymmetry of the 2D frame, which is swaying laterally under gravity loading. It is also noted that at relatively small values of seismic intensity, the ratio of

median residual to peak transient demand to the X -direction frame (Fig. 6.51) is larger than it is for the Y -direction frame (Fig. 6.52). This is an aspect having an influence on the probability to exceed a given limit state expressed either in terms of residual drift or transient drift or in terms of both the quantities (see Section 6.6.4). Such RHA results are consistent with predictions made from PA results. In particular, the spectral accelerations at collapse predicted from PAs (Table 6.1) are very close to values based on median drift response from RHAs.

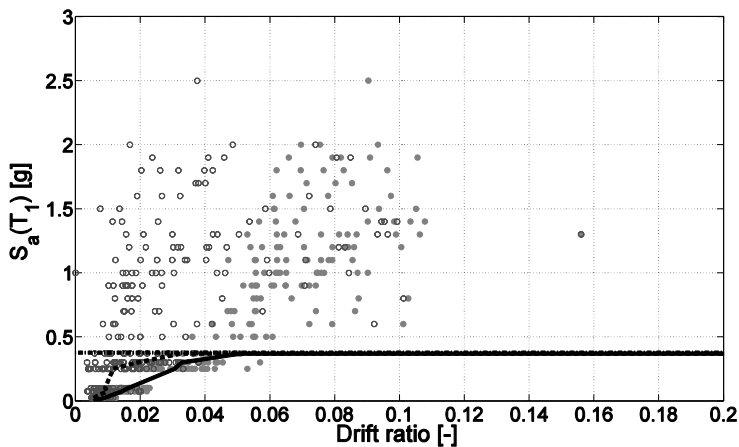


Figure 6.51 Peak transient and residual drift ratios for 1971/79-2D-X model.

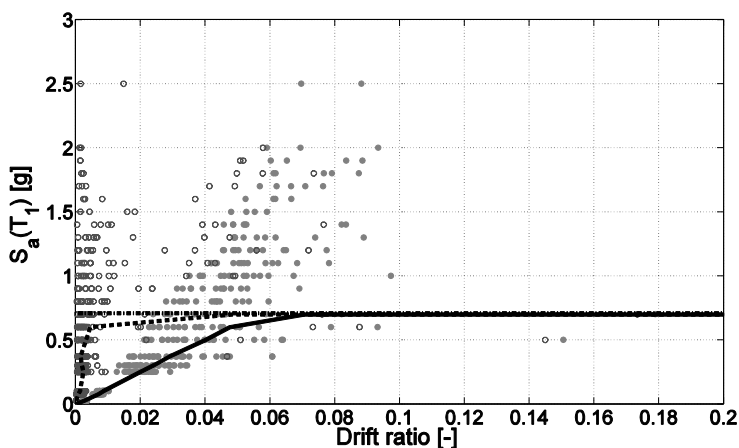


Figure 6.52 Peak transient and residual drift ratios for 1971/79-2D-Y model.

Figures (6.53) and (6.54) allow comparing the X and Y direction response of the 1991 building. Similarly to the 1971/79 frames, the ratio of residual to peak transient drift is larger for the X -direction than it is for the Y -direction frame, which is also consistent

with predictions from PA results. Differently from the 1971/79 frame, the X -direction frame is characterized by a small initial (gravity-induced) drift. This will have consequences on fragilities and probabilities of failure calculated considering both residual and transient drifts as discussed in the Section.(6.6.3) Also in this case the spectral accelerations at collapse predicted from PAs and ATC guidelines are in good agreement with the median drift response from RHAs.

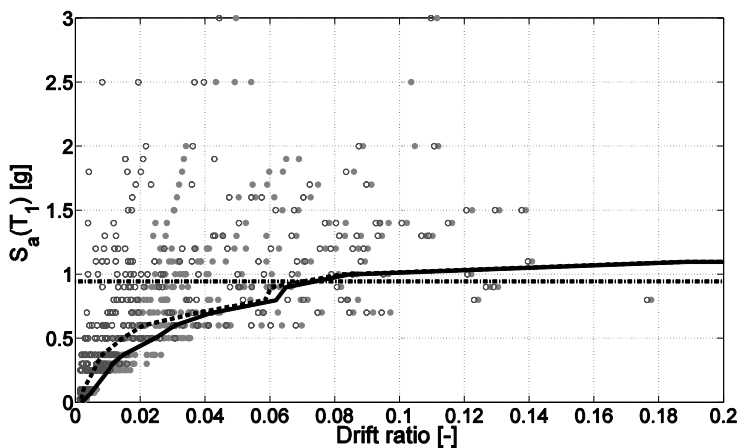


Figure 6.53 Peak transient and residual drift ratios for the 1991-2D-X model.

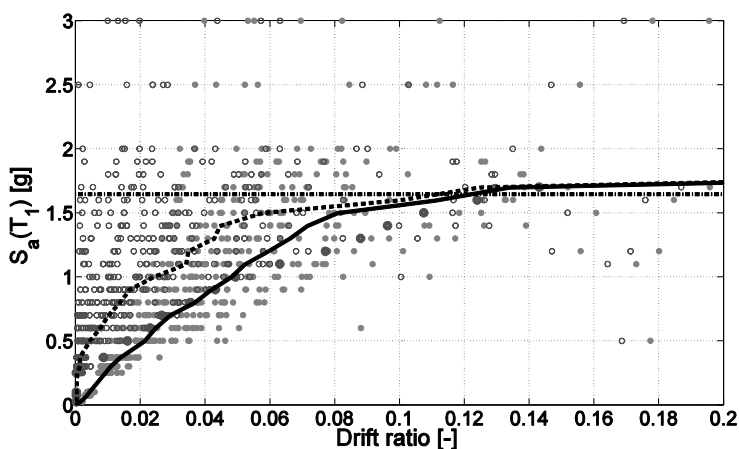


Figure 6.54 Peak transient and residual drift ratios for the 1991-2D-Y model.

Figures (6.55) and (6.56) report the drift ratio demands for 1991-3D-Y *fully continuous* model and *partially continuous* model, respectively. It can be observed that the assumption made about the different out-of-plane behaviour in the two models strongly influences their seismic response. Moreover, predictions of $S_{a,collapse}$ from PA results (Table 6.1) largely overestimate the collapse earthquake intensity, therefore they are

not represented in Figures (6.55) and (6.56). Such an inability of PA results to anticipate the dynamic response, as well as the large difference in response of the 1991-3D-Y models and 1991-2D-Y models, is discussed in the following.

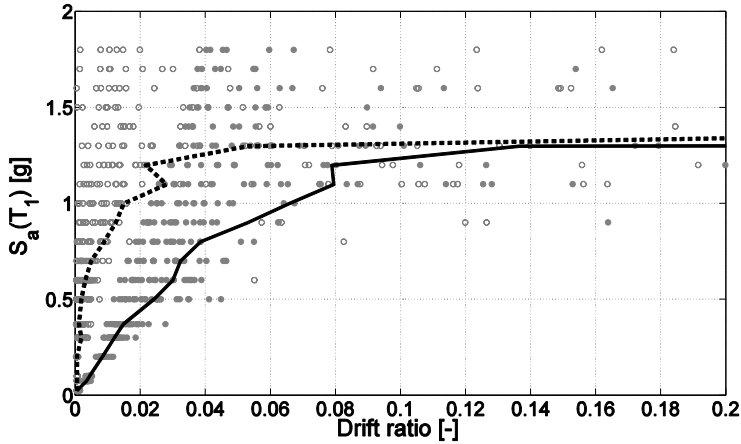


Figure 6.55 Peak transient and residual drift ratios for the *fully continuous* 1991-3D-Y model.

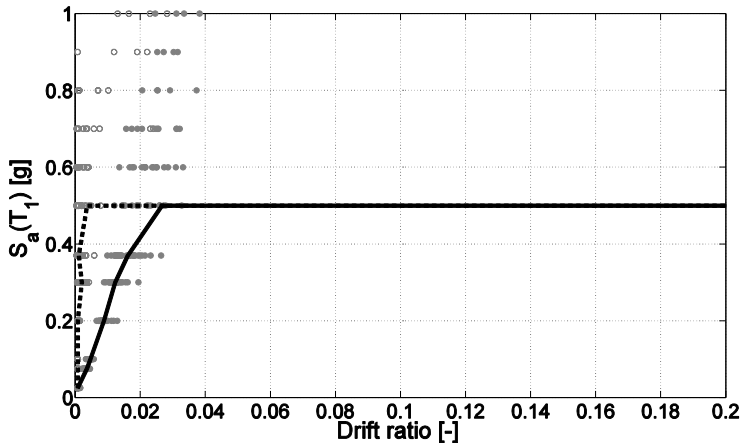


Figure 6.56 Peak transient and residual drift ratios for the *partially continuous* 1991-3D-Y model.

In order to compare the global performance predicted by the 3D models and 2D ones, in Figure (6.57), the median drift demands to the three-dimensional models and to the 1991-2D-Y frame are reported.

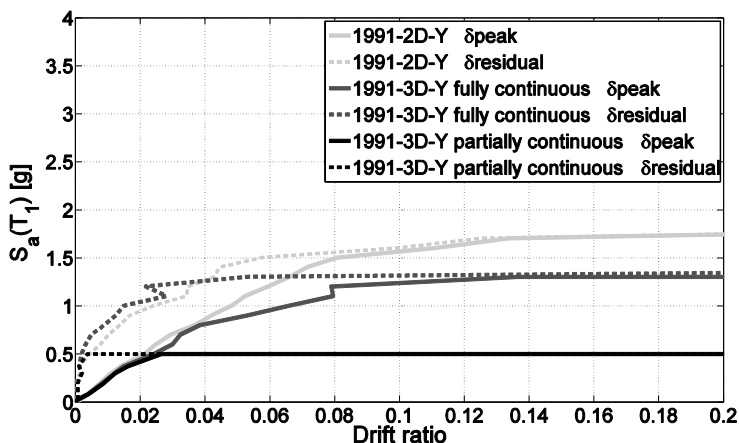


Figure 6.57 Peak transient and residual drifts ratio for the 1991-3D-Y models and the corresponding 1991-2D-Y frame.

For spectral accelerations up to about 0.5 g , all models show a similar median drift demand. At larger spectral accelerations the behaviour changes radically. In case of a 3D model, the number of GMs inducing global collapse increases much more rapidly than it does for a 2D model. Such a large difference in response is due to the activation of a different collapse mechanism.

Collapse of the 1991-2D-Y frame occurs with a column-sway mode (Fig. 6.58a). The same type of collapse mechanism is also exhibited by the X-direction 2D frames (Fig. 6.58b). The collapse mechanism of the 1991-3D-Y model is instead characterized by relatively complex three-dimensional instability of roof trusses (Fig. 6.59c), a mode of response which cannot be captured by 2D models. Similarly, PA is not able to highlight such a type of failure mode, because it is generally carried out with first-mode proportional loading vectors. The details of the collapse mode depend on the GM, because high-frequency modes of transverse vibration of planar trusses are activated depending on the GM frequency content. Clearly, the fully continuous 3D model leads to a better structural response than the partially continuous 3D model, because roof instability is delayed at larger levels of spectral acceleration by introducing continuity of the joint bending moments. Thus, the fully continuous 3D model approaches the response of the 2D model for which such roof instability is a priori excluded.

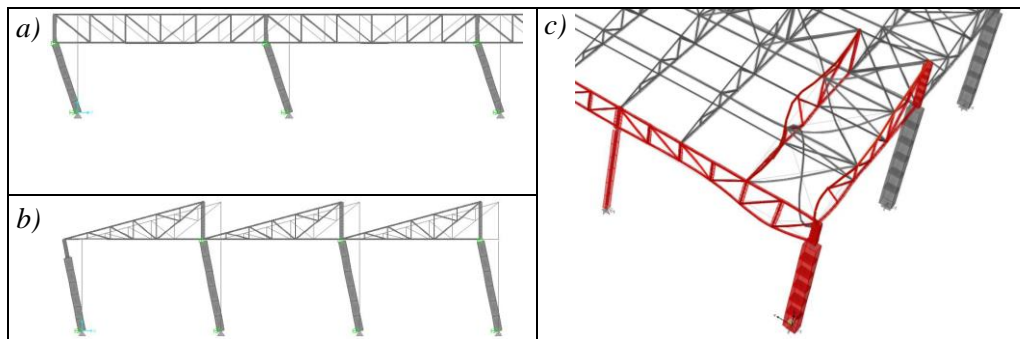


Figure 6.58 Collapse mechanisms: (a) 1991-2D-Y frame; (b) 1991-2D-X frame; (c) 1991-3D-Y model.

The results in Figures (6.57) and (6.58) suggest that a 3D model is mandatory to capture the possibility of (complex) out-of-plane truss buckling modes involving multiple roof members. Evaluating accurately such buckling modes and corresponding earthquake intensities is difficult, because they strongly depend on the degree of restraint exerted by all members connecting to a joint. The results from RHAs of the two alternative 3D models highlight the large variability of response with the type of roof truss model (Figs. 6.57).

A fully nonlinear analysis of the 3D structure, i.e. including nonlinearity of also roof elements as well as failure of end member connections, is the only rigorous approach allowing a realistic response to be traced. However, it has to be considered that such a 3D model would be extremely cumbersome and it cannot be considered affordable for a routine application of the probabilistic methodology. The partially continuous 3D model appears to be a reasonable compromise between accuracy (fidelity to reality) and tractability based on the following reasoning: (i) the in-plane roof behaviour is traditionally assessed assuming pinned joints because the truss behaviour is dominating and bending moments can be considered a secondary source of global strength and stiffness; (ii) using pinned joints for out-of-plane displacements, i.e. completely neglecting continuity of moments for out-of-plane joint displacements, may eventually lead to initially unstable structures, an excessively conservative modelling assumption. Figure (6.59) reports a comparison of the counted medians of all the analysed structural models, computed from peak transient drift response. It can be observed that the 1971/79 portion is characterized by lower spectral acceleration leading to the collapse, identified as the acceleration level at which the median curve becomes horizontal. Moreover, the *X*-direction results, both for 1991-2D and 1971/79-2D models, as the analysis direction characterized by the worst response in terms of spectral acceleration leading to collapse.

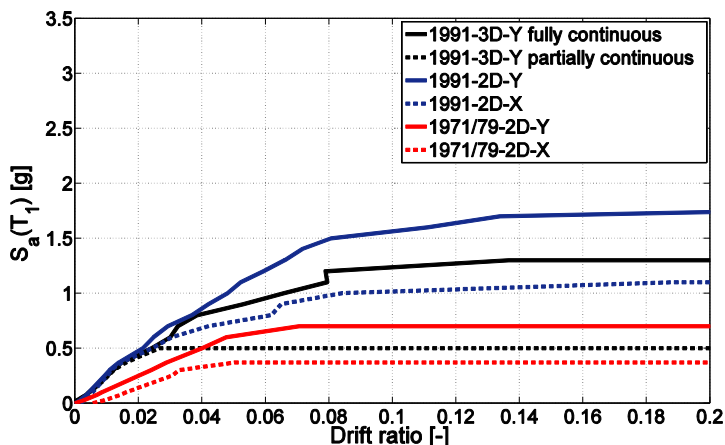


Figure 6.59 Counted median comparison for the analysed structural models.

Finally, for a better comprehension of the computation of fragility curves according to Eq. (6.18), in Figures from (6.60) to (6.65) the results of the performed MSA are reported in the range of non-collapse cases ($\delta < \delta_U$) for the considered models together with a bar-plot of the number of RHAs leading to collapse. In these figures, the black solid line and the black dashed line represent, respectively, the counted median of peak transient drift resulting from the analyses and the median of non-collapse cases, for which a lognormal distribution was assumed. The blue lines refer to the same entities, computed for residual drifts. In the same Figures, red dotted lines represent the drift capacity limitations assumed both for peak transient and residual drift.

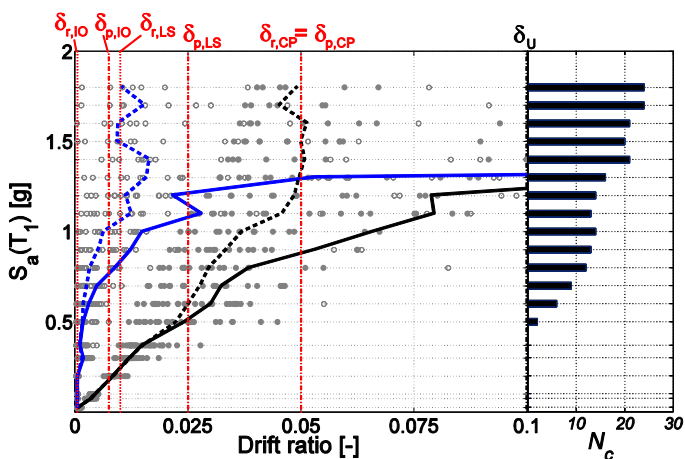


Figure 6.60 Results of MSA for *fully continuous* 1991-3D-Y model.

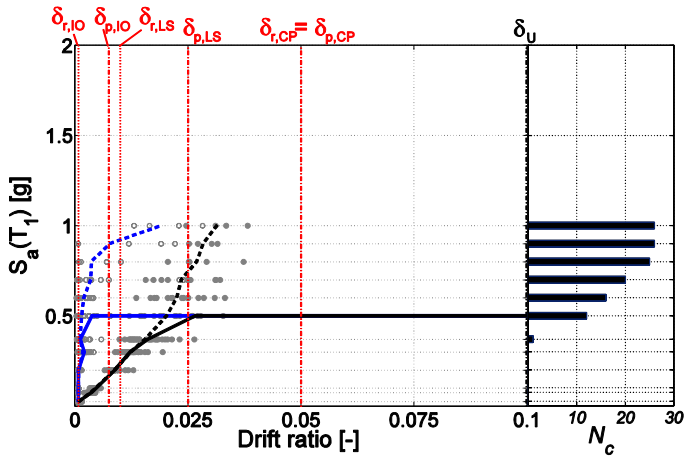


Figure 6.61 Results of MSA for *partially continuous* 3D-1991-Y model.

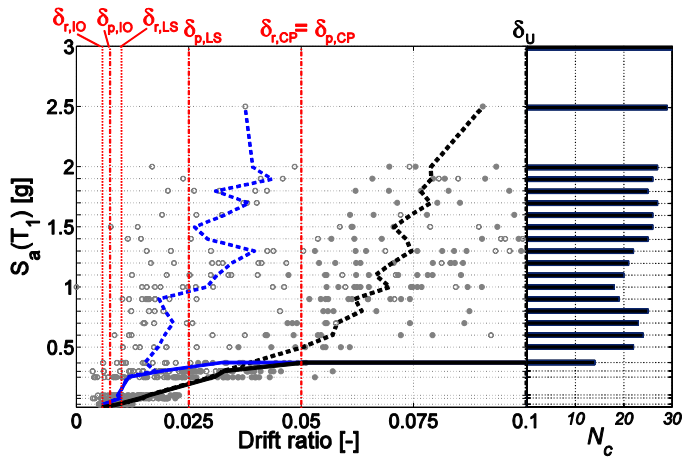


Figure 6.62 Results of MSA for 2D-1971/79-2D-X model.

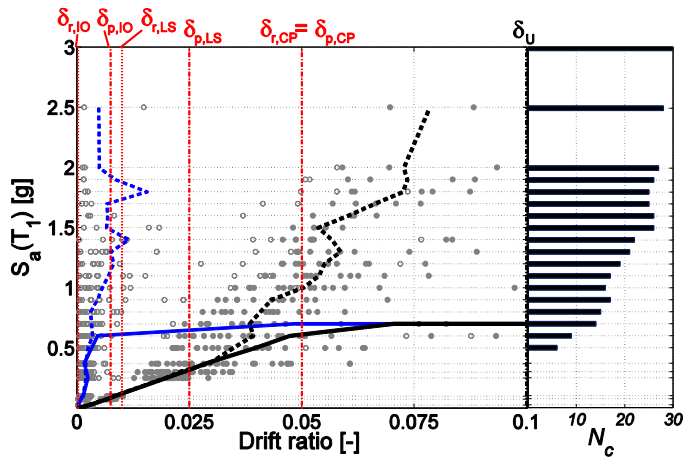


Figure 6.63 Results of MSA for 2D-1971/79-2D-Y model.

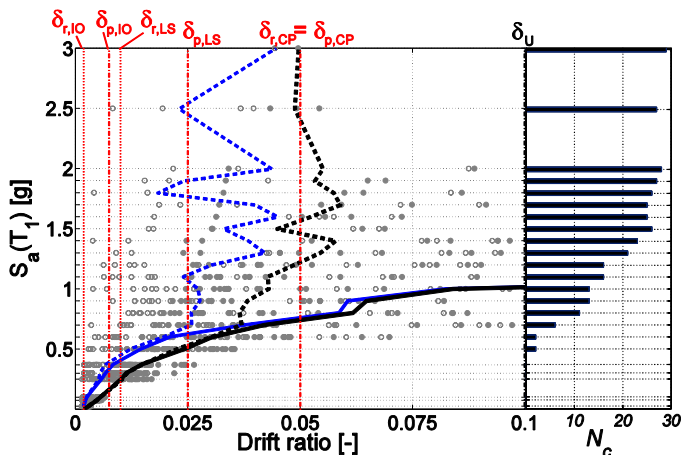


Figure 6.64 Results of MSA for 2D-1991-2D-X model.

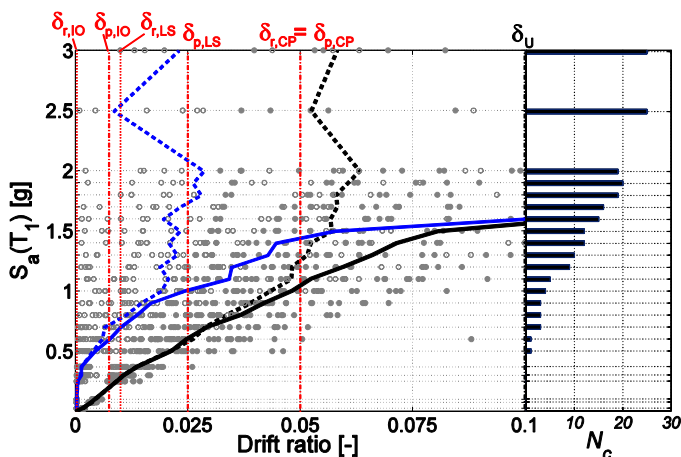


Figure 6.65 Results of MSA for 2D-1991-2D-Y model.

6.6.2.2. Local force demands

Regarding local failures of 2D-models, some general results are given in the following. Figure (6.66) shows two samples of force demand on members belonging to the 1991-2D-Y model. Starting from the value due to gravity loads (N_G), the axial force demand increases linearly (elastic response) at small levels of spectral acceleration. But when a plastic mechanism has been formed in the main frame (plastic hinges at bottom and top ends of each column), the axial force demand remains practically constant. Some variation in the force demand can still remain because: (i) masses on the roof are distributed to also the top chord nodes and roof members are linear elastic; (ii) the peak force demand to roof elements may not occur at the time of maximum displacement because of local higher modes of vibration superimposing to the global first-mode response. The vertical dashed line shown in Figure (6.66) corresponds to the axial

force capacity (N_{CAP}). Figure (6.66a) refers to a member the seismic force demand of which never exceeds the capacity, while Figure (6.66b) is for a member originally subjected to compressive force due to gravity loads and subsequently undergoing buckling failure due to earthquake loads. Many of such local failure modes were detected for the existing structures, thus highlighting the importance to monitor local force demand to those elements.

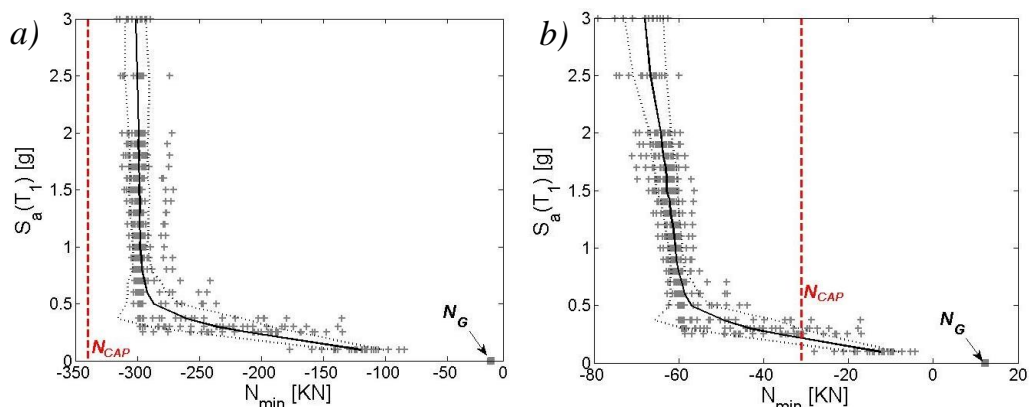


Figure 6.66 Results of MSA in terms of member axial force for two elements of the 1991-2D-Y model.

Table (6.4) provides the number of roof members showing any of the failure modes described in Section (6.5.3), out of the total number of roof members. Besides, the number of elements failing because of each one of the exhibited failure modes is also given, out of the total number of failing elements.

Table 6.4 Summary of local failures of roof members.

Critical roof members		Number of elements failing by mode i / Total number of failing elements				
Structural Model	Number of failing elements/Total number	Member Buckling $N_{R,c}$	tension failure of the net cross section $N_{R,yt}$	Bolt shear failure $N_{R,bv}$	Bolt bearing failure $N_{R,bf}$	Connection fracturing in tension - compression $N_{R,ct}; N_{R,cc}$
1991-2D-Y	16/97	10/16	0/16	6/16	0/16	0/16
1991-2D-X	36/69	20/36	11/36	5/36	0/36	0/36
1971/79-2D-Y	12/97	6/12	0/12	6/12	0/12	0/12
1971/79-2D-X	342/414	207/342	88/342	47/342	0/342	0/342

6.6.3. Fragility curves

As already stated, fragility curves were computed both considering as EDP only the peak transient drift and considering this one in conjunction with the residual drift.

In the following, a comparison of the fragility curves obtained from the univariate distribution of peak transient drifts for the analysed models (see Sect. 6.5.1) is performed first. Then, a comparison is done between the fragility curves obtained considering a truncated and non-truncated joint distribution of peak transient and residual drift demands (see Sect. 6.5.2); then, a comparison is made between fragility curves obtained with univariate and bivariate distributions of the EDPs. Finally, fragility curves representative of the local failure of some structural members are given (see Sect. 6.5.3).

6.6.3.1. Fragility curves from the univariate distribution of peak transient drift

For the computation of the fragility curves according to Eq. (6.18), the transient drift ratio capacities corresponding to the considered IO, LS and CP performance levels were assumed equal to 0.0075, 0.025 and 0.05, as resulting from ASCE (2000) indications for existing steel frame structures.

As already stated, the limit drift introduced to exclude entering a region where the model is not trustworthy (Vamvatsikos and Cornell, 2002) was assumed equal to $\delta_U = 0.1$. Figure (6.67) shows the fragility curves for the 1991-3D-Y *partially continuous* and *fully continuous* model. As previously discussed, at low seismic intensities the behaviour of the two models is almost the same, as shown by the fragility curves at IO limit state. At higher intensity levels, the behaviour of the two models drastically changes and the *partially continuous* model exhibits early out-of-plane failure of roof trusses, so that its fragility curve at the LS limit state actually coincides with the curve at CP limit state of the *fully continuous* model.

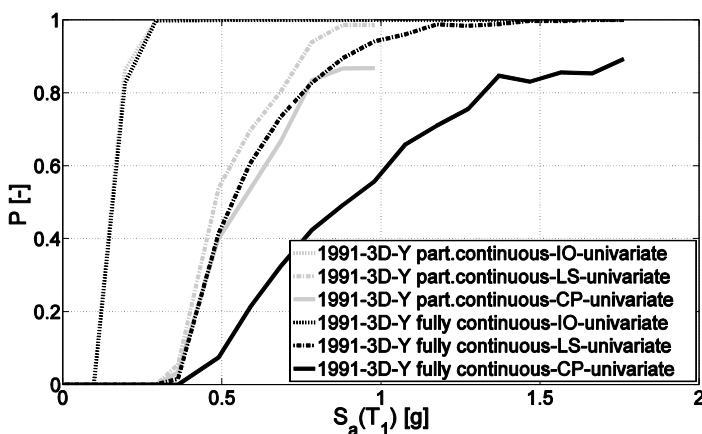


Figure 6.67 Fragility curves for 3D models.

Figure (6.68) shows the fragilities for both the X- and Y-directions of the 1971/79 building, for the three considered limit states. It can be seen that the structural behaviour is quite different in the two directions, and that the model in the X-direction exhibits larger failure probabilities, given the intensity measure level, at each limit state. The differences at the IO limit state are believed to be related to the entity of the drift due to gravitational loads, that is close to the onset of the yielding in the first plastic hinge. This aspect is exacerbated by a high sensitivity to P-Delta effects, as testified by the large α_e value (Table 6.1). This may explain the high values of the failure probability given IM, for the LS and CP limit states. Moreover, as shown from both PA and RHAs, this structure exhibits the lower R_{max} and $S_{a,collapse}$.

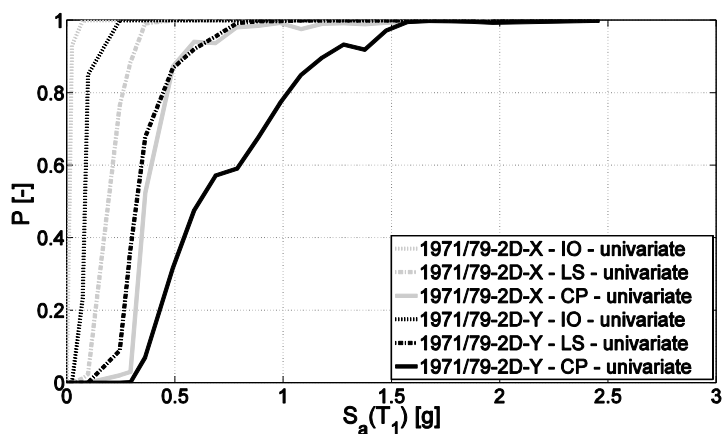


Figure 6.68 Fragility curves for 1971/79 2D-models in X and Y direction.

Fragility curves for the 1991-2D models in X- and Y-directions are shown in Figure (6.69). It can be observed that, unlike the 1971-2D models, at the IO limit state the fragility curves are practically coincident, while they are significantly different at the CP limit state. Intermediate differences have been obtained for the LS limit state. This behaviour can be explained on the basis of the period of vibration and the influence of P-Delta effects. The period of elastic vibration is similar in the two directions of the building. At high performance levels, i.e. at small earthquake intensities, the demand is sufficiently small to make P-Delta effects negligible. Since the period of vibration is about 1 s for both directions, the displacement demand can be approximately estimated by the “equal-displacement” rules, which justifies the similar values of the fragilities at the IO limit state. When low performance levels are investigated, such as the CP limit state, the significance of P-Delta effects is much more important and can make the difference. Indeed, as previously commented, the sensitivity to P-Delta effects is larger when the earthquake acts along the X-direction than it is in case of earthquakes acting

in the Y -direction. Consequently, the fragility at the CP limit state is larger for the X -direction structure than it is for the Y -direction structure.

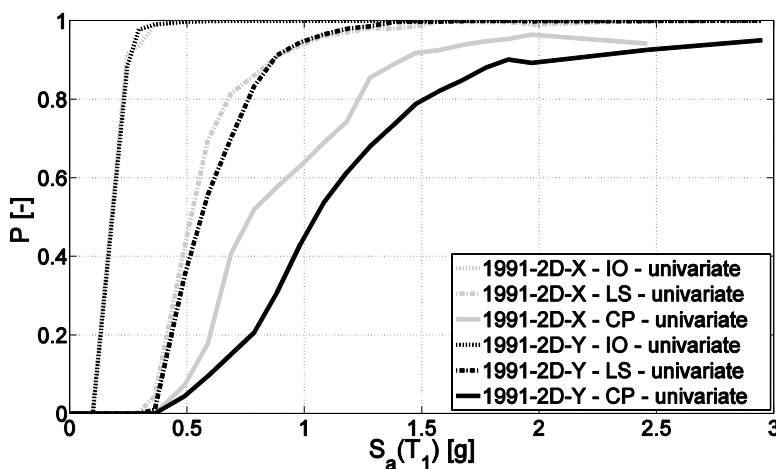


Figure 6.69 Fragility curves for 1991 2D-models in X and Y direction.

6.6.3.2. Comparison of fragility curves from bivariate distribution of EDPs

In this sub-Section, the influence of considering a *truncated* and a *non-truncated* bivariate distribution of peak transient and residual drifts, given that $IM=x$ and given that no global dynamic instability collapse occurred, is discussed (Section 6.5.2).

Figures from (6.70) to (6.75) show, for the considered models, the fragility curves obtained under the two assumptions. Comparing red and black lines in the Figures, it can be noticed that the truncation of the domain of the bivariate distribution of peak and residual drifts does not produce significant effects, except for the IO limit state in 1991-3D-Y models and for the LS and CP in the 1991-2D-X and 1991-2D-Y models. The differences at the IO limit state are related to the fact that the truncation discussed in Section (6.5.4.2), regards a region of low δ_p and δ_r values (see Fig. 6.46).

The differences at the LS and CP limit states are related to the specific distribution of the residual drift with respect to the peak one; in fact, in those cases in which the residual drift is close to the peak one, the (δ_p, δ_r) bins are distributed in a region close to the $\delta_p = \delta_r$ line (see Figure 6.37). In such cases, the truncation of the JPDF domain produces effects on the fragility curve.

Anyway, in all the cases in which appreciable differences can be observed, the truncation reported in Figure (6.37) leads to probability values minor than the non-truncated case. This suggests to employ such a truncation only in those cases in which a particularly accurate estimate of the failure probability from the joint distribution of peak transient and residual drift is required.

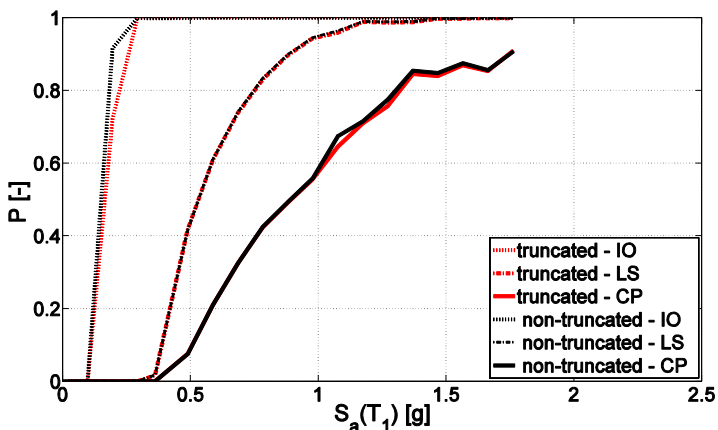


Figure 6.70 Comparison of fragility curves of *fully continuous* 1991-3D-Y model, obtained under different assumptions regarding the bivariate distribution of the demands.

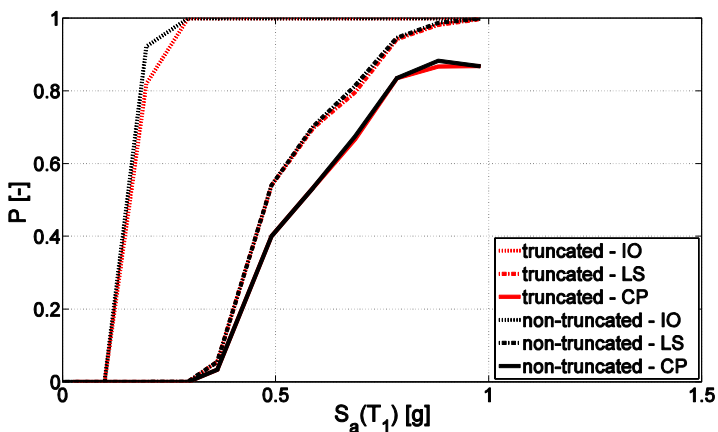


Figure 6.71 Comparison of fragility curves of *partially continuous* 1991-3D-Y model, obtained under different assumptions regarding the bivariate distribution of the demands.

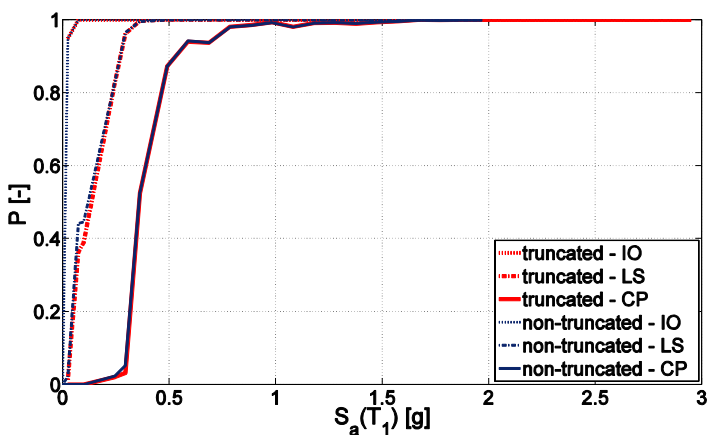


Figure 6.72 Comparison of fragility curves of 1971/79-2D-X model, obtained under different assumptions regarding the bivariate distribution of the demands.

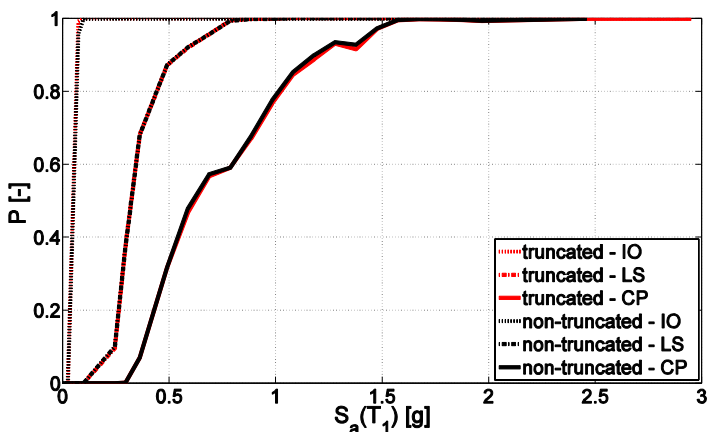


Figure 6.73 Comparison of fragility curves of 1971/79-2D-Y model, obtained under different assumptions regarding the bivariate distribution of the demands.

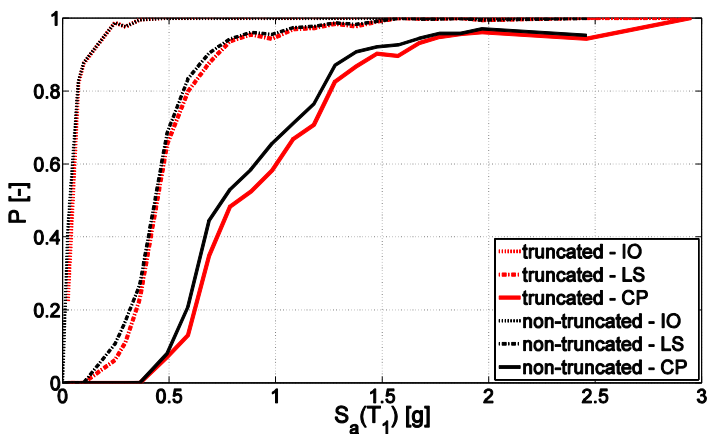


Figure 6.74 Comparison of fragility curves of 1991-2D-X model, obtained under different assumptions regarding the bivariate distribution of the demands.

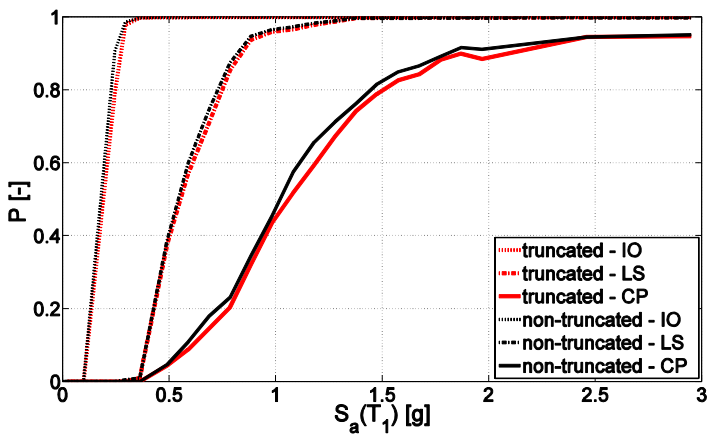


Figure 6.75 Comparison of fragility curves of 1991-2D-Y model, obtained under different assumptions regarding the bivariate distribution of the demands.

6.6.3.3. Comparison of fragility curves from univariate and bivariate distribution of EDPs

The following Figures from (6.76) to (6.81) show example comparisons of fragility curves obtained assuming as EDP the peak transient drift (univariate distribution of demands) and those calculated considering as EDPs the peak transient and residual drifts (bivariate distribution of demands). Non-truncated curves from the previous Section are considered in the comparison.

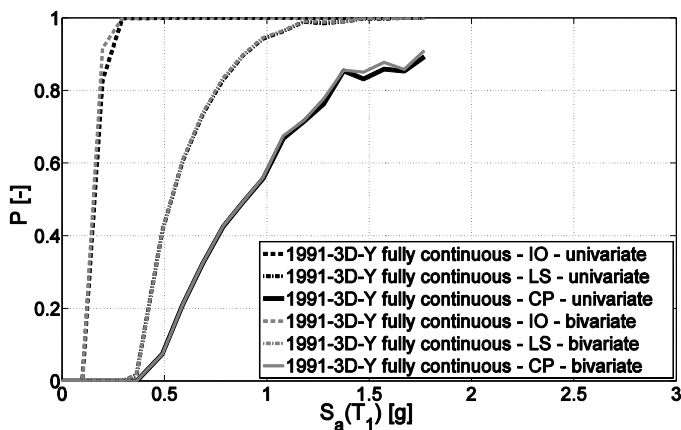


Figure 6.76 Comparison of fragility curves obtained from univariate and bivariate distribution of demands for the *fully continuous* 1991-3D-Y model.

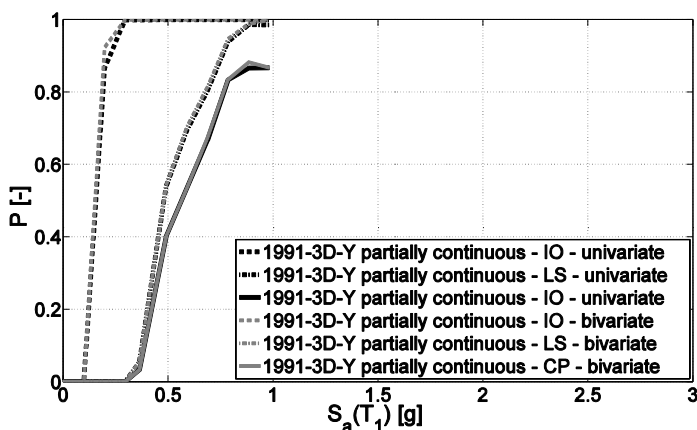


Figure 6.77 Comparison of fragility curves obtained from univariate and bivariate distribution of demands for the *partially continuous* 1991-3D-Y model.

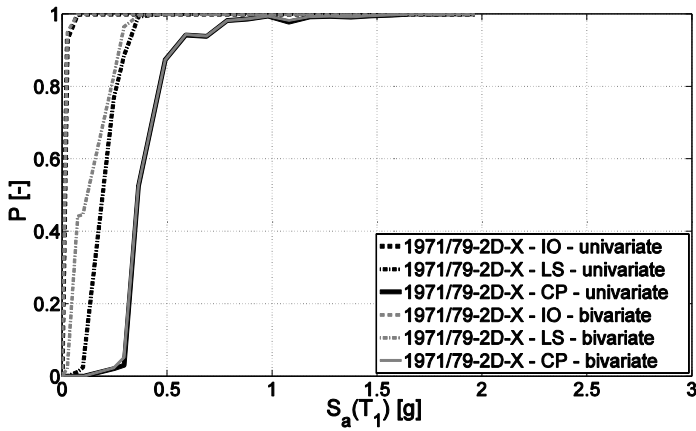


Figure 6.78 Comparison of fragility curves obtained from univariate and bivariate distribution of demands for the 1971/79-2D-X model.

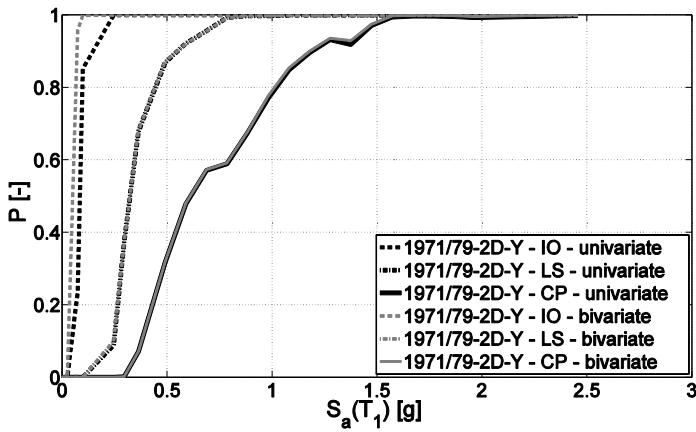


Figure 6.79 Comparison of fragility curves obtained from univariate and bivariate distribution of demands for the 1971/79-2D-Y model.

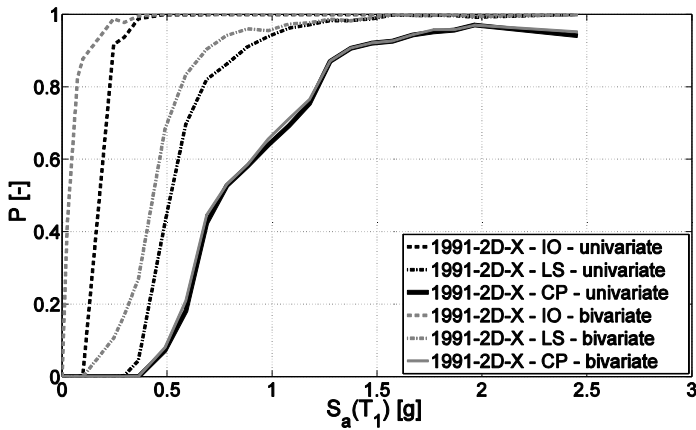


Figure 6.80 Comparison of fragility curves obtained from univariate and bivariate distribution of demands for the 1991-2D-X model.

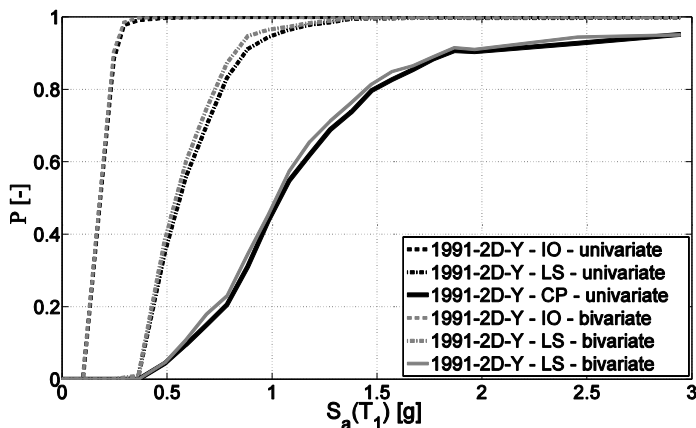


Figure 6.81 Comparison of fragility curves obtained from univariate and bivariate distribution of demands for the 1991-2D-Y model.

It can be observed that considering a bivariate distribution provides probabilities of failure, given IM, always greater than those obtained by means of a univariate distribution. For the analysis in the Y-direction (1991-3D-Y models; 1971/79-2D-Y model and 1991-2D-Y model), minor differences can be observed computing fragilities from peak transient drift or from the bivariate distribution of peak transient and residual drift. On the contrary, in the X-direction significant differences in the fragility curves can be observed. In fact, from the results of the analyses it can be noticed that for both the 1971/79-2D-X (see Fig. 6.78) and the 1991-2D-X (see Fig. 6.81) structures, at the CP limit state, the two types of fragility curves (for univariate and bivariate distributions) are practically coincident, because the residual drift demand deriving from the structural analyses is always smaller than the transient drift demand, while capacity limits are coincident (see Figure 6.51 for 1971/79-2D-X and 6.53 for 1991-2D-X model). The largest effect of including limitations on the residual drifts is expected to appear in the calculation of fragilities for the LS and, especially, the IO limit states. However, the changes in the calculated fragilities can be either large or small, because of the structure peculiar response. For example, Figure (6.78) shows no significant effect at the IO limit state, while Figure (6.81) shows large difference. Indeed, the 1971/79-2D-X frame is subject to a relatively large initial (gravity induced) drift (Fig. 6.51). As mentioned above, such an initial drift is the assumed residual drift capacity at the IO limit state; it is relatively large and close to the peak drift capacity for the 1971/79-2D-X frame. On the other hand, median residual drift demands results to be relatively small with respect to median transient demands (Fig. 6.51), because of the flexibility of the structure associated with large peak drifts and small inelasticity. Thus, introducing a limit to the residual drift did not change significantly the total

seismic fragility of the 1971/79-2D-X frame. An opposite trend is revealed by the 1991-2D-X frame: the ratio of the residual and transient drift capacity is small while the ratio of the median residual and transient drift demand is large (Fig. 6.53). Consequently, the frequency of exceeding the IO limit state because of an excessive residual drift has a strong effect on the total computed fragility (Fig. 6.81).

6.6.3.4. Fragility curves of roof members

Figure (6.82) shows fragility curves for local failures, obtained on the basis of the procedure outlined in Section (6.5.3), for two members extracted from the “1991-2D-Y” and “1991-2D-X” model, respectively. Similar curves were obtained for each element of the analysed structural models. Figure (6.82a) corresponds to the case in which the capacity falls between the axial force acting on the member due to gravitational loads (N_G) and the one corresponding to the lower level of IM. In other words, this is the case of a frame which can withstand gravitational loads, but for a whatever small value of spectral acceleration the probability that the demand exceed the capacity is close to 1. Considering that IMs ranging between 0 and 0.25 g were not investigated (i.e. 0.025 g is the lowest IM value considered), a linear approximation of the fragility curve was adopted in the aforementioned range. The case shown in Figure (6.82b) is obtained for a capacity falling between the axial force demands at the lower level of IM and those corresponding to the formation of a fully plastic mechanism. Other possible limit cases are: (i) a capacity larger than the axial force obtained at the formation of the plastic mechanism, which corresponds to a probability of failure equal to zero; (ii) a capacity lower than the axial force due to gravitational loads, which corresponds to a probability of failure equal to 1. This latter case never occurs in the analysed models. This behaviour is observed for all the examined structures. Similar considerations apply for the fragility of column base welds.

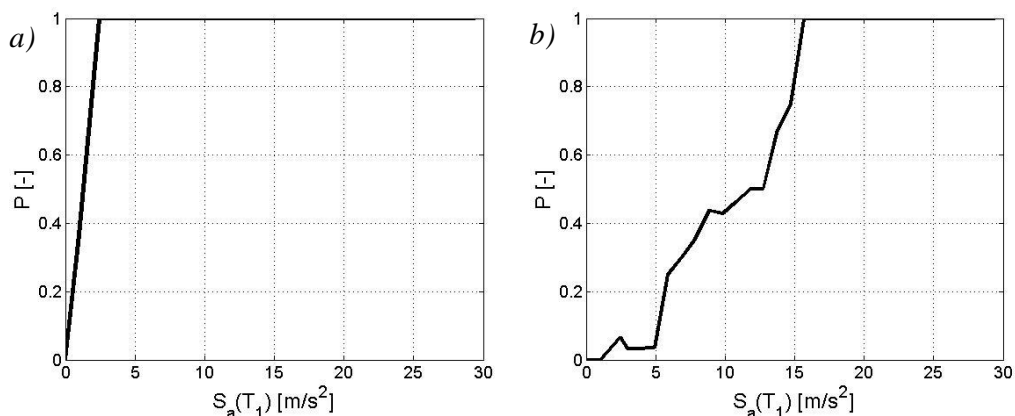


Figure 6.82 Fragility curves for two members belonging to 1991-2D-Y (a) and 1991-2D-X (b) models.

6.6.4. Failure probability

6.6.4.1. Probability of global failure

Given the hazard (Section 6.6.1) and the fragilities discussed above (Section 6.6.3), the annual probability of failure (P_f) can be computed according to the approaches outlined in Section 6.5. The annual failure probabilities for the considered limit states, calculated on the basis of the peak transient drifts are reported in Table (6.5).

Table 6.5 Probabilities of failure based on the peak transient drift.

Structural model	<i>IO</i>	<i>LS</i>	<i>CP</i>
1971/79-2D-X	3.7E-02	1.2E-03	2.0E-04
1971/79-2D-Y	5.7E-03	3.3E-04	7.0E-05
1991-2D-X	5.1E-03	4.7E-04	1.9E-04
1991-2D-Y	5.0E-03	3.9E-04	1.1E-04
1991-3D-Y “fully continuous”	5.9E-03	4.2E-04	1.7E-04
1991-3D-Y “partially-continuous”	6.0E-03	4.3E-04	3.4E-04

As a general outcome, the *Y*-direction frames are generally more reliable than *X*-direction frames: this is because of the larger stiffness and strength observed for *Y*-direction frames.

Failure probabilities values confirm the 1971/79-2D-X as the worst model among the analysed ones. This is related to its high deformability, the relatively low flexural strength of its column base plates (see Sect. 6.3.2.1) and its dimensions. In fact, due to the gravitational loads, the extreme perimeter columns are subjected to significant drifts and to a bending moment approximately equal to the 80% of the flexural strength. Therefore, as anticipated by the PA (the model is characterized by the lower R_{max} , $S_{a,collapse}$ and the higher α_e), the 1971/79-2D-X is characterised, at each limit state, by failure probabilities of approximately one order of magnitude greater than those of the other structural models.

Regarding the other structural models, comparable values of the failure probabilities can be observed at IO limit state. Even if the “1991” building is stiffer than the “1971/79” building and characterised by lower drift demands, as testified by all the structural analysis results, the lower flexibility also results into a lower period of vibration ($T=1$ s for the “1991” structure and $T=1.6$ s for the “1971-1979” structure). Accordingly, the probability of exceeding any given value of the spectral acceleration is higher for the “1991” building. The annual probability of failure, which is the convolution of the two terms (Eq. 6.16), compensates these two opposite aspects and

assumes values of the same order of magnitude in 1991 models and the 1971/79-2D-Y one. The considerations previously discussed for the IO limit apply in the whole field of stable structural response. When the structure encounters larger displacements, P-Delta effects become more important and can change significantly the probability of failure. This phenomenon partially affects the Life Safety (LS) limit state. In fact, the x -direction is characterized by larger values of P_f than the y -direction both in case of the “1991” and the “1971-1979” structures. This is related to the larger sensitivity of the x -directions to the P-Delta effects. The influence of P-Delta effects becomes very large when the Collapse Prevention (CP) limit state is considered. This can be observed comparing $P_{f,CP}$ values with respect those obtained at LS limit state, as well as comparing $P_{f,CP}$ values for the different structural models. It can be noticed as the different failure modes that can involve roof trusses, discussed in Section (6.5.3), lead to failure probabilities that almost double considering the 1991-2D-Y, the *fully continuous* 1991-3D-Y and the *partially continuous* 1991-3D-Y model.

In Table (6.6) the failure probabilities obtained considering a bivariate truncated distribution of peak transient and residual drift and the percentage variation with respect to a non-truncated one are reported in parentheses. Table (6.6) permits appreciating the influence of including residual drifts in the assessment and confirms the results of Figures (6.76) to (6.81). If transient and residual drift capacities are close each other, the inclusion of residual drifts in the calculation of P_f must obviously have a minor effect, because the residual drift demand is always smaller than the transient value. If the residual drift capacity is significantly smaller than the transient value, the influence of including residual drifts in the calculations will still depend on the distribution of demands. At a given level of spectral acceleration, if the median residual and transient drift demands are relatively similar, which is the case for stiff but weak structures, then the limit imposed to the residual drift is expected to have a remarkable influence on the calculated P_f . On the contrary, if the median transient drift demand is larger than the median residual drift demand, as in case of flexible and strong structures, the influence will be smaller though it may still be significant.

Table 6.6 Probabilities of failure based on the bivariate distribution of peak transient and residual drift. In parentheses the percentage variations with respect to the univariate distribution of peak transient drift reported in Table (6.5).

Structural model	<i>IO</i>	<i>LS</i>	<i>CP</i>
1971/79-2D-X	3.7E-02 (1.26)	6.7E-03 (454.30)	2.1E-04 (2.54)
1971/79-2D-Y	1.2E-02 (113.40)	3.4E-04 (3.62)	6.7E-05 (0.13)
1991-2D-X	6.6E-02 (1182.59)	1.2E-03 (152.06)	2.0E-04 (4.97)
1991-2D-Y	5.1E-03 (1.81)	4.2E-04 (6.92)	1.2E-04 (8.33)
1991-3D-Y “fully continuous”	6.3E-03 (6.48)	4.2E-04 (0.55)	1.7E-04 (0.35)
1991-3D-Y “partially-continuous”	6.3E-03 (4.14)	4.4E-04 (0.79)	3.4E-04 (0.38)

6.6.4.2. Probability of local failure

In a similar manner, the probabilities of exceedance of local member capacity were calculated for each structural member of the bi-dimensional models. Results are shown in Table (6.7) for the weakest element among roof members, together with the number of failing elements over the total.

Table 6.7 Annual probabilities of exceeding global drift ratio limits, given that no global collapse occurs.

Structural model	failing elements over the total	P_f of the weakest roof member
1971/79-2D-X	342/414	1.7E-02
1971/79-2D-Y	12/97	1.7E-02
1991-2D-X	36/69	5.1E-02
1991-2D-Y	16/97	5.1E-02

From Table (6.7) follows that a significant number of elements could require strengthening. Even if in modern codes the suppression of such mechanisms is mandatory, the assessment of their probability of failure gives a numerical quantification of the risk deriving from possible local failures. This provides an indication about the probability that, after strong earthquakes, the building, although not collapsed for global sidesway mechanism, would require the strengthening of at

least one roof element (the probabilities in Table 6.7 are referred to the weakest element).

Table (6.7) shows that the probabilities of failure associated to local mechanisms are, in general of the same order of magnitude than those related to the immediate occupancy limit state, computed from the bivariate distribution of peak transient and residual drifts (Table 6.6). Nevertheless, there could be cases in which differences of one order of magnitude can be observed, as in 1991-2D-Y structure.

Finally, it is worth noting that, since for the weakest elements the capacity falls between the axial force acting on the members due to gravitational loads and the one corresponding to the lower level of IM, the values of failure probabilities are influenced by the linear approximation assumed in the initial range of IM, reported in Figure (6.82a).

6.7. Conclusions

In this Chapter a probabilistic seismic performance assessment was performed for a case study industrial steel building, in order to compute fragility curves for some typical industrial structures and to provide failure probabilities useful for loss estimation (Petruzzelli *et al.*, 2012a and 2012b and Della Corte *et al.*, 2013). Failure mode considerations versus modelling assumptions and results of dynamic nonlinear analyses of different frame models, extracted from the case study buildings have been discussed. The analyses were based on sets of ground motion records consistent with site-specific probabilistic seismic hazard analysis. Integrating the hazard and the fragility curves for different limit states, annual probabilities of failure were obtained. The following are the main conclusions drawn from the study.

One main difficulty of the analysis was the modelling of column base connections. Though experimental and/or finite element studies should rigorously be carried out, it has been shown that using the well-known components method (EC3), along with some reasonable and cautionary assumptions, a plausible moment-rotation response can be obtained. Considering that the influence of in-cycle strength degradation (due to P-Delta) was expected to be larger to the one due to the cyclic degradation, such moment-rotation response was used in non-linear dynamic analyses. Nevertheless, a research need exist in the quantification of rotational capacity and strength degradation in existing steel structures.

The importance to take into account failure of roof bracing elements connecting parallel frames has been highlighted by comparing results from two limit cases: (i) fully active bracing members (three-dimensional models) and (ii) fully collapsed

bracing members (two-dimensional models). Moreover, two different hypothesis were assumed regarding the out of plane flexural behaviour of trusses joints (continuous and pinned joints) in three-dimensional models. Interestingly, the results highlight that the behaviour in case of fully active transverse bracing is not necessarily better than the behaviour of individual frames at large earthquake intensity.

In fact, using a 3D model highlighted the possibility of roof truss failure in the form of complex three dimensional instability modes, involving groups of roof truss members. Such failure modes cannot be predicted using 2D models, because of the intrinsic 3D features of transverse vibrations of planar trusses. The latter vibrations are able to trigger local P-Delta effects, which are responsible of the instability modes. This conclusion is valid for all industrial steel buildings featuring a roof truss structure with out-of-plane joint displacements. The above considerations directly reflect into fragility curves developed for both the 3D and 2D analysed models.

The assessment of spectral acceleration leading to collapse from FEMA 440 guidelines well agrees with the results of MSAs, except for those cases in which the above mentioned out-of-plane collapse of roof trusses occurs.

From the analysis of the seismic demands in terms of peak transient and residual drifts, a larger dispersion, at increasing IM levels, can be observed for residual drifts than the one characterizing peak drifts. This is in agreement with some studies of SDOF and MDOF systems available in literature (e.g. Uma *et al.*, 2010).

Including both residual and peak transient drifts in the seismic risk assessment could be either very important or rather unessential depending on the structural characteristics and the relative magnitude of limits on residual and transient drifts. Results obtained within this study suggests that, generally, residual drifts should be included in the analysis, unless it can be anticipated by clear reasoning that they would have a minor effect on the probability of failure. The results presented might be helpful in identifying the latter cases. Such comments on the influence of residual drift limitations are clearly valid beyond the specific case study of industrial buildings.

The possibility of truncating the domain of the bivariate distribution of peak transient and residual drifts, give that no global collapse occurred, is, in most of the analysed cases negligible. Appreciable differences can be observed in those cases in which the residual drift assumes values close to the peak drift, that is when the structure is approaching the collapse.

It was emphasized that fragility curves need to be accurately represented in the field of low seismic intensities, because smaller values of spectral accelerations are much more probable than larger values and they strongly affect the final result in terms of failure probability.

The need of suppressing undesired failure modes, such as roof collapse failure, emerged as a critical aspect in the case-study, and in general can affect failure probability estimates performed at the global structural level. A measure of the local failure probability was also given for each structural member. Referring to the weakest one, an indication of the probability of observing at least one local failure in a structure that did not encounter global collapse, is provided.

Finally, as a general outcome, it is noted that the probabilistic methodologies appear to be rather well established and consolidated, while guidelines need to be developed for modelling existing structures on a rational basis, especially connections and degradation phenomena.

Chapter 7 – SUMMARY AND CONCLUSIONS

In this thesis, seismic risk assessment and management of structures belonging to large industrial groups were addressed. The research was focused on the development and application of quantitative and practice-ready tools operating at different scales, ranging from the one of a large portfolio of structures to the one of the single building. In the following, a synthesis of the main outcomes deriving from the development of such scale-dependent procedures and from their application to real case-studies is reported.

7.1. Prioritization analysis based on Nominal Deficit

The proposed procedure for priority analysis at a “*large scale*” was based on a “nominal deficit” index, named NODE, defined as the difference of the current seismic demand and the one provided by the codes enforced at the time of the design. It allows to explicitly account for the evolution of seismic classification of the territory and evolution of codes, which may be reasonably believed as the main cause for performance deficit, if any. This index can be computed both without any visual inspection (“*desk study*”), in terms of PGA, and after a visual survey of the structures, in terms of spectral accelerations or base shears. Therefore, in the most unfavourable cases, NODE can be computed knowing only the location and the year of design. In many cases, these data are easy available from the analysis of the building stocks.

The NODE index does not allow a direct (absolute) estimate of expected loss, yet a comparison of deficit among a portfolio for which the same assumptions can be made, for this reason it is suitable for prioritization analysis only.

Although based on strong assumptions (the perfect code compliance and the absence of defects, among the others) and extremely synthetic (it compares only the seismic demand according to two different structural codes), the NODE index provides a quantitative and coherent measure of hazard and vulnerability. Moreover it may account explicitly for exposure, expressed both in terms of number of occupants and economic losses (property damage and business interruption), providing a relative measure of seismic risk. Therefore, it is believed that such an index can be useful to rank priorities, if it is applied consistently in the portfolio.

The definition of the behaviour factor q , or of equivalent measures of ductility and overstrength employed in the proposed indices, as well as in others proposed in literature, appears as one of the critical aspects of such a prioritization approach. In fact, the current seismic demand is inelastic and one assumption of the approach is that the demand at the time of design may be considered inelastic as well. More in general, the definition of behaviour factors for different code requirements, for example referring to typical structural typologies, materials and construction practice and, most of all, minimum code requirements, should provide a useful proxy of the actual seismic capacity.

Regarding the assessment of the capacity of structures designed in non-seismic sites, being the NODE index defined as a difference between demand and capacity, a zero capacity value can be adopted in the methodology. Nevertheless, the use of horizontal capacity obtained from literature, or from wind design requirements and their evolution with codes, is proposed. The case-study analysis confirmed that the adoption of horizontal capacity deriving from wind design can be important, especially for industrial portfolios, since they are frequently characterized by lightweight and/or large structures, for which the wind action could have been the most demanding at the time of design.

From the comparison of the ranking obtained applying nominal indices from literature and the NODE indices, a general consistency of such measures emerges. The NODE index is clearly characterized by a lower level of information with respect to those indices employing the slope of the linear approximation of the hazard curve at the site in the logarithmic plane. Nevertheless, the availability of coherent hazard studies strongly limits the use of these indices worldwide.

The “*NODE – NOminal DEficit - v.1.1 beta*” software was developed for implementing the proposed procedure in the Italian context. It allows to compute automatically, and for large portfolios of engineering structures, all of the indices discussed, taking into account the different information available. In fact, the software contains the site-by-site evolution of seismic hazard and wind design since 1909 and a seismic micro-zonation of subsoils for the whole Italian territory.

It is believed that such a tool may be helpful for the current research on seismic risk prioritization schemes and, eventually, for the realization of National seismic risk maps, as well as to the professional in assessing both seismic and wind action.

7.2. Fragility-based rapid seismic risk assessment

The “*meso scale*” procedure, intended to be applied to tens or hundreds of structures, consists in the rapid computation of expected loss due to earthquakes by the convolution of hazard, vulnerability and exposure. In particular, the procedure is based on the allocation of a fragility curve to the structure under investigation, obtained from literature or computed ad hoc. The use of “class” fragility curves is also feasible, depending on the scale of the portfolio.

Although the use of fragility curves can be considered a well-established methodology for computing seismic risk, significant differences exist among fragility functions computed in different geographical contexts, reflecting the differences in structural typologies, construction practice and materials. Such variability in terms of employed intensity measure, limit states and structural types to which they relate, makes the association of a fragility curve (or a set of fragility curves) to a specific structure (or class of structures) a non-trivial task.

A software suite named “*FRAME - Fragility-based rapid seismic Risk AssessMENT - v.1.0 beta*”, was developed in order to overcome these shortcomings, providing for the management and the manipulation of an inventory of fragility curves. The Syner-G project (Syner-G, 2009a and 2009b) and Hazus project (FEMA, 2003) fragility curves were included into the software, as well as the possibility of defining new user-defined ones.

The developed tool allows the conversion of the intensity measures and units employed in a fragility curve, as well as to compute statistics over an ensemble of fragility curves, selected by filtering the inventory according to a pre-defined taxonomy. This is believed to represent a suitable tool for comparing fragility curves derived from different studies and, eventually, defining fragility curves for classes of structures.

The inclusion in the software of seismic hazard at the global scale, from the GSHAP project, allows to compute worldwide the probability of exceeding a limit state, given a scenario PGA with 475 years return period. The inclusion in the software of a loss module allows the rapid assessment of seismic risk worldwide, expressed as the expected loss, given the scenario earthquake.

With specific reference to the Italian context, the inclusion of the curves of seismic hazard referred to project DPC-INGV S1, allows to characterize the probability of exceeding a specified limit state. In this case (or if a user-defined hazard curve is provided), the tool can provide the expected annual loss. The software also includes the

American hazard map from USGS, as well as the possibility of defining a user-defined hazard curve for the chosen intensity measure.

Managing fragility curves required to define an appropriate building taxonomy, that is necessary to classify fragility functions and to filter the database of available fragility curves in order to select only those matching the structural characteristics of the building under investigation or other search criteria such as methodology used for their calculation or geographical context to which they apply.

One main issue concern the harmonization of different fragility curves and the homogenization of intensity measurements and limit states adopted. The FRAME software allows to compare fragility curves, after checking their coherency in terms of intensity measure and number of considered limit states, allowing to define mean and confidence intervals from a given set of fragility functions. This is performed searching the best-fit distribution of the probability of exceedance, given an intensity measure level. The definition of new limit states from existing ones is also possible, as well as the conversion of one intensity measure into another.

It is believed that this software could represent a valuable contribution to the spread of quantitative procedures for the assessment of seismic risk and an instrument for the rapid evaluation of risk for relatively large building portfolios. Moreover the possibility of comparing fragility functions developed for the same structural typology, by different authors, for different geographical contexts, under different assumptions, can represent a valid instrument for the vulnerability of classes of buildings.

The loss estimates provided by the tools are believed to be useful to the stakeholders for the comparison of annual revenues with annual expected losses and the implementation of risk management strategies over the structural portfolio.

Finally, the measures of seismic risk provided by the tool could be used for performing a more accurate ranking of the structures belonging to the fraction of the portfolio obtained from a prioritization analysis.

7.3. Seismic risk assessment of an existing industrial steel building

The “*site-specific scale*” procedure presented in this thesis consists in the probabilistic seismic performance assessment of a case-study industrial steel building. The

motivations of this study rely, on one hand, on computing failure probabilities useful for loss estimation and, on the other hand, on the necessity of computing fragility curves, that could be used in a “*meso scale*” approach. In fact, although steel structures represent a large part of the industrial building stock of many countries, the analysis of their seismic vulnerability has been subject of relatively little investigation with respect to other types of existing structures and a lack in fragility curves developed for this specific structural typology can be observed in literature. Moreover, these structures are highly not-standardized ones, therefore a detailed knowledge, modelling and analysis of the structure are required, in order to obtain realistic measures of the seismic risk.

This remarks that simplified approach to seismic risk assessment are coarsely applicable to non-standardized structures like the analysed one. In fact, the seismic behaviour of such peculiar structures is strongly influenced by structural detailing, that should be investigated at the highest possible level of knowledge. Similarly, the structural modelling and the analysis methodology employed should be able to capture all the possible failure modes that can affect an existing structure, designed, in most cases, without explicit capacity design and ductility control. Moreover, at least the uncertainty in seismic input should be adequately taken into account.

Such an approach is particularly demanding, in terms of time and computational burden, therefore it may be appropriate when the confidence in vulnerability functions is particularly low and/or the consequence of failure are expected to be especially relevant.

The analysed structure was the main workshop building of one of the most risk-prone plants of the case-study portfolio, as resulting from the prioritization analysis.

The structure is composed of different portions, designed according to obsolete structural codes about both the definition of the seismic design action and the design of steel structures. As frequently occurs in industrial steel structures, the structural scheme is a moment resisting frame characterized by battened columns both sustaining the roof structure and resisting horizontal forces; the roof structure was made of lattice shed-type trusses and Pratt-type trusses, connected by slender bracing elements. The roof structure is characterized by a non-negligible deformability in its plane.

Wide-range Multi Stripe Analyses were performed on different structural models extracted from the case-study building, both two-dimensional and three-dimensional. The assumed engineering demand parameters (EDPs) were both peak transient and residual drifts, as well as local force demands in all the members of the roof structure. Non-linear time-history analyses were based on sets of ground motion records consistent with site-specific probabilistic seismic hazard analysis. Their selection was

performed on the basis of a disaggregation of the seismic hazard at the site of the facility. While the probabilistic methodologies employed at this scale are rather well established and consolidated, some findings emerged from this study, regarding modelling and structural analysis issues as well as quantitative risk assessment. They are briefly summarized in the following.

One difficulty of the analysis was the modelling of column base connections, because of the special geometrical detailing that was adopted by the building structural designers. Though experimental and/or finite element studies should rigorously be carried out, it has been shown that using the well-known components method (EC3), along with some reasonable and conservative assumptions, a plausible moment-rotation response can be obtained. Anyway, research needs remain in the quantification of rotational capacity and strength degradation.

Both global (storey sidesway) collapse and local failure modes (e.g. failure of roof members or connections) have been addressed, as well as pounding of adjacent buildings.

In order to reduce the computational burden connected to the analyses, the opportunity of considering two-dimensional instead of three-dimensional structural models was investigated. Non-linear incremental time history analyses performed on three-dimensional structural models highlighted the possibility of roof truss failure in the form of complex three dimensional instability modes. These failures, triggered by transverse vibration of planar trusses, cannot be predicted using 2D models. Therefore a full three-dimensional model could be employed in steel structures characterized by a deformable roof deck and truss joints not adequately constrained in the out of plane direction.

The need of suppressing undesired failure modes, such as roof collapse failure, emerged as a critical aspect in the case-study, and in general it can affect failure probability estimates performed at the global structural level. In this thesis, this local failure modes have been treated as “brittle” failure modes and their onset was checked after the analysis. A measure of the local failure probability was also given for each structural member.

Regarding the sidesway collapse, the importance of taking into account, in a probabilistic framework, the onset of dynamic instability was remarked and the possibility of including the residual drift in the assessment was discussed.

Analysis results confirmed that residuals are characterized by a larger dispersion than peak transient demands and showed that the effect of their inclusion in the assessment can be more or less significant, depending on the relative magnitude of capacity limits on residual and transient drifts. Results obtained within this study suggests that, generally, residual drifts should be included in the analysis.

7.4. Final Remarks

Regarding the possibility of considering the three procedures presented in this thesis as a unique framework for seismic risk assessment and management, the following considerations can be made.

The application of the large-scale procedure can represent a suitable solution for reducing the size of the portfolio under investigation. The possibility of performing a prioritization analysis as a desk study is feasible simply requesting to the plant the year of design of its structures. Alternatively, knowledge forms developed for the specific case-study could be applied for the visual inspection of the structures by an un-expert subject.

After the selection of the fraction of the portfolio deserving deeper investigation, the “meso-scale” procedure could be applied, performing a search for fragilities in the provided inventory that can suite the specific structure under investigation. Class fragility curves or curves computed *ad-hoc* for the specific structure could be applied. The obtained failure probabilities or, most likely, expected losses, could be used to rank the remaining part of the portfolio and identify a restricted portion to be investigated by means of an analytical approach.

The analytical evaluation of fragility curves requires particularly high efforts both in the modelling and analysis. This confirms the opportunity of performing such kind of analysis for a limited fraction of the portfolio under investigation, deriving from a prioritization scheme.

In Figure (7.1) the possibility of considering the procedures discussed in the thesis as general framework is shown. In the Figure, the “knowledge” boxes refer to the data regarding the structure under investigation. It is supposed that hazard and exposure are known at the level of detail requested by the scale of the procedure.

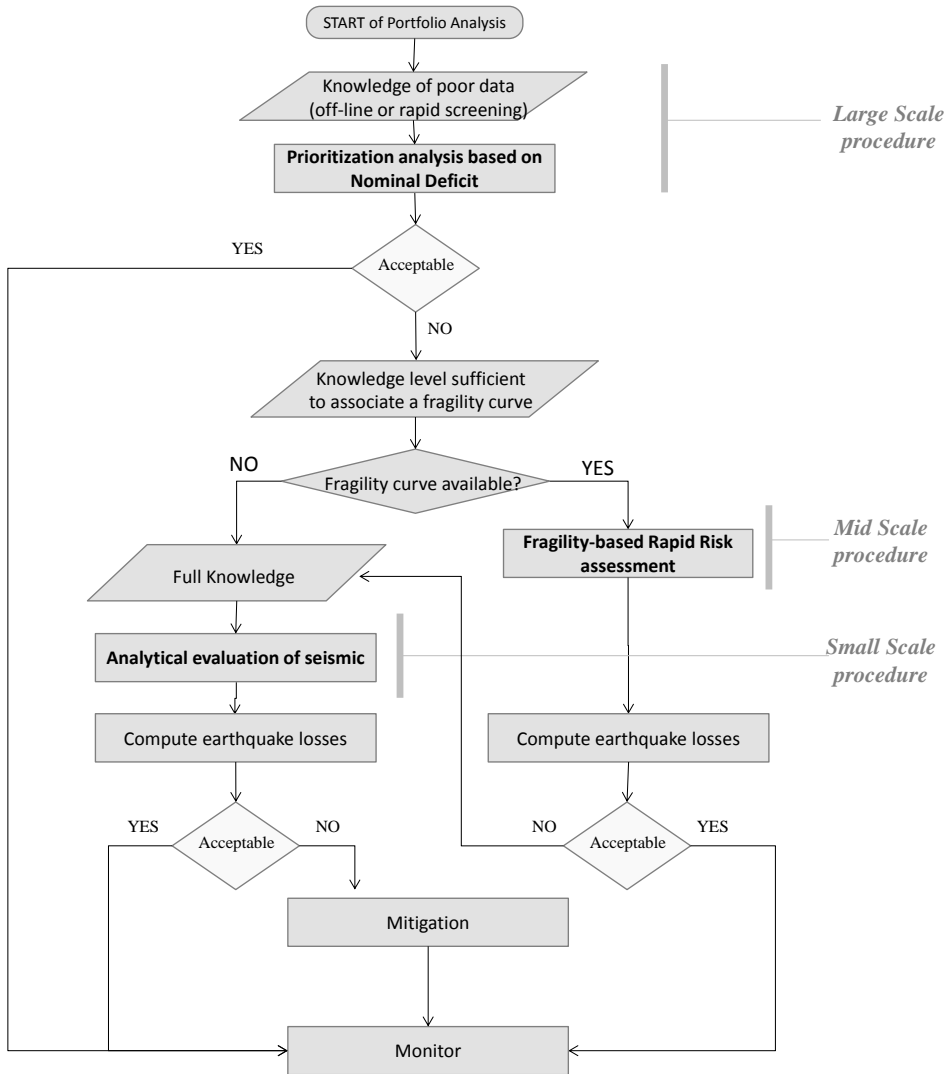


Figure 7.1 Scheme of the three scale-dependent procedures dealt in the thesis considered in a unified approach to seismic risk assessment and management .

REFERENCES

- Alavi, B. and Krawinkler, H. (2004). Behavior of moment-resisting frame structures subject to near-fault ground motions. *Earthquake Engineering and Structural Dynamics*, **33**(6): 678-706.
- Albanesi, T., Nuti, C. and Vanzi, I. (2004). Should we retrofit structure for earthquake protection?. *Proceedings of the 13th World Conference on Earthquake Engineering*. Vancouver, Canada, Paper No. 2562.
- Albarello, D. and Mucciarelli, M. (2002). Seismic hazard estimates using ill-defined macroseismic data at site. *Pure Applied Geophysics*, **159**: 1289-1304.
- Albarello, D., Azzaro, R., Barbano, M.S., D'Amico, V., D'Amico, S., Rotondi R., Tuvè, T. and Zonno, G. (2007). Valutazioni di pericolosità sismica in termini di intensità macrosismica utilizzando metodi di sito. Progetto INGV-DPC S1, Deliverable D9, <http://esse1.mi.ingv.it/d9.html>. (In Italian).
- Anagnostopoulos, S. A., Petrovski, J. and Bouwkamp, J.G. (1989). Emergency earthquake and stability assessment of buildings. *Earthquake Spectra*. **5**(3): 461-476.
- Angeletti, P., Bellina, A., Guagenti, E., Moretti, A. and Petrini, V. (1988). Comparison between vulnerability assessment and damage index. *Proceedings of the 9th World conference on Earthquake Engineering*, Tokyo-Kyoto, Japan, pp.181-186.
- ASCE (2000). *Pre-standard and Commentary for the Seismic Rehabilitation of Buildings*. FEMA 356. Reston, Virginia. American Society of Civil Engineers prepared for the Federal Emergency Management Agency.
- ASCE (2010). *Minimum design load for buildings and other structures*. ASCE 7-10.
- Aslani, H. and Miranda, E. (2004). Probability-based structural response analysis. *Engineering Structures* **27**(8): 1151-1163.
- Aslani, H. (2005). *Probabilistic Earthquake Loss Estimation and Loss Disaggregation in Buildings*. Ph.D. Thesis, John A. Blume Earthquake Engineering Centre, Dept. of Civil and Environmental Engineering Stanford University, 382 pp.
- Aslani, H. and Miranda, E. (2005). *Probabilistic earthquake loss estimation and loss disaggregation in buildings*. Report No. 157, The John A. Blume Earthquake Engineering Center, Stanford University, U.S.A.
- ATC Applied Technology Council, (1978). *Tentative provision for the development of seismic regulation for buildings*. Report No. ATC 3-06, Redwood City, California, U.S.A.
- ATC Applied Technology Council (1985). *Earthquake Damage Evaluation Data for California*, Report ATC-13, Redwood City, California, U.S.A.
- ATC Applied Technology Council (1996a). *Improved Seismic Design Criteria for California Bridges: Resource Document*. Report No. ATC-32-1, Redwood City, California, U.S.A.

- ATC Applied Technology Council, (1996b). *Seismic Evaluation and Retrofit of Concrete Buildings*. Report No. ATC-40, Redwood City, California, U.S.A.
- ATC Applied Technology Council (2003). *Procs. of FEMA-Funded Workshop on Communicating Earthquake Risk*. Report No. ATC-58-1, Redwood City, California, USA.
- ATC Applied Technology Council (2004). *Preliminary Evaluation of Methods for Defining Performance*. Report No. ATC-58-2, Redwood City, California, U.S.A.
- ATC Applied Technology Council (2005). *Improvement of nonlinear static seismic analysis procedures (FEMA 440)*. Prepared by Applied Technology Council, Redwood City, California, for Federal Emergency Management Agency, Washington, D.C.
- Badillo-Almaraz, H. Whittaker, A.S. and Reinhorn, A.M. (2007). Seismic Fragility of Suspended Ceiling Systems. *Earthquake Spectra*, **23(1)**: 21-40.
- Baggio, C., Bernardini, A., Colozza, R., Corazza, L., Della Bella, M., Di Pasquale, G., Dolce, M., Goretti, A., Martinelli, A., Orsini, G., Papa, F. and Zuccaro, G. (2000) *Manuale per la Compilazione della Scheda di I Livello di Rilevamento Danno, Pronto Intervento e Agibilità per Edifici Ordinari nell'Emergenza Post-sismica*, Servizio Sismico Nazionale e Gruppo Nazionale per la Difesa dai Terremoti. (In Italian).
- Baker, J. W. and Cornell, C.A. (2005). A vector-valued ground motion intensity measure consisting of spectral acceleration and epsilon. *Earthquake Engineering and Structural Dynamics*, **34**:1193-1217.
- Balbi, A., Frumento, S. and Penna, A. (2004). Una procedura integrate peer la valutazione della vulnerabilità sismica degli edifice scolastici. *Proceedings of the XI Congresso Nazionale ANIDIS L'ingegneria Sismica in Italia*, Genova. (In Italian).
- Ballio, G., Lagomarsino, S., Picardo, G. and Solari, G. (1999). Probabilistic analysis of Italian extreme winds: reference velocity and return criterion. *Wind and Structures*, **2(1)**: 51-68.
- Bartoli, G., Ricciardelli, F. and Solari, G. (2011). Historical evolution of Italian regulations on wind actions on structures and its implications on the design of steel structures. *Proceedings of the XXIII Congresso CTA: Le Giornate Italiane dell'Acciaio*, Ischia 9-12/10/2011, Italy. (In Italian).
- Basili, R., Kastelic, V., Valensise, G. and DISS Working Group (2009). *DISS3 tutorial series: Guidelines for compiling records of the Database of Individual Seismogenic Sources, version 3*. Rapporti Tecnici INGV, No. 108, 20.
- Bazzurro, P. and Cornell, C.A. (1999). Disaggregation of Seismic Hazard. *Bulletin of the Seismological Society of America*, **89(2)**: 501-520.
- Benedetti, D. and Petrini, V. (1984). On seismic vulnerability of masonry buildings: proposal of an evaluation procedure. *L'industria delle Costruzioni*, **18**: 67-68. (In Italian).

- Bernardini, A., Gori, R. and Modena, C. (1990). *Application of Coupled Analytical Models and Experimental Knowledge to Seismic Vulnerability Analyses of Masonry Buildings*. In Engineering Damage Evaluation and Vulnerability Analysis of Building Structures, A. Koridze, Omega Scientific, Oxon, U.K.
- Bernardis, G., Giorgetti F., Nieto, D. and Slejko, D. (1977). *Earthquakes Catalogue for Eastern Alps Region*. OGS, Trieste, computer printout. (In Italian).
- Bommer, J.J. (2002). Deterministic vs. probabilistic seismic hazard assessment: an exaggerated and obstructive dichotomy. *Special Issue Journal of Earthquake Engineering*, **6(1)**: 4373pp.
- Bommer, J.J., Abrahamson, N.A. (2006). Why do modern probabilistic seismic-hazard analyses often lead to increased hazard estimates?. *Bulletin of the Seismological Society of America*, **96**: 1967-1977.
- Bommer, J.J., and Alarcon, J.E. (2006). The prediction and use of peak ground velocity. *Journal of Earthquake Engineering*, **10(1)**: 1-31.
- Borzi, B., Calvi, G.M., Elnashai, A.S., Faccioli, E. and Bommer, J. (2001). Inelastic Spectra for Displacement-Based Seismic Design. *Soil Dynamics and Earthquake Engineering*, **21(3)**: 47-61.
- Borzi, B., Pinho, R. and Crowley, H. (2007). Simplified Pushover-Based Vulnerability Analysis for Large Scale Assessment of RC Buildings. *Engineering Structures*, **30(3)**: 804-820.
- Borzi, B., Crowley, H. and Pinho, R. (2008). Simplified pushover-based earthquake loss assessment (SP-BELA) method for masonry buildings. *International Journal of Architectural Heritage*, **2(4)**: 353-376.
- Borzi, B., Ceresa, P., Faravelli, M., Fiorini, E. and Onida, M. (2011). Definition of a prioritisation procedure for structural retrofitting of Italian school buildings. *Proceedings of the 3rd ECCOMAS Thematic Conference on Computation Methods in Structural Dynamics and Earthquake Engineering*, Corfu, Grecia, 25-28 May.
- Boschi, E., Ferrari, G., Gasperini, P., Guidoboni, E., Smriglio, G. and Valensise, G. (eds.) (1995). *Catalogo dei forti terremoti in Italia dal 461 a.C. al 1980*. ING-SGA, Bologna, 970 pp.
- Bradley, B.A., Dhakal, R.P., Cubrinovski, M., MacRae, G.A. and Lee, D.S. (2009). Seismic loss estimation for efficient decision making. *Bulletin of the New Zealand Society of Earthquake Engineering*, **42(2)**: 96-110.
- Bradley, B.A. (2010). Epistemic uncertainties in component fragility functions. *Earthquake Spectra*. **26(1)**: 41-62.
- Braga F., Dolce M., Liberatore D. (1982). A statistical study on damaged buildings and an ensuing review of the MSK-76 scale. *Proceedings of the 7th European Conference on Earthquake Engineering*, Athens, Greece. pp. 431-450.

- Brencich, A. (2010). Collapse of an industrial steel shed: A case study for basic errors in computational structural engineering and control procedures. *Engineering Failure Analysis* **17**: 213-225.
- Calvi, G.M., (1999). A displacement-based approach for vulnerability evaluation of classes of buildings. *Journal of Earthquake Engineering*, **3(3)**: 411-438.
- Calvi, G.M., Pinho, R., Mangenes, G., Bommer, J.J., Restrepo-Vélez, L.F. and Crowley, H. (2006). Development of seismic vulnerability assessment methodologies over the past 30 years. *Journal of Earthquake Tecnology*, ISET, **43(3)**: 75-104.
- Capozzi, V. (2009). *Comportamento sismico dei collegamenti nelle strutture prefabbricate*. Ph.D. Thesis in seismic risk, University of Naples Federico II, Naples, Italy. (In Italian).
- Cardona, O.D. and Yamin, L.E. (1997). Seismic Microzonation and Estimation of Earthquake Loss Scenarios: Integrated Risk Mitigation Project of Bogotá, Colombia. *Earthquake Spectra*, **13(4)**: 795-814.
- Carrozzo, M.T., De Visintini, G., Giorgetti, F. and Iaccarino, E. (1973). *General Catalogue of Italian Earthquakes*, CNEN, RT/PROT(73)12, Roma, 225 pp. (In Italian).
- Carrozzo, M.T., Cosentino, M., Ferlito, A., Giorgetti, F., Patané, G. and Ruscetti, M. (1975). Earthquakes catalogue of Calabria and Sicily (1783-1973). *Quaderni della Ricerca Scientifica*, 93, 216 pp. (In Italian).
- CEN (2004) Comité Européen de Normalisation. European Standard EN 1998-1 Eurocode 8: *Design of structures for earthquake Resistance*. Part 1: General rules, seismic actions and rules for buildings, Brussels, Belgium.
- CEN (2005). Comité Européen de Normalisation. EN 1993-1-8, Eurocode 3: *Design of steel structures* – Part 1-8: Design of joints. European Committee for Standardization, Brussels.
- Chapman, H.E., Oakden, G.J. and Lauder, M.K (2000). Seismic screening of bridges in New Zealand. *Proceedings of the 12th World Conference on Earthquake Engineering*, Auckland, New Zealand, paper No. 2083.
- Chioccarelli, E., Iervolino, I. (2010). Near-source seismic demand and pulse-like records: A discussion for L'Aquila earthquake. *Earthquake Engineering and Structural Dynamics*. **39(9)**: 1039-1069.
- CNR (1981). Norme CNR-UNI 10012/81: Azioni sulle costruzioni. ROMA - CNR DI NORME TECNICHE RELATIVE ALLE COSTRUZIONI (In Italian).
- CNR (1985). Norme CNR-UNI 10012/85: Azioni sulle costruzioni. (In Italian).
- CNR-DT (2008). Istruzioni per la valutazione delle azioni e degli effetti del vento sulle costruzioni. (In Italian).
- CNR-UNI (1964). Norme CNR-UNI 10012/64: Ipotesi di carico sulle costruzioni. (In Italian).

- CNR–UNI (1967). Norme CNR-UNI 10012/67: Ipotesi di carico sulle costruzioni. (In Italian).
- Colombi M., Borzi B., Crowley H., Onida M., Meroni F. and Pinho R. (2008). Deriving vulnerability curves using Italian earthquake damage data. *Bulletin of Earthquake Engineering*, **6(3)**: 485-504.
- Comerio, M.C., Landis, J.D., Firpo, C.J. and Monzon, J.P. (1996). Residential Earthquake Recovery, California Policy Seminar, University of California, Berkeley
- Cornell, C.A. (1968). Engineering seismic risk analysis. *Bulletin of the Seismological Society of America*, **58**: 1583-1606.
- Cornell, C.A. (1996). Calculating Building seismic performance reliability: abasis for multilevel design norms. *Proceedings of the 11th World Conference in Earthquake Engineering*, Acapuco, Mexixo, Paren No. 612.
- Cornell, C. A., and Krawinkler, H. (2000). Progress and changelles in seismic performance assessment. PEER News, April 3(2).
- Cosenza, E., Manfredi, G., Polese, M. and Verderame, G.M. (2005). A Multi-Level Approach to the Capacity Assessment of Existing RC Buildings, *Journal of Earthquake Engineering*, **9(1)**: 1-22.
- Crowley H. and Pinho R. (2004). Period-height relationship for existing european reinforced concrete buildings. *Journal of Earthquake Engineering*, **8(1)**: 93-119.
- Crowley, H., Pinho, R. and Bommer, J.J. (2004). A probabilistic displacement-based vulnerability assessment procedure for earthquake loss estimation. *Bulletin of Earthquake Engineering*, **2**: 173-219.
- Crowley H., Pinho R., Bommer J.J. and Bird, J.F., (2006). *Development of a displacement-based method for earthquake loss assessment*. European school for advanced studies in reduction of seismic risk, ROSE Research Report No. 2006/01, IUSS Press, Pavia, Italy.
- Crowley, H., Colombi, M., Calvi, G.M., Pinho, R., Meroni, F. and Cassera, A. (2008). Application of a prioritisation scheme for seismic intervention in school buildings in Italy, *Proceedings of the Fourteenth World Conference on Earthquake Engineering*. October 12-17, 2008, Beijing, China.
- Crowley, H., Colombi, M., Borzi, B., Faravelli, M., Onida, M., Lopez, M., Polli, D., Meroni, F., and Pinho, R. (2009). A comparison of seismic risk maps for Italy. *Bulletin of Earthquake Engineering*, **7 (1)**: 149-180.
- CS.LL.PP. (2008). D.M. 14/01/2008, Norme Tecniche per le Costruzioni. G.U. della Repubblica Italiana, 29, 4 febbraio 2008. (In Italian).
- Cua, G., Wald, D.J., Allen, T.I., Garcia, D., Worden, C.B., Gerstenberger, M., Lin, K. and Marano, A. (2010). “Best Practises” for Using Macro seismic Intensity and Ground Motion-Intensity Conversion equations for hazard and Loss Models in GEM1. GEM Technical Report 2010-4, GEM Foundation, Pavia, Italy.

- Culver, C., Lew, H.S., Hart, G.C and Pinkham, C.W. (1975). *Natural hazards evaluation of existing buildings*. Building Science Series, National Bureau of Standards, Washington D.C.
- Daniell, J.E. (2009). *Comparison and procedure of open source earthquake loss assessment packages*. Master degree in earthquake and engineering seismology. European school for advanced studies in reduction of seismic risk (Rose School).
- Daniell, J.E., Khazai, B., Wenzel, F. and Vervaeck A. (2011). The CATDAT damaging earthquakes database. *Nat Hazards Earth Syst Sci*, **11**:2235–51.
- Daniell, J.E, Vervaeck, A. (2012) CEDIM earthquake loss estimation series *research report 2012-01*. Karlsruhe: CEDIM; 2012.
- Da Silva, L.S, Rebelo, C., Nethercot, D., Marques, L. Simoes, R. and Vila Real, P.M.M. (2009). Statistical evaluation of the lateral-torsional buckling resistance of steel I-beams, Part 2: Vulnerability os steel properties. *Journal of Constructional Steel Research*, ELSEVIER, **65**: 832-849.
- D’Ayala, D. and Speranza, E. (2002). An Integrated Procedure for the Assessment of Seismic Vulnerability of Historic Buildings. *Proceedings of the 12th European Conference on Earthquake Engineering*, London, U.K., Paper No. 561 (on CD).
- Della Corte, G., De Matteis, G., Landolfo, R. and Mazzolani, F.M. (2002). Seismic analysis of MR steel frames based on refined hysteretic models of connections. *Journal of Constructional Steel Research*, **58**: 1331-1345.
- Della Corte, G., Iervolino, I. and Petruzzelli, F. (2013). Structural modelling issues in seismic performance assessment of industrial steel buildings. *Proceedings of the 4th ECCOMAS Thematic Conference on Computational Methods in Structural Dynamics and Earthquake Engineering*, Kos Island, Greece, 12-14 June, 2013.
- De Matteis, G., Landolfo, R. and Mazzolani, F.M. (1999). Diaphragm effect for industrial steel buildings under earthquake loading. *Journal of Constructional Steel Research*, **46(1-3)**: 357-358.
- Di Pasquale, G., Fralleone, A., Pizza, A.G., and Serra, C. (1999a). *Synthesis of the code evolution from the Royal decree issued after the Messina and Reggio earthquake up to the first Ministry decree issued after the law n.64/74*. La classificazione e la normative sismica italiana dal 1909 al 1984, De Marco, R. and Martini, M.G., Istituto Poligrafico e Zecca dello Stato, Roma.
- Di Pasquale, G., Fralleone, A., Pizza, A.G. and Serra, C., (1999b). *Relevant changes to the Italian seismic Code from 1909 to 1975 – a synoptic table*. La classificazione e la normative sismica italiana dal 1909 al 1984, De Marco, R. and Martini, M.G., Istituto Poligrafico e Zecca dello Stato, Roma.
- Di Pasquale, G., Orsini, G. Severino, M. (2001). Modello di valutazione di un indice di rischio sismico per edifici. *Proceedings of the X Congresso Nazionale ANIDIS L’ingegneria sismica in Italia*, Potenza-Matera. (In Italian).

- Di Pasquale G., Orsini G. and Romero R.W. (2005). New developments in seismic risk assessment in Italy. *Bulletin of Earthquake Engineering*, **3(1)**: 101-128.
- DL 74/12 (2012). Decreto-Legge n.74 del 06/06/2012, Interventi urgenti in favore delle popolazioni colpite dagli eventi sismici che hanno interessato il territorio delle province di Bologna, Modena, Ferrara, Mantova, Reggio Emilia e Rovigo, il 20 e il 29 maggio 2012. (12G0096). G.U. della Repubblica Italiana n.131 del 07/06/2012. (In Italian).
- DM 40/75 (1975). Decreto Ministeriale n. 40 del 03/03/1975, Approvazione delle norme tecniche per le costruzioni in zone sismiche. G.U. della Repubblica Italiana n. 93 dell'08/04/1975. (In Italian).
- DM 3/10/1978 (1978). Decreto Ministeriale del 3/10/1978, Criteri generali per la verifica della sicurezza delle costruzioni e dei carichi e sovraccarichi. G.U della Repubblica Italiana n.319 del 15/11/1978. (In Italian).
- DM 515/81 (1981). Decreto Ministeriale n. 515 del 03/06/1981, Classificazione a bassa sismicità $S = 6$ del territorio dei Comuni delle Regioni Basilicata, Campania e Puglia. G.U. della Repubblica Italiana n. 162 del 15/06/1981. (In Italian).
- DM 12/02/1982 (1982). Decreto Ministeriale del 12/02/1982, Aggiornamento delle Norme Tecniche relative ai Criteri generali per la verifica della sicurezza delle costruzioni e dei carichi e sovraccarichi. G.U della Repubblica Italiana n.56 del 26/02/1982 (In Italian).
- DM 208/84 (1984) Decreto Ministeriale del 19/06/1984, Norme tecniche per le costruzioni in zone sismiche,” G.U. della Repubblica Italiana n.208 del 30/07/1984. (In Italian).
- DM 24/01/1986 (1986). Decreto Ministeriale dei Lavori Pubblici del 24/01/1986, Norme Tecniche relative alle Costruzioni antisismiche. G.U. della Repubblica Italiana n.108 del 12/05/1986. (In Italian).
- DM. 16/01/1996 (1996a) Decreto Ministeriale del 16/01/1996, Norme tecniche per le costruzioni in zone sismiche. G.U. della Repubblica Italiana n. 29 del 05/02/1996. (In Italian).
- DM 16/01/1996 (1996b) Decreto Ministeriale del 16/01/1996, Norme tecniche relative ai criteri generali per la verifica di sicurezza delle costruzioni e dei carichi e sovraccarichi. G.U. della Repubblica Italiana n. 29 del 05/02/1996. (In Italian).
- Dolce M., Zuccaro G., Kappos A. and Coburn A. (1994). Report of the EAEE Working Group 3: Vulnerability and risk analysis. *Proceedings of 10th European Conference on Earthquake Engineering*, Vienna, Vol. 4, pp. 3049-3077.
- Dolce, M., Masi, A., Marino, M. and Vona, M. (2003). Earthquake Damage Scenarios of the Building Stock of Potenza (Southern Italy) Including Site Effects. *Bulletin of Earthquake Engineering*, **1(1)**: 115-140.
- Dowell, R.K., Seible, F.S. and Wilson, E.L. (1998). Pivot hysteretic model for reinforced concrete members. *ACI Structural Journal*, **95**: 607–617.

- DPC Dipartimento Protezione (1999). *LSU-1 Project: Censimento di Vulnerabilità degli Edifici Pubblici, Strategici e Speciali nella Regione Abruzzo, Basilicata, Calabria, Campania, Molise, Puglia e Sicilia*. Dipartimento della Protezione Civile, Rome. (In Italian).
- DPC Dipartimento Protezione Civile (2000). *Censimento di Vulnerabilità dell'Edilizia Corrente dei Centri Abitati, nelle Regioni Abruzzo, Calabria, Campania, Molise, Puglia e Sicilia*. Dipartimento della Protezione Civile, Rome. (In Italian).
- Dumova-Javanoska, E. (2000). Fragility curves for reinforced concrete structures in Skopje (Macedonia) region. *Soil Dynamics and Earthquake Engineering*, **19(6)**:455-466.
- Dumova-Jovanoska, E. (2004). Fragility Curves for RC Structures in Skopje Region, *Proceedings of the 13th World Conference on Earthquake Engineering*, Vancouver, Canada, Paper No. 3 (on CD).
- Eberhard, M.O., Mookerjee, A. and Parrish, M. (2001). *Uncertainties in Performance Estimates for RC Columns*. Richmond, CA: Pacific Earthquake Engineering Research Center <http://ce.washington.edu/~peera1>.
- ENEL (1977). *Catalogo dei terremoti italiani dall'anno 1000 al 1975*. Compilato da Geotecneco Spa, Roma, computer printout. (In Italian).
- Fabbrocino ,G., Iervolino I., Manfredi, G. and Salzano, E. (2004) Seismic early warning systems for the process industry. *Proceedings of 2nd International Conference on Structural Health Monitoring of Intelligent Infrastructure*, 16-18 November 2005,. Shenzhen (P.R. of China).
- Faccioli, E., Pessina, V., Calvi, G.M. and Borzi, B. (1999). A study on damage scenarios for residential buildings in Catania city. *Journal of Seismology*, **3(3)**: 327-343.
- Faccioli, E. and Pessina, V. (2000). *The Catania project: earthquake damage scenarios for a high risk area in the Mediterranean*. CNR-Gruppo Nazionale per la Difesa dai Terremoti, Rome, Italy.
- Faella, C., Piluso and V. Rizzano, G. (1999). *Structural steel semirigid connections-Theory, design and software*. CRC Press.
- Faenza, L. and Michelini, A. (2010). Regression analysis of MCS intensity and ground motion parameters in Italy and its application in Sakemaps. *Geophysical Journal International*, **180**:113-1152.
- Fah, D., Kind, F., Lang, K. and Giardini, D. (2001). Earthquake Scenarios for the City of Basel, *Soil Dynamics and Earthquake Engineering*, **21(5)**: 405-413.
- FEMA (2001). *HAZUS99 Estimated Annualized Earthquake Loss for the United State*. Report FEMA 366, Federal Emergency Management Agency, Washington, DC, U.S.A.
- Franchin, P., Pinto, P. E., and Pathmanathan, R. (2008) Assessing the adequacy of a single confidence factor in accounting for epistemic uncertainty. *Convegno*

- RELUIS: Valutazione e riduzione della vulnerabilità sismica di edifici esistenti in cemento armato*, Roma 29–30 maggio. (In Italian).
- Freeman, S.A., Nicoletti, J.P., and Tyrell, J.V. (1975). Evaluation of existing buildings for seismic risk - A case study of Puget Sound Naval Shipyard Bremerton, Washington. *Proceedings of the U.S. National Conference on Earthquake Engineering*, Berkeley, California, U.S.A., pp. 113-122.
- GdL (1999) Gruppo di Lavoro CPTI. *Catalogo Parametrico dei Terremoti Italiani*, versione 1 (CPTI99). INGV, Bologna. <http://emidius.mi.ingv.it/CPTI/>.
- Giardini, D., Grünthal, G., Shedlock, K. M. and Zhang, P. (1999). The GSHAP Global Seismic Hazard Map. *Annali di Geofisica* **42 (6)**: 1225-1228.
- Giorgetti, F. and Iaccarino, E. (1971). Italian Earthquake Catalogue from the Beginning of the Christian Age up to 1968. *Boll. Geof. Teor. Appl.*, XIII, 113 pp. (In Italian).
- Giovinazzi, S. and Lagomarsino, S. (2001). Una metodologia per l'analisi di vulnerabilità sismica del costruito. *X Congresso Nazionale L'ingegneria Sismica in Italia*, Potenza-Matera. (In Italian).
- Giovinazzi, S. and Lagomarsino, S. (2004). A Macro seismic Method for the Vulnerability Assessment of Buildings. *Proceedings of the 13th World Conference on Earthquake Engineering*, Vancouver, Canada, Paper No. 896 (on CD).
- Giovinazzi, S. (2005). *The Vulnerability Assessment and the Damage Scenario in Seismic Risk Analysis*, PhD Thesis, Technical University Carolo-Wilhelmina at Braunschweig, Braunschweig, Germany and University of Florence, Florence, Italy.
- Giovinazzi, S., and Lagomarsino, S. (2006) Vulnerability Methods and Damage Scenario for Seismic Risk Analysis as Support to Retrofit Strategies: an European Perspective. *NZSEE Conference*. Paper No. 14.
- Glaister, S., Pinho, R., (2003). Development of a simplified deformation based method for seismic vulnerability assessment. *Journal of Earthquake Engineering*, **7(S11)**: 107-140.
- GNDT (1993). *Rischio sismico di edifici pubblici. Parte I: aspetti metodologici*. CNR-Gruppo Nazionale per la Difesa dai Terremoti, Rome, Italy.
- Gòmes Capera, A.A., Meletti, C., Rebez, A. and Stocchi, M. (2007). *Mappe di pericolosità sismica in termini di intensità macrosismica utilizzando lo stesso impianto metodologico di MPS04*. Progetto INGV-DPC S1. Deliverable D7 <http://esse1.mi.ingv.it/d7.html>.
- Grant, D., Bommer, J.J., Pinho, R. and Calvi, G.M. (2006). *Defining priorities and timescales for seismic intervention in school buildings in Italy*. ROSE Research Report No. 2006/03, IUSS Press, Pavia, Italy.

- Grant, D.N., Bommer, J.J., Pinho, R., Calvi, G.M., Goretti, A. and Meroni, F. (2007). A prioritization scheme for seismic intervention in school buildings in Italy. *Earthquake Spectra*, **23(2)**: 291-314.
- Grases, J., Cascante, G. and Gajardo, E. (1992). *Proceeding of the Tenth World Conference on Earthquake Engineering*, Madrid, Vol.1, pp. 5777-5782.
- Grünthal, G. (1998). *Cahiers du Centre Européen de Géodynamique et de Séismologie: Volume 15 – European Macroseismic Scale 1998*. European Center for Geodynamics and Seismology, Luxembourg.
- Gulkan, P. and Sozen, M.A. (1977). Inelastic response of reinforced concrete structures to earthquake motions. In: *Reinforced Concrete Structures in Seismic Zone*, SP-53, American Concrete Institute (ACI), Detroit, U.S.A., pp 109-115 (reprinted from *journal of the American Concrete Institute*, **71(12)**: 604-610, 1974).
- Gupta, B. and Krawinkler, H. (1999). *Seismic demands for performance evaluation of steel moment resisting frame structures (SAC Task 5.4.3)*. Report No. 132, The John A. Blume Earthquake Engrg.Ctr., Stanford University, Stanford, California, U.S.A.
- Gupta, A. and Krawinkler, H. (2000). Estimation of seismic drift demands for frame structures. *Earthquake Engineering and Structural Dynamics*, **29(9)**:1287-1305.
- Hassan, A.F. and Sozen, M.A., (1997). Seismic vulnerability assessment of low-rise buildings in regions with infrequent earthquakes. *ACI Structural Journal*, **94(1)**: 31-39
- HAZUS (2003). *HAZUS-MH@MR4 Technical Manual*, Federal Emergency Management Agency (FEMA).
- Holmes, W.T., (2002). Background and history of the seismic hospital program in California. *Proceedings of the Seventh U.S. National Conference on Earthquake Engineering*. Boston, Massachusetts.
- Hoover, C.A. (1992). *Seismic Retrofit Policies: An evaluation of Local Practices in Zone 4 and their Application to Zone 3*. Oakland, California, EERI.
- Holzer, T.L. and Savage, J.C. (2013). Global earthquake fatalities and population. *Earthquake Spectra*, **29(1)**: 155-175.
- Ibarra L. F., Krawinkler H. (2005). *Global collapse of frame structures under seismic excitations*. Report No. 152, The John A. Blume Earthquake Engineering Center, Department of Civil and Environmental Engineering, Stanford University.
- ICC (2012) International Code Council 2012 *International Building Code (IBC-2012)*, United States.
- IEG Independent Evaluation Group (2007). *Development actions and the rising incident of disasters*, Washington, DC: The World Bank.
- Iervolino, I. Fabbrocino, G. and Manfredi, G. (2004). Fragility of standard industrial structures by a response surface based method. *Journal of Earthquake Engineering*, **8**: 927-946

- Iervolino, I., Manfredi, G., Polese, M., Verderame, G.M. and Fabbrocino G. (2007). Seismic risk of R.C. building classes. *Engineering Structures*, **29(5)**:813-820.
- Iervolino, I., Galasso, C. and Cosenza, E., (2010). REXEL: computer aided record selection for code-based seismic structural analysis. *Bulletin of Earthquake Engineering*, **8**: 339-362.
- Iervolino, I., Zollo, A., Erdik, M. (2011) Foreword to: Prospects and applications of earthquake early warning. *Soil Dynamics and Earthquake Engineering*. **31(2)**: 105.
- Iervolino I. and Petruzzelli, F. (2011). NODE v.1.0 beta: attempting to prioritize large-scale seismic risk of engineering structures on the basis of nominal deficit. *Proceedings of XIV Convegno ANIDIS 2011*, 18-22/11/11, Bari.
- ING (1981). *Catalogo dei terremoti italiani dal 1450 a.C. al 1980*. Rapporto interno, Roma.
- INGV-DPC S1 (2007). *Progetto S1. Proseguimento della assistenza al DPC per il completamento e la gestione della mappa di pericolosità sismica prevista dall'Ordinanza PCM 3274 e progettazione di ulteriori sviluppi*. Istituto Nazionale di Geofisica e Vulcanologia – Dipartimento della Protezione Civile.
- Jain, SK, Jennings, PC. (1985). Analytical models for low-rise buildings with flexible roof diaphragms. *Earthquake Engineering and Structural Dynamics*, **13**: 225–41.
- Jalayer, F. (2003). *Direct probabilistic seismic analysis: implementing non-linear dynamic assessments*. Ph.D Thesis, Department of Civil and Environmental Engineering, Stanford University, Stanford, California.
- Jalayer, F., Franchin, P. and Pinto, P.E. (2007). A scalar decision variable for seismic reliability analysis of RC frames. *Special issue of Earthquake Engineering and Structural Dynamics on Structural Reliability*, **36 (13)**: 2050-2079, June 2007.
- Jalayer F., and Cornell C. A. (2009). Alternative nonlinear demand estimation methods for probability-based seismic assessments. *Earthquake Engineering and Structural Dynamics*, **38**: 951-972.
- Jalayer, F., Iervolino, I. and Manfredi, G. (2010). Structural modeling uncertainties and their influence on seismic assessment of existing r.c. structures. *Structural Safety*, **32(3)**: 220-228.
- Jalayer, F., Elefante, L., Iervolino, I., Manfredi, G. (2011). Knowledge-based Performance Assessment of Existing RC Buildings. *Journal of Earthquake Engineering* **15(3)**: 362-389.
- Jaspart, J.P. (2000). General report: session on connections. *Journal of Constructional Steel Research* **55**: 69–89.
- JBDPA (1990). *Standard for seismic capacity assessment of existing reinforced concrete buildings*. Japanese Building Disaster Prevention Association, Ministry of Construction, Tokyo, Japan.
- Jeiswal, K. and Wald, D.J. (2013). Estimating Economic Losses from Earthquakes Using an Empirical Approach. *Earthquake Spectra*, **29(1)**: 309-324.

- Kanvinde, A.M. (2003). Methods to evaluate the dynamic stability of structures – Shake table tests and nonlinear dynamic analyses. (*EERI paper competition winner*), *Proceedings of EERI Meeting*, Portland, February.
- Kappos, A.J., Ptilakis, K. and Stylianidis, K.C. (1995). Cost-Benefit Analysis for the Seismic Rehabilitation of Buildings in Thessaloniki, Based on a Hybrid Method of Vulnerability Assessment, *Proceedings of the Fifth International Conference on Seismic Zonation*, Nice, France, Vol. 1, pp. 406-413.
- Kappos, A.J., Stylianidis, K.C. and Ptilakis, K. (1998). Development of Seismic Risk Scenarios Based on a Hybrid Method of Vulnerability Assessment, *Natural Hazards*, **17(2)**: 177-192.
- Kappos, A.J., Panagopoulos, G., Panagopoulos, C., Penelis, G. (2006) A hybrid method for the vulnerability assessment of RC and URM buildings. *Bulletin of Earthquake Engineering*. **4**: 391-413.
- Kilar, V. and Fajar, P. (1997). Simplified push-over analysis of asymmetric buildings. *Earthquake Engineering and Structural Dynamics*, **26(2)**: 233-249.
- Kilar, V. and Fajar, P. (2001). On the application of pushover analysis to the seismic performance evaluation of asymmetric buildings. *European Earthquake Engineering*, **15(1)**: 10-31.
- Kircher, C.A., Nassar, A.A., Kustu, O., Holmes, W.T. (1997a). Development of building damage functions for earthquake loss estimation. *Earthquake Spectra*, **13(4)**: 663-682.
- Kircher, C.A., Reitherman, R.K., Whitman, R.V., Arnold, C. (1997b). Estimation of earthquake losses to buildings. *Earthquake Spectra*, **13(4)**: 703-720.
- Kostov, M., Vaseva, E., Kaneva, A., Koleva, N., Varbanov, G., Stefanov, D., Darvarova, E., Solakov, D., Simeonova, S. and Cristockov, L. (2004). *Application to Sofia*. Report RISK-UE WP13.
- Kramer, S.L. (1996). *Geotechnical Earthquake Engineering*. Prentice-Hall, Upper Saddle River, New Jersey, U.S.A.
- Krawinkler, H. (1995). New trends in seismic design methodology. *Proceedings of the 10th European Conference on Earthquake Engineering*, Balkema, Rotterdam, The Netherlands, Vol. 2, pp. 821-830.
- Krawinkler, H. and Miranda, E. (2004). *Performance-based earthquake engineering, Earthquake Engineering: From Engineering Seismology to Performance-Based Engineering*. Chapter 9, pp. 9-1 to 9-59.
- Krawinkler, H. (2005). *Van Nuys Hotel Building Testbed Report: Exercising Seismic Performance Assesment*. Paper No. PEER 2005/11 Pacific Earthquake Engineering Research Center. Department of Civil and Environmental Engineering Stanford University.
- L 122/12 (2012). Legge n. 122 del 1/08/2012, Conversione in legge, con modificazioni, del decreto-legge 6 giugno 2012, n. 74, recante interventi urgenti in favore delle popolazioni colpite dagli eventi sismici che hanno interessato il

- territorio delle province di Bologna, Modena, Ferrara, Mantova, Reggio Emilia e Rovigo, il 20 e il 29 maggio 2012. (12G0148) G.U. della Repubblica Italiana n.180 del 03/08/2012. (In Italian).
- L 1684/62 (1962). Legge n.1684 del 25/11/1962, Provvedimenti per l'edilizia, con particolari prescrizioni per le zone sismiche. Supplemento Ordinario n. 1 alla G.U. della Repubblica Italiana n. 326 del 22/12/1962. (In Italian).
- L 1684/62 (1962). Legge n.1684 del 25/12/1962, Provvedimenti per l'edilizia, con particolari prescrizioni per le zone sismiche. Supplemento Ordinario n.1 alla G.U. della Repubblica Italiana n. 326 del 22/12/1962. (In Italian).
- L 64/74 (1974). Legge n.64 del 02/02/1974, Provvedimenti per le costruzioni con particolari prescrizioni per le zone sismiche. G.U. della Repubblica Italiana n. 76 del 21/3/1974. (In Italian).
- Lanzo, G. and Silvestri, F. (1999). *Risposta sismica locale*. Hevelius Edizioni, Benevento, Italy. (In Italian).
- LESSLOSS (2005). *Report on Building Stock Data and Vulnerability Data for each Case Study*. Deliverable 84.
- Liel, L.B. and Lynch, K.P. (2009). *Vulnerability and reinforced concrete frame buildings and their occupants in the 2009 L'Aquila, Italy earthquake*. University of Colorado, Natural Hazards Center.
- Lignos, D.G., Krawinkler, H. and Whittaker, A.S. (2008). Shaking table collapse tests of two scale models of a 4-story moment resisting steel frame. *Proceedings of the 14th World Conference on Earthquake Engineering*, October 12-17, Beijing, China.
- M.LL.PP. (1996). Circolare del Ministero dei Lavori Pubblici n.156 del 4/7/1996, Istruzioni per l'applicazione delle Norme tecniche relative ai criteri generali per la verifica di sicurezza delle costruzioni e dei carichi e sovraccarichi di cui al Decreto Ministeriale 16 gennaio 1996. G.U. della Repubblica Italiana. (In Italian).
- M.LL.PP. (1997). Circolare del Ministero dei Lavori Pubblici n. 65 del 10/04/1997 Istruzioni per l'applicazione delle Norme tecniche per le costruzioni in zone sismiche di cui al Decreto Ministeriale 16 gennaio 1996. G.U. della Repubblica Italiana n. 97 del 28/04/1997. (In Italian).
- Mac Rae, G.A. and Kawashima, K. (1997), Post Earthquake Residual Displacements of Bilinear Oscillators, *Earthquake Engineering and Structural Dynamics*, **26**: 701-716.
- Magliulo, G., Ercolino, M., Petrone, C., Coppola, O. and Manfredi, G. (2012). The influence of connections on the seismic response exhibited by precast structures during Emilia earthquake. *Progettazione Sismica*, **3(4)**: 121-130. (In Italian).
- Mahin, S.A., Bardero, V.V. (1975). *An evaluation of same method for predicting seismic behaviour of reinforced concrete buildings*. Report No. EERC 75/05. Earthquake Engineering Research Center, University of California, Berkeley, California, U.S.A.

- Margottini, C., Molin, D. and Serva, L. (1992). Intensity versus ground motion: A new approach using Italia data. *Engineering Geology*, **33**: 45-58.
- Mastrogiuseppe, S., Rogers, C.A., Tremblay, R. and Nedisan, C.D. (2008). Influence of nonstructural components on roof diaphragm stiffness and fundamental periods of single storey steel buildings. *Journal of Constructional Steel Research*, **64**: 214-227.
- McGuire, R.K. (2001). Deterministic vs. probabilistic earthquake hazards and risks. *Soil Dynamics and Earthquake Engineering*, **21**: 377-384.
- McGuire, R.K. (2004). *Seismic Hazard and Risk Analysis*. EERI Monograph No. 10.
- Medina, R., and Krawinkler, H. (2003). Global collapse of frame structures under seismic excitations. *Report No. PEER 2003/15*, Pacific Earthquake Engineering Research Center, University of California at Berkeley, Berkeley, California.
- Medvedev, S. and Sponheuer, W. (1969). MSK Scale of Seismic Intensity. *Proceeding of Fourth World Conference of Earthquake Engineering*, Santiago, Chile Vol.1 p.A2.
- Maireless, H., Pinho, R., Bento, R. and Antoniou, S. (2006). Verification of an adaptive pushover technique for the 3D case. *Proceedings of the 1st European Conference on Earthquake Engineering and Seismology*, Geneva, Switzerland, Paper No. 619.
- Meletti, C., Patacca, E. and Scandone, P. (2000). Construction of a seismotectonic model: the case of Italy. *Pageoph*, **157**: 11-35.
- Meletti, C. and Montaldo, V. (2007). *Stime di pericolosità sismica per diverse probabilità di superamento in 50 anni: valori di ag*. Progetto INGV-DPC S1, Deliverable D2, <http://esse1.mi.ingv.it/d2.html>. (In Italian).
- Miranda, E. and Akkar, S., (2003). Dynamic instability of simple structural systems. *Journal of Structural Engineering*, ASCE, **129(12)**: 1722-1726.
- Miranda, E., and Aslani, H. (2003). *Probabilistic response assessment for building-specific loss estimation*. Report No. *PEER 2003/03*, Pacific Earthquake Research Center, Richmond, California.
- Mitrani-Reiser, J., (2007). *An ounce of prevention: probabilistic loss estimation for performance-based earthquake engineering*. Thesis, California Institute of Technology, Pasadena, California.
- Moehle, J.P. and Deierlein, G.G. (2004). A framework for performance-based earthquake engineering. *Proceeding of 13th World Conference on Earthquake Engineering*, Canadian Association for Earthquake Engineering under auspices of International Association of Earthquake Engineering, Vancouver, Canada, Paper No. 679.
- Montaldo, V. and Meletti, C., (2007). *Valutazione del valore della ordinata spettrale a 1sec e ad altri periodi di interesse ingegneristico*. Progetto DPC-INGV S1, Deliverable D3, <http://esse1.mi.ingv.it/d3.html>.

- Monti, G. and Alessandri, S. (2008). Confidence factors for concrete and steel strength. *Convegno RELUIS: Valutazione e riduzione della vulnerabilità sismica di edifici esistenti in cemento armato*, Roma 29–30 Maggio 2008. (In Italian).
- Mosalam, K.M., Ayala, G., White, R.N. and Roth, C. (1997). Seismic Fragility of LRC Frames with and without Masonry Infill Walls. *Journal of Earthquake Engineering*, **1(4)**: 693-720.
- Mouroux P. and Le Brun B. (2006). Presentation of RISK-UE project. *Bulletin of Earthquake Engineering*, **4(4)**: 323-339.
- MunichRe (2012). Earthquake, flood, nuclear accident. *Topics GEO*, Issue 2012: Natural catastrophes 2011, Analyses, assessments, positions.
- Murphy, J.R. and O'Brien, L.J. (1977) The correlation of peak ground acceleration amplitude with seismic intensity and other physical parameters. *Bulletin of Seismological Society of America*. **67(3)**: 877-915.
- Musson, R.W., and Gruntal, G. (2010). The comparison of macroseismic intensity scales. *Journal Seismology*. **14**:413-428.
- Mwafy, A.M. and Elnashai, A. S. (2002). Calibration of force reduction factors of RC buildings. *Journal of Earthquake Engineering*, **6(2)**: 239-273.
- NZSEE (2003). *Assessment and improvement of the structural performance of buildings in earthquakes [draft]*. New Zealand Society for Earthquake Engineering, Wellington, New Zealand.
- OPCM 3274 (2003). Ordinanza del Presidente del Consiglio dei Ministri n. 3274 del 20/03/2003, Primi elementi in materia di criteri generali per la classificazione sismica del territorio nazionale e di normative tecniche per le costruzioni in zona sismica. G.U. della Repubblica Italiana n. 105 dell'8/5/2003. (In Italian).
- OPCM 3431 (2005). Ordinanza del Presidente del Consiglio dei Ministri n. 3431 del 03/5/2005, Ulteriori modifiche ed integrazioni all'ordinanza del Presidente del Consiglio dei Ministri n. 3274 del 20 marzo 2003. G.U. della Repubblica Italiana n.107 del 10/5/2005. (In Italian).
- OPCM 3519 (2006). Ordinanza del Presidente del Consiglio dei Ministri n. 3519 del 28/04/2006, Criteri generali per l'individuazione delle zone sismiche e per la formazione e l'aggiornamento degli elenchi delle medesime zone. G.U. della Repubblica Italiana n. 108 del 11/05/06. (In Italian).
- Orsini G., (1999). A model for buildings' vulnerability assessment using the Parameterless Scale of Seismic Intensity (PSI). *Earthquake Spectra*, **15(3)**: 463-483.
- Ozdemir, P., Boduroglu, M.H., Ilki, A., (2005). Seismic safety screening method. *Proceedings of the International Workshop on Seismic Performance Assessment and Rehabilitation of Existing Buildings (SPEAR)*, Ispra, Italy, April 4-5. Paper No. 23.
- Pagni, C.A. and Lowes, L.N. (2006). Fragility Functions for Older Reinforced Concrete Beam-Column Joints. *Earthquake Spectra*, **22(1)**: 215-238.

- Pampanin, S., Christopoulos, C. and Priestley, M.J.N. (2002). Residual Deformations in the Performance Based Seismic Assessment of Frame Structures, *Research Report ROSE-2002/02*, University of Pavia, Pavia, Italy.
- Pampanin, S., Christopoulos, C. and Priestley, M.J.N. (2003). Performance-Based Seismic Response of Frame Structures Including Residual Deformations. Part II: Multi-Degree-of-Freedom Systems. *Journal of Earthquake Engineering (JEE)*, **7(1)**: 119-147.
- Pampanin, S., Christopoulos, C., Chen, T-H., (2006). Development And Validation of a Metallic Haunch Seismic Retrofit Solution for Existing Under-Designed RC Frame Buildings. *Earthquake Engineering and Structural Dynamics*, **35**: 1739-1766.
- Parisi, F. (2010). *Non-linear seismic analysis of masonry buildings*, Ph.D. Thesis in Seismic Risk, University of Naples Federico II, Naples, Italy.
- Parisi, F., Augenti, N. (2013). Earthquake damages to cultural heritage constructions and simplified assessment of artworks. *Engineering Failure Analysis*, doi: j.engfailanal.2013.01.005.
- Park, Y-J. and Ang, A.H-S. (1985). Mechanistic Seismic Damage Model for Reinforced Concrete. *Journal of Structural Engineering*. **111(4)**: 722-739.
- PCI Precast/Prestressed Concrete Institute (2010) *PCI Design Handbook precast and prestressed concrete*, 7th Edition, Helmuth Wilden, P. E., FPCI.
- Penelis, G.G., and Kappos, A.J. (2002). 3-D pushover analysis: The issue of torsion. *Proceedings of the 12th European Conference on Earthquake Engineering*, London, U.K., Paper No. 15.
- Perruzza, L. (2005). Probable shakings in Italy in 50 years since 2003: trials, perspectives and limitations for the 3rd generation seismic hazard maps. *Bollettino di Geofisica Teorica e Applicata*.
- Petersen, M.D., Frankel, A.D., Harmsen, S.C., Mueller, C.S., Haller, K.M., Wheeler, R.L., Wesson, R.L., Zeng, Y., Boyd, O.S., Perkins, D. M., Luco, N., Field, E.H., Wills, C.J. and Rukstales, K. S., (2008), *Documentation for the 2008 Update of the United States National Seismic Hazard Maps*, U.S. Geological Survey Open-File Report 2008-1128, 61 pp.
- Petruzzelli, F., Jalayer, F., Iervolino, I. and Manfredi, G. (2010) Optimal Programming of In-situ Tests and Inspections for Existing Buildings. *Proceedings of 14th European Conference on Earthquake Engineering*, Ohrid, Republic of Macedonia, August 29 – September 4.
- Petruzzelli F, Della Corte G. and Iervolino, I. (2012a). Seismic Risk Assessment of an Industrial Steel Building. Part 1: Modelling and Analysis. *Proceedings of the 15th World Conference on Earthquake Engineering*, Lisboa, PT, Paper No.3086;
- Petruzzelli F, Della Corte G., Iervolino I. (2012b). Seismic Risk Assessment of an Industrial Steel Building. Part 2: Fragility and failure Probabilities. *Proceedings of the 15th World Conference on Earthquake Engineering*, Lisboa, PT, Paper No.3088;

- Petruzzelli F., Della Corte G. and Iervolino, I. (2011a). Modelli e analisi preliminari di edifici industriali esistenti in acciaio per la valutazione del rischio sismico. *Proceedings of the XXIII Congresso CTA Le giornate Italiane della Costruzione in Acciaio*, 9-12 ottobre 2011, Lacco Ameno, Ischia (NA) (In Italian)
- Petruzzelli F., Della Corte G. and Iervolino, I. (2011b). Rischio sismico di edifici industriali esistenti in acciaio: un caso studio. *Proceedings of the XIV Convegno ANIDIS 2011*, 18-22/11/11, Bari (In Italian).
- Pinho, R., Bomber, J.J. and Glaister, S., (2002). A simplified approach to displacement-based earthquake loss estimation analysis. *Proceedings of the 12th European Conference on Earthquake Engineering*, London, UK, September 9-13. Paper No. 738.
- Pitilakis, K., Gazepis, C. and Anastasiadis, A. (2004). Design response spectra and soil classification for seismic code provisions. *Proceedings of 13th World conference on Earthquake Engineering*. Vancouver, B.C., Canada. August 1/6/2004. Paper No. 2904.
- Polese, M. (2002). *Un approccio a Doppio Livello per la valutazione della Vulnerabilità Sismica delle Strutture in C.A.* Ph.D Thesis in Structural Engineering. Università degli Studi di Napoli Federico II. (In Italian).
- Porter, K. A., Kiremidjian, A. S. and Le Grue, J. S. (2001). Assembly-Based Vulnerability for Buildings and Its Use in Performance Evaluation. *Earthquake Spectra*, **17 (2)**: 291-312.
- Porter, K.A. (2002). *Preliminary EDP List*. Richmond, CA: Pacific Earthquake Engineering Research Center, www.peertestbeds.net/Crosscutting.htm.
- Porter, K.A., (2003). An overview of PEER's performance-based earthquake engineering methodology. *Proceeding of Ninth International Conference on Applications of Statistics and Probability in Civil Engineering*. San Francisco, California.
- Porter, K., Kennedy, R. and Bachman, R. (2007). Creating Fragility Functions for Performance-based Earthquake Engineering. *Earthquake Spectra*. **23(2)**: 471-489
- Postpischl, D. (ed.), (1985). *Catalogo dei terremoti italiani dall'anno 1000 al 1980*. Quaderni della Ricerca Scientifica, 114, 2B, Bologna, 239 pp.
- Priestley, M.J.N., 1997. Displacement-based seismic assessment of reinforced concrete buildings. *Journal of Earthquake Engineering*, **1(1)**: 157-192.
- RD 193/09 (1909). Regio Decreto n.193 del 18/04/1909, Norme tecniche ed igieniche obbligatorie per le riparazioni ricostruzioni e nuove costruzioni degli edifici pubblici e privati nei luoghi colpiti dal terremoto del 28 dicembre 1908 e da altri precedenti elencati nel R.D. 15 aprile 1909. G.U del Regno d'Italia n.95 del 22/04/1909. (In Italian).
- RDL 573/15 (1915). Regio Decreto Legge n. 573 del 29/04/1915 che riguarda le norme tecniche ed igieniche da osservarsi per i lavori edilizi nelle località colpite dal terremoto del 13 gennaio 1915. G.U. del Regno d'Italia n. 117 del 11/05/1915. (In Italian).

- RDL 2089/24 (1924). Regio Decreto Legge n. 2089 del 23/10/1924, Norme tecniche ed igieniche di edilizia per le località colpite dal terremoto. G.U. del Regno d'Italia n. 303 del 30/12/1924. (In Italian).
- RDL 431/27 (1927). Regio Decreto Legge n. 431 del 13/03/1927, Norme tecniche ed igieniche di edilizia per le località colpite dai terremoti. G.U. del Regno d'Italia n. 82 del 8/04/1927. (In Italian).
- RDL 640/35 (1935). Regio Decreto Legge n. 640 del 25/03/1935, Nuovo testo delle norme tecniche di edilizia con speciali prescrizioni per le località colpite dai terremoti. G.U. del Regno d'Italia n. 120 del 22/05/1935. (In Italian).
- RDL 2105/37 (1937). Regio Decreto Legge n. 2105 del 22/11/1937, Norme tecniche di edilizia con speciali prescrizioni per le località colpite dai terremoti. G.U. del Regno d'Italia n. 298 del 27/12/1937. (In Italian).
- Reiter, L. (1990) *Earthquake Hazard Analysis: Issues and Insights*, Columbia University Press.
- Restrepo-Vélez, L.F. and Magenes, G. (2004). Simplified Procedure for the Seismic Risk Assessment of Unreinforced Masonry Buildings. *Proceedings of the 13th World Conference on Earthquake Engineering*, Vancouver, Canada, Paper No. 2561 (on CD).
- Restrepo-Vélez, L.F. (2005). *A Simplified Mechanics-Based Procedure for the Seismic Risk Assessment of Unreinforced Masonry Buildings*, PhD Thesis, European School for Advanced Studies in Reduction of Seismic Risk (ROSE School), Pavia, Italy.
- Ricci, P. (2010). *Seismic vulnerability of existing RC buildings*. Ph.D. Thesis in Seismic Risk, University of Naples "Federico II", Naples, Italy.
- Ricci, P., De Luca, F., and Verderame, G.M. (2011). 6th April 2009 earthquake, Italy: reinforced concrete building performance. *Bulletin of Earthquake Engineering and Structural Dynamics*, **40(8)**: 925-944.
- Rodgers, J.E. and Mahin, S.A. (2003). Effects of connection hysteretic degradation on the seismic behavior of steel moment-resisting frames. *PEER Report 2003/13*, Pacific Earthquake Engineering Research Center, University of California, Berkeley.
- Rossetto T. and Elnashai A. (2003). Derivation of vulnerability functions for European-type RC structures based on observational data. *Engineering Structures*, **25(10)**: 1241-1263.
- Rossetto T. and Elnashai A. (2005). A new analytical procedure for the derivation of displacement-based vulnerability curves for populations of RC structures. *Engineering Structures*, **7(3)**: 397-409.
- Rota, M., Penna, A. and Strobbia, C.L. (2008). Processing Italian damage data to derive typological fragility curves. *Soil Dynamics and Earthquake Engineering*, **28(10-11)**: 933-947.

- Rovida, A., Camassi, R., Gasperini, P. and Stucchi, M. (2011). *CPT111, the 2011 version of the Parametric Catalogue of Italian Earthquakes*. Milano, Bologna, <http://emidius.mi.ingv.it/CPTI>.
- Ruiz-Garcia, J. and Miranda, E. (2005). Performance-based assessment of existing structures accounting for residual displacements, *Technical Report* No. 153. John A. Blume Earthquake Engineering Center, Stanford University, Stanford, CA.
- Sabetta, F., Goretti, A., Lucantoni, A. (1998). Empirical fragility curves from damage surveys and estimated strong ground motion. *Proceedings of the 11th European Conference on Earthquake Engineering*, Paris, France, September 6-11.
- Saiidi, M. and Sozen, M.A. (1981). Simple nonlinear seismic analysis of R/C structures. *Journal of Structural Division, ASCE*, **107(5)**: 973-952.
- Santo, A., De Falco, M. and Di Crescenzo, G. (2013). *Macrozonazione sismica del territorio italiano in categorie del sottosuolo (scala 1:100000)*. Dipartimento di Ingegneria Civile Edile ed Ambientale, Università di Napoli Federico II. Personal communication.
- Sarabandi, P., Pachakis, D., King, S. and Karemidjian, A. (2004). Empirical fragility functions from recent earthquake. *Thirteenth World Conference on Earthquake Engineering*, Vancouver, Canada.
- Scawthorn, C. (2011). Disaster Casualties – Accounting for Economic Impacts and Diurnal Variation. In *Human Casualties in Earthquakes: Progress in Modelling and Mitigation*, ed. Spence, .R, So, E., Scawthorn, C., Springer, New York
- SEAOC, Structural Engineering Association Of California. (1995). *Vision 2000, A Framework for Performance-Based Engineering*. Structural Engineers Association of California. Sacramento, California.
- SERGISAI Working Group (1997) *First Year Progress Report of the SERGISAI Project*. European Commission Directorate General XII for Science and Development Environmental and Climate 1994-1998, Climatology and Natural Hazard.
- Shinozuka, M., Feng, M.Q., Kim, H.K. and Kim S.H. (2000). Nonlinear static procedure for fragility curve development. *Journal of Engineering Mechanics*, **126**: 1287-1295.
- Shome, N. and Cornell, C.A., (2000) Structural Seismic Demand Analysis: Consideration of “Collapse”. *8th ACSE Specialty Conference on Probabilistic Mechanics and Structural Reliability*, PMC2000-119.
- Sieberg, A., (1930). Geologie der Erdbeben, *Handbuch der Geophysik* **2(4)**: 552-555.
- Singhal, A., Kiremidjian A.S. (1996). Method for probabilistic evaluation of seismic structural damage. *ASCE Journal of Structural Engineering*, **122(12)**: 1459-1467.
- Singhal, A, Kiremidjian, AS. (1997). *A method for earthquake motion-damage relationships with application to reinforced concrete frames*. State University of New York at Buffalo: National Center for Earthquake Engineering Research Report NCEER-97-0008.

- Singhal, A., Kiremidjian A.S. (1998). Bayesian Updating of Fragility with Application to RC Frames. *Journal of Structural Engineering*, ASCE, **124**(8): 922-929.
- Slejko, D. (1996). *Pericolosità sismica del territorio nazionale, versione PS.4*. GNDT, rapporto tecnico per il Dipartimento della Protezione Civile, Trieste, 8 pp.
- Slejko, D., Peruzza, L. and Rebez A. (1998). Seismic hazard maps of Italy. *Annali di Geofisica*, **41**: 183-214.
- Smith, W., (2005). The challenge of earthquake risk assessment. *Seism. Res. Lett.*, **76**: 415-416.
- Sokol, Z. and Wald, F. (1997) Experiments with T-stubs in Tension and Compression. *Research Report, ČVUT, Prague*.
- Sorensen, M.B., Stromeyer, D. and Grunthal, G. (2008). Estimation of macroseismic intensity-new attenuation and intensity vs. ground motion relations for different parts of Europe. In *Fourteenth Word Conference on Earthquake Engineering*, Beijing, China.
- Spallarossa, D. and Barani, S., (2007). *Disaggregazione della pericolosità sismica in termini di M-R-ε*. Progetto DPC-INGV S1, Deliverable D14, <http://esse1.mi.ingv.it/d14.html>. (In Italian).
- Spence R.J.S., Coburn A.W., Sakai S. and Pomonis A. (1991). A parameterless scale of seismic intensity for use in the seismic risk analysis and vulnerability assessment. *International Conference on Earthquake, Blast and Impact*, Manchester, UK, September 19-20. pp. 19-30.
- Spence, R., Coburn, A.W. and Pomonis, A. (1992). Correlation of Ground Motion with Building Damage: The Definition of a New Damage-Based Seismic Intensity Scale. *Proceeding of the Tenth Word Conference of Earthquake Engineering*, Madrid, Spain Vol. 1 pp 551-556.
- Stucchi, M., Camassi, R. and Monachesi, G. (1993). *NT: il catalogo "di lavoro" del GNDT*. GNDT, rapporto interno, Milano, 80 pp.
- Stucchi, M. and Zerga, A. (1994). Criteri di compilazione ed analisi del contenuto di NT.1, un catalogo di "lavoro" del GNDT. *Atti del 12° Convegno del GNGTS*, Roma, 24-26 novembre 1993, I, pp. 311-320.
- Stucchi, M., Meletti, C., Montaldo, V., Crowley, H., Calvi, G.M. and Boschi, E., (2011). Seismic Hazard Assessment (2003–2009) for the Italian Building Code. *Bulletin of the Seismological Society of America*, **101**: 1885-1911.
- Suita, K., Yamada, S., Kasai, K., Shimada, Y., Tada, M. and Matsuoka, Y. (2009). Full scale shaking table collapse experiment on a 4-story steel moment frame: Part 2 detail of collapse behaviour. *Proceedings of the International Conference on Behaviour of Steel Structures in Seismic Areas (STESSA 2009)*, Yokohama, Japan, pp. 131-136.
- Syner-G, Systemic Seismic Vulnerability and Risk Analysis for Buildings, Lifeline Networks and Infrastructures Safety Gain (2009a). Project Coordinator: Prof.

- Pitilakis, K.(Aristotle University of Thassaloniki) Deliverable D3.2-*Fragility functions for common RC building types in Europe*.
- Syner-G, Systemic Seismic Vulnerability and Risk Analysis for Buildings, Lifeline Networks and Infrastructures Safety Gain (2009b). Project Coordinator: Prof. Pitilakis, K.(Aristotle University of Thassaloniki) Deliverable D3.1-*Fragility functions for common masonry building types in Europe*.
- Tena-Colunga, A. and Abrams, DP. (1996). Seismic behavior of structures with flexible diaphragms. *Journal of Structural Engineering*, ASCE **122(4)**: 439–45.
- Tremblay, R., Rogers, C., Martin, E. and Yang, W. (2004). Analysis, testing and design of steel roof deck diaphragms for ductile earthquake resistance. *Journal of Earthquake Engineering*, **8(5)**: 775–816.
- Tselentis, G.A. and Danciu, L. (2008). Empirical Relationship between Modified Mercalli Intensity and Engineering Ground-Motion Parameters in Greece. *Bulletin of Seismological Society of America*. **98(4)**: 1863-1875.
- Uma, SR., Pampanin, S., and Christopoulos, C. (2006). A probabilistic framework to develop performance objectives Based on Maximum and Residual Deformations. *Proceedings of the 1st ECEES*. Geneva, Switzerland. Paper No.731.
- Uma, SR, Pampanin S, and Christopoulos, C. (2010). Development of probabilistic framework for performance-based seismic assessment of structures considering residual deformations. *Journal of Earthquake Engineering*, **14(7)**: 1092–1111.
- Vamvatsikos, D. and Cornell, C.A. (2002). Incremental dynamic analysis. *Earthquake Engineering and Structural Dynamics*, **31**: 491–514.
- Vasishth, U.C., Murray, R.H. and Jacobson, J.S. (1995). Seismic prioritization and retrofit of bridges in Washington State. *Proceedings of the 15th International Conference on Seismic Zonation*, Nice, France, pp. 518-525.
- Veneziano, D., Sussman, J.M., Gupta, U. and Kunnumkal, S.M. (2002). Earthquake Loss under Limited Transportation Capacity: Assessment, Sensitivity and Remediation. *Proceedings of the Seventh US National Conference on Earthquake Engineering*, Boston, U.S.A. (on CD).
- Verderame G.M., De Luca F., Ricci P. and Manfredi G. (2011). Preliminary analysis of a soft storey mechanism after the 2009 L’Aquila earthquake. *Earthquake Engineering and Structural Dynamics*. **40(8)**:925-944.
- Vian, D. and Bruneau, M. (2003). Tests to structural collapse of single degree of freedom frames subjected to earthquake excitations. *Journal of Structural Engineering*, **129(12)**: 1676-1685.
- Vinale, F. (ed.) (2000). *Indirizzi per studi di microzonazione sismica*. AMRA, Naples, Italy. (In Italian).
- Wald, D.J., Quitoriano, V., Heaton, T., Kanamori, H. Scrivner, C.W. and Worden, B.C. (1999a). Rapid generation of peak ground-motion and intensity maps for earthquake in southern California. *Earthquake Spectra*, **15**: 537-556.

-
- Wald, D.J., Quitoriano, V., Heaton, T. and Kanamori, H. (1999b). Relationship between peak ground acceleration, peak ground velocity and Modified Mercalli Intensity in California. *Earthquake Spectra*, **15**: 557-564.
- Wald, F. Sokol, Z., Steenhuis C.M. and Jaspert, J.P. (2008) Component method for steel column bases; Special issue, *HERON* **53(1/2)**: 3-20.
- Whitman, R.V., Reed J.W., Hong S.T., (1973). Earthquake Damage Probability Matrices. *Proceedings of the 5th World Conference on Earthquake Engineering*, Rome, Italy, June 25-29. Vol. 2, pp. 2531-2540.
- Wilson, E.L. (2002). *Three-dimensional static and dynamic analysis of structures*. Berkeley (CA, USA). Computers & Structures, Inc.
- World Bank (1993). *World development report 1993: Investing in Health*. Oxford University Press, New York.
- Yakut, A., (2004). Preliminary seismic performance assessment procedure for existing RC buildings. *Engineering Structures* **26(10)**: 1447-1461.
- Zareian, F. and H., Krawinkler (2009). *Simplified performance based earthquake engineering*, Report No. 169. The John A. Blume Earthquake Engineering Center, Stanford University, U.S.A.
- Zonno, G., coord.(1998). *Rapporto Finale CNR-IRRS alla Commissione Europea*, ContattoENV4-CT96-0279, pp. 95-102.

Appendix A – EVOLUTION OF WIND DESIGN PRESCRIPTIONS IN ITALY

The first Italian provisions for the definition of wind loads were contained in the CNR 10012 of 1964 (CNR-UNI, 1964). Before this guidelines (not compulsory), wind loads were quantified according to common practice. According to the document, no internal pressure was defined and kinetic pressure coefficients were defined in an approximate way, without any consideration about soil roughness and wind gusts. The document also provided the first Italian map of reference kinetic pressures, unchanged in CNR guidelines of 1967 (CNR-UNI, 1967). Italian territory was divided into four zones, with a reference kinetic pressure ranging between 0.6 and 1.2 KN/m². The design wind pressure was, therefore, defined as follows:

$$p = c \cdot k \cdot q \quad (\text{A.1})$$

where, c was a shape and exposure coefficient, k was a slenderness coefficient and q was the kinetic pressure. This latter was defined as a function of the reference kinetic pressure (defined at an height of 20 meters from soil) and of building height.

The first compulsory document for the quantification of wind loads was the Ministry Decree 18407 of 1978 (DM 18407/78, 1978), which implemented the CNR guidelines approach. The CNR instructions of 1981 (CNR, 1981), introduced the concept of reference wind speed, defined as the wind speed measured at 10 meters of height, on open field, averaged on 10 minutes and associated to a return period of 50 years. In absence of specific studies, a value of 32 m/s was assumed, which results to be major than the current provisions. This value had to be transformed into a kinetic pressure, by means of coefficients taking into account for height variability and wind gusts. The big increasing in wind action made this prescriptions largely disregarded by professionals. For this reason in 1982, a Ministry Decree (DM, 1982) and its explanatory document (M.LL.PP.,1982), confirmed the approach of the previous code, neglecting the abovementioned guidelines.

A significant change in wind design was issued with CNR guidelines of 1985 (CNR,1985), in which some contradictory provisions with respect to the DM of 1982 were given, in particular a reduced value of the reference speed of 30 m/s.

The Decree remained compulsory till 1996, when the D.M. of 16/01/1996 (DM,1996b) and its explanatory document (MM.LL.PP., 1996) were issued. By means of these codes the wind design was radically renewed and the wind pressure was defined as stated in Eq. (A.2)

$$p = q_{ref} \cdot C_e \cdot C_p \cdot C_d \quad (\text{A.2})$$

in which, q_{ref} was the reference kinetic pressure and C_e , C_p , C_d were the exposure, shape and dynamic coefficients, respectively.

Moreover, a new map of wind speeds, implementing the recent improvements in wind engineering, replaced the 1967 map of reference pressures (Ballio *et al.*, 1999).

For what concerning the pressure coefficient, they remained substantially unchanged after the introduction of both the Decree of 1996 and the NIBC.

Finally, the more recent CNR-DT guidelines of 2008 (CNR-DT,2008) implemented several relevant theoretical and design aspects, such as dynamic and aeroelastic effects, vortices detachment, definition of coefficients for quantification of design pressure, use of experimental measurement in design.

In Table (A.1) a summary of Italian wind design codes and guidelines is reported. The wind design actions reported in these documents have been implemented in *NODE v.1.1 beta* for the definition, according to the proposed “large-scale” approach for prioritization, of a measure of the horizontal capacity alternate to the one deriving from seismic design.

Table A.1. Summary of the codes for wind design in Italy considered in the “large-scale” prioritization approach and implemented in *NODE v.1.0 beta*.

Year	Code
1964	CNR-UNI 10012/64
1967	CNR-UNI 10012/67
1978	DM LL PP 03/10/1978 n.18407
1982	DM LL PP 12/02/1982 and Circ. M LL PP n.22631
1985	CNR 10012/85
1996	DM LLPP 16/01/1996 and Circ. M LL PP n.156
2006	CNR/DT206/06
2008	DM LL PP 14/01/2008
2008	CNR/DT 207/08

Appendix B – MAIN CHARACTERISTICS OF THE CASE-STUDY PORTFOLIO

Table (B.1) reports the main characteristics of the case-study portfolio structures, analysed in the “large scale” approach. In the Table are reported, for each structure: the construction material (“constr. mat.” column), the design year, the number of storeys, the shape of the plan layout, the maximum dimensions in the two plan directions (L_X and L_Y), the maximum building height (H_{max}), the total load to the roof structure (p), the behaviour factor assumed for the prioritization analysis (q), the Occupancy Loss Ratio (OLR). Regarding the construction material, PRC-L refers to precast lattice structures. Regarding L_X and L_Y , those cases in which more than one entry is reports, the planar shape was different from the rectangular one, therefore, the different entries refer to the dimensions of different portion of the structure

Table B.1. Main characteristics of case-study structures.

#	Structural Unit ID	constr. mat.	design year	n_s	Shape	L_X [m]	L_Y [m]	$H_{m_{ax}}$ [m]	P [K N /m ²]	q [-]	OL R [-]
1	PLANT-01_wh1_su1_ST_1971	steel	1971	1	RECT	216	96	11	1.85	1.5	0.46
2	PLANT-01_wh1_su2_ST_1971	steel	1971	1	RECT	216	96	11	1.85	1.5	0.46
3	PLANT-01_wh1_su1_ST_1991	steel	1991	1	RECT	36	96	11	1.91	2.5	0.08
4	PLANT-01_wh1_su2_ST_1991	steel	1991	1	RECT	36	96	11	1.91	2.5	0.08
5	PLANT-02_wh1_PRC_1988	PRC	1988	1	RECT	70	54	9.19	3.4	2.5	0.24
6	PLANT-02_wh1_PRC_1995	PRC	1995	1	RECT	65	54	11.5	2.9	2.5	0.24
7	PLANT-03_wh1_PRC_1988	PRC	1988	1	RECT	60	50	7.15	3.0	2.5	0.12
8	PLANT-04_wh1_su1_PRC_1977	PRC	1977	1	RECT	48	48	8.6	2.6	2.5	0.05
9	PLANT-04_wh1_su2_PRC_1977	PRC	1977	1	RECT	48	48	8.6	2.6	2.5	0.38
10	PLANT-04_wh1_su3_PRC_1970	PRC	1970	1	RECT	100	48	8.6	2.7	1.5	1.00
11	PLANT-04_wh2_su1_PRC_1991	PRC	1991	1	RECT	45	50	7.55	3.2	2.5	0.10
12	PLANT-04_wh2_su2_PRC_1988	PRC	1988	1	RECT	30	80	7.55	3.1	2.5	0.05
13	PLANT-04_wh2_su3_PRC_1988	PRC	1988	1	RECT	30	80	7.55	3.1	2.5	0.05
14	PLANT-04_wh2_su4_PRC_1988	PRC	1988	1	RECT	30	80	7.55	3.1	2.5	0.05
15	PLANT-04_wh2_su5_PRC_1988	PRC	1988	1	RECT	30	80	7.55	3.1	2.5	0.05
16	PLANT-04_wh2_su6_PRC_2005	PRC	2005	1	RECT	15	70	7.55	3.5	3.5	0.29

Appendix B – Main characteristics of the case-study portfolio

17	PLANT-04_wh3_PRC_2002	PRC	2002	1	RECT	70	45	8.6	2.6	3.5	0.29
18	PLANT-05_wh1_su1_PRC_1993	PRC	1993	1	RECT	40	72	13.4	3.4	2.5	0.06
19	PLANT-05_wh1_su2_PRC_1993	PRC	1993	1	RECT	60	72	13.4	3.3	2.5	0.09
20	PLANT-05_wh1_su3_PRC_1993	PRC	1993	1	RECT	60	72	13.4	3.3	2.5	0.09
21	PLANT-05_wh1_su4_PRC_1993	PRC	1993	1	RECT	40	72	13.4	3.4	2.5	0.06
22	PLANT-05_wh1_su5_PRC_1993	PRC	1993	1	RECT	40	70	13.4	3.4	2.5	0.06
23	PLANT-05_wh1_su6_PRC_1993	PRC	1993	1	RECT	60	70	13.4	3.3	2.5	0.09
24	PLANT-05_wh1_su7_PRC_1993	PRC	1993	1	RECT	60	70	13.4	3.3	2.5	0.09
25	PLANT-05_wh1_su8_PRC_1993	PRC	1993	1	RECT	40	70	13.4	3.4	2.5	0.06
26	PLANT-06_wh1_PRC_1993	PRC	1993	1	RECT	100	105	9	2.5	2.5	0.19
27	PLANT-07_wh1_su1_ST_1987	steel	1987	1	RECT	72	60	12.5	1.89	2.5	0.12
28	PLANT-07_wh1_su2_ST_1987	steel	1987	1	RECT	72	60	12.5	1.89	2.5	0.12
29	PLANT-07_wh2_ST_1987	steel	1987	1	RECT	144	84	12.5	1.86	2.5	0.24
30	PLANT-07_wh3_su1_ST_2007	steel	2007	2	RECT	144	36	18	1.90	3.5	0.05
31	PLANT-07_wh3_su2_ST_2007	steel	2007	1	RECT	144	24	18	1.95	3.5	0.05
32	PLANT-08_wh1_su1_PRC_1934	PRC-L	1934	1	RECT	30	70	7.5	2.5	1.5	0.19
33	PLANT-08_wh1_su2_PRC_1934	PRC-L	1934	1	RECT	40	70	7.5	3.3	1.5	0.24
34	PLANT-08_wh1_su3_PRC_1934	PRC-L	1934	1	RECT	30	70	7.5	3.3	1.5	0.19
35	PLANT-08_wh1_su4_PRC_1960	PRC-L	1960	1	RECT	100	30	7.5	3.2	1.5	0.27
36	PLANT-08_wh1_su5_ST_1971	steel	1971	1	RECT	100	40	10	2.11	1.5	0.35
37	PLANT-08_wh2_ST_1971	steel	1971	1	RECT	70	80	10	2.08	1.5	0.95
38	PLANT-09_wh1_su1_ST_1973	steel	1973	1	RECT	90	20	14.5	2.18	1.5	0.31
39	PLANT-09_wh1_su2_ST_1973	steel	1973	1	RECT	20	80	14.5	2.19	1.5	0.26
40	PLANT-09_wh1_su3_ST_1973	steel	1973	1	RECT	90	20	14.5	2.18	1.5	0.31
41	PLANT-09_wh1_su4_ST_1973	steel	1973	1	T	20 40 40	20 40 20	14.5	2.09	1.5	0.55
42	PLANT-10_wh1_su1_PRC_1974	PRC	1974	1	RECT	96	48	9.1	3.0	1.5	0.44
43	PLANT-10_wh1_su2_PRC_1974	PRC	1974	1	RECT	96	32	9.1	3.0	1.5	0.29
44	PLANT-10_wh1_su3_PRC_1978	PRC	1978	1	RECT	48	48	8.5	3.1	2.5	0.21
45	PLANT-11_wh1_PRC_1988	PRC	1988	1	RECT	63	32.5	7.5	3.1	2.5	0.13
46	PLANT-11_wh2_PRC_1988	PRC	1988	1	RECT	63	32.5	7.5	3.1	2.5	0.13
47	PLANT-11_wh3_PRC_1988	PRC	1988	1	RECT	60	32.5	7.5	3.1	2.5	0.10
48	PLANT-11_wh4_PRC_1988	PRC	1988	1	RECT	60	32.5	7.5	3.1	2.5	0.46
49	PLANT-12_wh1_PRC_2001	PRC	2001	1	RECT	80	120	9.5	2.6	3.5	0.29
50	PLANT-13_wh1_su1_ST_1963	steel	1963	1	RECT	168	252	8.6	1.83	1.5	0.29
51	PLANT-13_wh1_su2_ST_1963	steel	1963	1	RECT	192	252	8.6	1.83	1.5	0.10
52	PLANT-14_wh1_su1_ST_1968	steel	1968	1	RECT	97.5	40	13	1.91	1.5	0.12
53	PLANT-14_wh1_su2_ST_1968	steel	1968	1	RECT	97.5	40	13	1.91	1.5	0.43

Appendix B – Main characteristics of the case-study portfolio

54	PLANT-15_wh1_su1_ST_1969	steel	1969	1	RECT	80	112	9	1.86	1.5	0.24
55	PLANT-15_wh1_su2_ST_1969	steel	1969	1	L	64 48	16 96	9	1.89	1.5	0.24
56	PLANT-15_wh1_su3_ST_1969	steel	1969	1	RECT	96	96	9	1.86	1.5	0.24
57	PLANT-15_wh1_su4_ST_1969	steel	1969	1	RECT	80	132	9	1.87	1.5	0.24
58	PLANT-15_wh1_su5_ST_1969	steel	1969	1	RECT	112	132	9	1.86	1.5	0.24
59	PLANT-15_wh1_su6_ST_1969	steel	1969	1	RECT	96	132	9	1.86	1.5	0.24
60	PLANT-16_wh1_su1_PRC_1962	PRC-L	1962	1	RECT	128	32	10.5	4.1	1.5	0.24
61	PLANT-16_wh1_su2_PRC_1962	PRC-L	1962	1	RECT	64	32	10.5	4.2	1.5	0.14
62	PLANT-16_wh2_PRC_1962	PRC-L	1962	1	RECT	176	32	10.5	4.1	1.5	0.39
63	PLANT-16_wh3_su1_PRC_1962	PRC-L	1962	2	RECT	128	16	12.5	3.9	1.5	0.24
64	PLANT-16_wh3_su2_PRC_1962	PRC-L	1962	2	RECT	64	16	12.5	4.0	1.5	0.00
65	PLANT-16_wh3_su3_PRC_1962	PRC-L	1962	2	RECT	176	16	12.5	3.9	1.5	0.00
66	PLANT-16_wh3_su4_PRC_1962	PRC-L	1962	1	RECT	128	128	10.5	4.0	1.5	0.00
67	PLANT-16_wh3_su5_PRC_1962	PRC-L	1962	1	RECT	176	112	10.5	4.0	1.5	0.71
68	PLANT-16_wh4_ST_1969	steel	1969	1	RECT	28	14	8.15	2.12	1.5	0.95
69	PLANT-16_wh5_su1_ST_1969	steel	1969	1	RECT	49	14	8.15	2.08	1.5	0.02
70	PLANT-16_wh5_su2_ST_1969	steel	1969	1	RECT	49	14	8.15	2.08	1.5	0.02
71	PLANT-16_wh5_su3_ST_1969	steel	1969	1	RECT	32	64	8.15	1.94	1.5	0.02
72	PLANT-17_wh1_su1_PRC_1919	PRC-L	1919	1	RECT	72	96	7.5	4.0	1.5	0.25
73	PLANT-17_wh1_su2_PRC_1919	PRC-L	1919	1	RECT	99	96	7.5	3.2	1.5	0.34
74	PLANT-17_wh1_su3_PRC_1919	PRC-L	1919	1	L	27 72	84 54	7.5	4.1	1.5	0.50
75	PLANT-17_wh1_su4_PRC_1919	PRC-L	1919	1	L	99 9	36 102	7.5	4.0	1.5	0.58
76	PLANT-18_wh1_su1_PRC_1976	PRC	1976	1	RECT	160	50	10	2.9	2.5	0.52
77	PLANT-18_wh1_su2_PRC_1976	PRC	1976	1	RECT	160	50	10	2.9	2.5	0.52
78	PLANT-18_wh1_su3_PRC_1996	PRC	1996	1	RECT	40	20	10	3.3	3.5	0.14
79	PLANT-18_wh1_su4_PRC_1996	PRC	1996	1	RECT	60	90	10	2.9	3.5	0.00
80	PLANT-19_wh1_su1_ST_1968	steel	1968	1	RECT	90	72	10	1.88	1.5	0.52
81	PLANT-19_wh1_su2_ST_1968	steel	1968	1	RECT	108	72	10	1.87	1.5	0.55
82	PLANT-19_wh1_su3_ST_1968	steel	1968	1	RECT	90	90	10	1.86	1.5	0.52
83	PLANT-19_wh1_su4_ST_1968	steel	1968	1	RECT	108	90	10	1.86	1.5	0.55

Appendix C – MAIN CHARACTERISTICS OF RECORDS EMPLOYED IN NON-LINEAR TIME-HISTORY ANALYSES

Table C.1. Basic record characteristics for $T_R=475$ years set

Earthquake name	Station ID	Moment Magnitude	Fault Mechanism	Epicentral Distance [km]	EC8 Site class
L'Aquila earthquake, 2009	MI03	5.6	Normal	5.9015	B
Friuli 4th shock, 1976	FRC	5.9	Thrust	16.8309	B
Val Nerina, 1980	NRC	5	n/a	10.6285	B
Friuli, 1976	GMN	5.1	n/a	4.3876	B
App. lucano, 1998	LRG	5.6	Normal	6.6332	B
Friuli, 1976	FRC	5	Thrust	7.6747	B
L'Aquila earthquake, 2009	AQK	5.6	Normal	9.3502	B
App. lucano, 1998	LRG	5.6	Normal	6.6332	B
Friuli, 1976	FRC	5	Thrust	7.6747	B
L'Aquila earthquake, 2009	MI05	5.6	Normal	5.3021	B
L'Aquila earthquake, 2009	AQK	5.6	Normal	9.3502	B
Friuli 3rd shock, 1976	FRC	5.9	Thrust	17.2939	B
Gran Sasso, 2009	AQK	5.4	Normal	16.1638	B
Irpinia, 1981	CNV0	5.2	Normal	10.1286	B
Irpinia, 1981	CNV0	5.2	Normal	10.1286	B
Friuli 4th shock, 1976	FRC	5.9	Thrust	16.8309	B
Friuli, 1976	GMN	5.1	n/a	4.3876	B
Gran Sasso, 2009	AQG	5.4	Normal	12.2872	B
Gran Sasso, 2009	AQK	5.4	Normal	16.1638	B
App. umbro-marchigiano, 1997	NRC	5.2	Normal	19.2315	B
Friuli, 1977	TLM1	5.3	Thrust	11.3944	B
L'Aquila earthquake, 2009	AQG	5.6	Normal	15.1391	B
L'Aquila earthquake, 2009	BZZ	5.6	Normal	6.9007	B
Gran Sasso, 2009	AQG	5.4	Normal	12.2872	B
Friuli 3rd shock, 1976	FRC	5.9	Thrust	17.2939	B
L'Aquila Earthquake, 2009	BZZ	5.6	Normal	6.9007	B
Gran Sasso, 2009	AQK	5.1	Normal	12.1648	B
L'Aquila Earthquake, 2009	AQG	5.6	Normal	15.1391	B
Val Nerina, 1980	NRC	5	n/a	10.6285	B
L'Aquila Earthquake, 2009	MI05	5.6	Normal	5.3021	B

Table C.2. Basic record characteristics for $T_R=475$ years set

Earthquake name	Station ID	Moment Magnitude	Fault Mechanism	Epicentral Distance [km]	EC8 Site class
Friuli 4th shock, 1976	GMN	5.9	Thrust	4.6987	B
L'Aquila mainshock, 2009	AQA	6.3	Normal	4.6338	B
Friuli 2nd shock, 1976	GMN	5.6	Thrust	14.9642	B
Friuli 1st shock, 1976	TLM1	6.4	Thrust	21.7205	B
L'Aquila mainshock, 2009	AQV	6.3	Normal	4.8698	B
L'Aquila mainshock, 2009	AQG	6.3	n/a	4.3919	B
L'Aquila mainshock, 2009	AQK	6.3	Normal	5.6501	B
L'Aquila mainshock, 2009	AQK	6.3	Normal	5.6501	B
Friuli 1st shock, 1976	TLM1	6.4	Thrust	21.7205	B
Friuli 2nd shock, 1976	GMN	5.6	Thrust	14.9642	B
L'Aquila mainshock, 2009	AQG	6.3	n/a	4.3919	B
L'Aquila mainshock, 2009	AQV	6.3	Normal	4.8698	B
Friuli 4th shock, 1976	GMN	5.9	Thrust	4.6987	B
L'Aquila mainshock, 2009	AQA	6.3	Normal	4.6338	B
Friuli 4th shock, 1976	FRC	5.9	Thrust	16.8309	B
Friuli 3rd shock, 1976	NRC	5.6	Normal	20.0486	B
Friuli 3rd shock, 1976	GMN	5.9	Thrust	5.2292	B
Friuli 4th shock, 1976	FRC	5.9	Thrust	16.8309	B
L'Aquila earthquake, 2009	MI03	5.6	Normal	5.9015	B
App. lucano, 1998	LRG	5.6	Normal	6.6332	B
Umbria-Marche 3rd shock, 1997	NRC	5.6	Normal	20.0486	B
L'Aquila earthquake, 2009	AQK	5.6	Normal	9.3502	B
App. lucano, 1998	LRG	5.6	Normal	6.6332	B
Potenza earthquake, 1990	BRN	5.8	Strike-slip	26.7062	B
L'Aquila earthquake, 2009	MI05	5.6	Normal	5.3021	B
Friuli 3rd shock, 1976	FRC	5.9	Thrust	17.2939	B
L'Aquila earthquake, 2009	AQK	5.6	Normal	9.3502	B
Gran Sasso, 2009	AQK	5.4	Normal	16.1638	B
Friuli 2nd shock, 1976	FRC	5.6	Thrust	26.2079	B
Gran Sasso, 2009	AQG	5.4	Normal	12.2872	B

Table C.3. Basic record characteristics for $T_R=975$ years set

Earthquake name	Station ID	Moment Magnitude	Fault Mechanism	Epicentral Distance [km]	EC8 Site class
South Iceland, 2000	ST2482	6.5	strike slip	15	B
Campano Lucano, 1980	ST276	6.9	normal	16	B
South Iceland, 2000	ST2484	6.5	strike slip	7	B
South Iceland, 2000	ST2484	6.5	strike slip	7	B
Montenegro (aftershock), 1979	ST73	6.2	thrust	8	B
Campano Lucano, 1980	ST276	6.9	normal	16	B
Montenegro, 1979	ST62	6.9	thrust	25	B
South Iceland(aft.shock), 2000	ST2488	6.4	strike slip	11	B
Umbria Marche, 1997	ST60	6	normal	11	B
Montenegro (aftershock), 1979	ST73	6.2	thrust	8	B
Friuli (aftershock), 1976	ST35	6	thrust	21	B
Umbria Marche, 1997	ST60	6	normal	11	B
Montenegro, 1979	ST63	6.9	thrust	24	B
Erzincan, 1992	ST205	6.6	strike slip	13	B
Friuli (aftershock), 1976	ST28	6	thrust	14	B
South Iceland(aft.shock), 2000	ST2484	6.4	strike slip	12	B
South Iceland, 2000	ST2562	6.5	strike slip	21	B
Montenegro, 1979	ST63	6.9	thrust	24	B
Friuli (aftershock), 1976	ST24	6	thrust	14	B
Ano Liosia, 1999	ST1259	6	normal	14	B
Montenegro, 1979	ST62	6.9	thrust	25	B
Ano Liosia, 1999	ST1259	6	normal	14	B
Ano Liosia, 1999	ST1258	6	normal	14	B
Friuli (aftershock), 1976	ST28	6	thrust	14	B
Friuli (aftershock), 1976	ST35	6	thrust	21	B
Ano Liosia, 1999	ST1100	6	normal	16	B
Ano Liosia, 1999	ST1100	6	normal	16	B
Ano Liosia, 1999	ST1257	6	normal	18	B
Ano Liosia, 1999	ST1141	6	normal	19	B
South Iceland(aft.shock), 2000	ST2482	6.4	strike slip	21	B

Table C.4. Basic record characteristics for $T_R=2475$ years set

Earthquake name	Station ID	Moment Magnitude	Fault Mechanism	Epicentral Distance [km]	EC8 Site class
Erzincan, 1992	ST205	6.6	strike slip	13	B
Montenegro, 1979	ST63	6.9	thrust	24	B
Campano Lucano, 1980	ST276	6.9	normal	16	B
South Iceland, 2000	ST2484	6.5	strike slip	7	B
Montenegro, 1979	ST63	6.9	thrust	24	B
Montenegro, 1979	ST62	6.9	thrust	25	B
South Iceland, 2000	ST2482	6.5	strike slip	15	B
Campano Lucano, 1980	ST276	6.9	normal	16	B
South Iceland, 2000	ST2484	6.5	strike slip	7	B
Montenegro, 1979	ST67	6.9	thrust	16	B
Montenegro (aftershock), 1979	ST73	6.2	thrust	8	B
South Iceland (aft.shock) 2000	ST2488	6.4	strike slip	11	B
Umbria Marche, 1997	ST60	6	normal	11	B
Montenegro (aftershock), 1979	ST73	6.2	thrust	8	B
Friuli (aftershock), 1976	ST35	6	thrust	21	B
Umbria Marche, 1997	ST60	6	normal	11	B
Panisler, 1983	ST133	6.6	strike slip	33	B
Friuli (aftershock), 1976	ST28	6	thrust	14	B
South Iceland (aft.shock) 2000	ST2484	6.4	strike slip	12	B
Umbria Marche, 1997	ST228	6	normal	38	B
Campano Lucano, 1980	ST99	6.9	normal	33	B
South Iceland, 2000	ST2562	6.5	strike slip	21	B
Duzce 1, 1999	ST3134	7.2	oblique	11	B
Strofades, 1997	ST171	6.6	oblique	38	B
Erzincan, 1992	ST205	6.6	strike slip	13	B
Friuli (aftershock),1976	ST24	6	thrust	14	B
Panisler, 1983	ST133	6.6	strike slip	33	B
Ano Liosia, 1999	ST1259	6	normal	14	B
Montenegro, 1979	ST62	6.9	thrust	25	B
Duzce 1, 1999	ST3141	7.2	oblique	26	B